An Empirical Method of Ascertaining the Null Points from a Dedicated Short-Range Communication (DSRC) Roadside Unit (RSU) at a Highway On/Off-Ramp

Jonathan B. Walker, P.E.

Dissertation submitted to the faculty of the Virginia Polytechnic Institute and State University in partial fulfillment of the requirements for the degree
of

Doctor of Philosophy
In
Civil Engineering

Kevin Heaslip, Chair
Thidapat Chantem
Ryan Gerdes
Taylor Lochrane

August 2, 2018
Fall Church, VA

Keywords: Dedicated Short-Range Communications (DSRC), Null Points, Reflection Coefficients, Transmission Coefficients, Roadside Unit (RSU), Vehicle-to-Infrastructure (V2I), Vehicle-to-Vehicle (V2V), Planning Strategy

Copyright © 2018, Jonathan Walker

An Empirical Method of Ascertaining the Null Points from a Dedicated Short-Range Communication (DSRC) Roadside Unit (RSU) at a Highway On/Off-Ramp

Jonathan B. Walker, P.E.

ABSTRACT (Academic)

The deployment of dedicated short-range communications (DSRC) roadside units (RSUs) allows a connected or automated vehicle to acquire information from the surrounding environment using vehicle-to-infrastructure (V2I) communication. However, wireless communication using DSRC has shown to exhibit null points, at repeatable distances. If the wireless connection is poor or non-existent, the V2I safety application will not obtain sufficient data to perform the operation services. In other words, a poor wireless connection between a vehicle and infrastructure (e.g., roadside unit) could hamper the performance of a safety application.

This research is intended to contribute towards the area of V2I communications using a DSRC RSU along a highway on/off ramp. The main research question will focus on answering the following question: *"Is there a more robust empirical method in determining the null points from a DSRC RSU installed on a highway on/off ramp?"*

Two existing models were leveraged to analyze null points: 1) signal strength loss (i.e., a free space path loss model, or FSPL, in Appendix A) and 2) the existing horizontal and vertical polarization null points from a DSRC RSU. Using empirical data from two different field tests, the existing horizontal and vertical polarization null point model was shown to contain limitations in short distances from the DSRC RSU. Moreover, the existing horizontal and vertical polarization model for null points was extremely challenging to replicate with over 15 DSRC RSU data sets. After calculating the null point for several DSRC RSU heights, the paper noticed a limitation of the existing horizontal and vertical polarization null point model with over 15 DSRC RSU data sets (i.e., the model does not account for null points along the full length of the FSPL model).

An extended horizontal and vertical polarization model is proposed that calculates the null point from a DSRC RSU. There are 18 model comparisons of the packet counts and signal strengths at various thresholds as perspective extended horizontal and vertical polarization models. This paper compares the predictive ability of 18 models and measures the fit. Finally, a predication graph is depicted with the neural network's probability profile for packet counts =1 when greater than or equal to 377. Likewise, a python script is provided of the extended horizontal and vertical polarization model in Appendix C.

An Empirical Method of Ascertaining the Null Points from a Dedicated Short-Range Communication (DSRC) Roadside Unit (RSU) at a Highway On/Off-Ramp

Jonathan B. Walker, P.E.

ABSTRACT (Public)

The deployment of dedicated short-range communications (DSRC) roadside units (RSUs) allows a connected or automated vehicle to acquire information from the surrounding environment using vehicle-to-infrastructure (V2I) communication. However, wireless communication using DSRC has shown to exhibit null points, at repeatable distances. The null points are significant and there was unexpected loss in the wireless signal strength along the pathway of the V2I communication. If the wireless connection is poor or non-existent, the V2I safety application will not obtain sufficient data to perform the operation services. In other words, a poor wireless connection between a vehicle and infrastructure (e.g., RSU) could hamper the performance of a safety application.

For example, a designer of a V2I safety application may require a minimum rate of data (or packet count) over 1,000 meters to effectively implement a Reduced Speed/Work Zone Warning (RSZW) application. The RSZW safety application is aimed to alert or warn drivers, in a Cooperative Adaptive Cruise Control (CACC) platoon, who are approaching a work zone. Therefore, the packet counts and/or signal strength threshold criterion must be determined by the developer of the V2I safety application. Thus, we selected an arbitrary criterion to develop an empirical method of ascertaining the null points from a DSRC RSU.

The research motivation focuses on developing an empirical method of calculating the null points of a DSRC RSU for V2I communication at a highway on/off-ramp. The intent is to improve safety, mobility, and environmental applications since a map of the null points can be plotted against the distance between the DSRC RSU and a vehicle's onboard unit (OBU). The main research question asks: "What is a more robust empirical method, compared to the horizontal and vertical laws of reflection formula, in determining the null points from a DSRC RSU on a highway on/off ramp?"

The research objectives are as follows:

1. Explain where and why null points occur from a DSRC RSU (Chapter 2)
2. Apply the existing horizontal and vertical polarization model and discuss the limitations of the model in a real-world scenario for a DSRC RSU on a highway on/off ramp (Chapter 3 and Appendix A)
3. Introduce an extended horizontal and vertical polarization null point model using empirical data (Chapter 4)
4. Discuss the conclusion, limitations of work, and future research (Chapter 5).

The simplest manner to understand where and why null points occur is depicted as two sinusoidal waves: direct and reflective waves (i.e., also known as a two-ray model). The null points for a DSRC RSU occurs because the direct and reflective waves produce a destructive

interference (i.e., decrease in signal strength) when they collide. Moreover, the null points can be located using Pythagorean theorem for the direct and reflective waves.

Two existing models were leveraged to analyze null points: 1) signal strength loss (i.e., a free space path loss model, or FSPL, in Appendix A) and 2) the existing horizontal and vertical polarization null points from a DSRC RSU. Using empirical data from two different field tests, the existing horizontal and vertical polarization null point model was shown to contain limitations in short distances from the DSRC RSU. Moreover, the existing horizontal and vertical polarization model for null points was extremely challenging to replicate with over 15 DSRC RSU data sets. After calculating the null point for several DSRC RSU heights, the paper noticed a limitation of the existing horizontal and vertical polarization null point model with over 15 DSRC RSU data sets (i.e., the model does not account for null points along the full length of the FSPL model).

An extended horizontal and vertical polarization model is proposed that calculates the null point from a DSRC RSU. There are 18 model comparisons of the packet counts and signal strengths at various thresholds as perspective extended horizontal and vertical polarization models. This paper compares the predictive ability of 18 models and measures the fit. Finally, a predication graph is depicted with the neural network's probability profile for packet counts =1 when greater than or equal to 377. Likewise, a python script is provided of the extended horizontal and vertical polarization model in Appendix C.

Consequently, the neural network model was applied to 10 different DSRC RSU data sets at 10 unique locations around a circular test track with packet counts ranging from 0 to 11. Neural network models were generated for 10 DSRC RSUs using three thresholds with an objective to compare the predictive ability of each model and measure the fit. Based on 30 models at 10 unique locations, the highest misclassification was 0.1248, while the lowest misclassification was 0.000. There were six RSUs mounted at 3.048 (or 10 feet) from the ground with a misclassification rate that ranged from 0.1248 to 0.0553. Out of 18 models, seven had a misclassification rate greater than 0.110, while the remaining misclassification rates were less than 0.0993. There were four RSUs mounted at 6.096 meters (or 20 feet) from the ground with a misclassification rate that ranged from 0.919 to 0.000. Out of 12 models, four had a misclassification rate greater than 0.0590, while the remaining misclassification rates were less than 0.0412.

Finally, there are two major limitations in the research: 1) the most effective key parameter is packet counts, which often require expensive data acquisition equipment to obtain the information and 2) the categorical type (i.e., decision tree, logistic regression, and neural network) will vary based on the packet counts or signal strength threshold that is dictated by the threshold criterion. There are at least two future research areas that correspond to this body of work: 1) there is a need to leverage the extended horizontal and vertical polarization null point model on multiple DSRC RSUs along a highway on/off ramp, and 2) there is a need to apply and validate different electric and magnetic (or propagation) models.

Acknowledgements

First, my wife has provided unwavering support for three decades as I continue to translate my dreams into reality. As our son states, “To conquer your dreams, you will need to stay woke.”

Second, I would like to acknowledge Dr. Kevin Heaslip for guidance as an advisor and some of the most exciting courses at Virginia Tech. University. Also, I have a deep respect for the committee members: Dr. Chantem, Dr. Gerdes, and Dr. Lochrane. Likewise, Dr. Kathleen Hancock has been instrumental in all aspects of the Ph.D. program.

Third, the United States Department of Transportation (USDOT) staff and co-workers are too numerous to list, but they were the key to successful research, data, advice, support, and guidance.

A special thank you to Andrea Vann Easton, a good friend for two decades, for proofreading, grammar checking, and formatting the dissertation.

However, I would be remiss if I did not mention Tom Gilmore, Ph.D., who has provided cerebral conversations, encouragement, and wisdom over the past two decades.

Finally, I would like to thank my kids, family, and friends for words of encouragement.

Table of Contents

List of Figures

List of Tables

Chapter 1. Introduction

Section 1.1. Research Background

The deployment of dedicated short-range communications (DSRC) roadside units (RSUs) allows a connected or automated vehicle to acquire information from the surrounding environment, such as a traffic light's signal phase and timing, using vehicle-to-infrastructure (V2I) communication [1]. However, the optimal location of the roadside equipment may be physically infeasible to be repositioned or limited by cost and/or the deployment schedule [2]. The antenna has become an effective means of distributing electrical charges and current in a specific direction for wireless communications via a DSRC RSU. Yet, wireless communication using DSRC has shown to exhibit null points, at repeatable distances. If the wireless connection is poor or non-existent, the safety application will not obtain sufficient data to perform the operation services.

In the past decade, tremendous advancements in vehicle-to-vehicle (V2V) and V2I communications have shown cooperative adaptive cruise control (CACC) platooning can improve highway traffic flow and decrease fuel consumption as well as increase safety, comfort, convenience, and customer satisfaction [3]. In general, CACC is a connected/automated vehicle (CAV) technique that merges three driver-assisted elements:

1. Traditional Cruise Control (TCC), whereby the constant speed is automatically maintained by the vehicle's electronic system
2. Adaptive Cruise Control (ACC), which maintains a constant gap between the lead and following vehicle using radar (or similar) technology
3. DSRC, which is used to communicate with CAVs based on the transmission and reception of Basic Safety Message (BSM) data sets [4].

The advantages of CACC are reducing vehicle crashes among equipped vehicles, allowing vehicles to travel safely at close distances in a platoon formation, and increasing roadway capacity.

Simulation models have shown that CACC platooning can be achieved safely based on two collision models that measure the vehicle's emergency braking performance: a) a stochastic model coded in Matlab/Simulink and b) a deterministic model with closed-form solutions [5]. Also, there is a need for accurate coordinated vehicle controls and vehicle placements that will improve the organized departures of a CACC-equipped vehicle from a highway environment [6]. Therefore, a number of simulations have focused on complex algorithms that guarantee maximum traffic flow, minimum collisions, and proper vehicle controls as well as vehicle braking [7]. Unfortunately, most simulations do not account for the accrual electromagnetic properties of V2V or V2I communications.

In addition, a poor wireless connection between a vehicle and infrastructure (e.g., RSU) could hamper the performance of a safety application. For example, the red-light violation warning (RLVW), a V2I safety application defined in the U.S. Department of Transportation (USDOT) Connected Vehicle Reference Implementation Architecture (CVRIA), enables a connected vehicle approaching an instrumented signalized intersection to receive information from the

infrastructure (e.g., RSU) regarding the signal timing and the geometry of the intersection (e.g., signal phase and timing or SPaT). The CVRIA states that there is a mechanism to obtain the vehicle location and motion of the surrounding vehicles from the RSU. A poor wireless connection could obstruct the RLVW application from alerting the driver in time to avoid the traffic conflict.

Likewise, the wireless communication using DSRC has shown to exhibit null points, at repeatable distances, where the data packets/messages have dropped near the RSU—the source of radio frequency (RF). The reflection of the DSRC RSU traveling wave will have a destructive effect, which may produce a significant signal loss (or null point). This research will focus on an empirical method of ascertaining the null points in DSRC RSU at a highway off/off ramp as a function of distance and data package loss.

Section 1.2. Research Motivation

As shown in Figure 1-1, the research motivation focuses on developing an empirical method of calculating the null points of a DSRC RSU for V2I communication at a highway on/off-ramp. Normally, a DSRC RSU will be installed near a highway on/off ramp and will radiate an RF signal in a circular pattern (i.e., assuming an omnidirectional antenna). Figure 1-2 depicts a front view of a CACC platoon on a highway and a CACC vehicle entering the CACC platoon with the assistance of a DSRC RSU located near a highway on/off ramp. The intent is to improve safety, mobility, and environmental applications since a map of the null points can be plotted against the distance between the DSRC RSU and a vehicle's onboard unit (OBU).

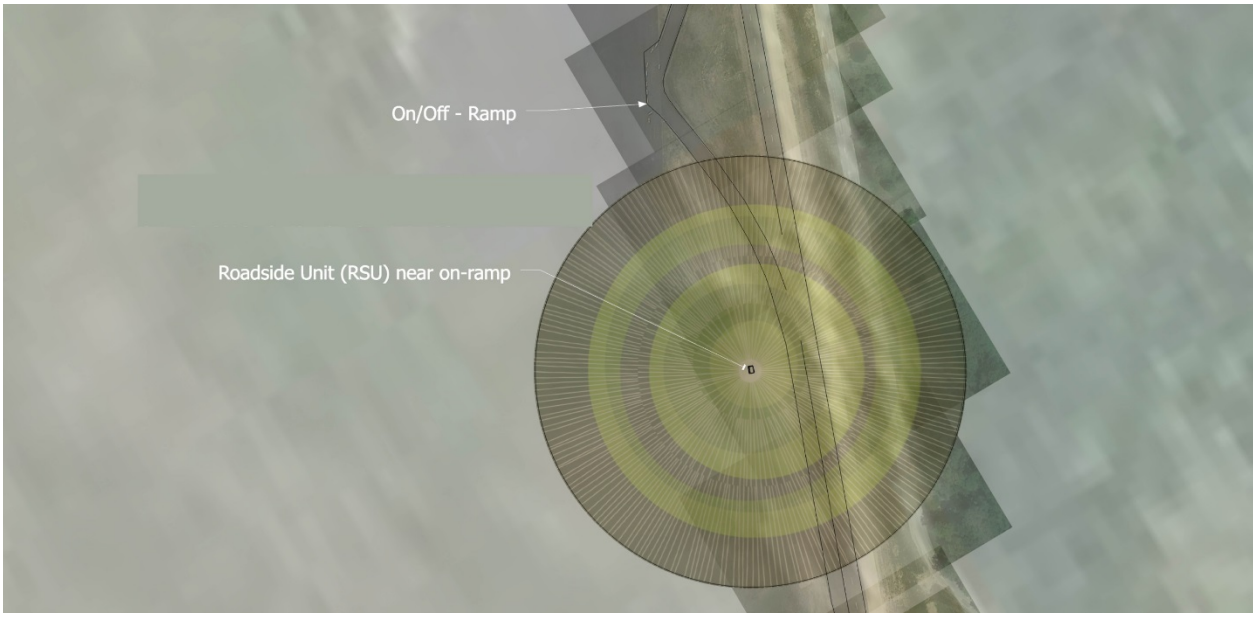

Figure 1-1. The top view of a DSRC RSU that is located near a highway on/off ramp; the RF signal radiates in a circular pattern using an omnidirectional antenna.

For example, a designer of a V2I safety application may require a minimum rate of data (or packet count) to effectively implement a V2I safety application such as Reduced Speed/Work Zone Warning (RSZW). The RSZW safety application is aimed to alert or warn drivers, in a

CACC platoon, who are approaching a work zone. If a CACC platoon is operating above the posted work zone speed limit, it is essential to maintain a minimum rate of data (or packet count) between the vehicle and infrastructure to warn the drivers approaching a work zone.

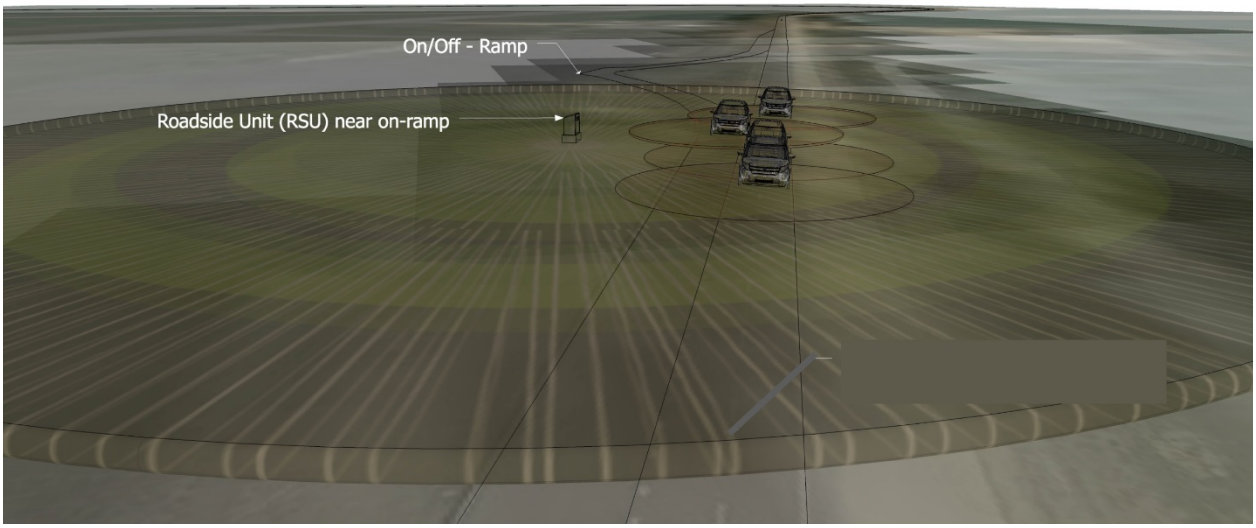

Figure 1-2. The front view of a DSRC RSU that is located near a highway on/off ramp with a CACC platoon and the RF signal radiates in a circular pattern using an omnidirectional antenna.

Section 1.3. Research Question, Objectives, Benefits, and Approach

Section 1.3.1. Research Question

The main research question focuses on the following: "What is a more robust empirical method, compared to the horizontal and vertical laws of reflection formula, in determining the null points from a DSRC RSU on a highway on/off ramp?"

Section 1.3.2. Research Objectives

The research objectives are as follows:

1. Explain where and why null points occurred from a DSRC RSU and introduce an existing horizontal and vertical polarization model along with the shortcomings of the model (Chapter 2)
2. Apply the existing horizontal and vertical polarization model and discuss the short comings of the model in a real-world scenario for a DSRC RSU on a Highway Off-Ramp (Chapter 3 and Appendix A)
3. Introduce an extended horizontal and vertical polarization model and apply the new extended model on base-line data (Chapter 4)
4. Discuss the limitations of the research and future research (Chapter 5).

Section 1.3.3. Research Benefits

The research benefits include:

1. Academic/Theoretical Benefit
    a. Using empirical and theoretical techniques, a horizontal and vertical polarization model is extended to account for long-range distances from a DSRC RSU because the existing model is only sufficient for short-range distances.
    b. The extended horizontal and vertical polarization model is portable and can be utilized with different datasets and customized scenarios.
2. Practical Benefit
    a. A low-cost and structured deployment strategy is presented for a DSRC RSU, which accounts for null points at a highway on/off ramp. The deployment strategy will reduce the initial planning cost, using free data/tools, while accounting for wireless communication constraints and environmental changes.
    b. The extended horizontal and vertical polarization model can be used to account for unexplained signal strength loss and packet counts in both short-range and long-range distances from the DSRC RSU.

Section 1.3.4. Dissertation Organization and Research Approach

The dissertation is organized to achieve the research objectives based on the research motivation. As shown in Figure 1-3, the research approach is segmented into chapters as follows:

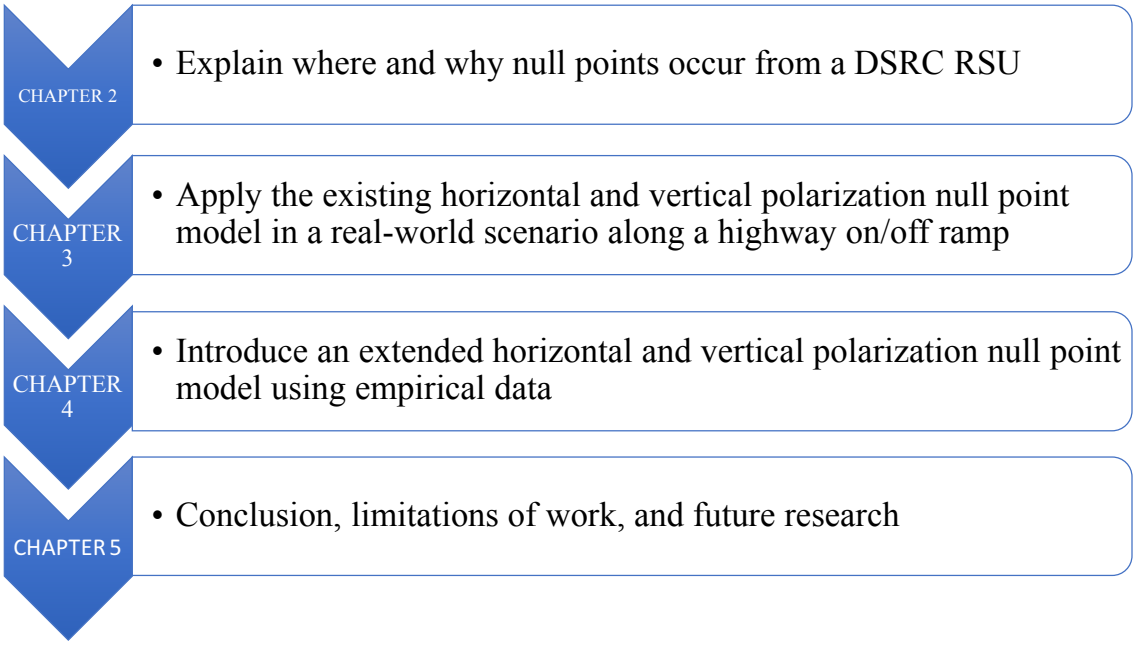

Figure 1-3. The research approach is segmented into four chapters (i.e., Chapters 2 through 5).

The first chapter provides an overview of the research that shows the correlation between the purpose, research method, and final results. Chapter 1 comprises the research background, motivation, question, objectives, benefits, and approach. The second, third, and fourth chapters describe the following: a) an abstract with the overall purpose of the chapter, b) the research background with the current state of practice, c) a research approach with the final results, and d) a discussion followed by references. The fifth chapter restates the research objective, summarizes the main results, and addresses future research. The appendix provides fundamental principles, a sample data file, and programming scripts.

Section 1.4. References

[1] J. Walker and K. Heaslip, "A Low-Cost Real-World Planning Strategy For Deploying a Dedicated Short-Range Communications Roadside Unit on a Highway Off-Ramp," *Transportation Research Board*, pp. 1–19, 2017.

[2] J. Walker, "The Fundamental Principles of Antenna Theory for (V2I) Deployments," in *Vehicle-to-Vehicle and Vehicle-to-Infrastructure Communications: A Technical Approach*, F. Hu, Ed. Boca Raton: CRC Press: Taylor & Francis Group, 2018, pp. 207–220.

[3] M. T. Hayat, H. Park, and B. L. Smith, "Connected Vehicle Enabled Freeway Merge Assistance system-field test: Preliminary results of driver compliance to advisory," *IEEE Intelligent Vehicle Symposium Proceedings*, no. IV, pp. 1017–1022, 2014.

[4] S. E. Shladover, C. Nowakowski, X.-Y. Lu, and R. Ferlis, "Cooperative Adaptive Cruise Control (CACC) Definitions and Operating Concepts," no. November 2014. p. 27.

[5] J. Fishelson, "Platooning Safety and Capacity in Automated Electric Transportation," Utah State University, 2013.

[6] E. Meissner, T. Chantem, and K. Heaslip, "Optimizing Departures of Automated Vehicles From Highways While Maintaining Mainline Capacity," *IEEE Transactions on Intelligent Transportation Systems.*, vol. 17, no. 12, pp. 3498–3511, Dec. 2016.

[7] D. Desiraju, T. Chantem, and K. Heaslip, "Minimizing the Disruption of Traffic Flow of Automated Vehicles During Lane Changes," *IEEE Transactions on Intelligent Transportation Systems.*, vol. 16, no. 3, pp. 1249–1258, Jun. 2015.

[8] National Highway Traffic Safety Administration (NHTSA), "Federal Motor Vehicle Safety Standards; V2V Communications." National Highway Traffic Safety Administration (NHTSA), Department of Transportation (DOT) ACTION:, Washington, D.C., pp. 1–392, 2016.

[9] Federal Highway Administration, "Crash Data Analyses for Vehicle-to- Infrastructure Communications for Safety Applications," Washington, D.C., 2012.

[10] J. Harding, G. Powell, R. Yoon, J. Fikentscher, C. Doyle, D. Sade, M. Lukuc, J. Simons, and J. Wang, "Vehicle-to-Vehicle Communications : Readiness of V2V Technology for Application," no. August. p. 327, 2014.

[11] National Highway Traffic Safety Administration (NHTSA), "Vehicle Safety Communications Project Final Report DOT HS 810 591," 2006.

[12] Federal Highway Administration, "2015 FHWA Vehicle to Infrastructure Deployment Guidance and Products." Washington, D.C., p. 30, 2014.

[13] D. Ou, Y. Yang, L. Xue, and D. Dong, "Optimal Connectivity-Based Deployment of Roadside Units for Vehicular Networks in Urban Areas," *Transportation Research*

Record: Journal of the Transportation Research Board, vol. 2559, no. 2559, pp. 46–56, Jan. 2016.

[14] G. G. M. Nawaz Ali, P. H. J. Chong, S. K. Samantha, and E. Chan, "Efficient data dissemination in cooperative multi-RSU Vehicular Ad Hoc Networks (VANETs)," *Journal of Systems and Software*, vol. 117, pp. 508–527, Jul. 2016.

[15] M. Kafsi, P. Papadimitratos, O. Dousse, T. Alpcan, and J.-P. Hubaux, "VANET Connectivity Analysis," 2009.

[16] T. Yan, W. Zhang, G. Wang, and Y. Zhang, "Access Points Planning in Urban Area for Data Dissemination to Drivers," *IEEE Transactions on Vehicular Technology*, vol. 63, no. 1, pp. 390–402, Jan. 2014.

[17] C. M. Silva, W. Meira, and J. F. M. Sarubbi, "Non-Intrusive Planning the Roadside Infrastructure for Vehicular Networks," *IEEE Transactions on Intelligent Transportation Systems.*, vol. 17, no. 4, pp. 938–947, 2016.

[18] O. Trullols, M. Fiore, C. Casetti, C. F. Chiasserini, and J. M. Barcelo Ordinas, "Planning roadside infrastructure for information dissemination in intelligent transportation systems," *Computer Communications*, vol. 33, no. 4, pp. 432–442, 2010.

[19] V. D. Khairnar and S. N. Pradhan, "Simulation Based Evaluation of Highway Road Scenario between DSRC/802.11p MAC Protocol and STDMA for Vehicle-to-Vehicle Communication," *Journal of Transportation Technologies*, vol. 3, no. 1, pp. 88–104, 2013.

[20] M. Shulman and R. K. Deering, "Third Annual Report of the Crash Avoidance Metrics Partnership, April 2003 - March 2004," Washington, D.C., 2005.

[21] R. Miucic, Z. Popovic, and S. M. Mahmud, "Experimental characterization of DSRC signal strength drops," in *2009 12th International IEEE Conference on Intelligent Transportation Systems*, 2009, pp. 1–5.

[22] E. Zöchmann, K. Guan, and M. Rupp, "Two-Ray Models in mmWave Communications," pp. 225–229, 2017.

[23] IEEE Vehicular Technology Society Sponsored, *IEEE Standard for Wireless Access in Vehicular Environments (WAVE)— Networking Services IEEE*. New York: The Institute of Electrical and Electronics Engineers, Inc., 2016.

[24] V. Shivaldova, A. Winkelbauer, and C. F. Mecklenbrauker, "Signal-to-noise ratio modeling for vehicle-to-infrastructure communications," *2014 IEEE 6th International Symposium on Wireless Vehicular Communications WiVeC 2014 - Proc.*, 2014.

[25] V. Shivaldova, A. Winkelbauer, and C. F. Mecklenbrauker, "Vehicular Link Performance: From Real-World Experiments to Reliability Models and Performance Analysis," *IEEE Vehicular Technology Magazine*, vol. 8, no. 4, pp. 35–44, 2013.

[26] V. Shivaldova and C. F. Mecklenbräuker, "Quantization-based Complexity Reduction for Range-dependent Modified Gilbert Model," *Proc. IEEE Sens. Array Multichannel Signal Process. Work.*, pp. 345–348, 2014.

[27] V. Shivaldova, A. Winkelbauer, and C. F. Mecklenbr, "Realistic Performance Model for Vehicle-to-Infrastructure Communications," no. c, pp. 557–561, 2014.

[28] V. Shivaldova, A. Paier, D. Smely, and C. F. Mecklenbräuker, "On roadside unit antenna measurements for vehicle-to-infrastructure communications," *IEEE International Symposium on Personal, Indoor and Mobile Radio Communications PIMRC*, pp. 1295–1299, 2012.

[29] W. H. Hayt, Jr., *Engineering Electromagnetics*, Fifth Edition. New York: McGraw-Hill, Inc., 1989.
[30] L. V. Bewley, *Two Dimensional Fields in Electrial Engineering*, 1st ed. New York: Dover Publications, 1963.
[31] D. Corson and P. Lorrain, *Introducing to Electromagnetic Fields and Waves*. San Franscisco: W.H. Freeman, 1962.
[32] R. Wilson, "Propagation Losses Through Common Building Materials 2.4 GHz vs 5 GHz," *Magis Network, Inc.*, pp. 1–28, 2002.
[33] R. E. Collins, *Antennas and Radio Wave Propagation*. New York: McGraw-Hill, Inc., 2014.
[34] S. L. Salas and E. Hille, *Calculus: One and Several Variables*, 3rd ed. John Wiley and Sons, Inc., 1978.
[35] R. Plonsey and R. E. Collin, *Principles and Applications of Electromagnetic Fields*. McGraw-Hill, Inc., 1961.
[36] M. Javid and P. M. Brown, *Field Analysis and Electromagnetics*. New York: McGraw-Hill, Inc., 1963.
[37] E. C. Jordan and K. G. Balmain, *Electromagnetic Waves and Radiating Systems*, 2nd ed. Englewood Cliffs: Dorling Kindesley Pearson Education, 2015.
[38] J. D. Kraus, *Electromagnetics*, 4th ed. New York: McGraw-Hill, Inc., 1992.
[39] J. E. Parton, S. J. . Owen, and M. S. Raven, *Applied Electromagnetics*. Palgrave Macmillan, 1985.
[40] D. T. Paris and F. K. Hurd, *Basic Electromagnetic Theory*. McGraw-Hill, Inc., 1969.
[41] R. C. Weast and S. M. Selby, Eds., *Standard Mathematical Tables*, Seventeent. The Chemical Rubber Co., 1969.
[42] S. Ramo, J. R. Whinnery, and T. Van Duzer, *Fields and Waves in Communication Electronics*, 3rd ed. New York: John Wiley and Sons, Inc., 2008.
[43] K. F. Sander and G. A. L. Reed, *Transmission and Propagation of Electromagnetic Waves*, 2nd ed. New York: Cambridge University Press, 1986.
[44] D. K. Cheng, *Field and Wave Electromagnetics*, Second Edi. Reading, Mass.: The Addison-Wesley, 1989.
[45] R. Valenzuela, "A ray tracing approach to predicting indoor wireless transmission," *IEEE 43rd Veh. Technol. Conf.*, pp. 214–218, 1993.
[46] A. M. Bodzin and L. Cirucci, "A Land-Use-Planning Simulation Using Google Earth.," *Sci. Scope*, vol. 32, no. 7, pp. 30–38, 2009.
[47] I. Janssen and A. Rosu, "Measuring sidewalk distances using Google earth," *BMC Med. Res. Methodol.*, vol. 12, no. 39, p. 10, 2012.
[48] S. Bayless, A. Guan, A. Shaw, M. Johnson, G. Pruitt, and B. Abernathy, "Recommended Practices for DSRC Licensing and Spectrum Management: A Guide for Management, Regulation, Deployment, and Administration for Connected Vehicle Environment.," 2015.
[49] F. C. Commission, "Equipment Authorization Order & Accredited Testing Laboratories FCC Equipment Authorization Process," 2017. [Online]. Available: https://transition.fcc.gov/oet/ea/presentations/files/may17/10-EA_Accredited-Labs-GT-Final.pdf.
[50] C. Kwok, R. F. Jr. Cleveland, and D. L. Means, "Evaluating Compliance with FCC Guidelines for Human Exposure to Radiofrequency Electromagnetic Fields Supplement C," 1997.

[51] J. D. M. S. J. L. U. Robert F. Cleveland and Standards, “OET bulletin 65: Evaluating compliance with FCC guidelines for human exposure to radiofrequency electromagnetic fields,” 1997.
[52] Cisco Systems, “White Paper on Antenna Patterns and Their Meaning,” San Jose, 2007.
[53] Linx Technology, “Application Note,” Merlin, 2012.
[54] A. S. C. of the I. A. and Propagation and Society, “IEEE Standard Definitions of Terms for Antennas,” 1993.
[55] Campbell Scientific, “The Link Budget and Fade Margin (Application Notes).” Campbell Scientific, Inc., Logan, 2016.
[56] T. Vincenty, “Direct and Inverse Solutions of Geodesics on the Ellipsoid With Application of Nested Equations,” *Surv. Rev.*, vol. 23, no. 176, pp. 88–93, 1975.
[57] T. Vincenty, “Geodetic inverse solution between antipodal points,” *Richard Rapp Geodetic Science Ohio State University*. 1975.

Chapter 2. Explain Where and Why Null Points Occur from a DSRC RSU and Investigate an Existing Horizontal and Vertical Polarization Model

Section 2.1. Title

Explain where and why null points occur from a DSRC RSU and investigate an existing horizontal and vertical polarization model.

Section 2.2. Abstract

To understand where and why null points occur, there is a need to represent DSRC as a sinusoidal wave and show the impact due to the ground surface (i.e., a change in the coefficients between an open space and a ground surface). Then, a two-ray model can be used to theoretically and visually discuss the null points for a DSRC RSU because the direct and reflective waves produce a destructive interference (i.e., decrease in signal strength) when they collide. The theoretical model corresponds to Pythagorean theorem from the direct and reflective waves. The horizontal (d_h^k) and vertical (d_v^k) polarization models were used to show the impact of a DSRC RSU's height, both mathematically and visually. Using the formula by Miucic et al., the horizontal and vertical polarization null points were calculated for several DSRC RSU heights.

When leveraged with V2V technology, V2I communication will enable a broader range of safety, mobility, and environmental applications. The V2I communication standards have been designed for the use of an RSU that broadcasts via DSRC. However, wireless communication using DSRC has shown to exhibit null points, at repeatable distances. If the wireless connection is poor or non-existent, the safety application will not obtain sufficient data to perform the operation services.

For example, the RSZW is a safety application that requires a constant rate of data (or packet count) between the vehicle and infrastructure to warn the drivers who approach a work zone. This chapter focuses on a rigorous derivation of the reflection and transmission fields because a number of publications make a correlation in equating the DSRC RSU's null points and mounting height with the vehicle's onboard unit (OBU). Thus, the reflection and transmission fields were used to analyze the impact of a DSRC RSU's mounting height at a highway on/off ramp. Moreover, the chapter has successfully derived the existing horizontal and vertical polarization null point model for determining null points in relation to various DSRC RSU heights.

Unfortunately, the existing horizontal and vertical polarization null point model are limited to short distances from the DSRC RSU. After calculating the null point for several DSRC RSU heights, the paper noticed a limitation of the existing horizontal and vertical polarization null point model (i.e., the model does not account for null points along the full length of the free space path loss, or FSPL, model).

In summary, the chapter discusses the following:

1. A two-ray model can be used to show how two out-of-phase electrical and magnetic fields produce a null point after one sinusoidal wave reflects off the earth's surface.
2. The horizontal (d_h^k) and vertical (d_v^k) polarizations models can be used to show the impact of a DSRC RSU's height (h_t), both mathematically and visually.

Section 2.3. Introduction

The past couple of years has seen increased potential to implement V2V and V2I communication technology due to the release of the National Highway Traffic Safety Administration (NHTSA) Notice of Proposed Rulemaking (NPRM) on V2V Communications. As a Federal agency under the USDOT, NHTSA has authority over U.S. motor vehicle safety and has been researching V2V and V2I communication technology for the past decade in partnership with the automotive industry, academic institutions, roadside equipment manufacturers, and many others [8]. When leveraged with V2V technology, V2I communication will enable a broader range of safety, mobility, and environmental applications since the communication technology has been designed to work as an interoperable unit for intelligent transportation systems (ITS) [9] [7] [6] [5]. As noted in the NHTSA readiness report on V2V communication, V2I communication can be utilized in numerous safety applications such as red light violation warning, curve speed warning, reduced speed zone warning, and railroad crossing violation warning [10]. But, a poor wireless connection between a vehicle and infrastructure (e.g., RSU) could hamper the performance of a safety application [11]. Because the Federal Communication Commission (FCC) designated the 5.9 GHz band for ITS services aimed at public safety communication, NHTSA and its partners have tested DSRC as a V2I communication medium [8]. As the FCC allocation of 5.9 GHz and the NHTSA NPRM have greatly increased the likelihood that multiple car manufacturers will implement the standards set forth in both regulations, this chapter focuses on V2I communication using DSRC via an RSU.

V2I research using DSRC has increased in recent years because the existing roadway infrastructure (e.g., Ethernet/fiber optic connection, highway gantry, power cabinet) can be used to reduce total deployment cost [12]. An initial literature search showed that several simulation-based planning strategies assume a strong RF signal strength between the DSRC RSU and the vehicle's OBU through V2I wireless communication [13] [14] [15] [16] [17] [18]. In other words, the simulation-based planning strategies do not account for RF signal attenuation due to path loss, reflection, diffraction, refraction, or scattering. Khairnar and Pradhan examined the importance of uninterrupted wireless communication connection, and their simulations revealed that an OBU is forced to drop over 80 percent of the data packets/messages if the wireless connection is not maintained or constant [19]. Eventually, the OBU's software does not have enough data to perform a given operation (e.g., red light violation, work zone alert), which implies an adverse consequence for the V2V or V2I safety application(s) because the wireless connection is not constant.

More specifically, the wireless communication using DSRC has shown to exhibit null points, at repeatable distances, where the data packets/messages have dropped near the RSU—the source of RF. In 2005, NHTSA and the Crash Avoidance Metrics Partnership (CAMP) documented early signs of null points (or "null zones") in field experiments and stated, "These [null zones] were most likely caused by the expected phenomenon of reflected signals canceling out the direct signal under specific sender-receiver geometries" [20]. In 2006, NHTSA conducted an extensive field study testing the maximum DSRC ranges and identified null points for V2V communication, even though there was a clear line-of-sight between the RSU and vehicle's OBU [11].

In 2009, Miucic, Popovic, and Mahmud provided key formulas to predict the null points, using DSRC, based on a geometric triangle RF reflection model; however, the formulas make a major assumption that holds the DSRC RSU's mounting height equal to the vehicle's OBU [21]. Likewise, Zöchmann, Guan, and Rupp provided predicted null points based on a geometric ellipse and assumed the DSRC RSU's mounting height is equal to the vehicle's OBU [22]. In a real-world V2I deployment, the RSU's mounting height may be restricted by the existing roadway infrastructure surrounding limitations (e.g., a fixed highway gantry height or fixed height of traffic signal enclosure).

Finally, the literature has revealed that the majority of DSRC RSU field experiences utilized a vertically (or linearly) polarized antenna. Although, original equipment manufacturers can produce vertically and horizontally polarized antenna, this chapter only elaborates on the vertically polarized antenna, since both derivations are similar in nature.

Section 2.4. Study Background

In general, the V2I communication standards have been designed around the use of an RSU that broadcasts via DSRC [23]. DSRC describes a specific type of IEEE 802.11 standard in operation that is customized for ITS. Moreover, the FCC has allocated 75 MHz (5.850 to 5.925 GHz), in the United States, as a primary service under CFR 47 Parts 90 and 95. Three sets of standards are commonly used for DSRC operation:

1. One developed under the IEEE 802.11.p standard
2. Two under SAE J2735 and SAE J2945
3. Several standards under IEEE 1609 [10].

The IEEE standard for Wireless Access in Vehicular Environments (WAVE) is a radio communication system that strives to provide interoperable service between the automotive and transportation industry. These services comprise of communications between vehicles and RSUs (i.e., V2I), between vehicles (i.e., V2V), and between vehicles and other devices (i.e., V2X). The wireless connectivity is achieved through a 5.9 GHz media using the WAVE standards. Thus, the planning strategies for a DSRC RSU are vital to the success of a robust wireless connection and an adequate reaction time for the V2I application. If the wireless connection is poor or non-existent, the safety application will not obtain sufficient data to perform the operation services.

The Institute of Telecommunications has published numerous scholarly papers associated with field experiments using IEEE 802.11p standards through V2I and V2V communications via roadside equipment [24] [25] [26] [27] [28] [25]. The scientific staff is part of the faculty in Electrical Engineering and Information Technology at Vienna University of Technology (https://www.nt.tuwien.ac.at). Shivaldova et al. have published six notable papers that explore implementation in the field using V2I communication to and from a DSRC RSU with mobile vehicles. The papers provide a function to calculate data throughput and packets loss using DSRC RSUs on existing highway infrastructure. Yet, the function does not account for null points near the RSU.

Section 2.5. Where and Why Null Points Occur for a DSRC RSU

Section 2.5.1. A Theoretical and Visual Perspective on Null Points for a DSRC RSU

Section 2.5.1.1. The Impact of a Ground Surface on Reflection and Transmission Fields

There is a major impact on the reflection and transmission fields due to the ground surface (i.e., a change in the coefficients between an open space and a ground surface). The RF signal transmitted by a DSRC RSU is rarely the result of a traveling wave captured directly between the RSU and an OBU in a vehicle. More likely, the traveling wave is the result of multipath signals, both directly and indirectly, with different amplitudes and phases of an electromagnetic wave.

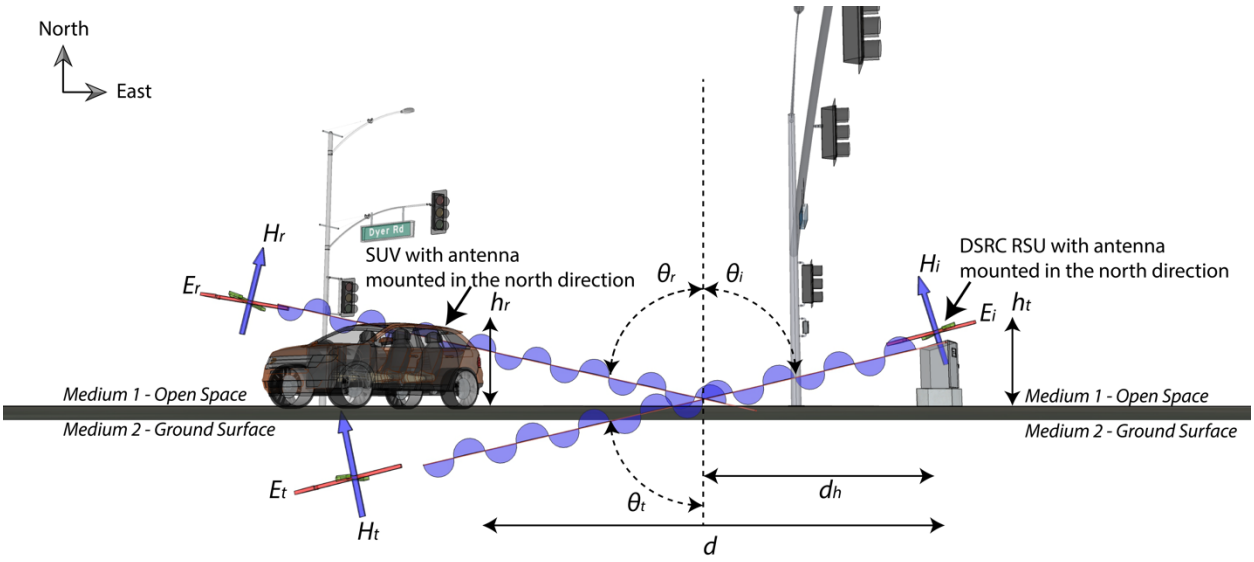

Figure 2-1. The reflection electric and magnetic fields (Er and Hr) and transmitted electric and magnetic fields (Et and Ht) at the ground surface (medium 2) in relation to open space (medium 1).

Figure 2-1 is a realistic view with vertical and horizontal waves between the RSU and OBUs in a vehicle. A traveling wave will be partially reflected from the surface and partially absorbed by the ground surface. The figure depicts the essential variables in wave reflection and transmission.

The mounting height of the DSRC RSU antenna (or transmitter) is h_t and the mounting height of the vehicle antenna (or receiver) is h_r. The incident electric and magnetic fields are denoted as Ei and Hi, respectively. The reflective electric and magnetic fields are denoted as Er and Hr, respectively. The transmitted electric and magnetic fields are denoted as Et and Ht, respectively. At a single transmission frequency, the angle of incidence (θ_i) and angle of reflection (θ_r) are equal with the angle of transmission (θ_t). Between the DSRC RSU and vehicle antennas, there is a distance of d and the null distance for the horizontal polarization is d_h. The open space (or air) is medium 1, and the ground surface is medium 2.

When a DSRC RSU is mounted near the ground, the angle of incidence (θ_i) is close to 90 degrees and termed a grazing angle [21]. For an angle of incidence (θ_i) at 90 degrees, the Fresnel reflection and transmission coefficients for both the perpendicular and parallel polarization are undefined since the cosine of 90 degrees is zero. Similarly, an angle of incidence (θ_i) at 85 and 80 degrees will be 8.71 percent and 17 percent, respectively, of the ratio between the intrinsic impedances (η) of air and the street/road (or a given medium). Thus, the height of the antenna will impact the angle of traveling waves that graze at the street/road (or a given medium) and reflected to the OBU in a vehicle from the DSRC RSU.

Section 2.5.1.2. Where and Why Null Points Occur for a DSRC RSU?

As shown in Figure 2-2, the null points for a DSRC RSU occur because the direct and reflective waves produce a destructive interference (i.e., decrease in signal strength) when they collide. The null points can be located using Pythagorean theorem for the direct and reflective waves. The reflected electric and magnetic fields will impact the direct wave as constructive or destructive interference. A zero-degree phase shift will produce a constructive interference with the direct wave, and a 180-degree phase shift will produce a destructive interference with the direct wave. The destructive interference will produce a decrease in the signal strength of the direct wave, which is termed a null point. In other words, the direct and reflective waves will cancel each other when they are 180 degrees out-of-phase.

A DSRC RSU's electric and magnetic fields can be depicted as two sinusoidal waves: direct and reflective waves (i.e., also known as a two-ray model). There are at least three essential characteristics in a two-ray model: a) the direct wave is normally the shortest line-of-site distance between the transmitter and receiver antennas (d_{t3}), b) the reflective wave is the sinusoidal wave that reflects off an imperfect conductor ($\sigma_2 \neq \infty$) such as the earth's surface ($d_{t1} + d_{t2}$) or a highway barrier object, and c) the height of the transmitter and receiver antennas.

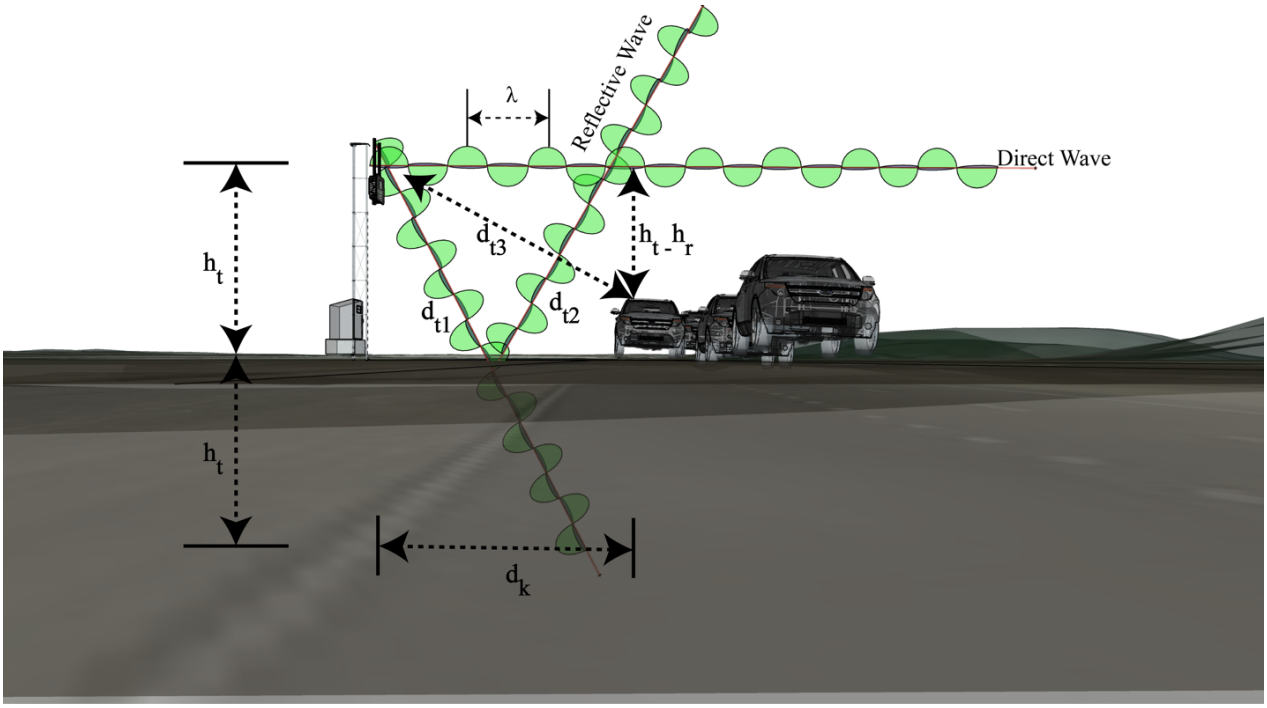

Figure 2-2. A direct wave (d_{t3}) is propagating from DSRC RSU while the reflective wave (d_{t1} + d_{t2}) collides with the earth's surface at height (h_t).

Using Figure 2-2, the three essential characteristics in a two-ray model are described as follows:

1. First, the direct wave (d_{t3}) will propagate, in free space, while decreasing in signal strength by the square of the distance traveled. The free space model is used to estimate the signal loss based on the frequency of the incident electric and magnetic fields.
2. Second, the reflective wave will propagate at an angle in the direction of the earth's surface (d_{t1} + d_{t2}). A portion of the electric and magnetic fields will transmit into the earth surface while the remaining electric and magnetic fields will reflect off the earth's surface (d_{t2}). The reflected electric and magnetic fields will shift in phase. As discussed previously, the phase shift is caused by a difference in intrinsic impedance between the incident electric and magnetic fields traveling in free space ($\sigma_2 = 0$) and the earth's surface ($\sigma_2 \neq \infty$). For instance, the reflective electric and magnetic fields are sinusoidal waves that can shift by a few degrees (or out-of-phase) once the incident electric and magnetic fields collide with the earth's surface.
3. Third, the location of a reflection will depend on the relative height of the transmitting antennas and the reflective properties of the earth's surface when deploying a DSRC RSU.

As depicted in Figure 2-2, the two-ray model can be formulated using Pythagorean theorem for the direct and reflective waves as follows:

$$directive\ wave: d_{t3} = \sqrt{(h_t - h_r)^2 + {d_k}^2} \quad (1)$$

$$reflective\ wave: d_{t1} + d_{t2} = \sqrt{(h_t + h_r)^2 + {d_k}^2} \quad (2)$$

Section 2.5.1.3. Horizontal and Vertical Polarization Null Points for a DSRC RSU

Using a modified Pythagorean theorem, a slightly modified model can be used to locate the null points both for a horizontal and vertical polarized DSRC RSU antenna. The reflection of the DSRC RSU traveling wave will have a destructive effect, which may produce a significant signal loss (or null point), on the resultant wave due to the law of reflection and Briggs Law [28] [27]. This subsection focuses on calculating critical distances of each null point of distributive traveling waves by a DSRC RSU. NHTSA's Vehicle Safety Communications project conducted field experiments on DSRC, during which null points were observed at various distances due to multipath reflections [33]. Miucic et al. [21] have documented DSRC signal strength null points and derived the critical distance that should be accounted for in planning strategies.

In Miucic et al., the null points can be determined for the horizontal (d_h^k) and vertical (d_v^k) polarizations, whereby $k = 0$ is the first critical null point, $k = 1$ is the second critical null point, $k = 2$ is the third critical null point, and so on. Each of the critical null points depends on the RF spectrum (or the more commonly used wave length λ of a given frequency in meters). For a vertically polarized wave, the null point will occur when the direct and indirect waves are equal but opposite in magnitude (i.e., out of phase by 180 degrees or $\frac{\lambda_i}{2} + k\lambda_i$). For a horizontal polarization wave, the null point will occur at $\lambda_i + k\lambda_i$.

$$d_h^k = \sqrt{\left(\frac{4h_r h_t - (\lambda_i + k\lambda_i)^2}{2(\lambda_i + k\lambda_i)}\right)^2 - (h_t - h_r)^2} \quad (3)$$

$$d_v^k = \sqrt{\left(\frac{4h_r h_t - (\lambda_i/2 + k\lambda_i)^2}{2(\lambda_i/2 + k\lambda_i)}\right)^2 - (h_t - h_r)^2} \quad (4)$$

The relative antenna heights between the DSRC RSU (h_t) and OBU in a vehicle (h_r) will govern the null points based on the path distance of d between the DSRC RSU and vehicle antennas.

Section 2.5.1.4. Horizontal and Vertical Polarization Null Points vs. the Height of a DSRC RSU

Now, the horizontal (d_h^k) and vertical (d_v^k) polarization models are used to show the impact of a DSRC RSU's height, both mathematically and visually. Using the formula by Miucic et al., the horizontal and vertical polarization null points were calculated for several DSRC RSU heights, in meters, 1, 1.524, 2.438, 3, 5, and 7.620. Table 2-1 and Table 2-2 provide the null points, in meters, for K=0 through K=5 for the horizontal and vertical polarization. Plotting the horizontal and vertical polarization results only provides a straight line on the X-Y axis, so it is challenging to render any significant conclusions. Therefore, the horizontal and vertical polarization results are depicted in a real-world environment using Google Maps and Google Earth. For each DSRC

RSU height (h_t), the horizontal and vertical polarization columns are assigned a Red-Green-Blue (RGB) color scheme, which are reflected in Figure 2-3 through Figure 2-8.

For example, the horizontal (d_h^k) and vertical (d_v^k) polarization null points are 0.05981, 0.11967, 0.02987, 0.039853, 0.01986, and 0.02387 km for K=0 through K=2 with a DSRC RSU height (h_t) at 1 meter as shown in Table 2-1. The RGB color schemes are (136, 14, 79), (244, 143, 177), (230, 81, 0), (255, 204, 128), (255, 214,0), and (255, 234, 0) for a DSRC RSU height at 1 meter, respectively. The horizontal and vertical polarization null points are 0.0227, 0.02597, 0.01811, 0.020152, 0.015047, and 0.016442 km for K=3 through K=5 with a DSRC RSU height at 1.524 meters as shown in Table 2-2. The RGB color schemes are (136, 14, 79), (244, 143, 177), (230, 81, 0), (255, 204, 128), (255, 214,0), and (255, 234, 0) for a DSRC RSU height at 1.524 meters, respectively.

Table 2-1. The horizontal (d_h^k) and vertical (d_v^k) polarization null points for various DSRC RSU heights (h_t) for K=0 through K=2 with an assigned Red-Green-Blue color scheme.

Height of Transmitting Antenna (m)	Horizontal Polarization K=0 (Km)	Vertical Polarization K=0 (Km)	Horizontal Polarization K=1 (Km)	Vertical Polarization K=1 (Km)	Horizontal Polarization K=2 (Km)	Vertical Polarization K=2 (Km)
RGB Color	136, 14, 79	244,143,177	230, 81, 0	255,204,128	255, 214, 0	255, 234, 0
1.000	0.05981	0.11967	0.02987	0.039853	0.01986	0.02387
1.524	0.091174	0.197941	0.045549	0.065946	0.03032	0.03642
2.438	0.145891	0.291825	0.072903	0.097237	0.04855	0.058297
3.000	0.179496	0.359039	0.089701	0.119637	0.05975	0.071732
5.000	0.299166	0.642968	0.149515	0.214258	0.0996	0.119571
7.620	0.455933	0.911965	0.227867	0.3039	0.1518	0.182234

Table 2-2. The horizontal (d_h^k) and vertical (d_v^k) polarization null points for various DSRC RSU heights (h_t) for K=3 through K=5 with an assigned Red-Green-Blue color scheme.

Height of Transmitting Antenna (m)	Horizontal Polarization K=3 (Km)	Vertical Polarization K=3 (Km)	Horizontal Polarization K=4 (Km)	Vertical Polarization K=4 (Km)	Horizontal Polarization K=5 (Km)	Vertical Polarization K=5 (Km)
RGB Color	85, 139, 47	197,225,165	0, 96, 100	178,235,242	78, 52, 46	188,170,164
1.000	0.01485	0.017	0.01183	0.01317	0.00981	0.01073
1.524	0.0227	0.02597	0.01811	0.020152	0.015047	0.016442
2.438	0.036367	0.041592	0.02904	0.032299	0.02415	0.02637
3.000	0.044756	0.051183	0.03575	0.039753	0.029732	0.032468
5.000	0.07462	0.085329	0.05961	0.066286	0.049594	0.054151
7.620	0.11373	0.130054	0.09087	0.10103	0.075602	0.082544

In addition, the horizontal (d_h^k) and vertical (d_v^k) polarization models can be shown visually in regard to the impact of a DSRC RSU's height. In Figure 2-3 and Figure 2-4, the horizontal and vertical polarization null points are depicted using Google Maps and Google Earth, respectively. The horizontal and vertical polarization null points are 0.05981, 0.11967, 0.02987, 0.039853, 0.01986, and 0.02387 km for K=0 through K=2 with a DSRC RSU height (h_t) at 1 meter as shown in Table 2-1. The RGB color schemes are (136, 14, 79), (244, 143, 177), (230, 81, 0), (255, 204, 128), (255, 214,0), and (255, 234, 0) for a DSRC RSU height at 1 meter, respectively.

The horizontal (d_h^k) and vertical (d_v^k) polarization null points are 0.01485, 0.017, 0.01183, 0.01317, 0.00981, and 0.01073 km for K=3 through K=5 with a DSRC RSU height (h_t) at 1 meter as shown in Table 2-2. The RGB color schemes are (85, 139, 47), (197, 225, 165), (0, 96, 100), (178, 235, 242), (78, 52, 46), and (188, 170, 164) for a DSRC RSU height at 1 meter, respectively.

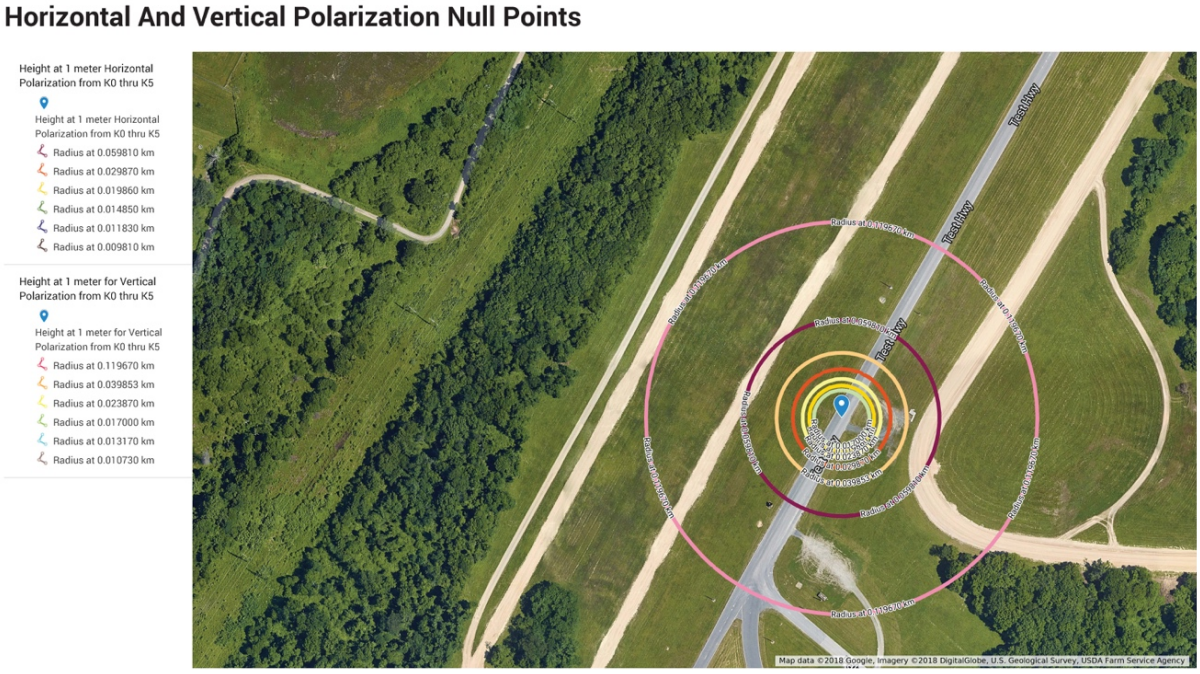

Figure 2-3. Using Google Maps, the horizontal (d_h^k) and vertical (d_v^k) polarization null points are depicted for K=0 to K=5 with a DSRC RSU height (h_t) at 1 meter using Red-Green-Blue color scheme.

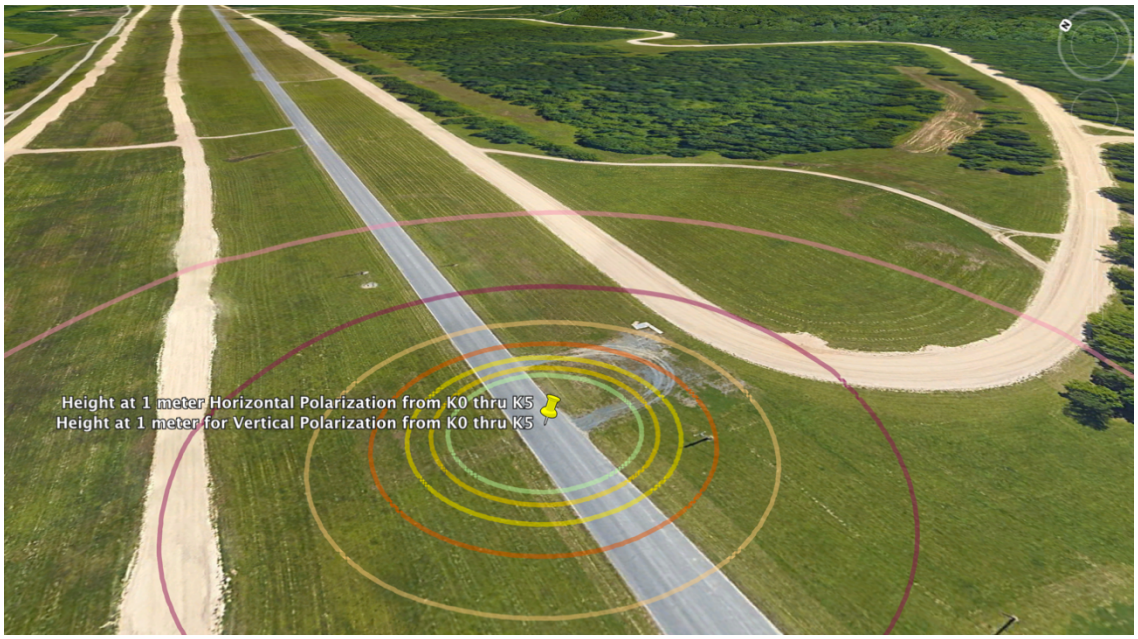

Figure 2-4. Using Google Earth, the horizontal (d_h^k) and vertical (d_v^k) polarization null points are depicted for K=0 to K=5 with a DSRC RSU height (h_t) at 1 meter using Red-Green-Blue color scheme.

In Figure 2-5 and Figure 2-6, the horizontal (d_h^k) and vertical (d_v^k) polarization null points are depicted using Google Maps and Google Earth, respectively. The horizontal and vertical polarization null points are 0.091174, 0.197941, 0.045549, 0.065946, 0.03032, and 0.03642 km for K=0 through K=2 with a DSRC RSU height (h_t) at 1.524 meters as shown in Table 2-1. The RGB color schemes are (136, 14, 79), (244, 143, 177), (230, 81, 0), (255, 204, 128), (255, 214,0), and (255, 234, 0) for a DSRC RSU height at 1.524 meters, respectively.

The horizontal (d_h^k) and vertical (d_v^k) polarization null points are 0.0227, 0.02597, 0.01811, 0.020152, 0.015047, and 0.016442 km for K=3 through K=5 with a DSRC RSU height (h_t) at 1.524 meters as shown in Table 2-2. The RGB color schemes are (85, 139, 47), (197, 225, 165), (0, 96, 100), (178, 235, 242), (78, 52, 46), and (188, 170, 164) for a DSRC RSU height at 1.524 meters, respectively.

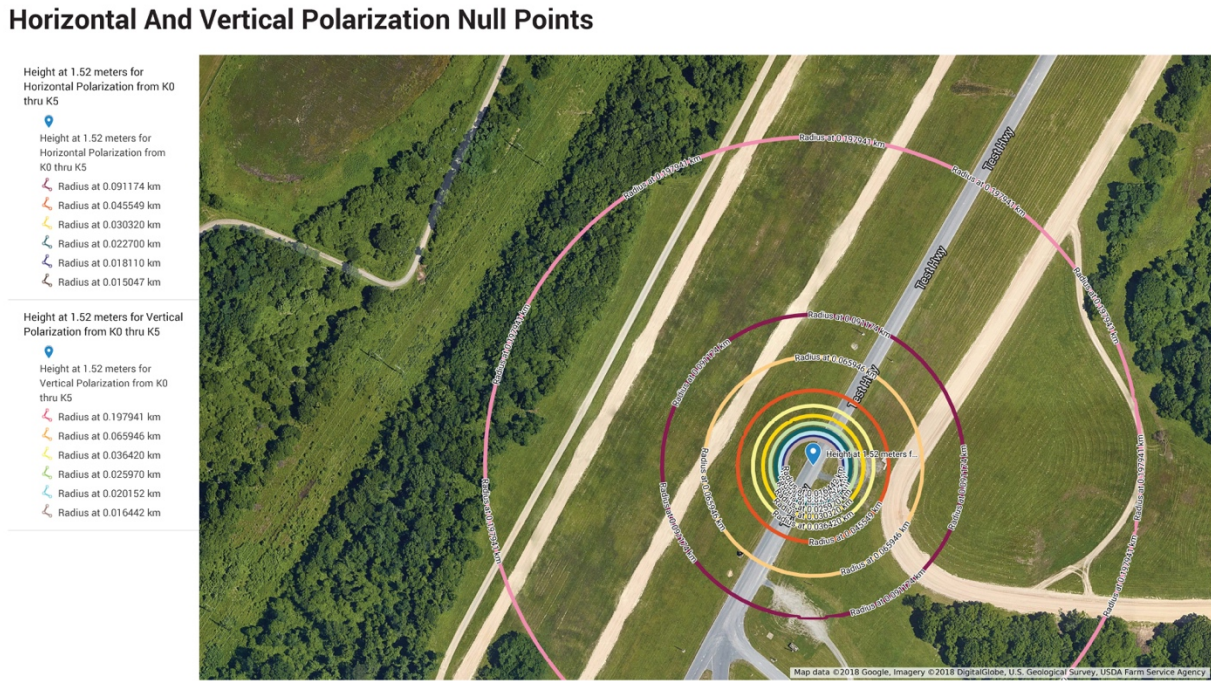

Figure 2-5. Using Google Maps, the horizontal (d_h^k) and vertical (d_v^k) polarization null points are depicted for K=0 to K=5 with a DSRC RSU height (h_t) at 1.524 meters using Red-Green-Blue color scheme.

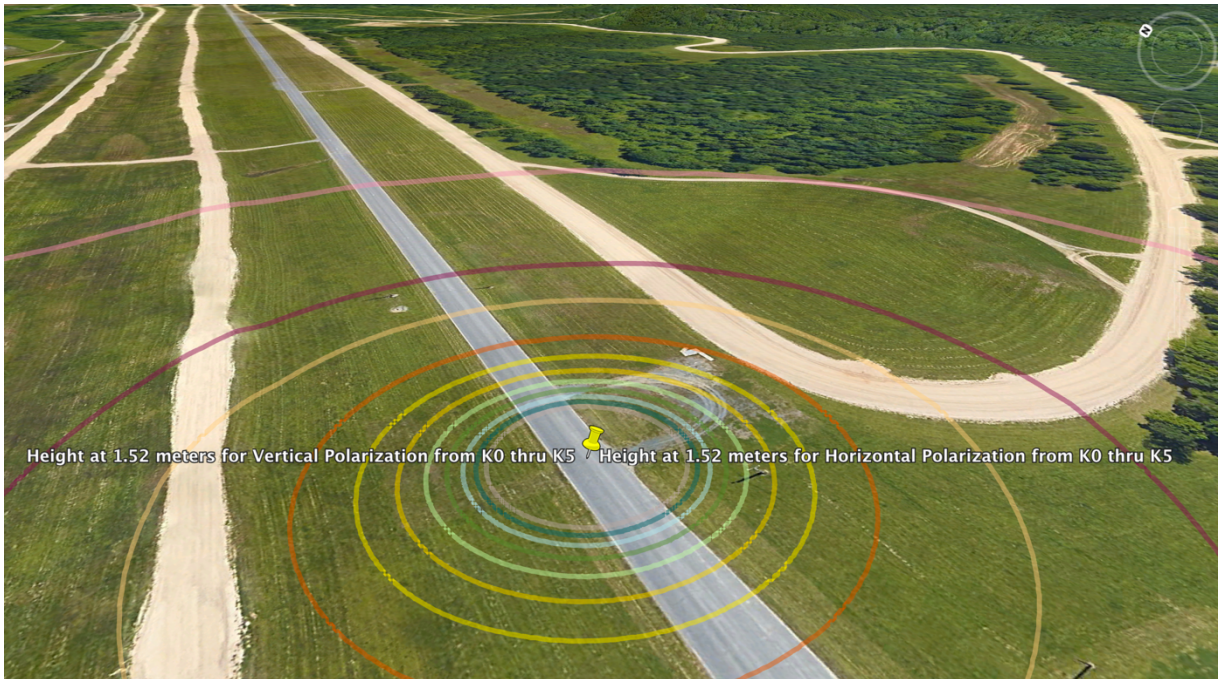

Figure 2-6. Using Google Earth, the horizontal (d_h^k) and vertical (d_v^k) polarization null points are depicted for K=0 to K=5 with a DSRC RSU height (h_t) at 1.524 meters using Red-Green-Blue color scheme.

In Figure 2-7 and Figure 2-8, the horizontal (d_h^k) and vertical (d_v^k) polarization null points are depicted using Google Maps and Google Earth, respectively. The horizontal and vertical polarization null points are 0.145891, 0.291825, 0.072903, 0.097237, 0.04855, and 0.058297 km for K=0 through K=2 with a DSRC RSU height (h_t) at 2.438 meters as shown in Table 2-1. The RGB color schemes are (136, 14, 79), (244, 143, 177), (230, 81, 0), (255, 204, 128), (255, 214,0), and (255, 234, 0) for a DSRC RSU height at 2.438 meters, respectively.

The horizontal (d_h^k) and vertical (d_v^k) polarization null points are 0.036367, 0.041592, 0.02904, 0.032299, 0.02415, and 0.02637 km for K=3 through K=5 with a DSRC RSU height (h_t) at 2.438 meters as shown in Table 2-2. The RGB color schemes are (85, 139, 47), (197, 225, 165), (0, 96, 100), (178, 235, 242), (78, 52, 46), and (188, 170, 164) for a DSRC RSU height at 2.438 meters, respectively.

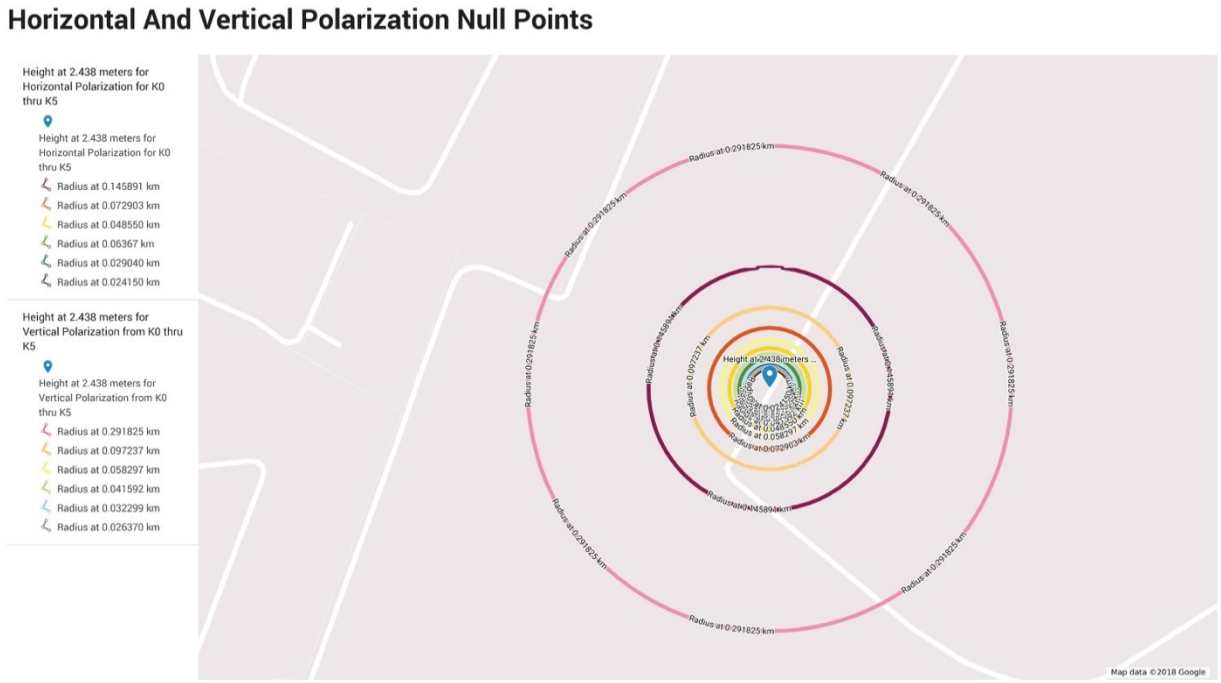

Figure 2-7. Using Google Maps, the horizontal (d_h^k) and vertical (d_v^k) polarization null points are depicted for K=0 to K=5 with a DSRC RSU height (h_t) at 2.438 meters using Red-Green-Blue color scheme.

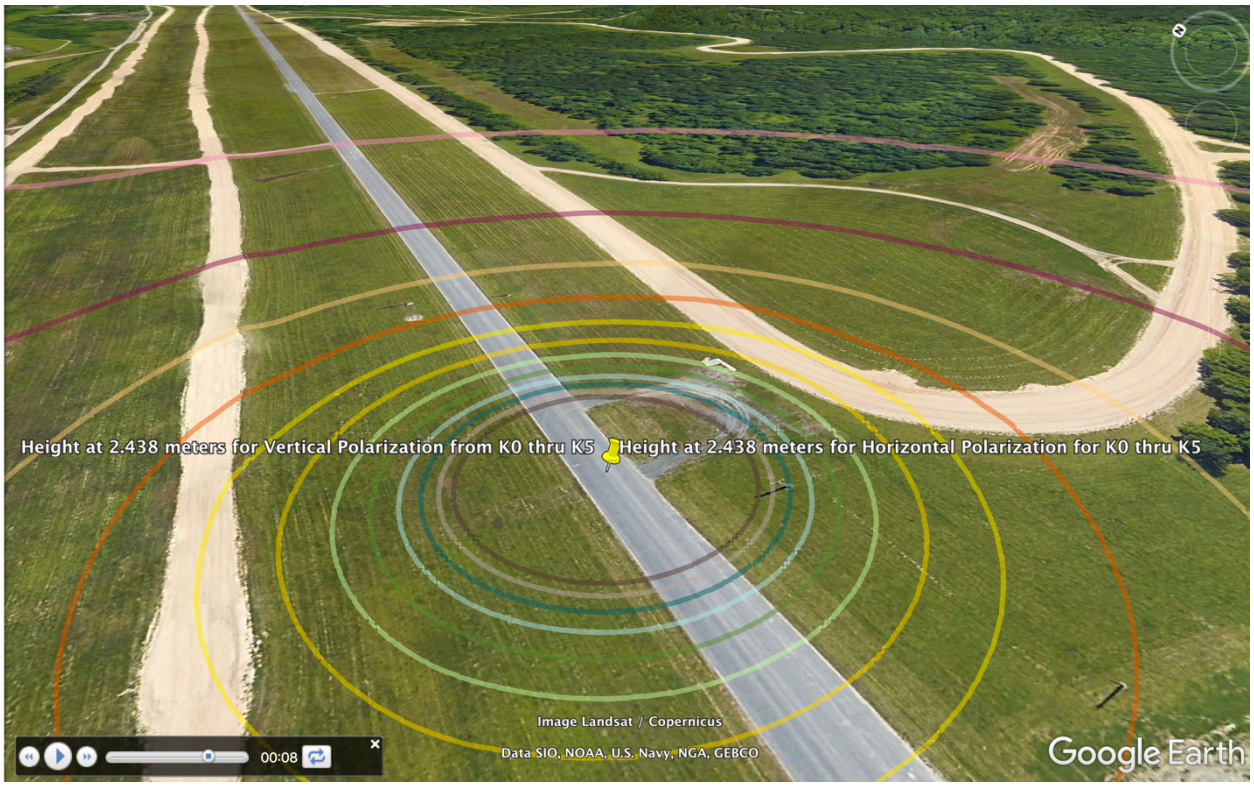

Figure 2-8. Using Google Earth, the horizontal (d_h^k) and vertical (d_v^k) polarization null points are depicted for K=0 to K=5 with a DSRC RSU height (h_t) at 2.438 meters using Red-Green-Blue color scheme.

In Figure 2-9 and Figure 2-10, the horizontal (d_h^k) and vertical (d_v^k) polarization null points are depicted using Google Maps and Google Earth, respectively. The horizontal and vertical polarization null points are 0.179496, 0.359039, 0.089701, 0.119637, 0.05975, and 0.071732 km for K=0 through K=2 with a DSRC RSU height (h_t) at 3.0 meters as shown in Table 2-1. The RGB color schemes are (136, 14, 79), (244, 143, 177), (230, 81, 0), (255, 204, 128), (255, 214,0), and (255, 234, 0) for a DSRC RSU height at 3.0 meters, respectively.

The horizontal (d_h^k) and vertical (d_v^k) polarization null points are 0.044756, 0.051183, 0.03575, 0.039753, 0.029732, and 0.032468 km for K=3 through K=5 with a DSRC RSU height (h_t) at 3.0 meters as shown in Table 2-2. The RGB color schemes are (85, 139, 47), (197, 225, 165), (0, 96, 100), (178, 235, 242), (78, 52, 46), and (188, 170, 164) for a DSRC RSU height at 3.0 meters, respectively.

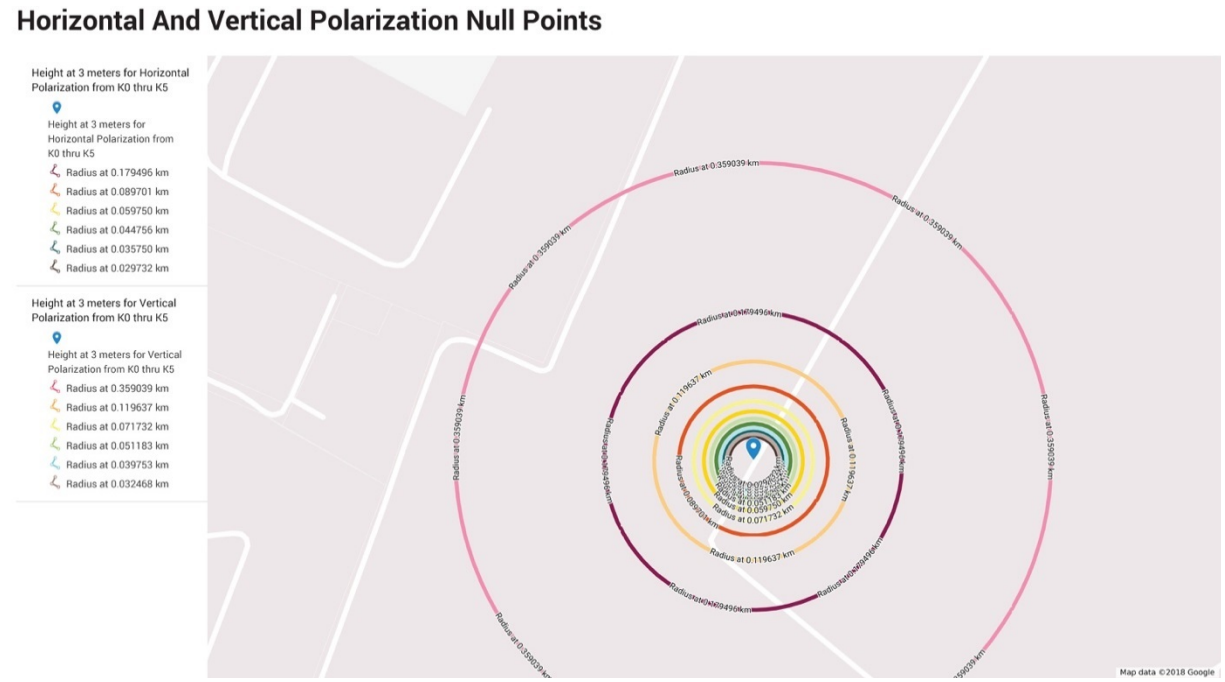

Figure 2-9. Using Google Maps, the horizontal (d_h^k) and vertical (d_v^k) polarization null points are depicted for K=0 to K=5 with a DSRC RSU height (h_t) at 3 meters using Red-Green-Blue color scheme.

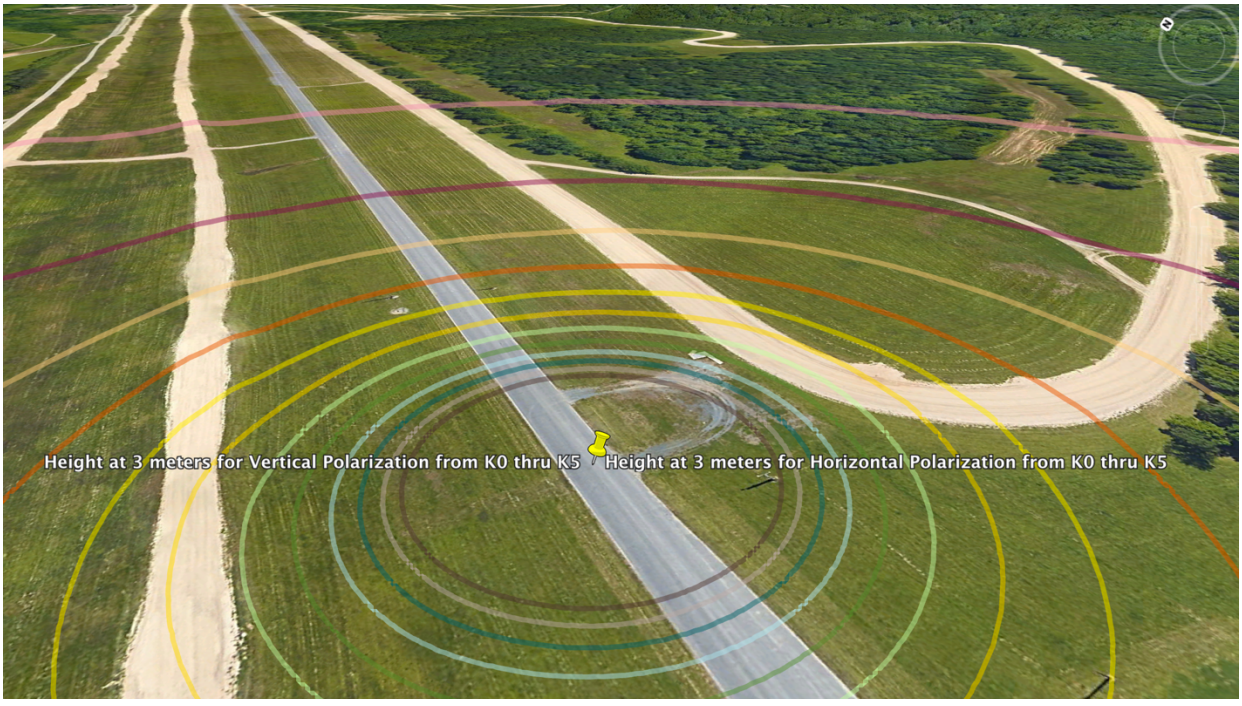

Figure 2-10. Using Google Earth, the horizontal (d_h^k) and vertical (d_v^k) polarization null points are depicted for K=0 to K=5 with a DSRC RSU height (h_t) at 3 meters using Red-Green-Blue color scheme.

In Figure 2-11 and Figure 2-12, the horizontal (d_h^k) and vertical (d_v^k) polarization null points are depicted using Google Maps and Google Earth, respectively. The horizontal and vertical polarization null points are 0.299166, 0.642968, 0.149515, 0.214258, 0.0996, and 0.119571 km for K=0 through K=2 with a DSRC RSU height (h_t) at 5.0 meters as shown in Table 2-1. The RGB color schemes are (136, 14, 79), (244, 143, 177), (230, 81, 0), (255, 204, 128), (255, 214,0), and (255, 234, 0) for a DSRC RSU height at 5.0 meters, respectively.

The horizontal (d_h^k) and vertical (d_v^k) polarization null points are 0.07462, 0.085329, 0.05961, 0.066286, 0.049594, and 0.054151 km for K=3 through K=5 with a DSRC RSU height (h_t) at 5.0 meters as shown in Table 2-2. The RGB color schemes are (85, 139, 47), (197, 225, 165), (0, 96, 100), (178, 235, 242), (78, 52, 46), and (188, 170, 164) for a DSRC RSU height at 5.0 meters, respectively.

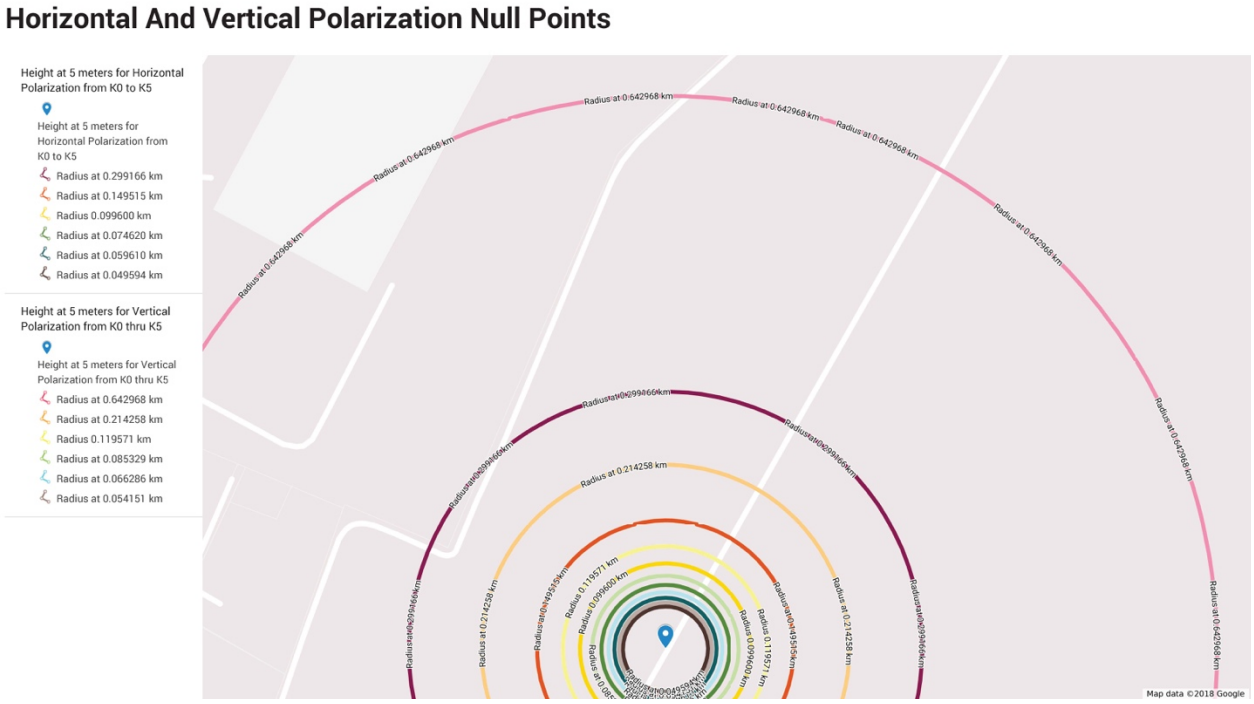

Figure 2-11. Using Google Earth, the horizontal (d_h^k) and vertical (d_v^k) polarization null points are depicted for K=0 to K=5 with a DSRC RSU height (h_t) at 5 meters using Red-Green-Blue color scheme.

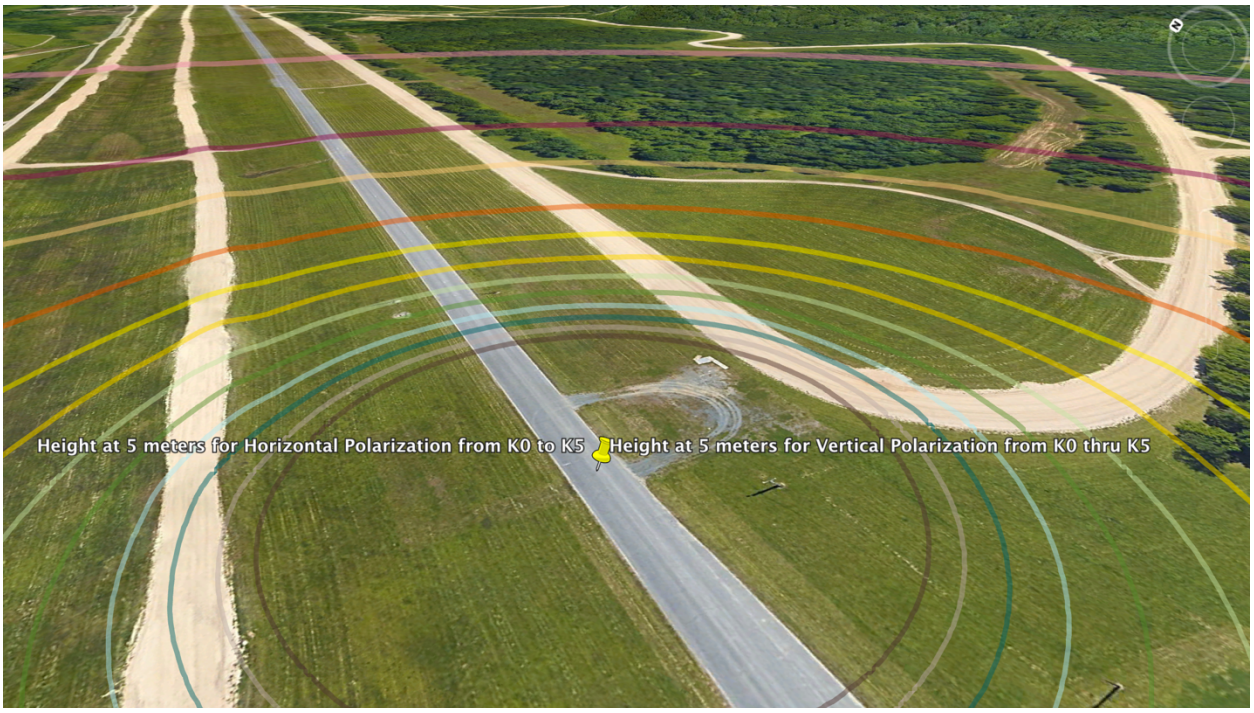

Figure 2-12. Using Google Earth, the horizontal (d_h^k) and vertical (d_v^k) polarization null points are depicted for K=0 to K=5 with a DSRC RSU height (h_t) at 5 meter using Red-Green-Blue color scheme.

In Figure 2-13 and Figure 2-14, the horizontal (d_h^k) and vertical (d_v^k) polarization null points are depicted using Google Maps and Google Earth, respectively. The horizontal and vertical polarization null points are 0.455933, 0.911965, 0.227867, 0.3039, 0.1518, and 0.182234 km for K=0 through K=2 with a DSRC RSU height (h_t) at 7.620 meters as shown in Table 2-1. The RGB color schemes are (136, 14, 79), (244, 143, 177), (230, 81, 0), (255, 204, 128), (255, 214,0), and (255, 234, 0) for a DSRC RSU height at 7.620 meters, respectively.

The horizontal (d_h^k) and vertical (d_v^k) polarization null points are 0.11373, 0.130054, 0.09087, 0.10103, 0.075602, and 0.082544 km for K=3 through K=5 with a DSRC RSU height (h_t) at 7.620 meters as shown in Table 2-2. The RGB color schemes are (85, 139, 47), (197, 225, 165), (0, 96, 100), (178, 235, 242), (78, 52, 46), and (188, 170, 164) for a DSRC RSU height at 7.620 meters, respectively.

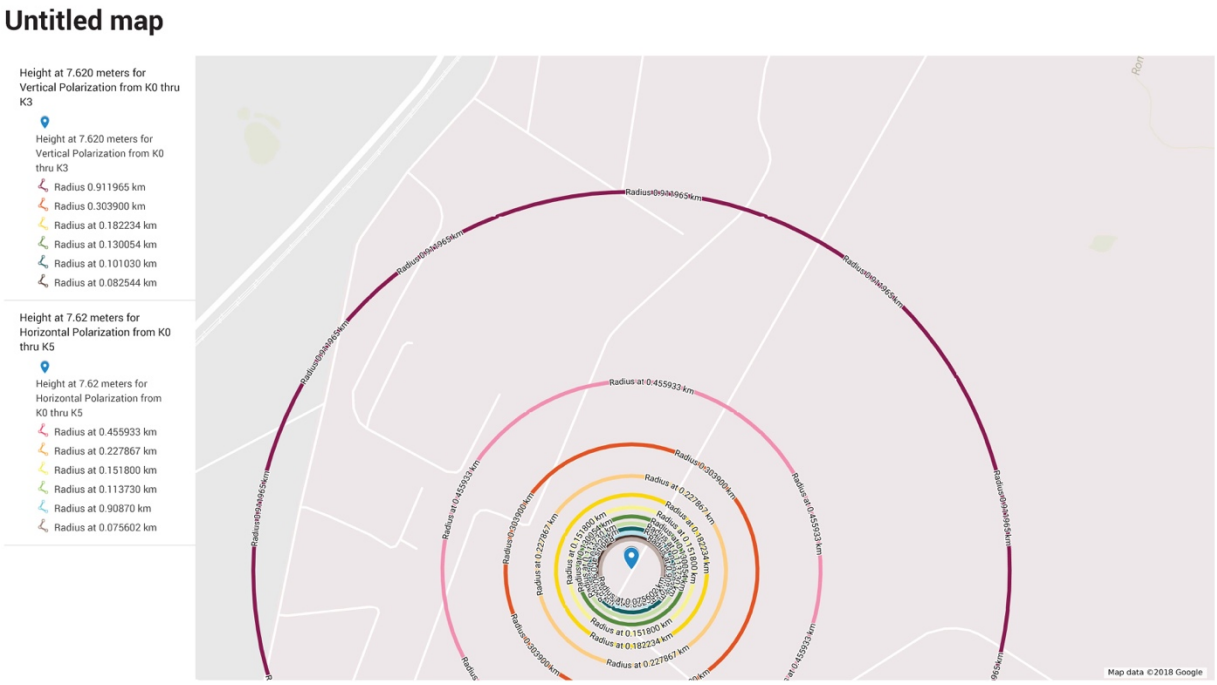

Figure 2-13. Using Google Earth, the horizontal (d_h^k) and vertical (d_v^k) polarization null points are depicted for K=0 to K=5 with a DSRC RSU height (h_t) at 7.620 meters using Red-Green-Blue color scheme.

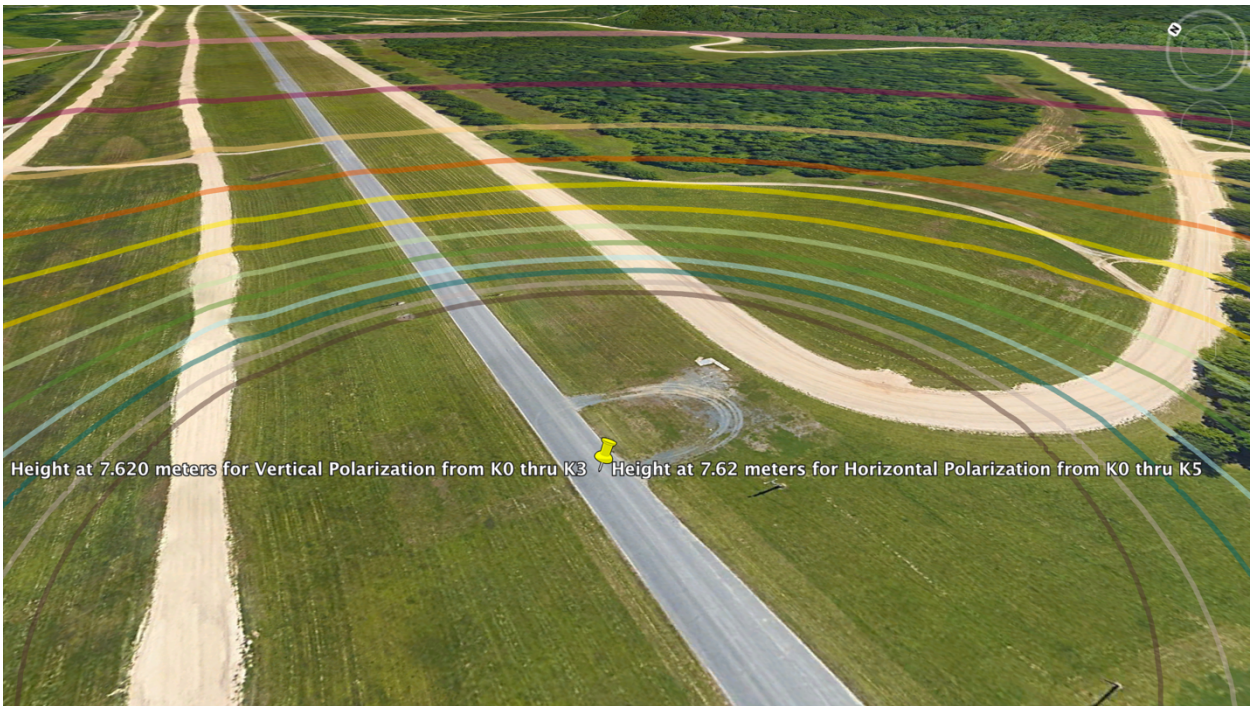

Figure 2-14. Using Google Earth, the horizontal (d_h^k) and vertical (d_v^k) polarization null points are depicted for K=0 to K=5 with a DSRC RSU height (h_t) at 7.620 meters using Red-Green-Blue color scheme.

Section 2.5.2. Limitations in the Existing Horizontal and Vertical Polarization Model along an FSPL

After calculating the null points for several DSRC RSU heights, there is a noticeable limitation of the existing horizontal (d_h^k) and vertical (d_v^k) polarization models that is related to the full length of the FSPL model. As discussed in detail within Appendix A, the DSRC RSU signal strength will decrease with the square of the separation distance because of the decrease in power flux density. In general, a manufacturer will produce an antenna with gain in reference to an isotropic antenna. The antenna gain for the radio hardware transmitter (source) and receiver (target) must be accounted for in the FSPL such that

$$\boldsymbol{FSPL(dB) = 20Log_{10}(d) + 20Log_{10}(f) + 92.45 - GTx - GRx} \quad (5)$$

whereby *d* is the distance from the transmitter (in kilometers), *f* is the signal frequency (in GHz), GTx is the transmitter gain (in dBi), and GRx is the receiver gain (in dBi). The antenna gain for the transmitter and receiver can be different in value, but the designer of the V2I system will make the final decision, which is often based on the V2I application or surrounding environment. Unfortunately, the existing horizontal and vertical polarization models do not account for the full length of the FSPL.

Therefore, we investigate the limitation of the horizontal polarization models using empirical packet count data that spans the full length of the FSPL. In Figure 2-15 through Figure 2-19, the empirical packet count data is displayed, using Google MyMaps, along the FSPL overlaid with the horizontal polarization model with a DSRC RSU mounting height of 7.620 meters. Thus, the horizontal polarization null points are 0.455933, 0.227867, and 0.1518 km for K=0 through K=2 with a DSRC RSU height (h_t) at 7.620 meters, respectively. The horizontal polarization null points are 0.11373, 0.09087, and 0.075602 km for K=3 through K=5 with a DSRC RSU height (h_t) at 7.620 meters, respectively.

In Figure 2-15, the empirical DSRC RSU packet count data is overlaid with the horizontal polarization null point model for K=0 to K=5 at a DSRC RSU height at 7.620 meters. The empirical DSRC RSU packet count data spans the full length of the FSPL. Moreover, the empirical null points are shown at various points throughout the path. In Figure 2-16, the empirical DSRC RSU data and null points are shown to spread beyond the horizontal polarization null point at K=0 for the full length of the FSPL. In Figure 2-17, the empirical DSRC RSU data and null points are shown between the horizontal polarization model between K=0 and K=1. In Figure 2-18, the empirical DSRC RSU data corresponds to the horizontal polarization at K=0. In Figure 2-19, the empirical DSRC RSU data and null points are overlaid with the horizontal polarization null model at K=0 thru K=5. Thus, the limitation of the horizontal polarization model does not correspond to null points from the empirical DSRC RSU packet counts except for K=0.

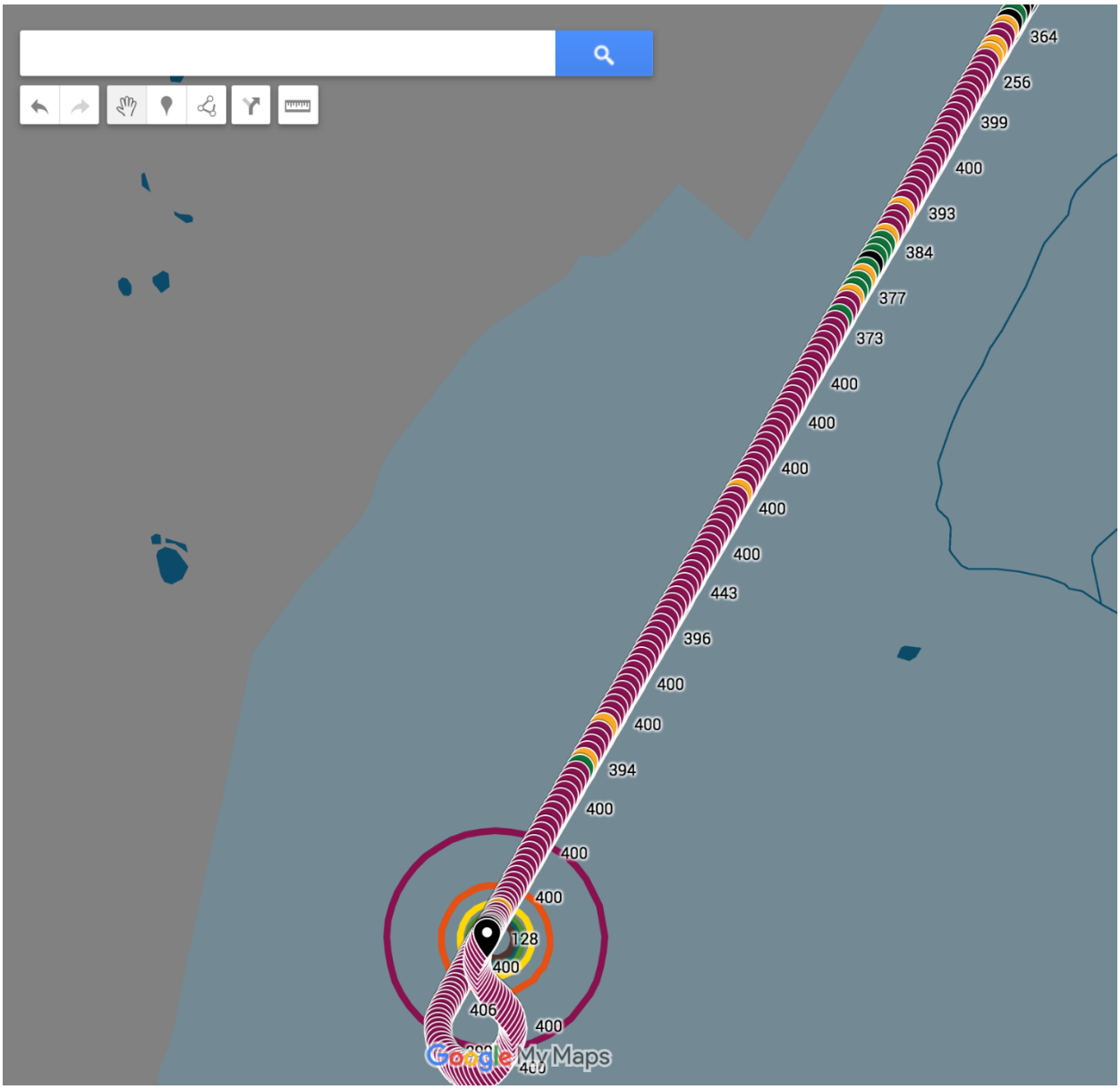

Figure 2-15. Using Google MyMaps, the empirical DSRC RSU packet count data is overlaid with the horizontal (d_h^k) polarization null point model for K=0 to K=5 at a DSRC RSU height (h_t) at 7.620 meters.

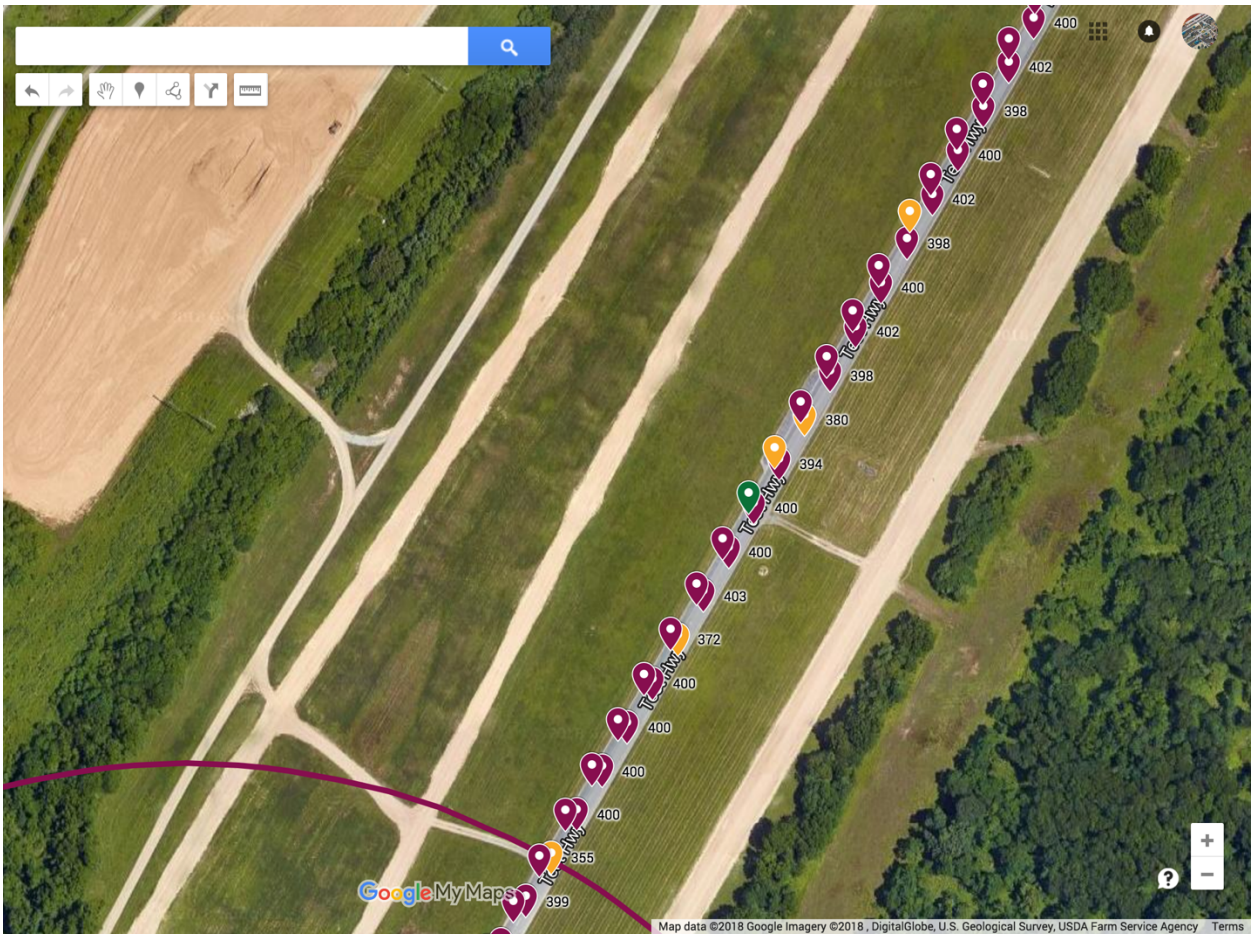

Figure 2-16. Using Google MyMaps, the empirical DSRC RSU packet count data and null points beyond the horizontal polarization null point at K=0 for the full length of the FSPL.

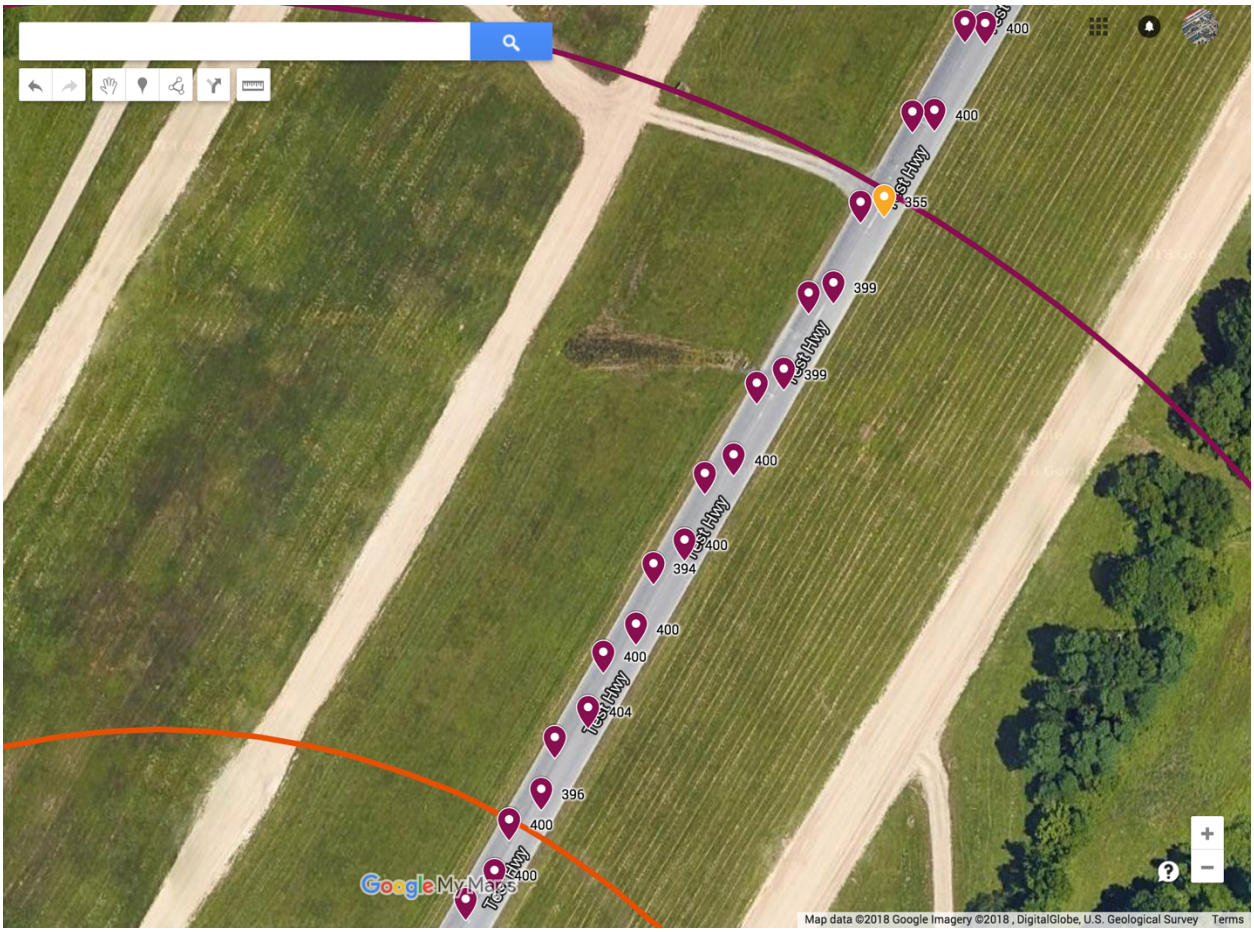

Figure 2-17. Using Google MyMaps, the empirical DSRC RSU packet count data and null points for the horizontal polarization model between K=0 and K=1.

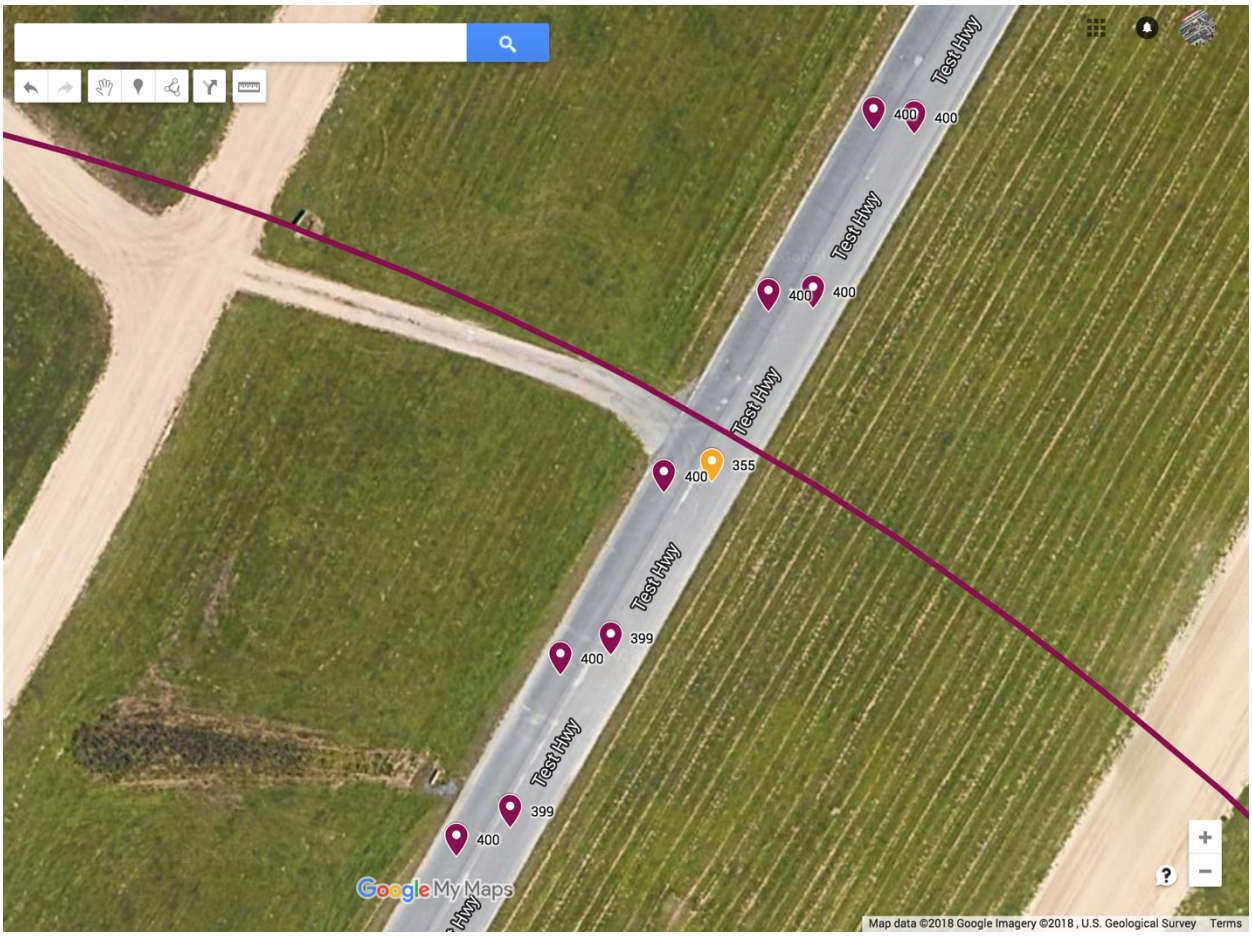

Figure 2-18. Using Google MyMaps, the empirical DSRC RSU packet count data corresponds to the horizontal polarization at K=0 for the full length of the FSPL.

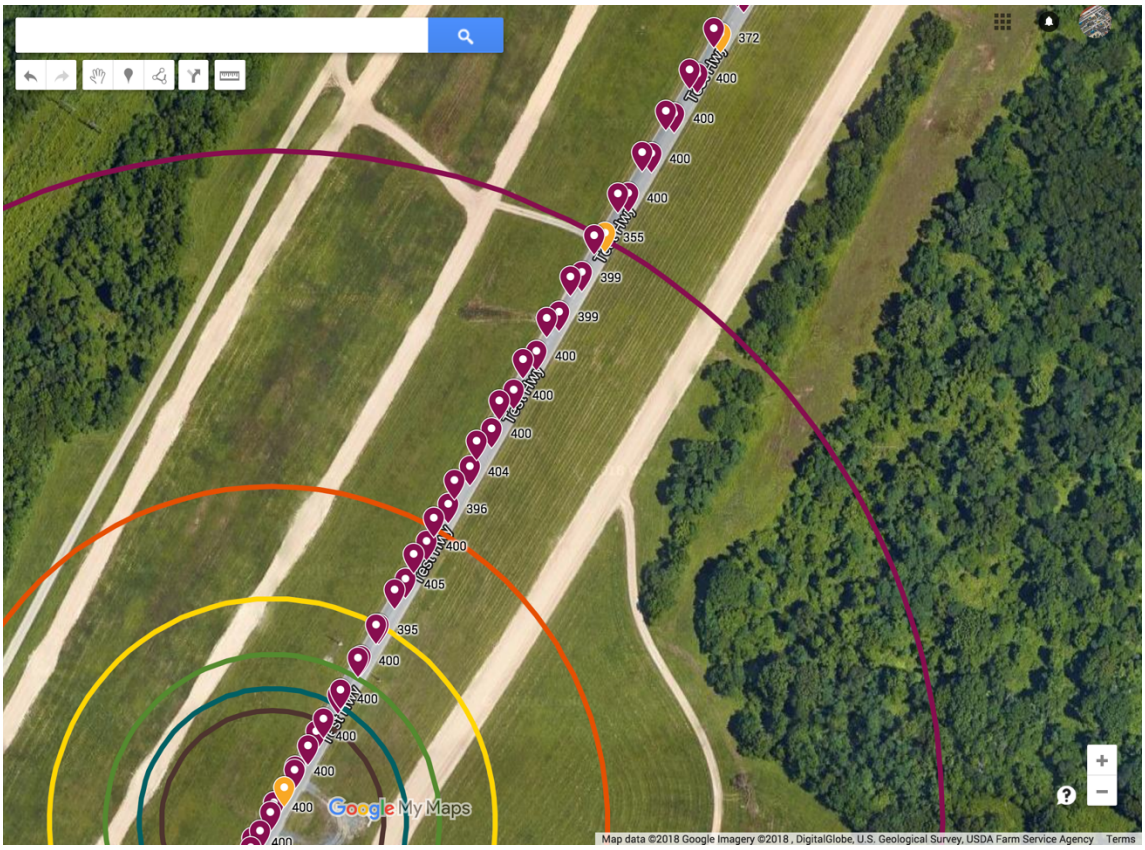

Figure 2-19. Using Google MyMaps, the empirical DSRC RSU packet count data and null points are overlaid with the horizontal polarization null model at K=0 thru K=5.

Section 2.6. Discussion

After calculating the null points for several DSRC RSU heights, there is a noticeable limitation of the existing horizontal (d_h^k) and vertical (d_v^k) polarization models because the model does not account for null points along the full length of the FSPL model. In Appendix A, a theoretical explanation of antenna theory is discussed with a focus on the FSPL as it relates to V2I deployment using a DSRC RSU. The antenna gain for a radio hardware transmitter (source) and receiver (target) must be accounted for in the FSPL whereby d is the distance from the transmitter (in kilometers). The empirical DSRC RSU packet count data spans the full length of the FSPL, which shows the empirical null points at various points throughout the path. Thus, the limitation of the horizontal polarization model does not correspond to null points from the empirical DSRC RSU packet counts except for K=0.

The next chapter applies the horizontal and vertical polarization null point model in a real-world scenario for a DSRC RSU on a highway off-ramp and confirms the limitation along the full length of the FSPL model. Moreover, the chapter focuses on developing a low-cost and structured deployment plan, for DSRC RSUs, applied on a highway off-ramp at exit 19A of the Capital Beltway, which encircles Washington, DC.

Section 2.7. References

[1] J. Walker and K. Heaslip, "A Low-Cost Real-World Planning Strategy For Deploying a Dedicated Short-Range Communications Roadside Unit on a Highway Off-Ramp," *Transportation Research Board*, pp. 1–19, 2017.

[2] J. Walker, "The Fundamental Principles of Antenna Theory for (V2I) Deployments," in *Vehicle-to-Vehicle and Vehicle-to-Infrastructure Communications: A Technical Approach*, F. Hu, Ed. Boca Raton: CRC Press: Taylor & Francis Group, 2018, pp. 207–220.

[3] M. T. Hayat, H. Park, and B. L. Smith, "Connected Vehicle Enabled Freeway Merge Assistance system-field test: Preliminary results of driver compliance to advisory," *IEEE Intelligent Vehicle Symposium Proceedings*, no. Iv, pp. 1017–1022, 2014.

[4] S. E. Shladover, C. Nowakowski, X.-Y. Lu, and R. Ferlis, "Cooperative Adaptive Cruise Control (CACC) Definitions and Operating Concepts," no. November 2014. p. 27.

[5] J. Fishelson, "Platooning Safety and Capacity in Automated Electric Transportation," Utah State University, 2013.

[6] E. Meissner, T. Chantem, and K. Heaslip, "Optimizing Departures of Automated Vehicles From Highways While Maintaining Mainline Capacity," *IEEE Transactions on Intelligent Transportation Systems.*, vol. 17, no. 12, pp. 3498–3511, Dec. 2016.

[7] D. Desiraju, T. Chantem, and K. Heaslip, "Minimizing the Disruption of Traffic Flow of Automated Vehicles During Lane Changes," *IEEE Transactions on Intelligent Transportation Systems.*, vol. 16, no. 3, pp. 1249–1258, Jun. 2015.

[8] National Highway Traffic Safety Administration (NHTSA), "Federal Motor Vehicle Safety Standards; V2V Communications." National Highway Traffic Safety Administration (NHTSA), Department of Transportation (DOT) ACTION:, Washington, D.C., pp. 1–392, 2016.

[9] Federal Highway Administration, "Crash Data Analyses for Vehicle-to- Infrastructure Communications for Safety Applications," Washington, D.C., 2012.

[10] J. Harding, G. Powell, R. Yoon, J. Fikentscher, C. Doyle, D. Sade, M. Lukuc, J. Simons, and J. Wang, "Vehicle-to-Vehicle Communications : Readiness of V2V Technology for Application," no. August. p. 327, 2014.

[11] National Highway Traffic Safety Administration (NHTSA), "Vehicle Safety Communications Project Final Report DOT HS 810 591," 2006.

[12] Federal Highway Administration, "2015 FHWA Vehicle to Infrastructure Deployment Guidance and Products." Washington, D.C., p. 30, 2014.

[13] D. Ou, Y. Yang, L. Xue, and D. Dong, "Optimal Connectivity-Based Deployment of Roadside Units for Vehicular Networks in Urban Areas," *Transportation Research Record: Journal of the Transportation Research Board*, vol. 2559, no. 2559, pp. 46–56, Jan. 2016.

[14] G. G. M. Nawaz Ali, P. H. J. Chong, S. K. Samantha, and E. Chan, "Efficient data dissemination in cooperative multi-RSU Vehicular Ad Hoc Networks (VANETs)," *Journal of Systems and Software*, vol. 117, pp. 508–527, Jul. 2016.

[15] M. Kafsi, P. Papadimitratos, O. Dousse, T. Alpcan, and J.-P. Hubaux, "VANET Connectivity Analysis," 2009.

[16] T. Yan, W. Zhang, G. Wang, and Y. Zhang, "Access Points Planning in Urban Area for Data Dissemination to Drivers," *IEEE Transactions on Vehicular Technology*, vol. 63, no. 1, pp. 390–402, Jan. 2014.

[17] C. M. Silva, W. Meira, and J. F. M. Sarubbi, “Non-Intrusive Planning the Roadside Infrastructure for Vehicular Networks,” *IEEE Transactions on Intelligent Transportation Systems.*, vol. 17, no. 4, pp. 938–947, 2016.
[18] O. Trullols, M. Fiore, C. Casetti, C. F. Chiasserini, and J. M. Barcelo Ordinas, “Planning roadside infrastructure for information dissemination in intelligent transportation systems,” *Computer Communications*, vol. 33, no. 4, pp. 432–442, 2010.
[19] V. D. Khairnar and S. N. Pradhan, “Simulation Based Evaluation of Highway Road Scenario between DSRC/802.11p MAC Protocol and STDMA for Vehicle-to-Vehicle Communication,” *Journal of Transportation Technologies*, vol. 3, no. 1, pp. 88–104, 2013.
[20] M. Shulman and R. K. Deering, “Third Annual Report of the Crash Avoidance Metrics Partnership, April 2003 - March 2004,” Washington, D.C., 2005.
[21] R. Miucic, Z. Popovic, and S. M. Mahmud, “Experimental characterization of DSRC signal strength drops,” in *2009 12th International IEEE Conference on Intelligent Transportation Systems*, 2009, pp. 1–5.
[22] E. Zöchmann, K. Guan, and M. Rupp, “Two-Ray Models in mmWave Communications,” pp. 225–229, 2017.
[23] IEEE Vehicular Technology Society Sponsored, *IEEE Standard for Wireless Access in Vehicular Environments (WAVE)— Networking Services IEEE*. New York: The Institute of Electrical and Electronics Engineers, Inc., 2016.
[24] V. Shivaldova, A. Winkelbauer, and C. F. Mecklenbrauker, “Signal-to-noise ratio modeling for vehicle-to-infrastructure communications,” *2014 IEEE 6th International Symposium on Wireless Vehicular Communications WiVeC 2014 - Proc.*, 2014.
[25] V. Shivaldova, A. Winkelbauer, and C. F. Mecklenbrauker, “Vehicular Link Performance: From Real-World Experiments to Reliability Models and Performance Analysis,” *IEEE Vehicular Technology Magazine*, vol. 8, no. 4, pp. 35–44, 2013.
[26] V. Shivaldova and C. F. Mecklenbräuker, “Quantization-based Complexity Reduction for Range-dependent Modified Gilbert Model,” *Proc. IEEE Sens. Array Multichannel Signal Process. Work.*, pp. 345–348, 2014.
[27] V. Shivaldova, A. Winkelbauer, and C. F. Mecklenbr, “Realistic Performance Model for Vehicle-to-Infrastructure Communications,” no. c, pp. 557–561, 2014.
[28] V. Shivaldova, A. Paier, D. Smely, and C. F. Mecklenbräuker, “On roadside unit antenna measurements for vehicle-to-infrastructure communications,” *IEEE International Symposium on Personal, Indoor and Mobile Radio Communications PIMRC*, pp. 1295–1299, 2012.
[29] W. H. Hayt, Jr., *Engineering Electromagnetics*, Fifth Edit. New York: McGraw-Hill, Inc., 1989.
[30] L. V. Bewley, *Two Dimensional Fields in Electrial Engineering*, 1st ed. New York: Dover Publications, 1963.
[31] D. Corson and P. Lorrain, *Introducing to Electromagnetic Fields and Waves*. San Franscisco: W.H. Freeman, 1962.
[32] R. Wilson, “Propagation Losses Through Common Building Materials 2.4 GHz vs 5 GHz,” *Magis Network, Inc.*, pp. 1–28, 2002.
[33] R. E. Collins, *Antennas and Radio Wave Propagation*. New York: McGraw-Hill, Inc., 2014.

[34] S. L. Salas and E. Hille, *Calculus: One and Several Variables*, 3rd ed. John Wiley and Sons, Inc., 1978.
[35] R. Plonsey and R. E. Collin, *Principles and Applications of Electromagnetic Fields*. McGraw-Hill, Inc., 1961.
[36] M. Javid and P. M. Brown, *Field Analysis and Electromagnetics*. New York: McGraw-Hill, Inc., 1963.
[37] E. C. Jordan and K. G. Balmain, *Electromagnetic Waves and Radiating Systems*, 2nd ed. Englewood Cliffs: Dorling Kindesley Pearson Education, 2015.
[38] J. D. Kraus, *Electromagnetics*, 4th ed. New York: McGraw-Hill, Inc., 1992.
[39] J. E. Parton, S. J. . Owen, and M. S. Raven, *Applied Electromagnetics*. Palgrave Macmillan, 1985.
[40] D. T. Paris and F. K. Hurd, *Basic Electromagnetic Theory*. McGraw-Hill, Inc., 1969.
[41] R. C. Weast and S. M. Selby, Eds., *Standard Mathematical Tables*, Seventeent. The Chemical Rubber Co., 1969.
[42] S. Ramo, J. R. Whinnery, and T. Van Duzer, *Fields and Waves in Communication Electronics*, 3rd ed. New York: John Wiley and Sons, Inc., 2008.
[43] K. F. Sander and G. A. L. Reed, *Transmission and Propagation of Electromagnetic Waves*, 2nd ed. New York: Cambridge University Press, 1986.
[44] D. K. Cheng, *Field and Wave Electromagnetics*, Second Edi. Reading, Mass.: The Addison-Wesley, 1989.
[45] R. Valenzuela, "A ray tracing approach to predicting indoor wireless transmission," *IEEE 43rd Veh. Technol. Conf.*, pp. 214–218, 1993.
[46] A. M. Bodzin and L. Cirucci, "A Land-Use-Planning Simulation Using Google Earth.," *Sci. Scope*, vol. 32, no. 7, pp. 30–38, 2009.
[47] I. Janssen and A. Rosu, "Measuring sidewalk distances using Google earth," *BMC Med. Res. Methodol.*, vol. 12, no. 39, p. 10, 2012.
[48] S. Bayless, A. Guan, A. Shaw, M. Johnson, G. Pruitt, and B. Abernathy, "Recommended Practices for DSRC Licensing and Spectrum Management: A Guide for Management, Regulation, Deployment, and Administration for Connected Vehicle Environment.," 2015.
[49] F. C. Commission, "Equipment Authorization Order & Accredited Testing Laboratories FCC Equipment Authorization Process," 2017. [Online]. Available: https://transition.fcc.gov/oet/ea/presentations/files/may17/10-EA_Accredited-Labs-GT-Final.pdf.
[50] C. Kwok, R. F. Jr. Cleveland, and D. L. Means, "Evaluating Compliance with FCC Guidelines for Human Exposure to Radiofrequency Electromagnetic Fields Supplement C," 1997.
[51] J. D. M. S. J. L. U. Robert F. Cleveland and Standards, "OET bulletin 65: Evaluating compliance with FCC guidelines for human exposure to radiofrequency electromagnetic fields," 1997.
[52] Cisco Systems, "White Paper on Antenna Patterns and Their Meaning," San Jose, 2007.
[53] Linx Technology, "Application Note," Merlin, 2012.
[54] A. S. C. of the I. A. and Propagation and Society, "IEEE Standard Definitions of Terms for Antennas," 1993.
[55] Campbell Scientific, "The Link Budget and Fade Margin (Application Notes)." Campbell Scientific, Inc., Logan, 2016.

[56] T. Vincenty, “Direct and Inverse Solutions of Geodesics on the Ellipsoid With Application of Nested Equations,” *Surv. Rev.*, vol. 23, no. 176, pp. 88–93, 1975.
[57] T. Vincenty, “Geodetic inverse solution between antipodal points,” *Richard Rapp Geodetic Science Ohio State University*. 1975.

Chapter 3. Applying the Existing Horizontal and Vertical Polarization Null Point Model and Discussing the Limitations of the Model in a Real-World Scenario for a DSRC RSU on a Highway On/Off-Ramp

Section 3.1. Title

Applying the horizontal and vertical polarization null point model and discussing the limitations of the model in a real-world scenario for a DSRC RSU on a highway off-ramp.

Section 3.2. Abstract

In the previous chapter, a designer of a V2I safety application required a minimum rate of data (or packet count) to effectively implement a V2I safety application such as RSZW. The RSZW safety application is aimed to alert or warn drivers, in a CACC platoon, who are approaching a work zone. If a CACC platoon is operating above the posted work zone speed limit, it is essential to maintain a minimum rate of data (or packet count) between the vehicle and infrastructure to warn the drivers approaching a work zone.

The deployment of DSRC RSUs allows a connected or automated vehicle to acquire information from the surrounding environment, such as a traffic light's signal phase and timing, using V2I communication. Several scholarly papers exist on planning strategies for DSRC RSU deployments using simulation without accounting for wireless communication constraints and environmental changes. This chapter proposes a hybrid empirical and theoretical based planning strategy for a highway off-ramp in a real-world environment. More specifically, the horizontal and vertical polarization model is applied in a real-world scenario along a highway on/off ramp.

Two existing models are leveraged to analyze null points: 1) signal strength loss (i.e., a FSPL model in Appendix A) and 2) the existing horizontal and vertical polarization null points from a DSRC RSU. The previous chapter discussed the limitation of the existing horizontal and vertical polarization null point model (i.e., the model does not account for null points along the full length of the FSPL model). The next chapter introduces an empirical method to obtain the null points along the full length of the FSPL model.

The research goal of this chapter focuses on developing a low-cost and structured deployment plan for DSRC RSUs with the following objectives:

- Use free planning tools
- Apply the deployment strategy in a real-world environment
- Utilize publicly available DSRC RSU data measurements
- Leverage existing ITS infrastructure when possible.

The proposed planning strategy includes three steps: 1) conduct a virtual site survey, 2) gather baseline performance data for the DSRC RSU equipment, and 3) generate a predictive radio frequency signal. The planning strategy was successfully applied on a highway off-ramp at exit 19A of the Capital Beltway, which encircles Washington, DC.

Section 3.3. Introduction

The deployment of DSRC RSUs has the potential to revolutionize the world's transportation systems by optimizing highway capacity and accelerating the pathway to highly connected and automated vehicles [1] [2] [3]. A DSRC RSU allows a connected or automated vehicle to acquire information from the surrounding environment, such as a traffic light's signal phase and timing, using V2I communication. Based on a review of the literature, several scholarly papers have been published on planning strategies for DSRC RSU deployments, both simulation and empirical based. This chapter proposes an extension of these previous studies by detailing an empirical-based planning strategy on a highway off-ramp in a real-world environment that leverages existing ITS infrastructure.

The main purpose of this strategy is to reduce initial deployment planning costs while accounting for wireless communication constraints and environmental changes. The process is twofold:

1. Propose a novel process that can be applied to most DSRC RSU deployment use cases
2. Apply the novel process to a highway off-ramp located on the Capital Beltway in Prince George's County, MD.

Section 3.4. Study Background

When leveraged with V2V technology, V2I communication will enable a broader range of safety, mobility, and environmental applications since the communication technology has been designed to work as an interoperable unit for ITS [4]. As noted in the NHTSA readiness report on V2V communication, V2I communication can be utilized in numerous safety applications such as red-light violation warning, curve speed warning, reduced speed zone warning, and railroad crossing violation warning.

The V2I communication standards have been designed around the use of an RSU that broadcasts via DSRC [5]. DSRC is a description of a specific type of IEEE 802.11 standard in operation that is customized for ITS. In the United States, the FCC has allocated 75 MHz (5.850 to 5.925 GHz) as a primary service under CFR 47 Parts 90 and 95. Three sets of standards are commonly used for DSRC operation:

1. One developed under the IEEE 802.11.p standard
2. Two under SAE J2735 and SAE J2945
3. Several standards under IEEE 1609 [4].

Thus, the planning strategies for a DSRC RSU are vital to the success of a robust wireless connection and an adequate reaction time for the V2I application. If the wireless connection is poor or non-existent, the safety application will not obtain sufficient data to perform the operation services. Thus, there is a need to develop a low-cost and structured deployment plan for DSRC RSUs.

Section 3.5. Research Approach

Section 3.5.1. Hybrid Empirical and Theoretical Approach Summary

This chapter presents an approach for a low-cost and real-world planning strategy to deploy a DSRC RSU applied to a highway off-ramp in the Washington, DC, area. The approach is structured to achieve the following:

1. Employ free tools for planning purposes
2. Identify a real-world site to deploy strategy
3. Utilize publicly available DSRC RSU data measurements in the process
4. Leverage existing ITS infrastructure to deploy DSRC RSUs when possible.

The proposed planning strategy includes three steps: 1) conduct a virtual site survey, 2) gather baseline performance data for the DSRC RSU equipment, and 3) generate a predictive RF signal. The chapter's main contributions are as follows:

4. Introduce a low-cost, virtual, five-step method to identify potential mounting locations of a DSRC RSU on existing infrastructure
5. Establish a free method to retrieve publicly available baseline performance data for the DSRC RSU without physically deploying the equipment in the region of interest
6. Apply a novel technique that utilizes baseline DSRC RSU data to generate to predictive RF signal:
    - Using the FSPL model
    - Applying the reflective coefficient theory for a ground surface
    - Calculating the location of destructive or null points from the horizontal/vertical polarization reflection.

In this chapter, the term predictive RF signals are key parameters that can be calculated using mathematical formulas. At times, the RF signal(s) can be measured, at a cost (e.g., equipment purchase/rental and hiring RF engineering experts). However, the research goal focuses on developing a low-cost development plan. The following sections describe the literature review, planning strategy approach, derivation of key RF propagation formulas, and results from a real-world use case.

Section 3.5.2. Planning Strategy Approach

The proposed planning strategy is a low-cost, structured approach to deploying a DSRC RSU with the following intent: a) use free tools to plan the deployment process, b) use publicly available data on the DSRC RSU to generate a predictive RF propagation model, and c) leverage existing ITS infrastructure to deploy a DSRC RSU with a focus on low deployment cost.

The following outlines the planning strategy approach:

1. **Conduct Virtual Site Survey**
   - Conduct a virtual site survey to identify a potential mounting location for a DSRC RSU on existing infrastructure
2. **Gather Baseline Performance Data on the DSRC RSU Equipment**
   - Retrieve baseline performance data of the DSRC RSU, without physically deploying the equipment in the region of interest, using the publicly available data submitted to the FCC by the manufacturer
3. **Generate a Predictive RF Signal**
   - Antenna Polarization
   - Determine the FSPL
   - Analyze the reflective coefficient
   - Calculate the horizontal and vertical polarization critical distance.

Section 3.5.2.1. Conduct Virtual Site Survey

Google Map™ and Google Earth™ are valuable tools in land-use planning and calculating the distance of road segments within a region of interest [22] [23]. Bodzin et al. developed a land-use planning simulation that can be used in multiple geographic areas for real-world planning decisions. Real-world planning is an inexpensive approach to identify existing infrastructure (e.g., electrical power, mounting poles, garners) and study the foliage over a period of time. Janssen et al. introduced a step-by-step Geographic Information System (GIS) protocol for researchers to measure the distance and coverage of sidewalks along roadways.

A virtual site survey allows investigation into a region of interest and enables initial planning of the surrounding environment for wireless coverage prediction. Utilizing the time lapse feature in Google Street View, the works of Bodzin and Janssen can be extended to survey the region of interest over a 7-year period. This chapter introduces a low-cost, virtual, six-step method to identify potential mounting locations of a DSRC RSU on existing infrastructure. The six steps are as follows:

1. Identify a potential DSRC RSU and retrieve the electrical network specifications/ constraints for the equipment
2. Using Google Map or Google Earth, search for an existing infrastructure with electrical/solar power to mount the DSRC RSU
3. Find the region of interest and record the essential road dimensions

4. Document the location of foliage, building, and physical structure surrounding the region of interest over various weather seasons (e.g., spring, winter, summer)
5. Obtain the latitude and longitude of the proposed mounting of the DSRC RSU
6. Apply for a DSRC license with the FCC, which is outlined in detail by FHWA-JPO-16-267 as well as limitations in the regulation, administrative practices, and deployment planning [48].

Google Maps was used to implement the virtual site survey on the Capital Beltway in Prince George's County, MD, with a focus on obtaining the latitude and longitude of an existing infrastructure with electrical/solar power.

Figure 3-1 presents four images of a highway off-ramp at exit 19A of the Washington, DC, Capital Beltway, departing I-495 North (Outer Loop) onto Route 50 East of the John Hanson Highway. The bottom-right photo is the region of interest from August 2009. The bottom-left photo is an image from October 2012. The top-left photo is an image from November 2016, while the top-right photo is a top view over the region of interest. These images are available using Google Street View under the time-lapse sliding bar. There is an automatic weather station with some form of power at latitude 38.941354 and longitude -76.856145 that was installed just before July 2012. This virtual site survey employs a free tool that can be used for planning purposes and provides a rapid visit to a region of interest when there is a need to identify existing infrastructure for mounting a DSRC RSU in a real-world environment.

Figure 3-1. Utilizing time lapse in Google Street View to conduct the virtual site survey.

Section 3.5.2.2. FCC RF Test Report

The DSRC RSU's manufacturers are responsible for demonstrating compliance with the FCC rules and requirements under an equipment certification process [24]. This process contains empirical data regarding the RF propagation characteristics of the DSRC RSU. The DSRC RSU test report is an equipment authorization issued by a recognized telecommunication certification body (TCB), and the testing is completed by an accredited, FCC-recognized testing laboratory. Moreover, the TCB is tasked with examining the test data, confirming the accuracy of the supporting documentations, ensuring the testing aligns with the appropriate FCC protocols, and ensuring the data validates the technical parameters [25] [26].

This section establishes a low-cost method of retrieving baseline performance data for the DSRC RSU without physically deploying the equipment at the region of interest. The baseline performance data is retrieved as follows:

1. Obtain the FCC Identification (FCC ID) for the DSRC RSU, which is located on the outside of the hardware
    - The first element is a three-character code with the Grantee Code
    - The second element is the Product Code
2. Using the FCC ID, retrieve the DSRC RSU test report
    - The DSRC-RSU test report is available online under Equipment Authorization Search at https://apps.fcc.gov/oetcf/eas/reports/GenericSearch.cfm
3. Record the data under Equivalent Isotropically Radiated Power (EIRP) measurements from the test report, which the test procedure defines as the power emitted by the antenna after accounting for losses (or gains) between the output signal generator to the antenna.
    - Document the tested frequencies, polarization, height of transmitter/receiver, data rate, EIRP, transmitter/receiver power, bandwidth, margin, and correction factor.

This chapter's research was conducted with an Arada System DSRC RSU with an FCC ID of XZB-MAXR552-4 (hereafter titled "RSU-XZB"). Per the FCC Testing Guidelines [26], the Locomate Commando RSU was tested and measured with a Spectrum Analyzer. The DSRC RSU was placed on a 0.8-meter height turntable that was rotated 360 degrees to search for the maximum radiation power. In the meanwhile, the receiver antenna was rotated in a vertical and horizontal direction from 1 meter to 4 meters for the maximum polar radiated power.

Figure 3-2 is a numerical plot and graph of data submitted by Arada Systems for their DSRC RSU under report number RF150120C04A for RSU-XZB. The plot shows a coalition between the EIRP measurements and data rate. There were other coalitions that were not as significant, so they were not presented on the figure to maintain a clear and concise graph. For example, the data sets were paired in the following channel/frequencies: test experiment numbers (or points) 1-2 = 172/5.860 GHz, points 3-4 = 174/5.870 GHz, points 5-6 = 175/5.875 GHz, points 7-8

points = 176/5.890 GHz, points 9-10 = 178/5.890 GHz, points 11-12 = 180/5.90 GHz, points 13-14 = 181/5.905 GHz, points 15-16 = 182/5.910 GHz, and points 17-18 = 184/5.920 GHz.

However, the DSRC RSU test report is a free data set that has been validated by an accredited testing laboratory. It can be used as a baseline data set without physically deploying the equipment in a region of interest.

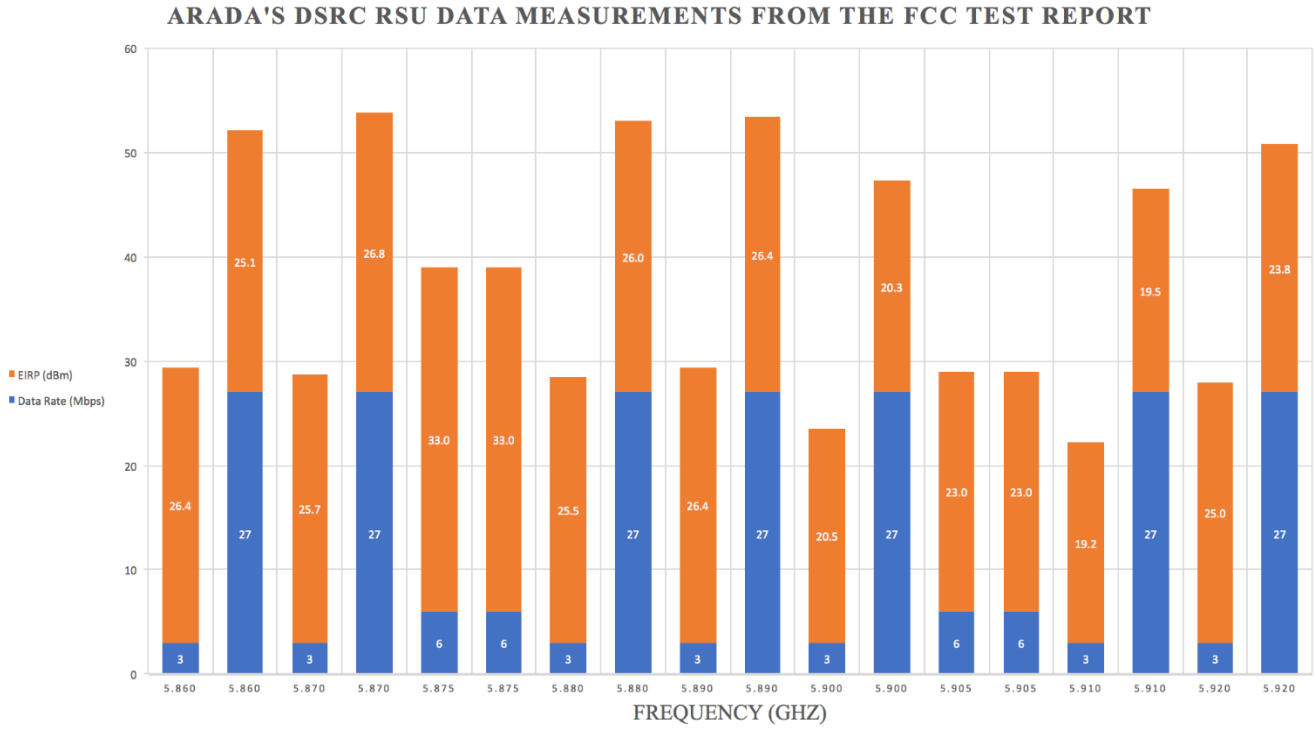

Figure 3-2. A plot of Arada's DSRC RSU data set from the FCC Test Report No. RF150120C04A.

Section 3.5.2.3. Generate a Predictive RF Signal

This subsection focuses on identifying and explaining three fundamental equations to generate a predictive RF signal using the baseline DSRC RSU data. The three fundamental equations are: 1) FSPL, 2) reflective coefficient, and 3) horizontal/vertical polarization null points at critical distances. The objective is to account for various RF signal gains and losses between the DSRC RSU and OBU in the vehicle, while accounting for wireless communication constraints and environmental change. This subsection provides examples of the fundamental principles of antenna polarization as a smooth transition into the reflection and transmission characteristics of a DSRC RSU.

Section 3.5.2.4. Fundamental Principles of Antenna Polarization

In the simplest form, an electromagnetic wave may be modeled as two sinusoidal signals in the horizontal and vertical planes traveling through space, which are the electric and magnetic fields [27] [28]. A traveling wave is considered vertically (or linearly) polarized if the electrical field is

moving in the vertical direction through space. A polarized antenna is sensitive to the mounting position and provides the best transmission/reception when the electrical fields are on the same plane.

In Figure 3-3, the sports utility vehicle (SUV) antenna is linearly polarized with the electrical field, which is traveling perpendicular (i.e., the left signal moving north and south) to the Earth's surface. The RSU antenna is linearly polarized, but the electric field is traveling parallel (i.e., the right signal moving east to west) to the Earth's surface. The DSRC RSU is mounted in the east direction, and the SUV antenna is mounted in the north direction. Therefore, the electric fields are not propagating on the same plane. In this scenario, a linearly polarized RSU antenna will receive the most energy from the SUV antenna when both antennas are physically mounted in the same direction and the electric fields are traveling on the same plane.

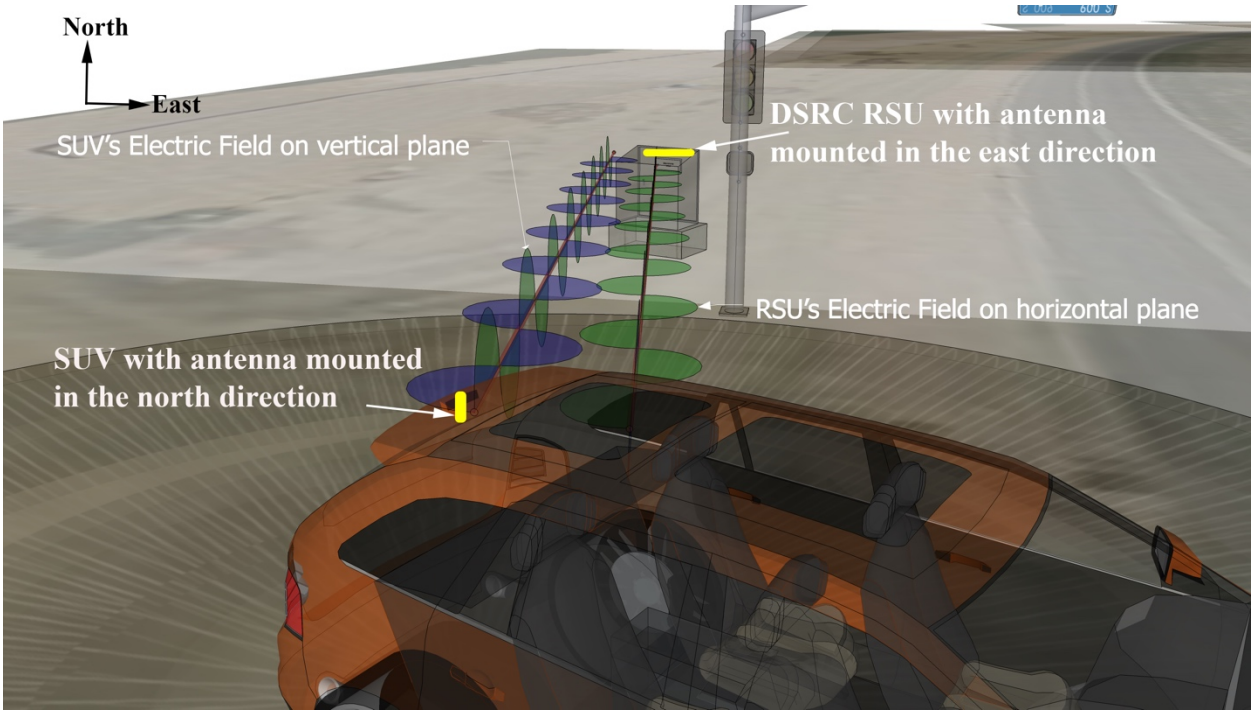

Figure 3-3. The SUV and RSU antennas are linearly polarized; however, the electromagnetic waves are not propagating on the same plane.

Section 3.5.2.5. Antenna Mounting

The polarization directly relates to the propagation direction (e.g., horizontal or vertical) of the electrical fields that depart from the antenna. An antenna can be designed with a sensitivity to the mounting direction, which implies the transmitting and receiving antennas must retain the same polarization for the best transmission/reception path. If the mounting direction is not observed during installation, the target will experience at least a 3-dB loss because the electrical fields are not propagating on the same plane. The antenna polarization and mounting direction are important factors in the reflective coefficient and polarization critical distance.

Section 3.5.2.6. FSPL Model

As an electromagnetic wave propagates from the DSRC RSU antenna in free space, the power density per unit area decreases in proportion to the frequency and the square of the distance traveled [29] [30]. As a baseline reference, the FSPL model can be used as an estimate of the signal loss in a non-atmospheric and non-reflective environment. As quoted from the IEEE standard 145-1993, the FSPL is "not due to dissipation, but rather to the fact that the power flux density decreases with the square of the separation distance" [31]. The equation for FSPL is presented below in terms of dB [27]:

$$FSPL = \left(\frac{4\pi df}{c}\right) \quad (1)$$

$$FSPL(dB) = 20Log_{10}\left(\frac{4\pi df}{c}\right) \quad (2)$$

$$FSPL(dB) = 20Log_{10}(d) + 20Log_{10}(f) + 20Log_{10}\left(\frac{4\pi}{c}\right) \quad (3)$$

$$FSPL(dB) = 20Log_{10}(d) + 20Log_{10}(f) + 92.45 \quad (4)$$

where c is the speed of light (3 x 10^8 m/s), d is the distance from the transmitter (in kilometers), and f is the signal frequency (in GHz).

Normally, a manufacturer will produce an antenna with gain in reference to an isotropic antenna. The antenna gain for the radio hardware transmitter (source) and receiver (target) must be accounted for in the FSPL such that:

$$FSPL(dB) = 20Log_{10}(d) + 20Log_{10}(f) + 92.45 - GTx - GRx \quad (5)$$

whereby d is the distance from the transmitter (in kilometers), f is the signal frequency (in GHz), GTx is the transmitter gain (in dBi), and GRx is the receiver gain (in dBi). Once again, the FSPL is a baseline reference for a DSRC RSU antenna, and the equation will be used after determining a critical threshold, as discussed in a later subsection.

Section 3.5.2.7. Reflective Coefficient – Conductive Properties of the Ground Surface

Because the DSRC RSU can be mounted at various heights, this subsection addresses the reflection and transmission coefficients of the ground surface surrounding the region of interest. The RF signal transmitted by a DSRC RSU is rarely the result of a traveling wave captured directly between the RSU and an OBU in a vehicle. More likely, the traveling wave is the result of multipath signals both directly and indirectly with different amplitudes and phases of an electromagnetic wave. Figure 3-4 is a realistic view with two sets of both vertical and horizontal waves between the RSU and OBUs in a vehicle. A traveling wave will be partially reflected from the surface and partially absorbed by the ground surface.

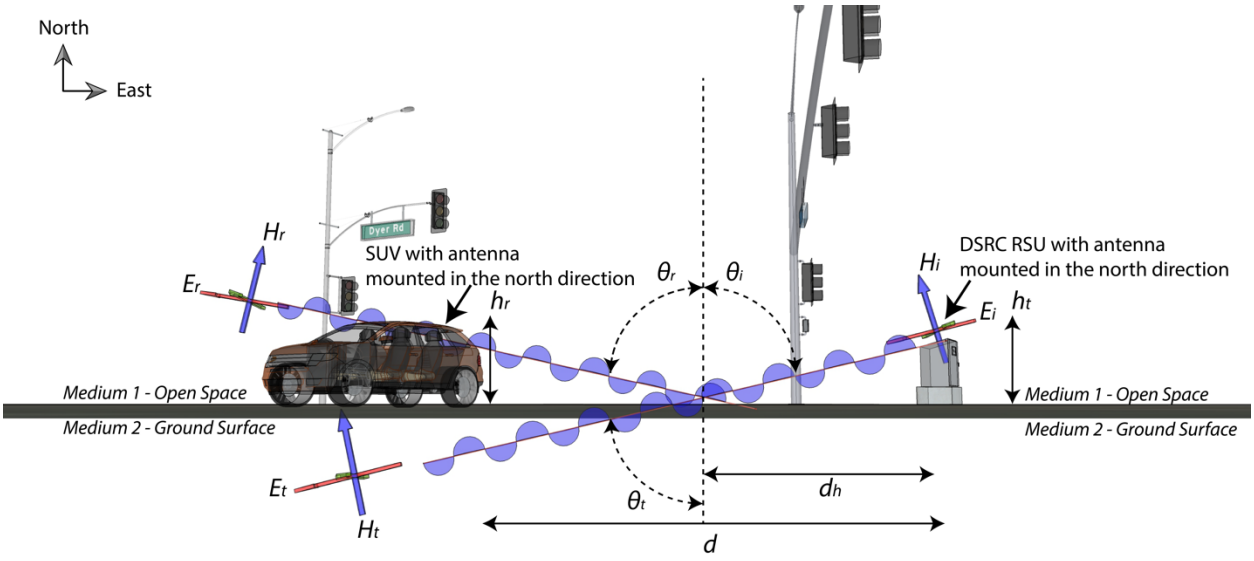

Figure 3-4. The reflection electric and magnetic fields (Er and Hr) and transmitted electric and magnetic fields (Et and Ht) at the ground surface (medium 2) in relationship to open space (medium 1).

The angle and level of reflection are based on several factors such as the electromagnetic wave frequency, the relative permittivity of the surface, the thickness of the surface material(s), and the angle of a traveling wave that approaches the material [32]. Wilson et al. conducted extensive measurements on 20 different materials (e.g., plexiglass, red brick, glass, and concrete) to estimate the reflectivity coefficients at 2.3 GHz and 5.25 GHz.

Figure 3-4 depicts the essential variables in wave reflection and transmission. The mounting height of the DSRC RSU antenna (or transmitter) is h_t and the mounting height of the vehicle antenna (or receiver) is h_r. The incident electric and magnetic fields are denoted as Ei and Hi, respectively. The reflective electric and magnetic fields are denoted as Er and Hr, respectively. The transmitted electric and magnetic fields are denoted as Et and Ht, respectively. At a single transmission frequency, the angle of incidence (θ_i) and angle of reflection (θ_r) are equal with the angle of transmission (θ_t). Between the DSRC RSU and vehicle antennas, there is a distance of d and the null distance for the horizontal polarization is d_h. The open space (or air) is medium 1, and the ground surface is medium 2.

When a DSRC RSU is mounted near the ground, the angle of incidence (θ_i) is close to 90 degrees and termed a grazing angle [21]. For an angle of incidence (θ_i) at 90 degrees, the Fresnel reflection and transmission coefficients for both the perpendicular and parallel polarization are undefined since the cosine of 90 degrees is zero. Similarly, an angle of incidence (θ_i) at 85 and 80 degrees will be 8.71 percent and 17 percent, respectively, of the ratio between the intrinsic impedances (η) of air and the street/road (or a given medium). Thus, the height of the antenna will impact the angle of traveling waves that graze at the street/road (or a given medium) and reflected to the OBU in a vehicle from the DSRC RSU.

Section 3.5.2.8. Horizontal and Vertical Polarization Null Points and Critical Distances

The reflection of the DSRC RSU traveling wave will have a destructive effect, which may produce a significant signal loss (or null point), on the resultant wave due to the law of reflection and Briggs Law [28] [27]. This subsection focuses on calculating critical distances of each null point of distributive traveling waves by a DSRC RSU. NHTSA's Vehicle Safety Communications project conducted field experiments on DSRC, during which null points were observed at various distances due to multipath reflections [33]. Miucic et al. [21] have documented DSRC signal strength null points and derived the critical distance that should be accounted for in planning strategies.

In Miucic et al., the null points can be determined for the horizontal (d_h^k) and vertical (d_v^k) polarizations, whereby $k = 0$ is the first critical null point, $k = 1$ is the second critical null point, $k = 2$ is the third critical null point, and so on. Each of the critical null points depends on the RF spectrum (or the more commonly used wave length λ of a given frequency in meters). For a vertically polarized wave, the null point will occur when the direct and indirect waves are equal but opposite in magnitude (i.e., out of phase by 180 degrees or $\frac{\lambda_i}{2} + k\lambda_i$). For a horizontal polarization wave, the null point will occur at $\lambda_i + k\lambda_i$.

$$d_h^k = \sqrt{\left(\frac{4h_r h_t - (\lambda_i + k\lambda_i)^2}{2(\lambda_i + k\lambda_i)}\right)^2 - (h_t - h_r)^2} \tag{6}$$

$$d_v^k = \sqrt{\left(\frac{4h_r h_t - (\lambda_i/2 + k\lambda_i)^2}{2(\lambda_i/2 + k\lambda_i)}\right)^2 - (h_t - h_r)^2} \tag{7}$$

Based on the null point formulas and as shown in Figure 3-4, the relative antenna heights between the DSRC RSU (h_t) and OBU in a vehicle (h_r) will govern the null points based on the path distance of d between the DSRC RSU and vehicle antennas. The direct and indirect waves contribute to the multipath signals when the relative difference in the antenna heights $|h_t - h_r|$ is much larger than the critical path distance d_c. The critical path distance d_c is calculated as follows [34]:

$$d_c = \frac{4\pi h_t h_r}{\lambda} \tag{8}$$

On average, the path loss will follow the free space loss equation. When the path distance (d) between the DSRC RSU and vehicle antennas is much greater than the critical path distance d_c, the relative difference in the antenna heights $|h_t - h_r|$ becomes very small (or $h_t \cong h_r$). Thus, the horizontal d_h^k and vertical d_v^k null points must be calculated and multipath loss is calculated as follows [34]:

$$PL_{multipath}(dB) = 40Log_{10}(d) - 20Log_{10}(h_t\, h_r) + 120 \tag{9}$$

whereby d is the path distance between the DSRC RSU and vehicle antennas (in kilometers), h_t is the height of the DSRC RSU in meters, and h_r is the height of the vehicle antenna in meters. As previously discussed, the height of the antenna will impact the amount of traveling waves that graze at the ground surface.

Section 3.6. Results

Section 3.6.1. Baseline Predictive RF Signal

Using the baseline performance data for the Arada System DSRC RSU, the FSPL and multipath loss were calculated based on a path distance d of 3 meters between the DSRC RSU and OBU as described in the test report number RF150120C04A. Also, the DSRC RSU and OBU were approximately the same height ($h_t \cong h_r$) at 1 meter. As shown in Table 3-1, the critical path distance d_c was calculated between 245.46 to 247.98 meters at 5.860 GHz and 5.920 GHz, respectively. Based on the baseline data, the FSPL can be applied for an OBU that is stationary at a distance of 3 meters and a height of 1 meter.

Table 3-1. FSPL and Multipath Loss from the Baseline Data and the Region of Interest at Latitude: 38.941354 and Longitude: -76.856145 for the Arada DSCR RSU

Frequency (GHZ)	EIRP (DBM)	FSPL (DB)	Multipath Loss (DB)	Critical Distance (M)
Baseline Predictive RF Signal				
5.860	26.35	57.35	19.08	245.46
5.870	25.70	57.37	19.08	245.88
5.880	25.50	57.38	19.08	246.30
5.890	26.40	57.39	19.08	246.72
5.900	20.52	57.41	19.08	247.14
5.910	19.16	57.42	19.08	247.56
5.920	25.00	57.44	19.08	247.98
Region of Interest Predictive RF Signal				
5.860	26.35	65.45	27.96	570.11
5.870	25.70	65.46	27.96	571.08
5.880	25.50	65.48	27.96	572.05
5.890	26.40	65.49	27.96	573.03
5.900	20.52	65.51	27.96	574.00
5.910	19.16	65.52	27.96	574.97
5.920	25.00	65.54	27.96	575.94

Section 3.6.2. Region of Interest Predictive RF Signal

Now, the same formulas can be applied at the site survey location of *Latitude:* 38.941354 and *Longitude:* -76.856145. Using the baseline performance data, the FSPL and multipath loss were calculated based on a path distance d of 7.62 meters between the DSRC RSU and OBU. The path distance is 7.62 meters to account for a lane width at 3.6576 meters, a weather station setback of 3.9624 meters, and a DSRC RSU height at 1.524 meters ($h_t \cong h_r$) As shown in Table 3-1, the critical path distance d_c was calculated between 570.11 to 575.94 meters at 5.860 GHz and 5.920 GHz, respectively.

Section 3.6.3. Region of Interest Predictive Horizontal Polarization Null Points

Finally, the horizontal (d_h^k) polarization null points are calculated for six critical distances, whereby $k = 0$ to 5. In Figure 3-5, Google Maps Pro was used to depict the critical null points at:

$d_h^0 = 91.17\ meters\ (Red\ Circle)$

$d_h^1 = 45.55\ meters\ (Yellow\ Circle)$

$d_h^2 = 30.32\ meters\ (Orange\ Circle)$

$d_h^3 = 22.70\ meters\ (Green\ Circle)$

$d_h^4 = 11.84\ meters\ (Blue\ Circle)$

$d_h^5 = 9.82\ meters\ (White\ Circle)$.

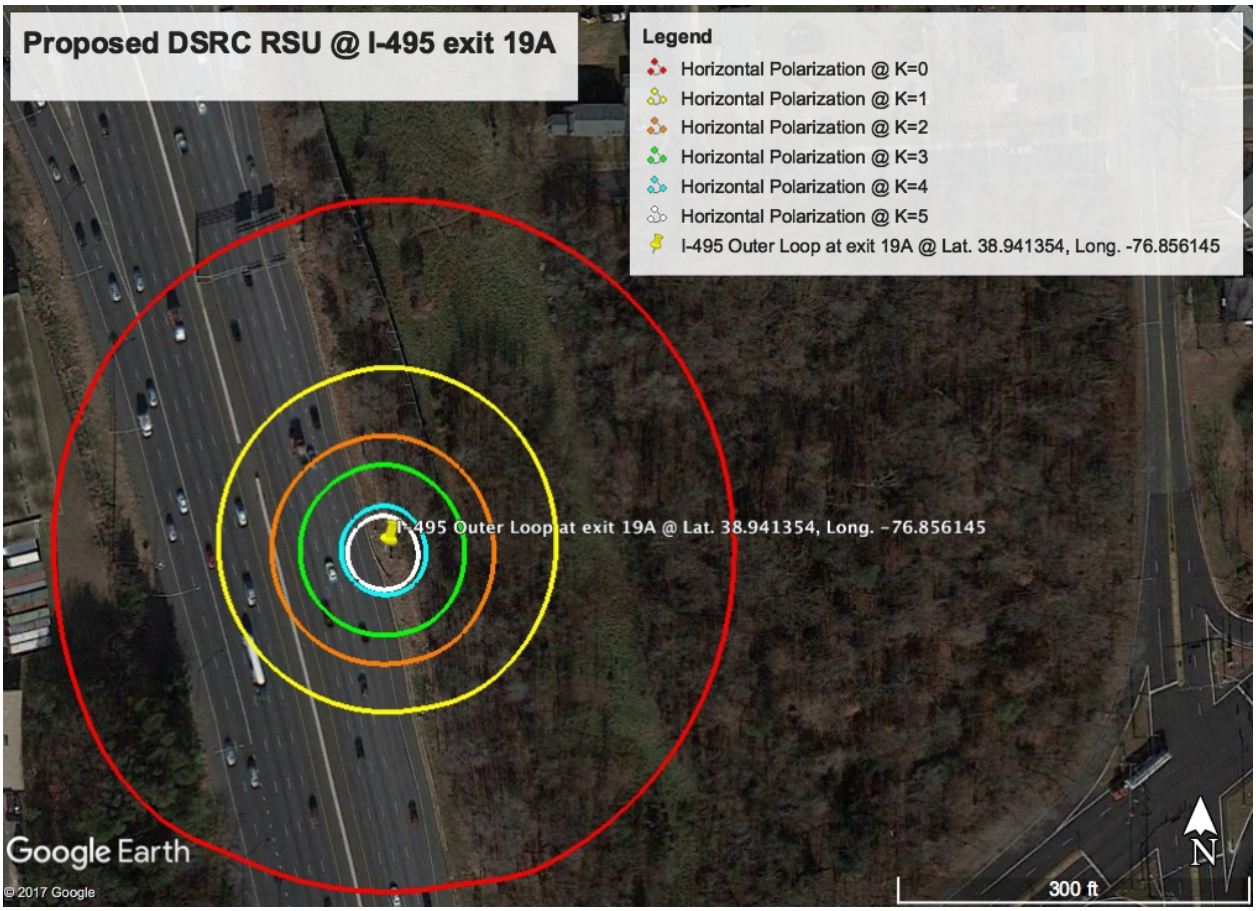

Figure 3-5. The predictive horizontal polarization null points for virtual site survey location at Latitude 38.941354 and Longitude -76.856145.

Section 3.7. Discussion

We applied the existing horizontal polarization model (d_h^k) in a real-world scenario along a highway on/off ramp. The proposed planning strategy was successfully applied on a highway off-ramp at exit 19A of the Capital Beltway. Also, we presented a low-cost planning approach for deploying a DSRC RSU without incurring equipment cost for testing equipment or hiring RF experts. Moreover, we utilized FCC test data, submitted by the DSRC RSU vendor, without purchasing the hardware to conduct initial calculations.

The FCC test data was used to calculate FSPL, critical distance, and the horizontal polarization null points for the potential location of a DSRC RSU. However, the maximum horizontal polarization distance is 91.17 meters for k=0 (i.e., the first critical null point), while the critical path distance d_c was calculated between 570.11 to 575.94 meters at 5.860 GHz and 5.920 GHz, respectively. In this real-world scenario, the horizontal polarization model does not account for null points along the full length of the FSPL model. Thus, the next chapter introduces an empirical method to obtain the null points along the full length of the FSPL model.

Section 3.8. References

[1] J. Walker and K. Heaslip, "A Low-Cost Real-World Planning Strategy For Deploying a Dedicated Short-Range Communications Roadside Unit on a Highway Off-Ramp," *Transportation Research Board*, pp. 1–19, 2017.

[2] J. Walker, "The Fundamental Principles of Antenna Theory for (V2I) Deployments," in *Vehicle-to-Vehicle and Vehicle-to-Infrastructure Communications: A Technical Approach*, F. Hu, Ed. Boca Raton: CRC Press: Taylor & Francis Group, 2018, pp. 207–220.

[3] M. T. Hayat, H. Park, and B. L. Smith, "Connected Vehicle Enabled Freeway Merge Assistance system-field test: Preliminary results of driver compliance to advisory," *IEEE Intelligent Vehicle Symposium Proceedings*, no. Iv, pp. 1017–1022, 2014.

[4] S. E. Shladover, C. Nowakowski, X.-Y. Lu, and R. Ferlis, "Cooperative Adaptive Cruise Control (CACC) Definitions and Operating Concepts," no. November 2014. p. 27.

[5] J. Fishelson, "Platooning Safety and Capacity in Automated Electric Transportation," Utah State University, 2013.

[6] E. Meissner, T. Chantem, and K. Heaslip, "Optimizing Departures of Automated Vehicles From Highways While Maintaining Mainline Capacity," *IEEE Transactions on Intelligent Transportation Systems.*, vol. 17, no. 12, pp. 3498–3511, Dec. 2016.

[7] D. Desiraju, T. Chantem, and K. Heaslip, "Minimizing the Disruption of Traffic Flow of Automated Vehicles During Lane Changes," *IEEE Transactions on Intelligent Transportation Systems.*, vol. 16, no. 3, pp. 1249–1258, Jun. 2015.

[8] National Highway Traffic Safety Administration (NHTSA), "Federal Motor Vehicle Safety Standards; V2V Communications." National Highway Traffic Safety Administration (NHTSA), Department of Transportation (DOT) ACTION:, Washington, D.C., pp. 1–392, 2016.

[9] Federal Highway Administration, "Crash Data Analyses for Vehicle-to- Infrastructure Communications for Safety Applications," Washington, D.C., 2012.

[10] J. Harding, G. Powell, R. Yoon, J. Fikentscher, C. Doyle, D. Sade, M. Lukuc, J. Simons, and J. Wang, "Vehicle-to-Vehicle Communications : Readiness of V2V Technology for Application," no. August. p. 327, 2014.

[11] National Highway Traffic Safety Administration (NHTSA), "Vehicle Safety Communications Project Final Report DOT HS 810 591," 2006.

[12] Federal Highway Administration, "2015 FHWA Vehicle to Infrastructure Deployment Guidance and Products." Washington, D.C., p. 30, 2014.

[13] D. Ou, Y. Yang, L. Xue, and D. Dong, "Optimal Connectivity-Based Deployment of Roadside Units for Vehicular Networks in Urban Areas," *Transportation Research Record: Journal of the Transportation Research Board*, vol. 2559, no. 2559, pp. 46–56, Jan. 2016.

[14] G. G. M. Nawaz Ali, P. H. J. Chong, S. K. Samantha, and E. Chan, "Efficient data dissemination in cooperative multi-RSU Vehicular Ad Hoc Networks (VANETs)," *Journal of Systems and Software*, vol. 117, pp. 508–527, Jul. 2016.

[15] M. Kafsi, P. Papadimitratos, O. Dousse, T. Alpcan, and J.-P. Hubaux, "VANET Connectivity Analysis," 2009.

[16] T. Yan, W. Zhang, G. Wang, and Y. Zhang, "Access Points Planning in Urban Area for Data Dissemination to Drivers," *IEEE Transactions on Vehicular Technology*, vol. 63, no. 1, pp. 390–402, Jan. 2014.

[17] C. M. Silva, W. Meira, and J. F. M. Sarubbi, “Non-Intrusive Planning the Roadside Infrastructure for Vehicular Networks,” *IEEE Transactions on Intelligent Transportation Systems.*, vol. 17, no. 4, pp. 938–947, 2016.
[18] O. Trullols, M. Fiore, C. Casetti, C. F. Chiasserini, and J. M. Barcelo Ordinas, “Planning roadside infrastructure for information dissemination in intelligent transportation systems,” *Computer Communications*, vol. 33, no. 4, pp. 432–442, 2010.
[19] V. D. Khairnar and S. N. Pradhan, “Simulation Based Evaluation of Highway Road Scenario between DSRC/802.11p MAC Protocol and STDMA for Vehicle-to-Vehicle Communication,” *Journal of Transportation Technologies*, vol. 3, no. 1, pp. 88–104, 2013.
[20] M. Shulman and R. K. Deering, “Third Annual Report of the Crash Avoidance Metrics Partnership, April 2003 - March 2004,” Washington, D.C., 2005.
[21] R. Miucic, Z. Popovic, and S. M. Mahmud, “Experimental characterization of DSRC signal strength drops,” in *2009 12th International IEEE Conference on Intelligent Transportation Systems*, 2009, pp. 1–5.
[22] E. Zöchmann, K. Guan, and M. Rupp, “Two-Ray Models in mmWave Communications,” pp. 225–229, 2017.
[23] IEEE Vehicular Technology Society Sponsored, *IEEE Standard for Wireless Access in Vehicular Environments (WAVE)— Networking Services IEEE*. New York: The Institute of Electrical and Electronics Engineers, Inc., 2016.
[24] V. Shivaldova, A. Winkelbauer, and C. F. Mecklenbrauker, “Signal-to-noise ratio modeling for vehicle-to-infrastructure communications,” *2014 IEEE 6th International Symposium on Wireless Vehicular Communications WiVeC 2014 - Proc.*, 2014.
[25] V. Shivaldova, A. Winkelbauer, and C. F. Mecklenbrauker, “Vehicular Link Performance: From Real-World Experiments to Reliability Models and Performance Analysis,” *IEEE Vehicular Technology Magazine*, vol. 8, no. 4, pp. 35–44, 2013.
[26] V. Shivaldova and C. F. Mecklenbräuker, “Quantization-based Complexity Reduction for Range-dependent Modified Gilbert Model,” *Proc. IEEE Sens. Array Multichannel Signal Process. Work.*, pp. 345–348, 2014.
[27] V. Shivaldova, A. Winkelbauer, and C. F. Mecklenbr, “Realistic Performance Model for Vehicle-to-Infrastructure Communications,” no. c, pp. 557–561, 2014.
[28] V. Shivaldova, A. Paier, D. Smely, and C. F. Mecklenbräuker, “On roadside unit antenna measurements for vehicle-to-infrastructure communications,” *IEEE International Symposium on Personal, Indoor and Mobile Radio Communications PIMRC*, pp. 1295–1299, 2012.
[29] W. H. Hayt, Jr., *Engineering Electromagnetics*, Fifth Edit. New York: McGraw-Hill, Inc., 1989.
[30] L. V. Bewley, *Two Dimensional Fields in Electrial Engineering*, 1st ed. New York: Dover Publications, 1963.
[31] D. Corson and P. Lorrain, *Introducing to Electromagnetic Fields and Waves*. San Franscisco: W.H. Freeman, 1962.
[32] R. Wilson, “Propagation Losses Through Common Building Materials 2.4 GHz vs 5 GHz,” *Magis Network, Inc.*, pp. 1–28, 2002.
[33] R. E. Collins, *Antennas and Radio Wave Propagation*. New York: McGraw-Hill, Inc., 2014.

[34] S. L. Salas and E. Hille, *Calculus: One and Several Variables*, 3rd ed. John Wiley and Sons, Inc., 1978.
[35] R. Plonsey and R. E. Collin, *Principles and Applications of Electromagnetic Fields*. McGraw-Hill, Inc., 1961.
[36] M. Javid and P. M. Brown, *Field Analysis and Electromagnetics*. New York: McGraw-Hill, Inc., 1963.
[37] E. C. Jordan and K. G. Balmain, *Electromagnetic Waves and Radiating Systems*, 2nd ed. Englewood Cliffs: Dorling Kindesley Pearson Education, 2015.
[38] J. D. Kraus, *Electromagnetics*, 4th ed. New York: McGraw-Hill, Inc., 1992.
[39] J. E. Parton, S. J. . Owen, and M. S. Raven, *Applied Electromagnetics*. Palgrave Macmillan, 1985.
[40] D. T. Paris and F. K. Hurd, *Basic Electromagnetic Theory*. McGraw-Hill, Inc., 1969.
[41] R. C. Weast and S. M. Selby, Eds., *Standard Mathematical Tables*, Seventeent. The Chemical Rubber Co., 1969.
[42] S. Ramo, J. R. Whinnery, and T. Van Duzer, *Fields and Waves in Communication Electronics*, 3rd ed. New York: John Wiley and Sons, Inc., 2008.
[43] K. F. Sander and G. A. L. Reed, *Transmission and Propagation of Electromagnetic Waves*, 2nd ed. New York: Cambridge University Press, 1986.
[44] D. K. Cheng, *Field and Wave Electromagnetics*, Second Edi. Reading, Mass.: The Addison-Wesley, 1989.
[45] R. Valenzuela, "A ray tracing approach to predicting indoor wireless transmission," *IEEE 43rd Veh. Technol. Conf.*, pp. 214–218, 1993.
[46] A. M. Bodzin and L. Cirucci, "A Land-Use-Planning Simulation Using Google Earth.," *Sci. Scope*, vol. 32, no. 7, pp. 30–38, 2009.
[47] I. Janssen and A. Rosu, "Measuring sidewalk distances using Google earth," *BMC Med. Res. Methodol.*, vol. 12, no. 39, p. 10, 2012.
[48] S. Bayless, A. Guan, A. Shaw, M. Johnson, G. Pruitt, and B. Abernathy, "Recommended Practices for DSRC Licensing and Spectrum Management: A Guide for Management, Regulation, Deployment, and Administration for Connected Vehicle Environment.," 2015.
[49] F. C. Commission, "Equipment Authorization Order & Accredited Testing Laboratories FCC Equipment Authorization Process," 2017. [Online]. Available: https://transition.fcc.gov/oet/ea/presentations/files/may17/10-EA_Accredited-Labs-GT-Final.pdf.
[50] C. Kwok, R. F. Jr. Cleveland, and D. L. Means, "Evaluating Compliance with FCC Guidelines for Human Exposure to Radiofrequency Electromagnetic Fields Supplement C," 1997.
[51] J. D. M. S. J. L. U. Robert F. Cleveland and Standards, "OET bulletin 65: Evaluating compliance with FCC guidelines for human exposure to radiofrequency electromagnetic fields," 1997.
[52] Cisco Systems, "White Paper on Antenna Patterns and Their Meaning," San Jose, 2007.
[53] Linx Technology, "Application Note," Merlin, 2012.
[54] A. S. C. of the I. A. and Propagation and Society, "IEEE Standard Definitions of Terms for Antennas," 1993.
[55] Campbell Scientific, "The Link Budget and Fade Margin (Application Notes)." Campbell Scientific, Inc., Logan, 2016.

[56] T. Vincenty, “Direct and Inverse Solutions of Geodesics on the Ellipsoid With Application of Nested Equations,” *Surv. Rev.*, vol. 23, no. 176, pp. 88–93, 1975.
[57] T. Vincenty, “Geodetic inverse solution between antipodal points,” *Richard Rapp Geodetic Science Ohio State University*. 1975.

Chapter 4. Introducing an Extended Horizontal and Vertical Polarization Model to Ascertain the Null Points from a DSRC RSU

Section 4.1. Title

Introducing an extended horizontal and vertical polarization model to ascertain the null points from a DSRC RSU

Section 4.2. Abstract

An extended horizontal and vertical polarization model are proposed that calculates the null point from a DSRC RSU. The extended model is applied to empirical data from the USDOT Federal Highway Administration (FHWA) that required a secure testing facility. Therefore, the latitude and longitude coordinates were expunged to withhold the testing location and maintain a certain level of confidentiality. Therefore, the latitude and longitude are converted into travel distances using the greater circle and Vincenty distance algorithms. The paper will use the Vincenty distance, but the model will work with less accurate latitude and longitude data such as the data acquisition system.

There are 18 model comparisons of the packet counts and signal strengths at various thresholds as perspective extended horizontal and vertical polarization models. The objective is to compare the predictive ability of each model and measure the fit. Finally, a predication graph is depicted with the neural network's probability profile for packet counts =1 when greater than or equal to 377. Likewise, a python script is provided of the extended horizontal and vertical polarization model in Appendix C.

Section 4.3. Introduction

Once again, the research motivation focuses on developing an empirical method of calculating the null points of a DSRC RSU. A designer of a V2I safety application may require a minimum rate of data (or packet count) over 1,000 meters to effectively implement a RSZW application. For example, the RSZW may require a constant flow of 400 packet counts per second for 1,000 meters before the work zone.

In Figure 4-1, we propose a process that introduces an extended horizontal and vertical polarization model to ascertain the null points from a DSRC RSU. Using statistical analysis, the packet count and signal strength can be used to determine thresholds to investigate potential DSRC RSU null points. The packet counts and signal strength threshold criterion must be determined by the developer of the V2I safety application before implementing the extended horizontal and vertical polarization model.

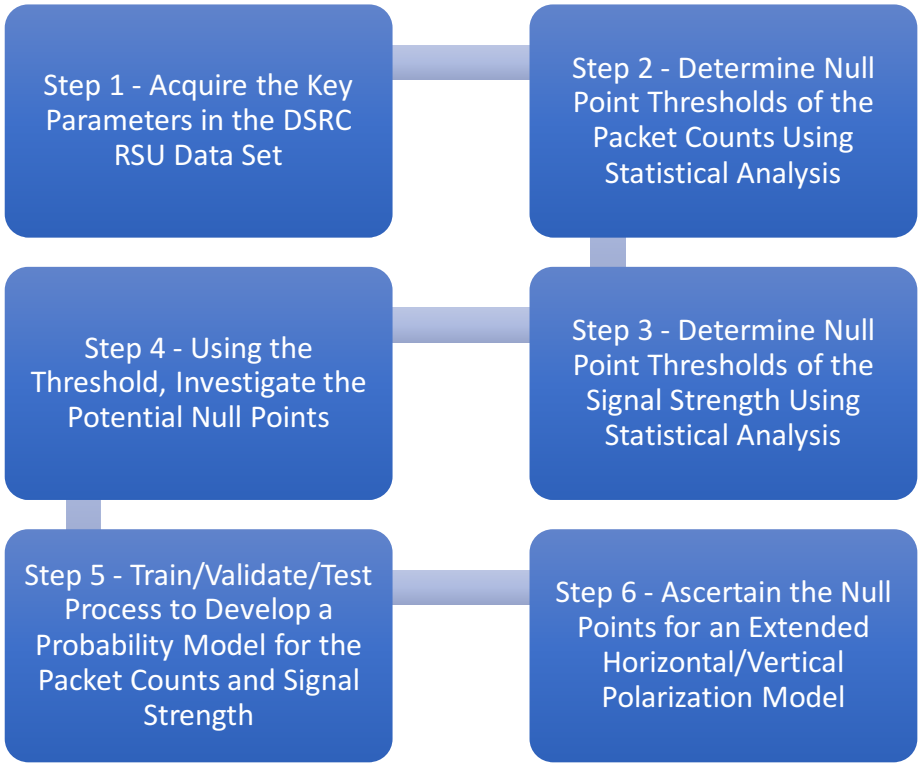

Figure 4-1. A block diagram of the process used to develop a model using a training-validation-test data set from a DSRC RSU.

Section 4.3.1. DSRC RSU Data Set from the Field Test

The DSRC RSU data set was retrieved from the USDOT FHWA as unpublished data. The latitude and longitude coordinates were expunged to withhold the testing location and maintain a certain level of confidentiality. Instead, the distance was calculated between the adjunct coordinate using at least two techniques that allow for data analysis: greater circle distance and Vincenty distance.

Section 4.4. Materials and Methods (Study Background)

Section 4.4.1. Description of FHWA's DSRC RSU Field Test

This subsection focuses on describing the field test environment where the DSRC RSU data set was retrieved. The field test was conducted by the USDOT FHWA at a secure testing facility with an open sky (i.e., for good GPS satellite reception) and limited infrastructure (e.g., no building, highway barriers). The DSRC RSU was a Cohda unit that was mounted approximately 18 feet above ground. The test equipment included two Agilent Spectrum Analyzer (Model No. 8563E), Agilent Vector Signal Analyzer (Model No. 89441A), an Anritsu Radion Communication Analyzer (Model No. MT8815A), and a Tektronix Digital Storage Oscilloscope (Model No. TDS3052). In Figure 4-2, the DSRC data set and test site are displayed, which

allows the creation of customized maps based on the latitude and longitude coordinate on the surface of the earth [https://support.google.com/mymaps/answer/3024396].

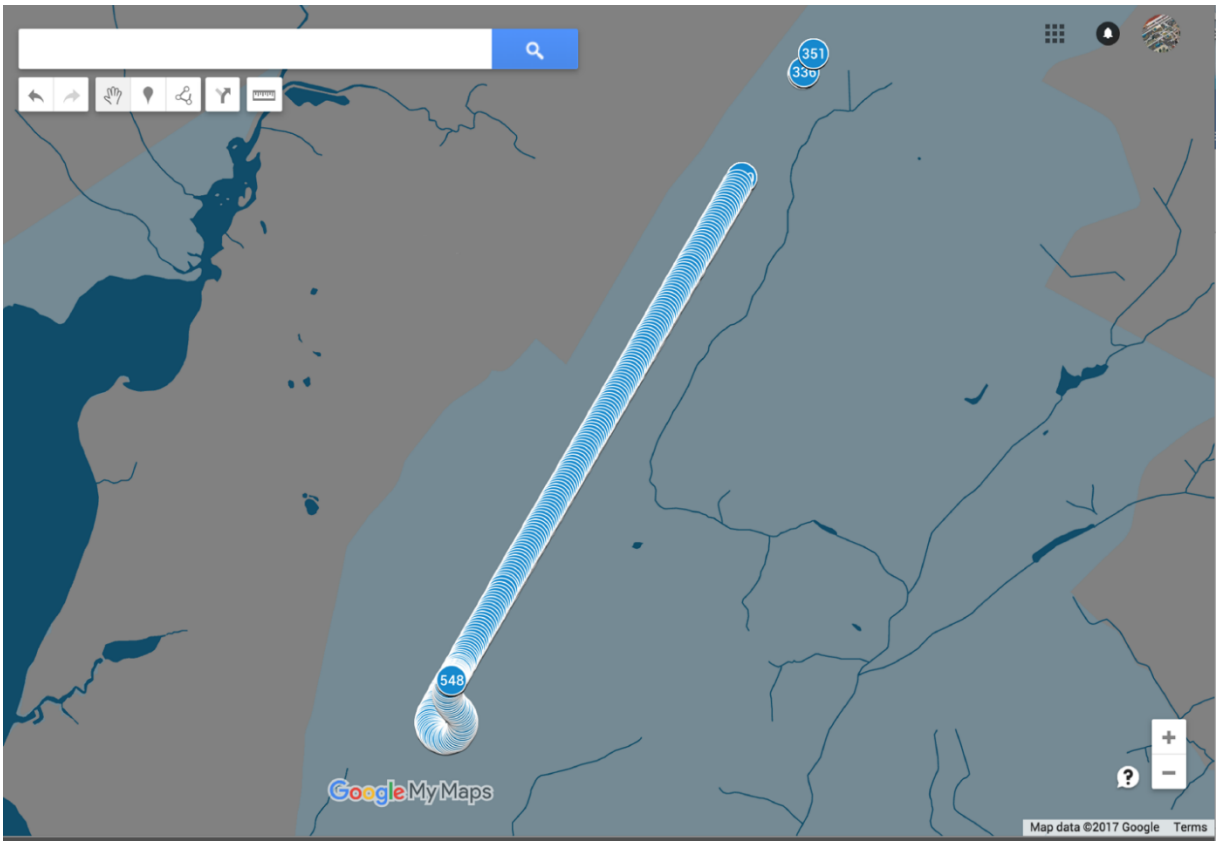

Figure 4-2. The DSRC data set and test site are displayed using Google My Maps.

Section 4.4.2. Vehicle Testing Segments

The vehicle testing segments (i.e., the region of interest) occurred along a straight 2-mile track and circular loops at each end of the track. At a rate of 10 times per second, the data acquisition system collected information from the DSRC RSU in a single test run (i.e., there were 10 data points per second). The 10 data points were averaged over one second because the data acquisition system had limited storage space. As shown in Figure 4-3, Figure 4-4, Figure 4-5, and Table 4-1, the vehicle testing segment can be divided into four segments, for future analysis.

Table 4-1. A single test run is divided into four segments for future analysis.

Segment	Data Points	Description	Figure
Segment 1			
Starting Mark	1- 52	Vehicle is stationary and 8 feet from the DSRC Road Side Unit	Xb

Segment	Data Points	Description	Figure
Southern Loop	53 – 129	Vehicle traveling along the circle which is south of the RSU	Xc
Segment 2			
Northern Testing Segment	130 – 306	Vehicle moving in the northern direction of track	Xd
Segment 3			
Vehicle Northern Stopped	307 – 320	Vehicle stopped in the northern direction	Xe
Northern Loop	321 – 351	Traveling along the circle that is north of the RSU	Xe
Segment 4			
Southern Testing Segment	352 – 530	Vehicle moving in the southern direction of track	Xf
Vehicle Southern Stopped	531 – 548	Vehicle stopped in the southern direction	Xb

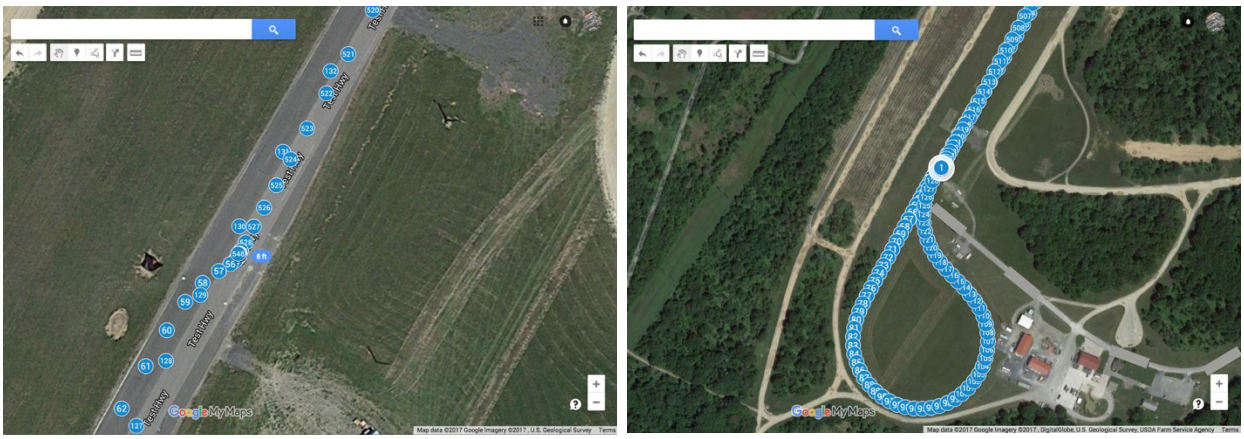

Figure 4-3. In the left image, the vehicle is stationary approximately 8 feet from the DSRC RSU (Data points 1- 52 and 531 – 548). In the right image, the vehicle is traveling along the circle, which is south of the DSRC RSU (Data points 53- 130).

Figure 4-4. In the left image, the vehicle is moving in the northern direction of the DSRC RSU (Data points 307 - 320). On the right image, the vehicle is stopped in the north direction (Data points 307 - 320) and traveling along the circle, which is north of the RSU (Data points 321 - 351).

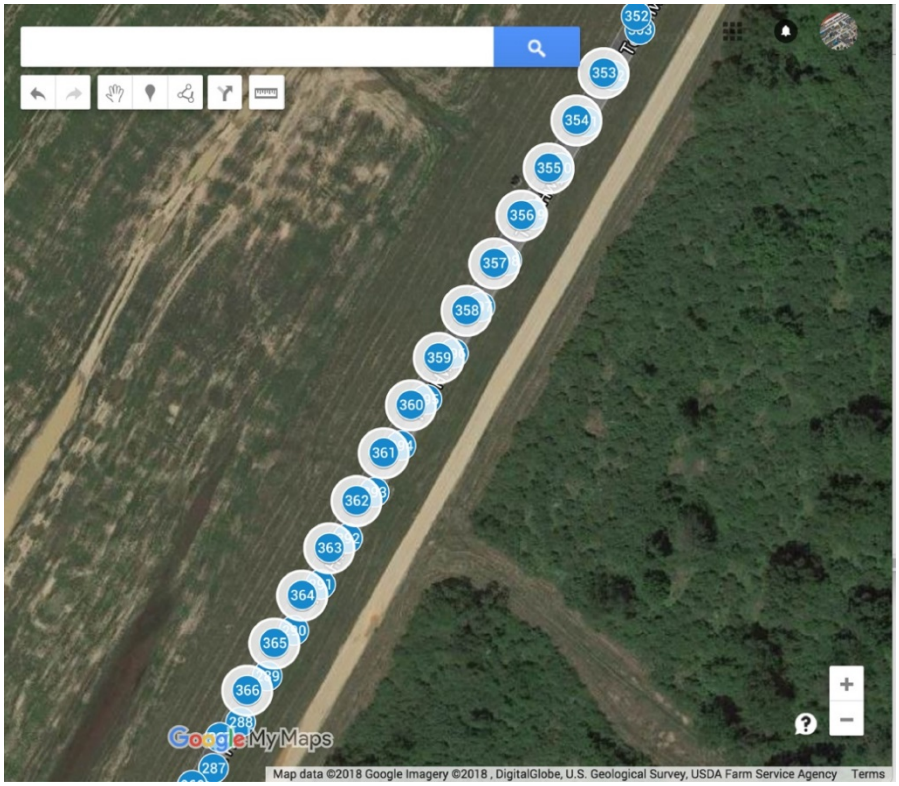

Figure 4-5. The vehicle moving in the southern direction of the DSRC RSU (Data points 352 - 530).

Section 4.4.3. Distance of the Vehicle Testing Segments

Before we introduce the novice technique, it is essential to convert the expunged latitude and longitude coordinates into distance traveled. The distance traveled from the DSRC RSU by the vehicle is obtained or calculated using the data acquisition system, greater circle distance, and the Vincenty distance [1]. The data acquisition system provides an estimated distance between

the vehicle and RSU. However, it is unclear which distance calculation(s) or mathematical technique(s) are used for the resulting values. Therefore, the greater circle and Vincenty algorithms are used to calculate the travel distance based on the latitude and longitude coordinates [56] [57]. The Vincenty algorithm is based on a spheroid earth with an accuracy of 0.5 millimeters or 0.020 inches. When possible, this paper uses the Vincenty travel distance for data analysis. However, there may be situations in the model development process that may require the data acquisition system travel distance, which may not be accounted for in this paper. In general, the model will work with any travel distance and is not limited to the greater circle or Vincenty travel distance.

The distance traveled by the vehicle is essential in data analysis (e.g., calculating null points, location of packet loss); therefore, the distance was calculated for vehicle testing segment 1 (Southern Loop), 2 (Northern Testing Segment), and 4 (Southern Testing Segment). Moreover, the distance of each vehicle segment is provided in at least three measurement sources/techniques: 1) the data acquisition system, 2) the greater circle distance calculation, and/or 3) the Vincenty distance calculation. The following briefly describes the three measurement sources/techniques:

- **Data Acquisition:** The data acquisition system provides an estimated distance between the vehicle and RSU; however, there was no clear explanation in the data set or technical staff available to provide information. Therefore, the paper utilized the techniques below to verify and compare the distance traveled by the vehicle (i.e., the error rate was not available).
- **Greater Circle Distance:** Using data from the acquisition system, the latitude and longitude coordinates are utilized to calculate the distance between two points using the great-circle distance on the surface of a sphere (i.e., the distance can be in error up to 0.3 percent when converting GPS coordinates to distance traveled).
- **Vincenty Distance:** Using data from the acquisition system, the latitude and longitude coordinates are utilized to calculate the distance between two points using the Vincenty's formulae based on the surface of a spheroid (i.e., accurate within 0.5 millimeters or 0.020 inches when converting GPS coordinates to distance traveled).

In segment 1 (Southern Loop), two measurement techniques were used to determine the diameter of the loop, which are the greater circle distance at 209.9 meters and the Vincenty at 209.88 meters. As depicted in Figure 4-6 and Table 4-2, the data points at 90 and 114 were utilized to calculate the distance.

Table 4-2. Two diameter measures of the southern loop, which are calculated from data points 90 to 114.

Segment 1: *Southern Loop (Data Points 90 to 114)*		
Measurement Technique	**meters**	**feet**
Greater Circle Distance	209.9	688.648294
Vincenty Distance	209.887	688.605643

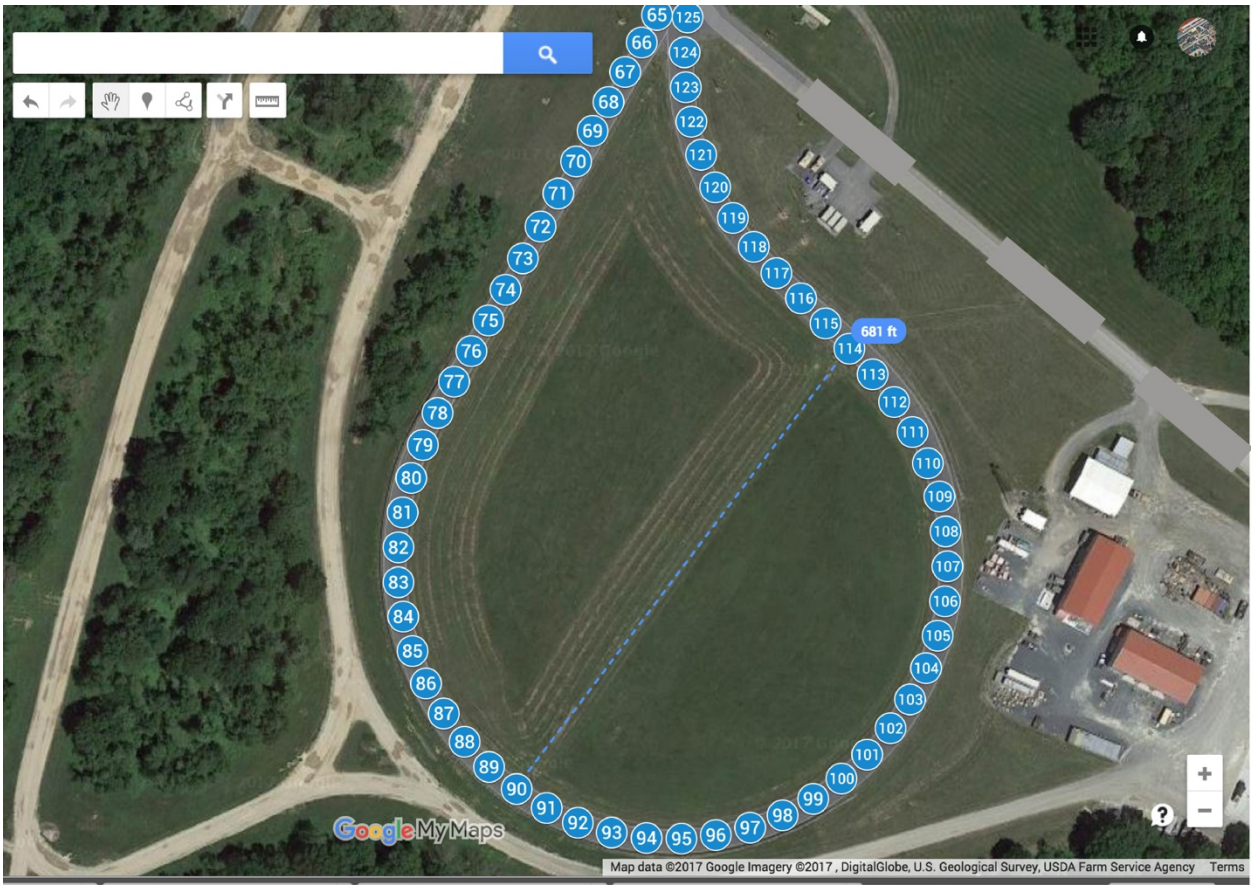

Figure 4-6. The diameter measure of the southern loop which are calculated from data points 90 to 114.

In segment 2 (Northern Testing Segment), three measurement techniques were used to determine the distance (or length) of the northern testing segment: 1) the data acquisition system at 3,624.75 meters, 2) the greater circle distance at 3,616 meters, and 3) the Vincenty distance at 3,615.97 meters. As depicted in Figure 4-7 and Table 4-3, the data points from 130 to 306 were utilized to calculate the northern testing segment. Also, the difference (or delta) in measurement is calculated against the data acquisition value, which is an estimated distance between the vehicle and RSU. As stated before, the error rate was not available for the data acquisition system, while the greater circle has an error rate of up to 0.3 percent and the Vincenty distance is accurate within 0.5 millimeters.

Table 4-3. Based on four measurement techniques, the distance (or length) of the northern testing segments from data points 130 to 306.

Segment 2: *Northern Testing Segment (Data Points 130-306)*				
Measurement Technique	**meters**	**Delta (meters)**	**feet**	**Delta (feet)**
Data Acquisition System	3624.75	0	11892.22441	0
Greater Circle Distance	3616	8.75	11863.51706	28.70735
Vincenty Distance	3615.979	8.771	11863.44816	28.77625

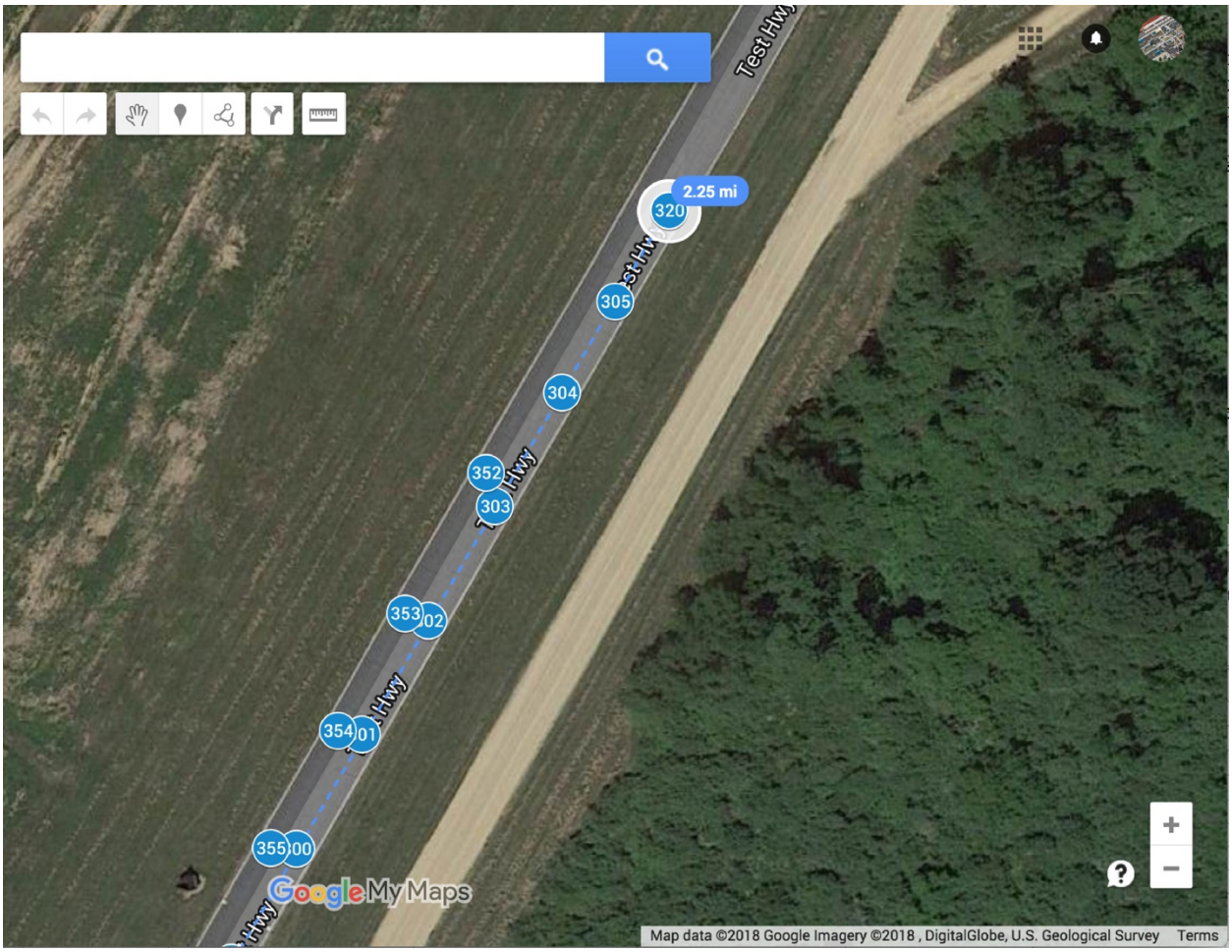

Figure 4-7. The distance (or length) of the northern testing segments from data points 130 to 306.

In segment 4 (Southern Testing Segment), three measurement techniques were used to determine the distance (or length) of the southern testing segment: 1) the data acquisition system at 3,575.11 meters, 2) the greater circle distance at 3,570 meters, and 3) the Vincenty distance at 3,570.116 meters. As depicted in Figure 4-8 and Table 4-4, the data points from 352 to 530 were utilized to calculate the southern testing segment. Also, the difference (or delta) in measurement is calculated against the data acquisition value, which is an estimated distance between the vehicle and RSU.

Table 4-4. Based on four measurement techniques, the distance (or length) of the southern testing segments from data points 352 to 530.

Segment 4: *Southern Testing Segments (Data Points 352-530)*				
Measurement Technique	**meters**	**Delta (meters)**	**feet**	**Delta (feet)**
Data Acquisition System	3575.11	0	11729.36352	0
Greater Circle Distance	3570	5.11	11712.6	16.76352
Vincenty Distance	3570.116	4.994	11712.979	16.38452

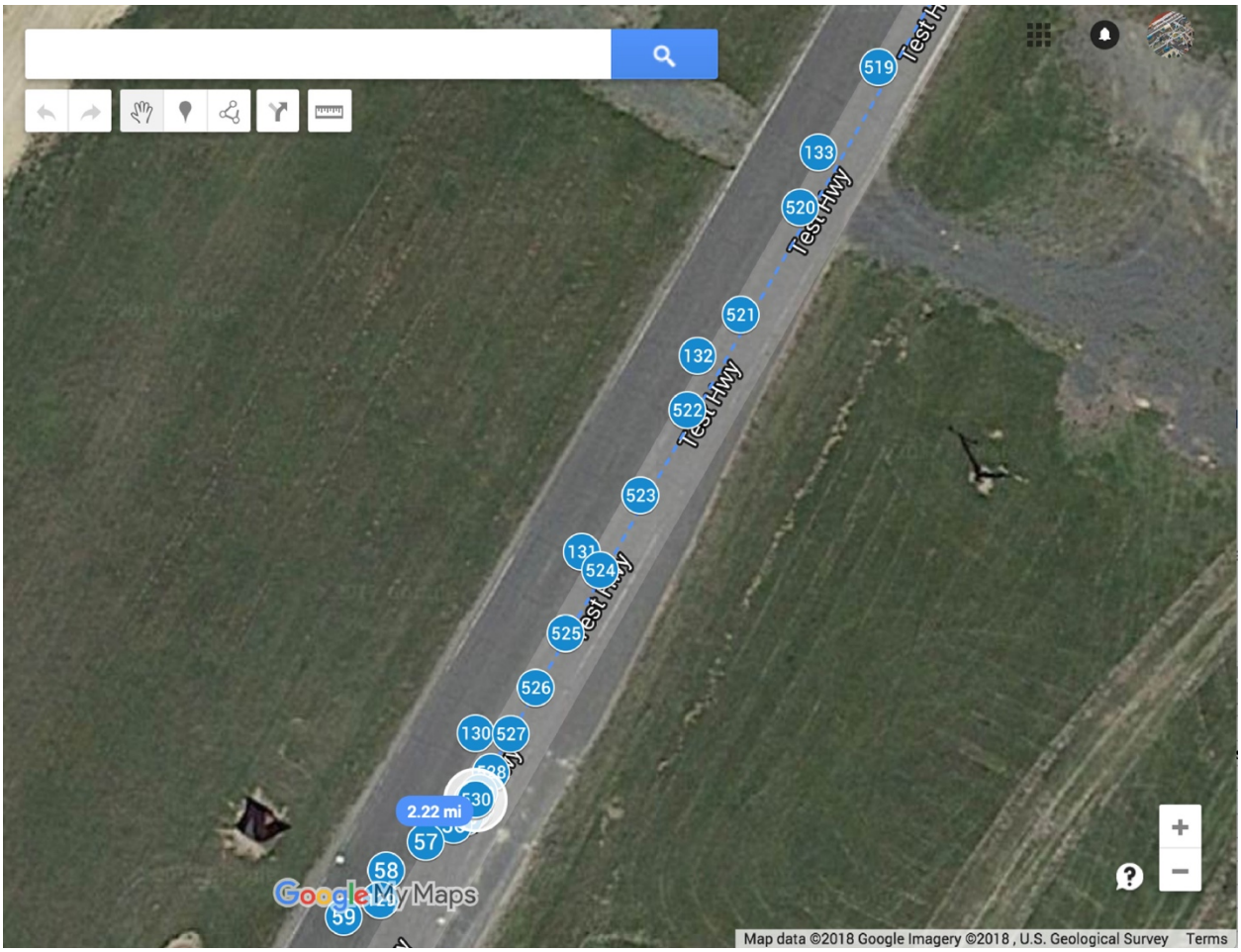

Figure 4-8. The distance (or length) of the southern testing segments from data points 352 to 530.

Section 4.4.4. Key Parameters in the DSRC RSU (Sample) Data Set (Step 1)

Based on the vehicle testing segments, the data set were collected from the data acquisition system at a rate of 10 times per second; however, the 10 data points were averaged over one second because the data acquisition system had limited storage space. In Table 4-5 through Table 4-7, the key parameters are listed along with the description and sample data for the DSRC RSU data set at a rate of 10 times per second.

Table 4-5. The key parameters of the DSRC RSU data set at a rate of 10 times per second (i.e., Each row of data is an average of 10 data points over one second) (1 of 3).

Epoch Time	Eastern Standard Time (hh:mm:ss)	Greater Circle Distance (meters)	Greater Circle Distance (feet)	Vincenty Distance (meters)	Vincenty Distance (feet)
1505327129	1:25:29 PM	0	0	0	0
1505327130	1:25:30 PM	0.028106117	0.09221167	0.028076058	0.092113051

Epoch Time	Eastern Standard Time (hh:mm:ss)	Greater Circle Distance (meters)	Greater Circle Distance (feet)	Vincenty Distance (meters)	Vincenty Distance (feet)
1505327131	1:25:31 PM	0.023845898	0.078234573	0.023808738	0.078112657
1505327132	1:25:32 PM	0.020464979	0.06714232	0.020456667	0.067115049
1505327133	1:25:33 PM	0.017178549	0.056360069	0.017181733	0.056370515

Epoch Time: The value represents the number of seconds elapsed since 00:00:00 on January 1, 1970, Coordinated Universal Time (UTC) as a system clock.

Eastern Standard Time: The eastern standard time is calculated into a human readable time from the Epoch time and displayed as two-digit hours, two-digit minutes, and two-digit seconds (hh:mm:ss).

Greater Circle Distances (meters): The greater circle (or orthodromic) distance was calculated from the expunged latitude and longitude coordinates in meters. The distance is calculated between two points along the surface of a spherical earth (i.e., the distance can be in error up to 0.3 percent when converting GPS coordinates to distance traveled).

Greater Circle Distance (feet): The greater circle (or orthodromic) distance was calculated from the expunged latitude and longitude coordinates in feet. The distance is calculated between two points along the surface of a spherical earth (i.e., the distance can be in error up to 0.3 percent when converting GPS coordinates to distance traveled).

Vincenty Distance (meters): The Vincenty distance was calculated from the expunged latitude and longitude coordinates in meters. More accurate than the greater circle distance, the distance is calculated between two points along the surface of a spheroid earth, developed by Thaddeus Vincenty (i.e., accurate within 0.5 millimeters when converting GPS coordinates to distance traveled).

Vincenty Distance (feet): The Vincenty distance was calculated from the expunged latitude and longitude coordinates in feet. More accurate than the greater circle distance, the distance is calculated between two points along the surface of a spheroid earth, developed by Thaddeus Vincenty (i.e., accurate within 0.020 inches when converting GPS coordinates to distance traveled).

Table 4-6. The key parameters of the DSRC RSU data set at a rate of 10 times per second (i.e., Each row of data is an average of 10 data points over one second) (2 of 3).

Data Acquisition System Range from RSU (meters)	Data Acquisition System Range from RSU (feet)	Data Acquisition System Maximum Range (meters)	Data Acquisition System Maximum Range (feet)	Packet Counts
2.75	9.022309711	2.75	9.022309711	128
2.65	8.694225722	2.75	9.022309711	400
2.65	8.694225722	2.75	9.022309711	400
2.65	8.694225722	2.75	9.022309711	400
2.65	8.694225722	2.75	9.022309711	400

Data Acquisition System Range from RSU (meters): The range from the RSU is recorded by the data acquisition system during the field test in meters.

Data Acquisition System Range from RSU (feet): The range from the RSU is recorded by the data acquisition system during the field test in feet (i.e., the error rate was not available).

Data Acquisition System Maximum Range (meters): The maximum range is an accumulate distance over the period of field testing and is recorded by the data acquisition system in meters (i.e., the error rate was not available).

Data Acquisition System Maximum Range (feet): The maximum range is an accumulate distance over the period of field testing and is recorded by the data acquisition system in feet (i.e., the error rate was not available).

Packet Counts: The packet counts represent data captured from the RSU at the given location.

Table 4-7. The key parameters of the DSRC RSU data set at a rate of 10 times per second (i.e., Each row of data is an average of 10 data points over one second) (3 of 3).

Signal A (dBm)	Noise A (dBm)	Signal A – Noise A (dBm)
-65.27	-101.87	36.6
-65.89	-101.66	35.77
-66.14	-101.77	35.63
-65.08	-101.76	36.68
-64.44	-101.67	37.23

Signal A (dBm): Signal A is the electromagnetic signal strength received from the RSU.

Noise A (dBm): The Noise A is the electromagnetic noise signal received from the RSU.

Signal A - Noise A (dBm): This is the difference between Signal A and Noise A.

Section 4.5. Statistical Analysis Techniques

Section 4.5.1. Statistical Analysis to Determine Null Point Thresholds Using Packet Counts (Step 2)

As stated earlier, the packet counts criterion must be determined by the developer of the V2I safety application. Therefore, we selected an arbitrary criterion of 400 packet counts per second. Statistical analysis was used to adjust the threshold to investigate potential null points from the packet counts. In Figure 4-9, the DSRC RSU packet counts is analyzed using a histogram and outlier box plot because the data set are discrete values that can be easy quantified. The histogram plot is a distribution graph with percent labels (the percent of column values represented by each histogram bar) and count labels (the frequency of column values represented by each histogram bar).

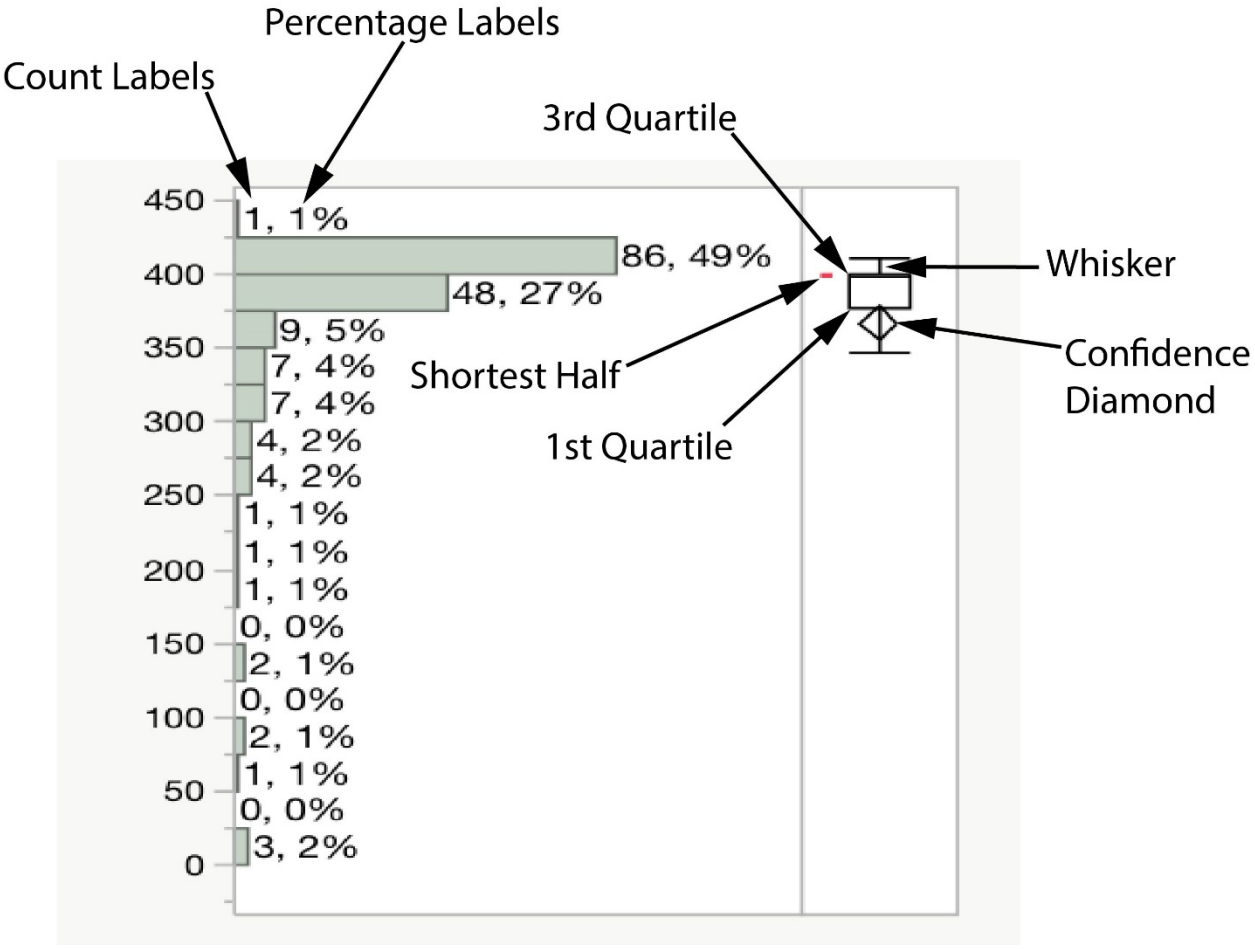

Figure 4-9.The DSRC RSU packet counts are analyzed to investigate potential DSRC RSU null points using a histogram and outlier box plot.

The outlier plot is a distribution diagram with the following characteristics:

1. The horizontal line within the box represents the median sample value;
2. The confidence diamond contains the mean and the upper and lower 95 percent of the mean. The mean is seen when a line crosses through the middle of the diamond. The top and bottom points of the diamond represent the upper and lower 95 percent of the mean;
3. The ends of the box represent the 25th (1st quartile) and 75th (3rd quartile) quantiles;
4. The difference between the 1st and 3rd quartiles is called the interquartile range;
5. The box has lines that extend from each end, sometimes called whiskers. The whiskers extend from the ends of the box to the outermost data point that falls within the distances computed as follows: a) 1st quartile - 1.5*(interquartile range) and b) 3rd quartile + 1.5*(interquartile range)
6. The bracket outside of the box identifies the shortest half (i.e., the red mark) is the most-dense 50 percent of the observations.

Section 4.5.2. Statistical Analysis to Determine Null Point Thresholds Using Signal Strength (Step 3)

Once again, the signal strength criterion must be determined by the developer of the V2I safety application. In Figure 4-10, the DSRC RSU signal strength is analyzed against the FSPL model ($\lambda = 0.999$) using a fit smoothing spline on field data based on a lambda value (e.g., $\lambda = 0.000586$ with R-Square = 0.964). As the value of lambda decreases, the error term of the spline model has more weight and the fit becomes more flexible and curved. As the value of lambda increases, the fit becomes stiff that approaches a straight line. The data points that are closest to the fitted curve have the most influence, and the influence increases as the value of λ decreases. In this paper, the arbitrary value of lambda criterion is adjusted as follows (i.e., the closer to 1.0, the better fit):
Arbitrary Threshold 1: R-Square value of approximately 0.95
Arbitrary Threshold 2: R-Square value of approximately 0.90.

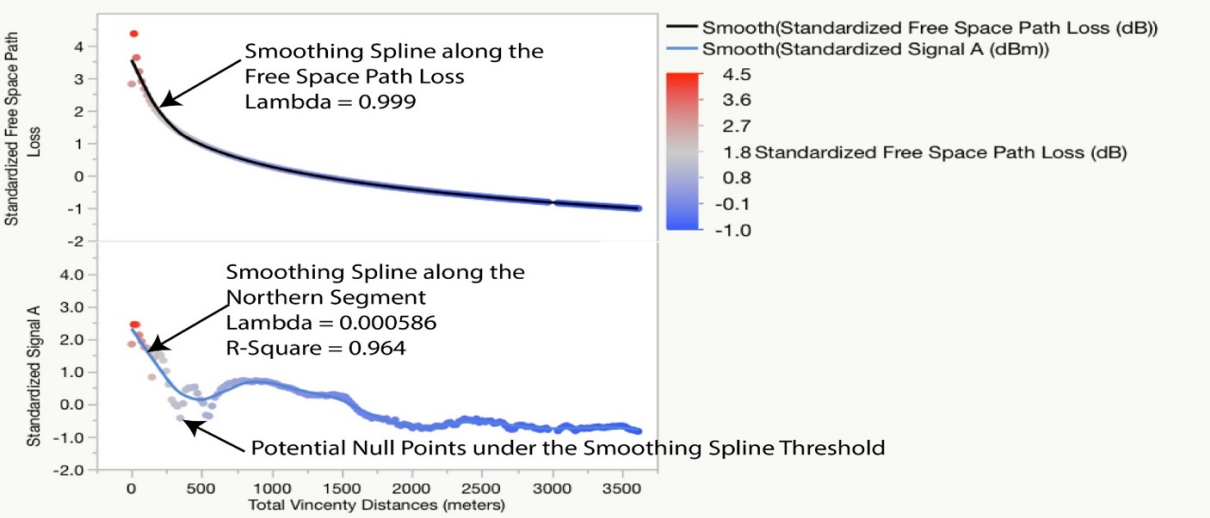

Figure 4-10. The DSRC RSU signal strength is analyzed to investigate potential DSRC RSU null points using a fit spline based on a lambda value (i.e., bottom image at $\lambda = 0.000586$ with a R-Square = 0.964).

As stated earlier, the empirical data was retrieved from a secure testing facility with an open sky (i.e., for good GPS satellite reception) and limited infrastructure (e.g., no building, highway barriers, or unauthorized personnel/vehicles). As shown in Figure 4-11, noise was limited and remained constant throughout the testing period because the staff members have full control over the radio frequency interference through a radio silence test procedure. In other words, the staff was able to notify all personnel, at the secure testing facility, of the radio silence period (i.e., no radio was allowed to broadcast during testing) and the noise was monitored during the testing period.

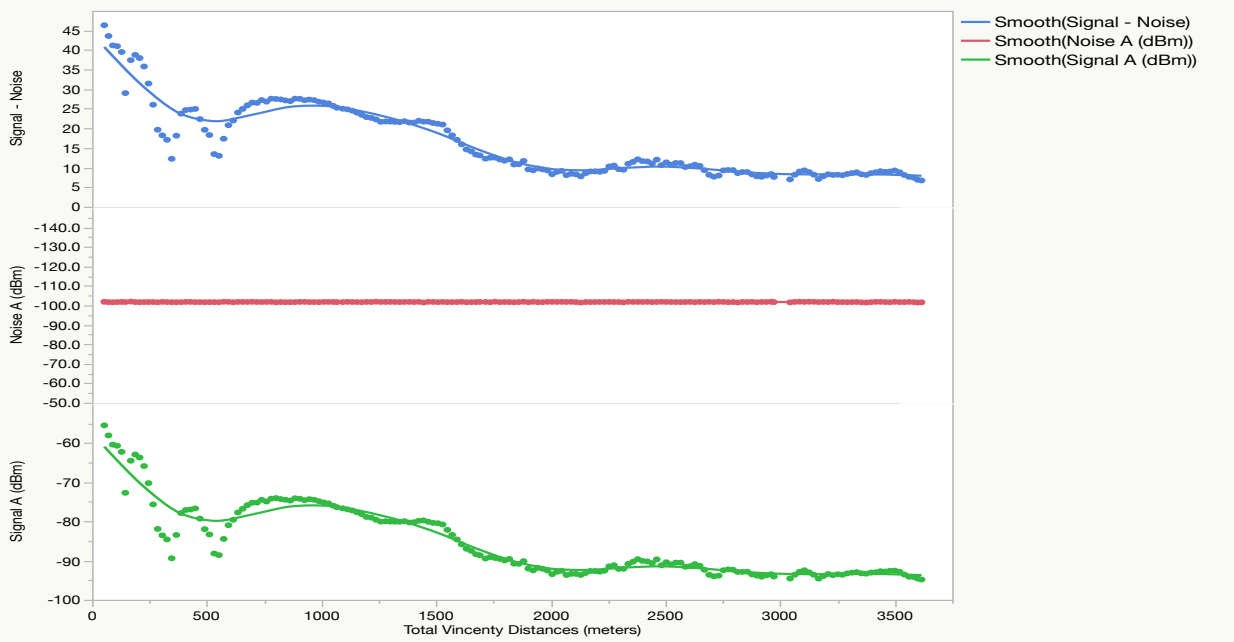

Figure 4-11. The noise was limited and remained constant at the secure testing facility because the staff members implemented a radio silence period during testing.

Section 4.5.3. Based on a V2I Safety Application Design Criterion, Selecting Thresholds to Investigate Potential DSRC RSU Null Points (Step 4)

Based on the software design criterion to select thresholds to investigate potential null points. This subsection focuses on selecting potential packet counts and signal strength thresholds. Based on the V2I safety application criterion, the statistical results should be used to determine potential null points from the packet counts and/or signal strength.

The field test confirms that packet counts decrease as the vehicle moves in the northern direction of the DSRC RSU. In Figure 4-12 (right image), the Quantiles report has a maximum packet count of 443 (100 percent), a median packet count of 399 (50 percent), a 75th percentile at 400 packets, and a 25th percentile at 377 packets. In Figure 4-12 (left image), the Outlier Box plot depicts a distribution of the northern direction with the horizontal line representing the median

sample value (i.e., 87 or 49 percent data points), the ends of the box represent 75th (or 3rd) and 25th (1st) quantiles, and the extended lines (or whiskers) represent 1st and 3rd quartiles + 1.5 (difference between the 1st and 3rd quartiles).

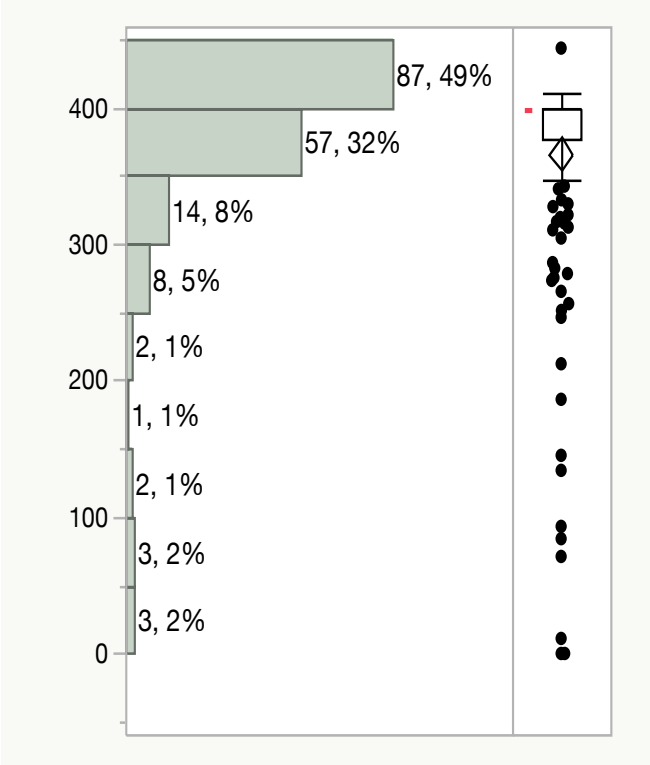

Percentage	Quantiles	Packet Counts
100.0%	maximum	443
99.5%		443
97.5%		404
90.0%		400
75.0%	quartile	400
50.0%	median	399
25.0%	quartile	377
10.0%		281
2.5%		77
0.5%		0
0.0%	minimum	0

Figure 4-12. The Outlier (left image) and Quantiles (right image) reports are the distribution of packet counts in the northern direction of the DSRC RSU (Data points 130 – 306).

In Figure 4-13, the packet counts are plotted against the vehicle travel distance to determine the potential null points based on thresholds. The packet counts are subdivided based on the Quantiles: 443 to 400 (100 percent to 75 percent), 399 (50 percent), 398 to 377 (50 percent to 25 percent), 376 - 281 (25 percent to 10 percent), and 280 to 0 (10 percent to 0 percent) packet counts.

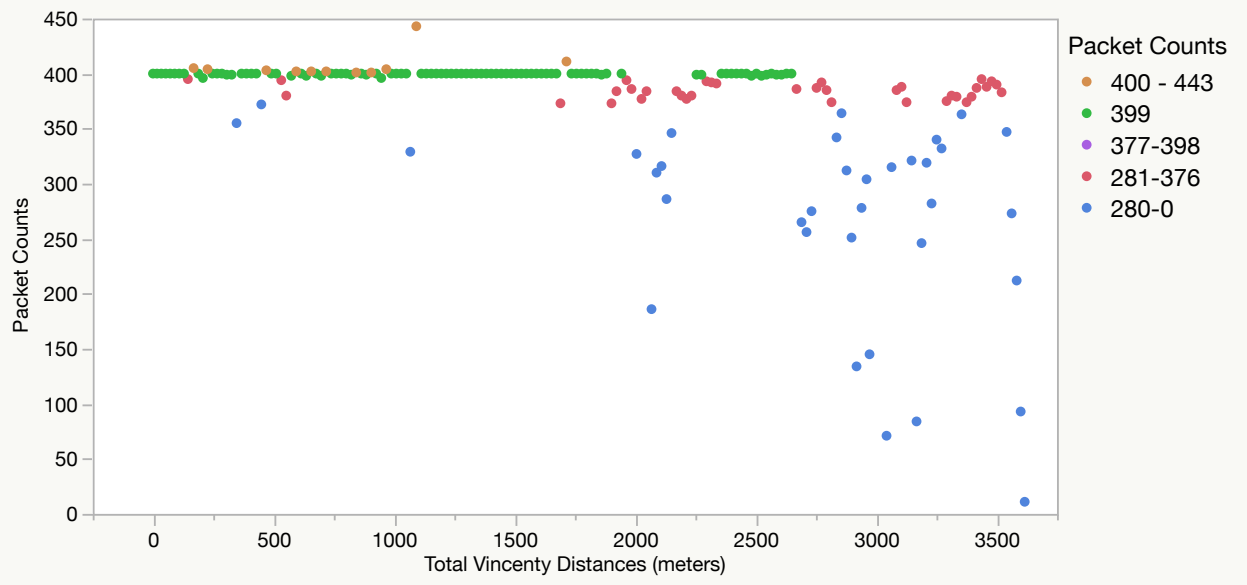

Figure 4-13. The packet counts are plotted against the vehicle travel distance to determine the potential null points based on thresholds.

In Figure 4-14, the packet counts are plotted against the vehicle travel distance using three threshold levels. The packet counts are subdivided based on the Quantiles: 443 to 400 (100 percent to 75 percent), 399 (50 percent), and 398 to 377 (50 percent to 25 percent). Thus, the packet counts are arbitrary subdivided as follows:

Arbitrary Threshold 1: 443 to 400 (100 percent to 75 percent)
Arbitrary Threshold 2: 399 (50 percent)
Arbitrary Threshold 3: 398 to 377 (50 percent to 25 percent).

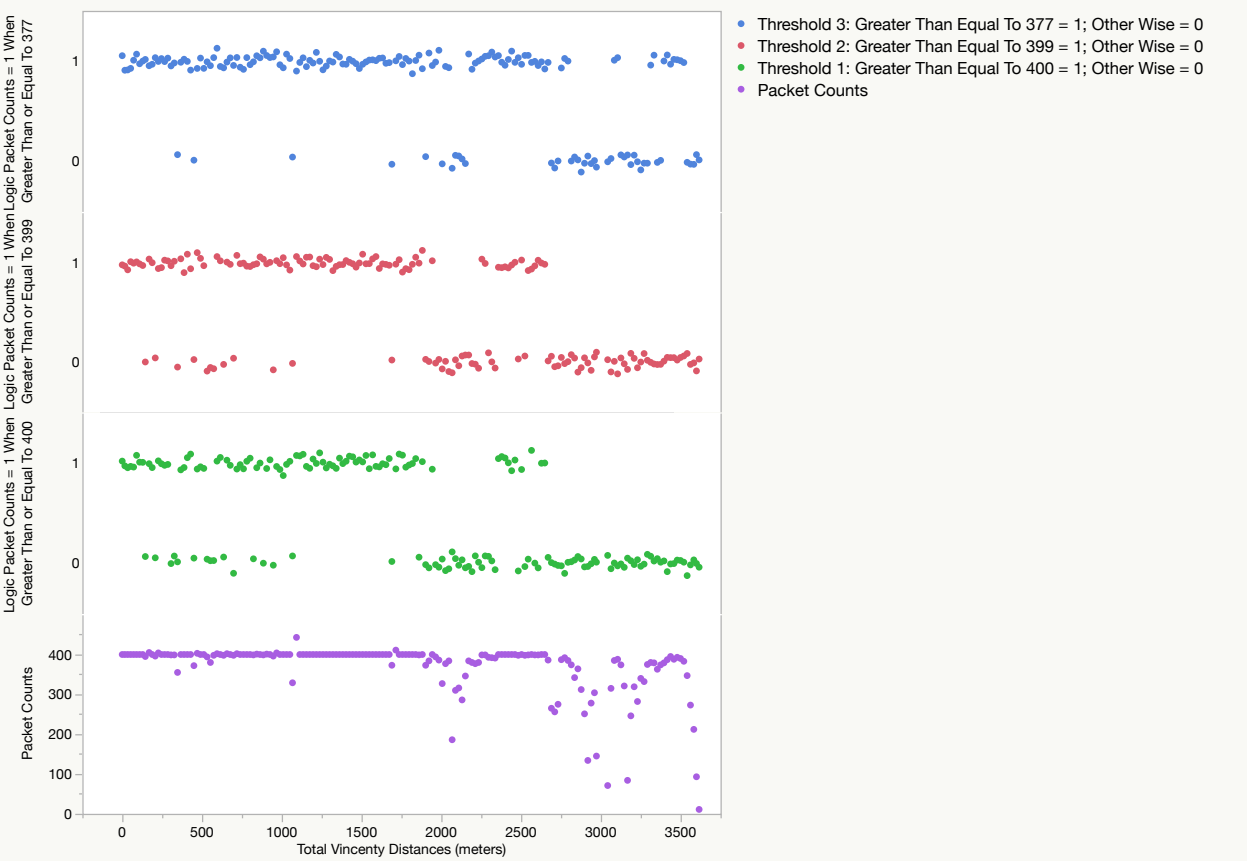

Figure 4-14. The packet counts are arbitrarily subdivided into threshold 1 (green), threshold 2 (red), and threshold 3 (blue).

In Figure 4-15, the potential signal strength thresholds are plotted to provide a visual perspective of the raw data. The DSRC RSU signal strength is plotted against the FSPL model ($\lambda = 0.999$) using fit smoothing spline and compared against two statistical ranges:

Arbitrary Threshold 1: Lambda = 0.000586; R-Square = 0.964
Arbitrary Threshold 2: Lambda = 0.110; R-Square = 0.895.

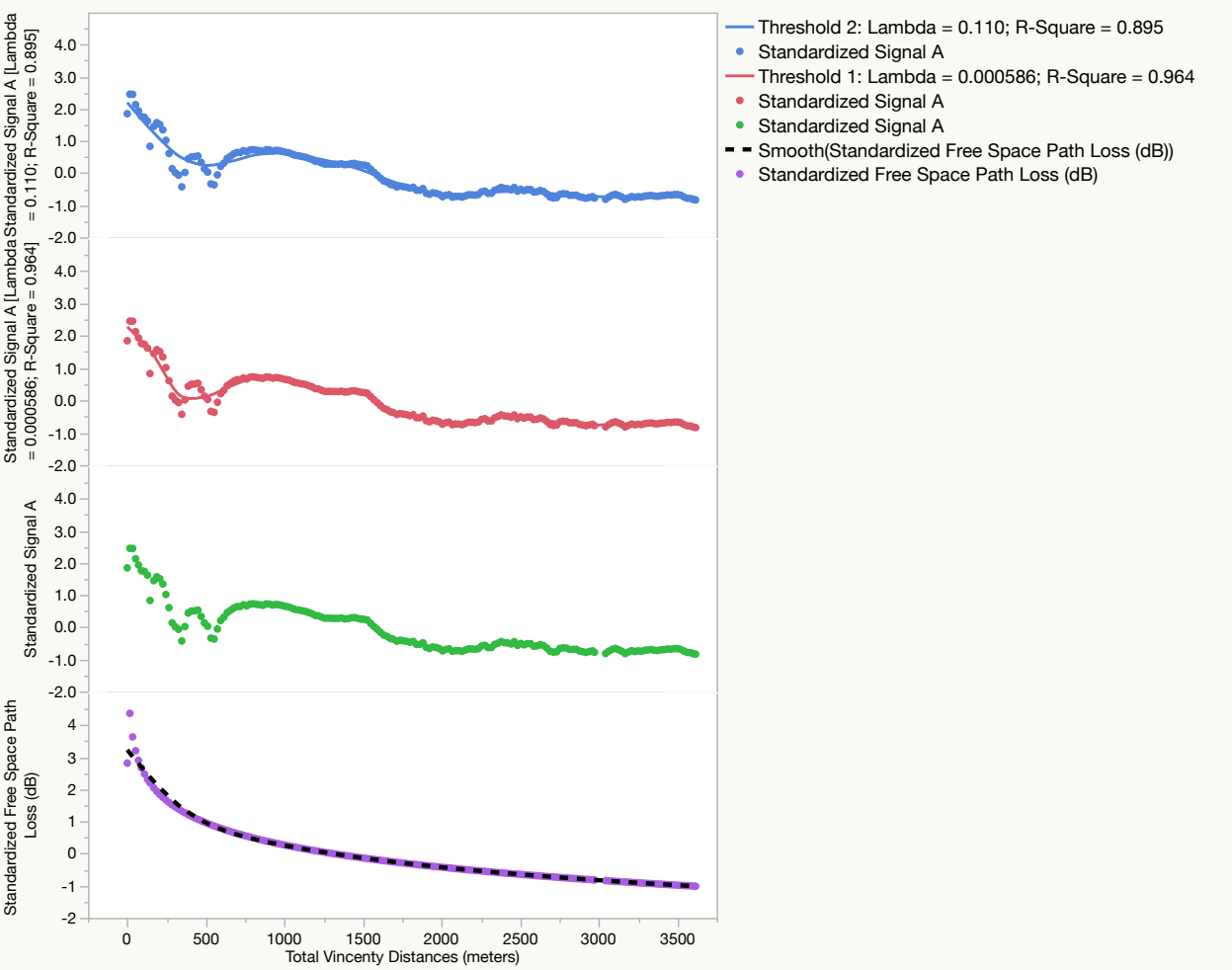

Figure 4-15. The DSRC RSU signal strength is analyzed to investigate potential DSRC RSU null points using a fit spline based on Thresholds 1 (Red line) and 2 (Blue line).

Section 4.5.4. Train/Validate/Test Data Set to Build Categorical Models (Step 5)

Using the DSRC RSU data set, the train-validate-test method is used to build various categorical model. This validation process uses part of a data set to estimate model parameters and the other part to assess the predictive ability of the model. After several trials, the data set is subdivided as follows:

1. The *Test* set is a final, independent assessment of the model's predictive ability (20 percent)
2. The *Validate (or Tune)* set is used to estimate the optimal value of the penalty, assesses or validates the predictive ability of the model (21 percent)
3. The *Train* set is used to estimate the model parameters (59 percent).

Section 4.5.5. Developing Categorical Models Using Packet Counts and Signal Strength Threshold (Step 6)

This subsection utilizes a statistical categorical variable model to develop a predictive formula by converting results of the packet counts and/or signal strength into binary data (i.e., one or zero). Therefore, the paper develops and compares three categorical models: Classification (Decision) Tree, Logistic Regression, and Neural Networks.

In Figure 4-16, a classification (decision) tree model is generated for packet counts =1 when greater than or equal to 399. The model recursively partitions data according to a relationship between the predictors and response values to generate a decision tree. The algorithm searches all possible splits of predictors to best predict the response. The confusion matrix has 64 predicted counts at zero with 14 misclassifications and 92 predicted counts at one with 5 misclassifications. The generalized R-Square is 0.7407 for training, 0.6287 for validation, and 0.5887 for testing.

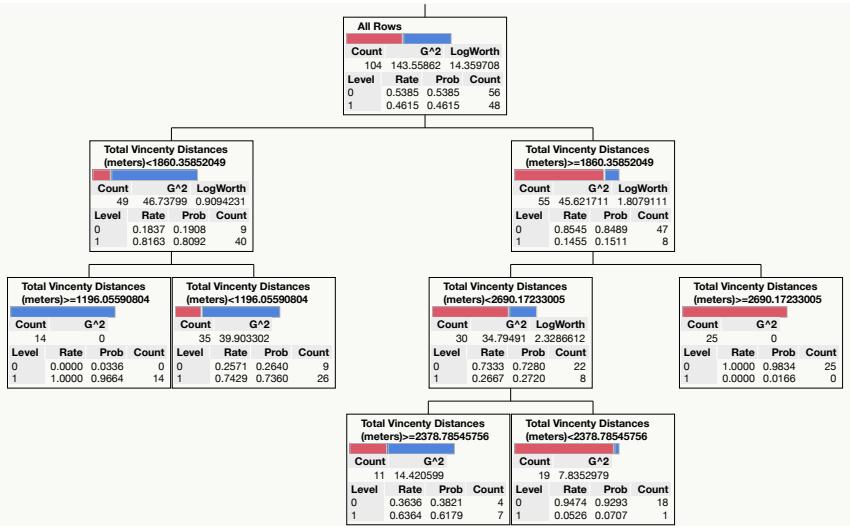

Figure 4-16. Using Classification (Decision) Tree, a categorical model was developed for packet counts = 1 when greater than or equal to 399.

In Figure 4-17, a logistic regression model is generated for packet counts =1 when greater than or equal to 399. A logistic regression model allows us to establish a relation between a binary packet count and a predictor travel distance variable, thereby leading to prediction formulas. The prediction formulas model the logit-transformed probability as a linear relationship with the predictor travel distance. A binary packet count can be represented as a zero/one or failure/success if the packet counts are subdivided based on the Quantiles. In other words, the prediction formulas give the most likely response as well as the probability of failure/success for each travel distance.

Logistic Plot

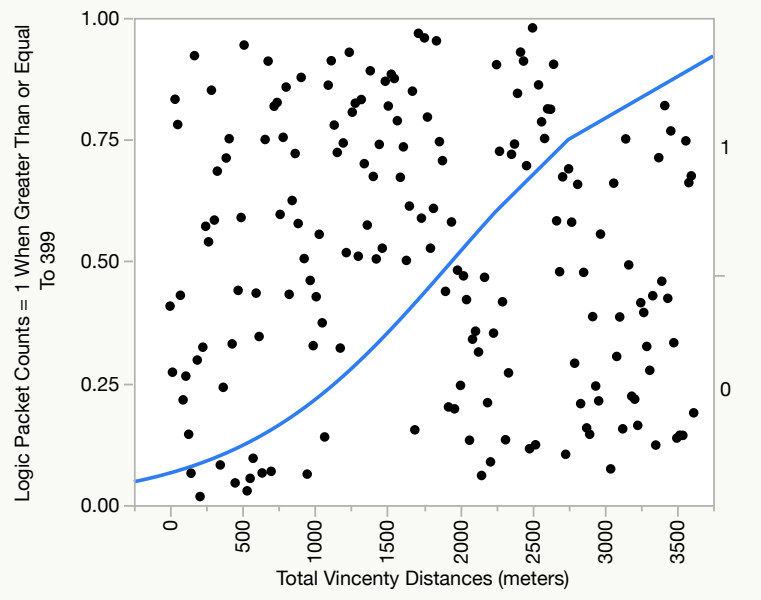

Figure 4-17. Using Logistic Regression, a categorical model was developed for packet counts = 1 when greater than or equal to 399.

Also, the binary packet counts are established as a zero (0) for values less than 399 and one (1) for values greater than or equal to 399 (i.e., 100 percent to 75 percent Quantiles). The horizontal axis contains the Total Vincenty Distance in meters, and the vertical axis contains the probability scale (i.e., 0.0 to 1.0). Each dot represents the actual Vincenty distance, in meters, along the horizontal axis. However, the dot is randomly placed along the vertical axis during the iteration process.

The confusion matrix has 64 predicted counts at zero with 14 misclassifications and 82 predicted counts at one with 15 misclassifications. The generalized R-Square is 0.4547 for training, 0.3840 for validation, and 0.4233 for testing.

In Figure 4-17, a neural network model is generated for packet counts =1 when greater than or equal to 377. To mitigate overfitting, the neural network model divides the original data into K subsets for a KFold validation. In turn, each of the K sets is used to validate the model fit on the rest of the data set and fitting a total of K models. Thus, the model selects the best validation statistic as a final model. A neural network model uses the following multi-layer functions:

a) Tangent Hyperbolic – The hyperbolic tangent function is a sigmoid function and the function transforms values to be between -1 and 1, which is a scaled version of the logistic function.
b) Linear – A linear function is most often used in the slope and intercept form.

c) Gaussian – A Gaussian function uses a radial basis function behavior, or when the response surface is Gaussian (normal) in shape.

The confusion matrix has 31 predicted counts at zero with 10 misclassifications and 131 predicted counts at one with 3 misclassifications. The generalized R-Square is 0.7069 for training, 0.6845 for validation, and 0.6698 for testing.

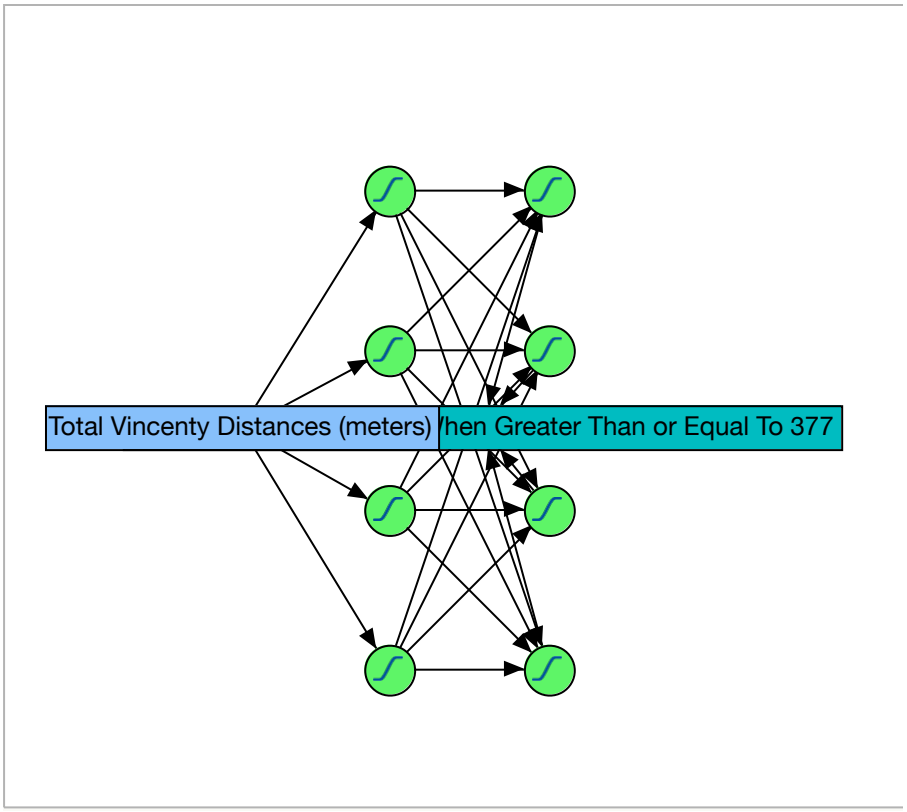

Figure 4-18. Using Neural Networks, a categorical model was developed for packet counts = 1 when greater than or equal to 377.

In Figure 4-19, there are 18 model comparisons of the packet counts and signal strengths at various thresholds. The objective is to compare the predictive ability of each model and measure the fit. Therefore, each row corresponds to a different model. As previously discussed, the most effective model is the neural network for packet counts =1 when greater than or equal to 377.

Model Comparison

Predictors

Measures of Fit for Logic Packet Counts = 1 When Greater Than or Equal To 400

Creator	.2 .4 .6 .8	Entropy RSquare	Generalized RSquare	Mean -Log p	RMSE	Mean Abs Dev	Misclassification Rate	N	AUC
Partition		0.5192	0.6842	0.3332	0.3249	0.2108	0.1429	175	0.9139
Fit Nominal Logistic		0.2782	0.4267	0.5003	0.4050	0.3341	0.2057	175	0.8383
Neural		0.5303	0.6941	0.3256	0.3136	0.2054	0.1314	175	0.9257

Measures of Fit for Logic Packet Counts = 1 When Greater Than or Equal To 399

Creator	.2 .4 .6 .8	Entropy RSquare	Generalized RSquare	Mean -Log p	RMSE	Mean Abs Dev	Misclassification Rate	N	AUC
Partition		0.5864	0.7407	0.2843	0.2890	0.1699	0.1086	175	0.9340
Fit Nominal Logistic		0.3020	0.4547	0.4797	0.3905	0.3218	0.1657	175	0.8506
Neural		0.6098	0.7597	0.2681	0.2800	0.1568	0.1086	175	0.9446

Measures of Fit for Logic Packet Counts = 1 When Greater Than or Equal To 377

Creator	.2 .4 .6 .8	Entropy RSquare	Generalized RSquare	Mean -Log p	RMSE	Mean Abs Dev	Misclassification Rate	N	AUC
Partition		0.4438	0.5777	0.3028	0.2965	0.1656	0.1086	175	0.9064
Fit Nominal Logistic		0.2401	0.3467	0.4137	0.3647	0.2618	0.2400	175	0.8355
Neural		0.5812	0.7069	0.228	0.2410	0.1160	0.0743	175	0.9307

Measures of Fit for Logic Standardized Signal A = 1 When Greater Than or Equal To Lambda = 0.000586

Creator	.2 .4 .6 .8	Entropy RSquare	Generalized RSquare	Mean -Log p	RMSE	Mean Abs Dev	Misclassification Rate	N	AUC
Partition		-0.004	-0.007	0.6938	0.5003	0.4958	0.4686	175	0.5000
Fit Nominal Logistic		-0.000	-0.001	0.6914	0.4991	0.4931	0.4686	175	0.5414
Neural		-0.004	-0.007	0.6938	0.5003	0.4958	0.4686	175	0.5000

Measures of Fit for Logic Standardized Signal A = 1 When Greater Than or Equal To Lambda = 0.110

Creator	.2 .4 .6 .8	Entropy RSquare	Generalized RSquare	Mean -Log p	RMSE	Mean Abs Dev	Misclassification Rate	N	AUC
Partition		0.5051	0.6709	0.3421	0.3336	0.2126	0.1600	175	0.9236
Fit Nominal Logistic		-0.001	-0.002	0.6919	0.4994	0.4979	0.4686	175	0.4510
Neural		0.5949	0.7485	0.28	0.2944	0.2068	0.1257	175	0.9681

Figure 4-19. A comparison of 18 categorical models with each row corresponding to different models.

In Figure 4-20, a predication graph is depicted with the neural network's probability profile for packet counts =1 when greater than or equal to 377. The probability is mapped against the total Vincenty distance on the x-axis. To mitigate overfitting, the neural network model uses K-Fold to divide the original data into K subsets, and each of the K sets is used to validate the model fit on the rest of the data (i.e., fitting a total of K models).

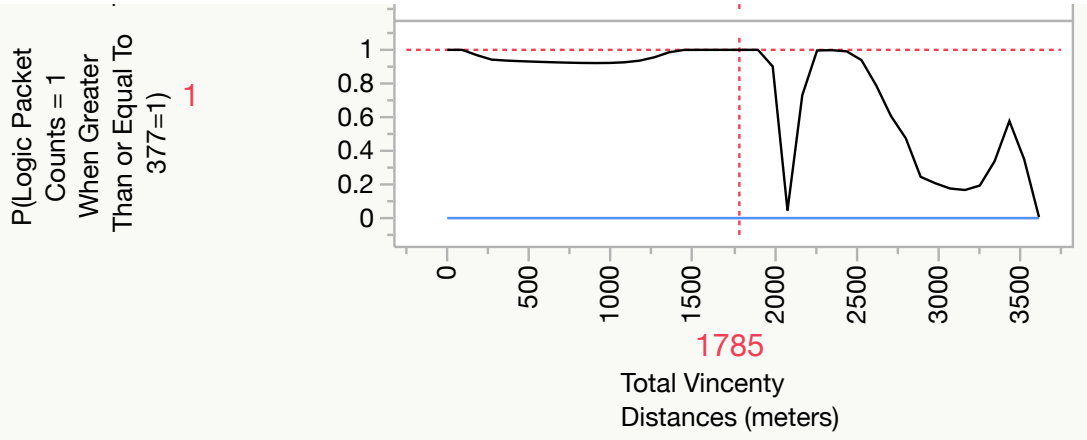

Figure 4-20. A predication graph is depicted with the neural network with misclassification of 0.0743 for a packet count threshold of 377.

In the next chapter, the neural network model will be utilized on a new data set, from a different location, to test our extended horizontal and vertical polarization models based on packet counts. The confusion matrix will be used to measure the effectiveness of the neural network model from a different location.

Section 4.6. References

[1] J. Walker and K. Heaslip, "A Low-Cost Real-World Planning Strategy For Deploying a Dedicated Short-Range Communications Roadside Unit on a Highway Off-Ramp," *Transportation Research Board*, pp. 1–19, 2017.

[2] J. Walker, "The Fundamental Principles of Antenna Theory for (V2I) Deployments," in *Vehicle-to-Vehicle and Vehicle-to-Infrastructure Communications: A Technical Approach*, F. Hu, Ed. Boca Raton: CRC Press: Taylor & Francis Group, 2018, pp. 207–220.

[3] M. T. Hayat, H. Park, and B. L. Smith, "Connected Vehicle Enabled Freeway Merge Assistance system-field test: Preliminary results of driver compliance to advisory," *IEEE Intelligent Vehicle Symposium Proceedings*, no. Iv, pp. 1017–1022, 2014.

[4] S. E. Shladover, C. Nowakowski, X.-Y. Lu, and R. Ferlis, "Cooperative Adaptive Cruise Control (CACC) Definitions and Operating Concepts," no. November 2014. p. 27.

[5] J. Fishelson, "Platooning Safety and Capacity in Automated Electric Transportation," Utah State University, 2013.

[6] E. Meissner, T. Chantem, and K. Heaslip, "Optimizing Departures of Automated Vehicles From Highways While Maintaining Mainline Capacity," *IEEE Transactions on Intelligent Transportation Systems.*, vol. 17, no. 12, pp. 3498–3511, Dec. 2016.

[7] D. Desiraju, T. Chantem, and K. Heaslip, "Minimizing the Disruption of Traffic Flow of Automated Vehicles During Lane Changes," *IEEE Transactions on Intelligent Transportation Systems.*, vol. 16, no. 3, pp. 1249–1258, Jun. 2015.

[8] National Highway Traffic Safety Administration (NHTSA), "Federal Motor Vehicle Safety Standards; V2V Communications." National Highway Traffic Safety Administration (NHTSA), Department of Transportation (DOT) ACTION:, Washington, D.C., pp. 1–392, 2016.

[9] Federal Highway Administration, "Crash Data Analyses for Vehicle-to- Infrastructure Communications for Safety Applications," Washington, D.C., 2012.

[10] J. Harding, G. Powell, R. Yoon, J. Fikentscher, C. Doyle, D. Sade, M. Lukuc, J. Simons, and J. Wang, "Vehicle-to-Vehicle Communications : Readiness of V2V Technology for Application," no. August. p. 327, 2014.

[11] National Highway Traffic Safety Administration (NHTSA), "Vehicle Safety Communications Project Final Report DOT HS 810 591," 2006.

[12] Federal Highway Administration, "2015 FHWA Vehicle to Infrastructure Deployment Guidance and Products." Washington, D.C., p. 30, 2014.

[13] D. Ou, Y. Yang, L. Xue, and D. Dong, "Optimal Connectivity-Based Deployment of Roadside Units for Vehicular Networks in Urban Areas," *Transportation Research Record: Journal of the Transportation Research Board*, vol. 2559, no. 2559, pp. 46–56, Jan. 2016.

[14] G. G. M. Nawaz Ali, P. H. J. Chong, S. K. Samantha, and E. Chan, “Efficient data dissemination in cooperative multi-RSU Vehicular Ad Hoc Networks (VANETs),” *Journal of Systems and Software*, vol. 117, pp. 508–527, Jul. 2016.
[15] M. Kafsi, P. Papadimitratos, O. Dousse, T. Alpcan, and J.-P. Hubaux, “VANET Connectivity Analysis,” 2009.
[16] T. Yan, W. Zhang, G. Wang, and Y. Zhang, “Access Points Planning in Urban Area for Data Dissemination to Drivers,” *IEEE Transactions on Vehicular Technology*, vol. 63, no. 1, pp. 390–402, Jan. 2014.
[17] C. M. Silva, W. Meira, and J. F. M. Sarubbi, “Non-Intrusive Planning the Roadside Infrastructure for Vehicular Networks,” *IEEE Transactions on Intelligent Transportation Systems.*, vol. 17, no. 4, pp. 938–947, 2016.
[18] O. Trullols, M. Fiore, C. Casetti, C. F. Chiasserini, and J. M. Barcelo Ordinas, “Planning roadside infrastructure for information dissemination in intelligent transportation systems,” *Computer Communications*, vol. 33, no. 4, pp. 432–442, 2010.
[19] V. D. Khairnar and S. N. Pradhan, “Simulation Based Evaluation of Highway Road Scenario between DSRC/802.11p MAC Protocol and STDMA for Vehicle-to-Vehicle Communication,” *Journal of Transportation Technologies*, vol. 3, no. 1, pp. 88–104, 2013.
[20] M. Shulman and R. K. Deering, “Third Annual Report of the Crash Avoidance Metrics Partnership, April 2003 - March 2004,” Washington, D.C., 2005.
[21] R. Miucic, Z. Popovic, and S. M. Mahmud, “Experimental characterization of DSRC signal strength drops,” in *2009 12th International IEEE Conference on Intelligent Transportation Systems*, 2009, pp. 1–5.
[22] E. Zöchmann, K. Guan, and M. Rupp, “Two-Ray Models in mmWave Communications,” pp. 225–229, 2017.
[23] IEEE Vehicular Technology Society Sponsored, *IEEE Standard for Wireless Access in Vehicular Environments (WAVE)— Networking Services IEEE*. New York: The Institute of Electrical and Electronics Engineers, Inc., 2016.
[24] V. Shivaldova, A. Winkelbauer, and C. F. Mecklenbrauker, “Signal-to-noise ratio modeling for vehicle-to-infrastructure communications,” *2014 IEEE 6th International Symposium on Wireless Vehicular Communications WiVeC 2014 - Proc.*, 2014.
[25] V. Shivaldova, A. Winkelbauer, and C. F. Mecklenbrauker, “Vehicular Link Performance: From Real-World Experiments to Reliability Models and Performance Analysis,” *IEEE Vehicular Technology Magazine*, vol. 8, no. 4, pp. 35–44, 2013.
[26] V. Shivaldova and C. F. Mecklenbräuker, “Quantization-based Complexity Reduction for Range-dependent Modified Gilbert Model,” *Proc. IEEE Sens. Array Multichannel Signal Process. Work.*, pp. 345–348, 2014.
[27] V. Shivaldova, A. Winkelbauer, and C. F. Mecklenbr, “Realistic Performance Model for Vehicle-to-Infrastructure Communications,” no. c, pp. 557–561, 2014.
[28] V. Shivaldova, A. Paier, D. Smely, and C. F. Mecklenbräuker, “On roadside unit antenna measurements for vehicle-to-infrastructure communications,” *IEEE International Symposium on Personal, Indoor and Mobile Radio Communications PIMRC*, pp. 1295–1299, 2012.
[29] W. H. Hayt, Jr., *Engineering Electromagnetics*, Fifth Edit. New York: McGraw-Hill, Inc., 1989.

[30] L. V. Bewley, *Two Dimensional Fields in Electrial Engineering*, 1st ed. New York: Dover Publications, 1963.
[31] D. Corson and P. Lorrain, *Introducing to Electromagnetic Fields and Waves*. San Franscisco: W.H. Freeman, 1962.
[32] R. Wilson, "Propagation Losses Through Common Building Materials 2.4 GHz vs 5 GHz," *Magis Network, Inc.*, pp. 1–28, 2002.
[33] R. E. Collins, *Antennas and Radio Wave Propagation*. New York: McGraw-Hill, Inc., 2014.
[34] S. L. Salas and E. Hille, *Calculus: One and Several Variables*, 3rd ed. John Wiley and Sons, Inc., 1978.
[35] R. Plonsey and R. E. Collin, *Principles and Applications of Electromagnetic Fields*. McGraw-Hill, Inc., 1961.
[36] M. Javid and P. M. Brown, *Field Analysis and Electromagnetics*. New York: McGraw-Hill, Inc., 1963.
[37] E. C. Jordan and K. G. Balmain, *Electromagnetic Waves and Radiating Systems*, 2nd ed. Englewood Cliffs: Dorling Kindesley Pearson Education, 2015.
[38] J. D. Kraus, *Electromagnetics*, 4th ed. New York: McGraw-Hill, Inc., 1992.
[39] J. E. Parton, S. J. . Owen, and M. S. Raven, *Applied Electromagnetics*. Palgrave Macmillan, 1985.
[40] D. T. Paris and F. K. Hurd, *Basic Electromagnetic Theory*. McGraw-Hill, Inc., 1969.
[41] R. C. Weast and S. M. Selby, Eds., *Standard Mathematical Tables*, Seventeent. The Chemical Rubber Co., 1969.
[42] S. Ramo, J. R. Whinnery, and T. Van Duzer, *Fields and Waves in Communication Electronics*, 3rd ed. New York: John Wiley and Sons, Inc., 2008.
[43] K. F. Sander and G. A. L. Reed, *Transmission and Propagation of Electromagnetic Waves*, 2nd ed. New York: Cambridge University Press, 1986.
[44] D. K. Cheng, *Field and Wave Electromagnetics*, Second Edi. Reading, Mass.: The Addison-Wesley, 1989.
[45] R. Valenzuela, "A ray tracing approach to predicting indoor wireless transmission," *IEEE 43rd Veh. Technol. Conf.*, pp. 214–218, 1993.
[46] A. M. Bodzin and L. Cirucci, "A Land-Use-Planning Simulation Using Google Earth.," *Sci. Scope*, vol. 32, no. 7, pp. 30–38, 2009.
[47] I. Janssen and A. Rosu, "Measuring sidewalk distances using Google earth," *BMC Med. Res. Methodol.*, vol. 12, no. 39, p. 10, 2012.
[48] S. Bayless, A. Guan, A. Shaw, M. Johnson, G. Pruitt, and B. Abernathy, "Recommended Practices for DSRC Licensing and Spectrum Management: A Guide for Management, Regulation, Deployment, and Administration for Connected Vehicle Environment.," 2015.
[49] F. C. Commission, "Equipment Authorization Order & Accredited Testing Laboratories FCC Equipment Authorization Process," 2017. [Online]. Available: https://transition.fcc.gov/oet/ea/presentations/files/may17/10-EA_Accredited-Labs-GT-Final.pdf.
[50] C. Kwok, R. F. Jr. Cleveland, and D. L. Means, "Evaluating Compliance with FCC Guidelines for Human Exposure to Radiofrequency Electromagnetic Fields Supplement C," 1997.

[51] J. D. M. S. J. L. U. Robert F. Cleveland and Standards, “OET bulletin 65: Evaluating compliance with FCC guidelines for human exposure to radiofrequency electromagnetic fields,” 1997.
[52] Cisco Systems, “White Paper on Antenna Patterns and Their Meaning,” San Jose, 2007.
[53] Linx Technology, “Application Note,” Merlin, 2012.
[54] A. S. C. of the I. A. and Propagation and Society, “IEEE Standard Definitions of Terms for Antennas,” 1993.
[55] Campbell Scientific, “The Link Budget and Fade Margin (Application Notes).” Campbell Scientific, Inc., Logan, 2016.
[56] T. Vincenty, “Direct and Inverse Solutions of Geodesics on the Ellipsoid With Application of Nested Equations,” *Surv. Rev.*, vol. 23, no. 176, pp. 88–93, 1975.
[57] T. Vincenty, “Geodetic inverse solution between antipodal points,” *Richard Rapp Geodetic Science Ohio State University*. 1975.

Chapter 5. Applying the Extended Horizontal and Vertical Polarization Model on a New Test Site to Ascertain the Null Points from a DSRC RSU

Section 5.1. Title

Applying the extended horizontal and vertical polarization model on a new test site to ascertain the null points from a DSRC RSU

Section 5.2. Abstract

The extended horizontal and vertical polarization model is applied on a new data set, from a different location, to test our model based on packet counts. The confusion matrix is used to measure the effectiveness of the neural network model from a different location. The extended model is applied to empirical data from the USDOT FHWA that required a secure testing facility. Therefore, the latitude and longitude coordinates were expunged to withhold the testing location and maintain a certain level of confidentiality.

Section 5.3. Materials and Methods (Study Background)

Section 5.3.1. Description of FHWA's DSRC RSU Field Test

This subsection focuses on describing the new field test environment where the DSRC RSU data set was retrieved. The field test was conducted by the USDOT FHWA at a secure testing facility with an open sky (i.e., for good GPS satellite reception) and limited infrastructure (e.g., no building, highway barriers). As shown in Figure 5-1, there are 10 different DSRC RSU data sets at 10 unique locations around a circular test track with packet counts ranging from 0 to 11. The DSRC RSUs are installed approximately 800 meters apart. There are six RSUs mounted approximately 3.048 meters (or 10 feet) from the ground: RSU-1, RSU-3, RSU-5, RSU-7, RSU-9, and RSU-11. There are four RSUs mounted approximately 6.096 meters (or 20 feet) from the ground: RSU-13, RSU-15, RSU-17, and RSU-19. The DSRC data set and test site are displayed, which allows the creation of customized maps based on the latitude and longitude coordinate on the surface of the earth [https://support.google.com/mymaps/answer/3024396].

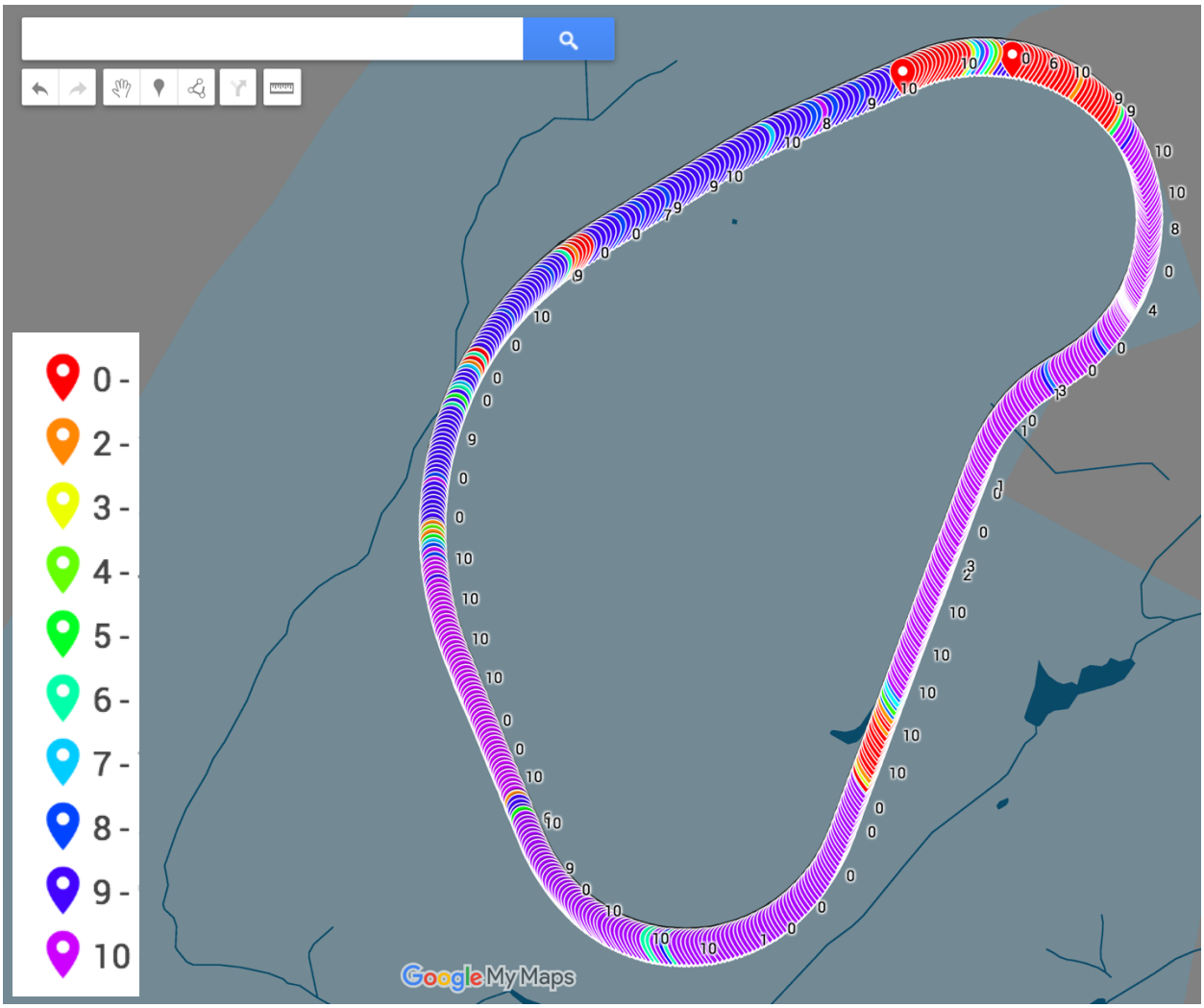

Figure 5-1. The new DSRC data set and test site are displayed, ranging from 0 to 10 packet counts, using Google My Maps.

Section 5.4. Determining and Using the Threshold based on Packet Counts to Investigate Potential Null Points (Step 2 and Step 4)

Based on the software design criterion to select thresholds to investigate potential null points. This subsection is focused on selecting potential packet counts thresholds. Based on the V2I safety application criterion, the statistical results should be used to determine potential null points from the packet counts.

Section 5.4.1. Determining and Using the Threshold based on Packet Counts to Investigate Potential Null Points (Step 2 and Step 4)

The vehicle testing segments (i.e., the region of interest) are based on each RSU's location as a frame of reference. For example, the packet counts from RSU-1 are depicted around a circular test track, in Figure 5-2, which is installed approximately 3.048 meters (or 10 feet) from the ground. The packet counts are detected near the DSRC RSU and 2,000 meters due to line-of-

sight RF propagation. At a rate of 10 times per second, the data acquisition system collected information from the DSRC RSU in a single test run (i.e., there were 10 data points per second). The 10 data points were averaged over one second because the data acquisition system had limited storage space.

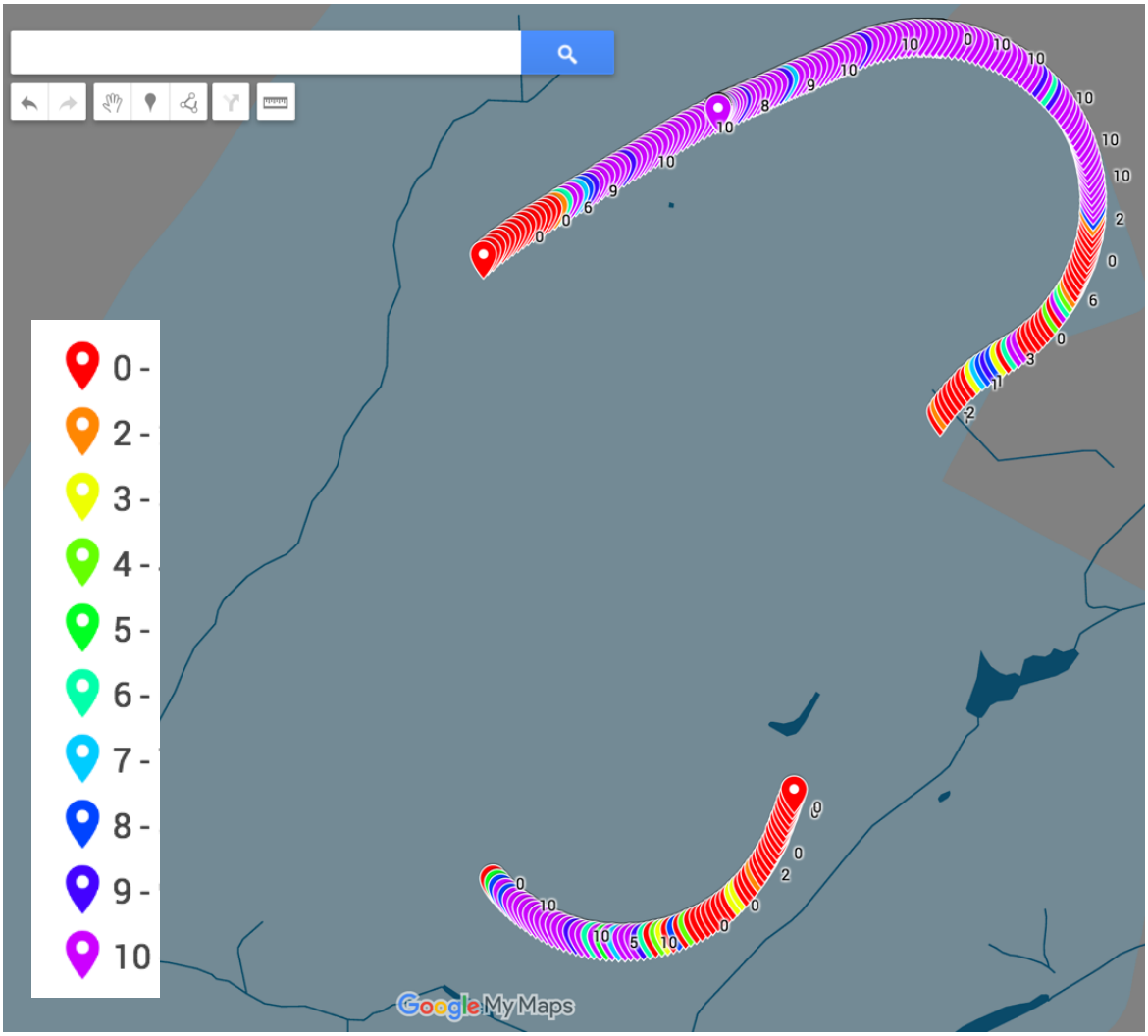

Figure 5-2. Packet counts from RSU-1 around a circular test track using Google My Maps.

As stated earlier, the packet counts criterion must be determined by the developer of the V2I safety application. Therefore, we selected an arbitrary criterion of 10 packet counts per second. Statistical analysis was used to adjust the threshold to investigate potential null points from the packet counts. In Figure 4-13, the packet counts are plotted against the vehicle travel distance to determine the potential null points based on three thresholds. For RSU-1, the three thresholds are for: a) Threshold 1 - packet counts greater than equal to 9, b) Threshold 2 - packet counts greater than equal to 8, and c) Threshold 3 - packet counts greater than equal to 7.

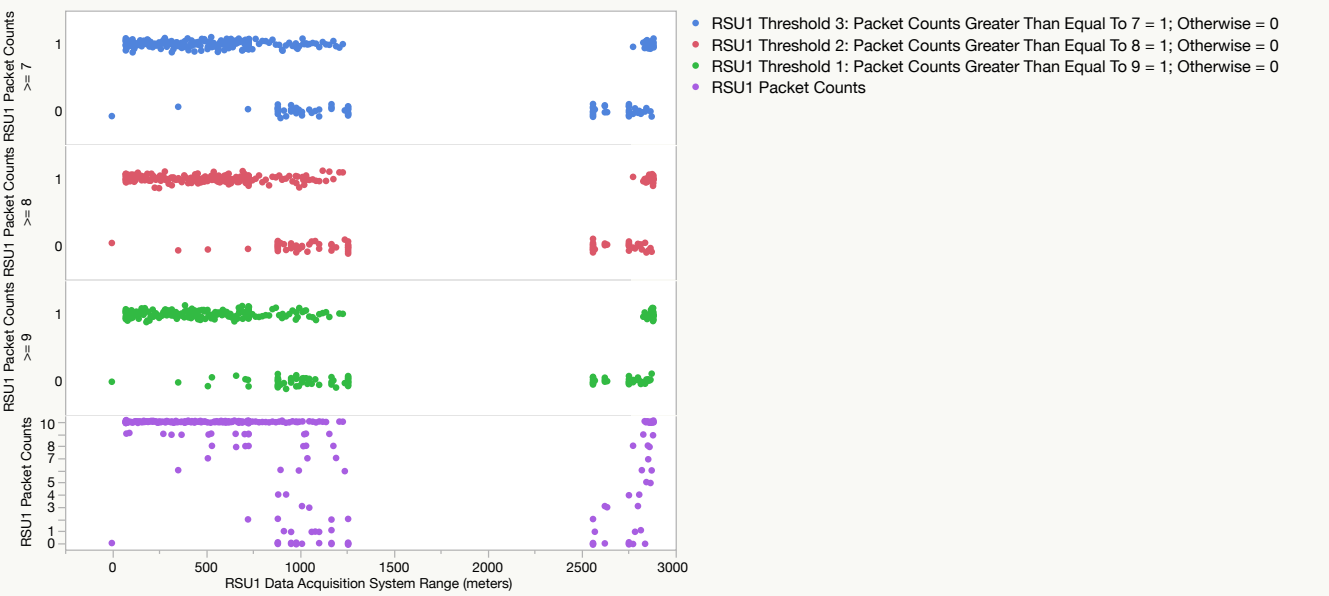

Figure 5-3. The three thresholds for packet counts from DSRC RSU-1

The packet counts from RSU-3 is depicted around a circular test track, in Figure 5-4, which is installed approximately 3.048 meters (or 10 feet) from the ground. The packet counts are detected near the DSRC RSU. At a rate of 10 times per second, the data acquisition system collected information from the DSRC RSU in a single test run (i.e., there were 10 data points per second). The 10 data points were averaged over one second because the data acquisition system had limited storage space. In Figure 4-13, the packet counts are plotted against the vehicle travel distance to determine the potential null points based on three thresholds. For RSU-3, the three thresholds are for: a) Threshold 1 - packet counts greater than equal to 9, b) Threshold 2 - packet counts greater than equal to 8, and c) Threshold 3 - packet counts greater than equal to 7.

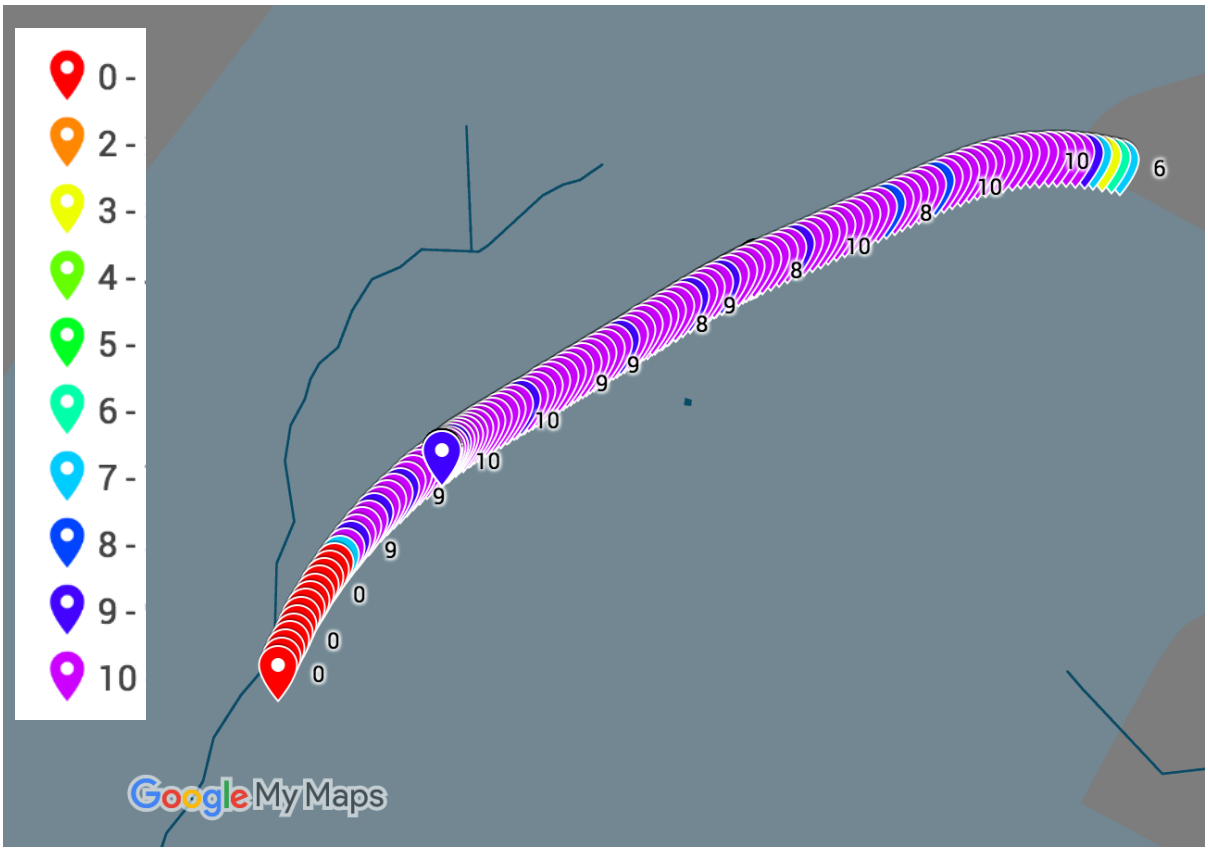

Figure 5-4. Packet counts from RSU-3 around a circular test track using Google My Maps.

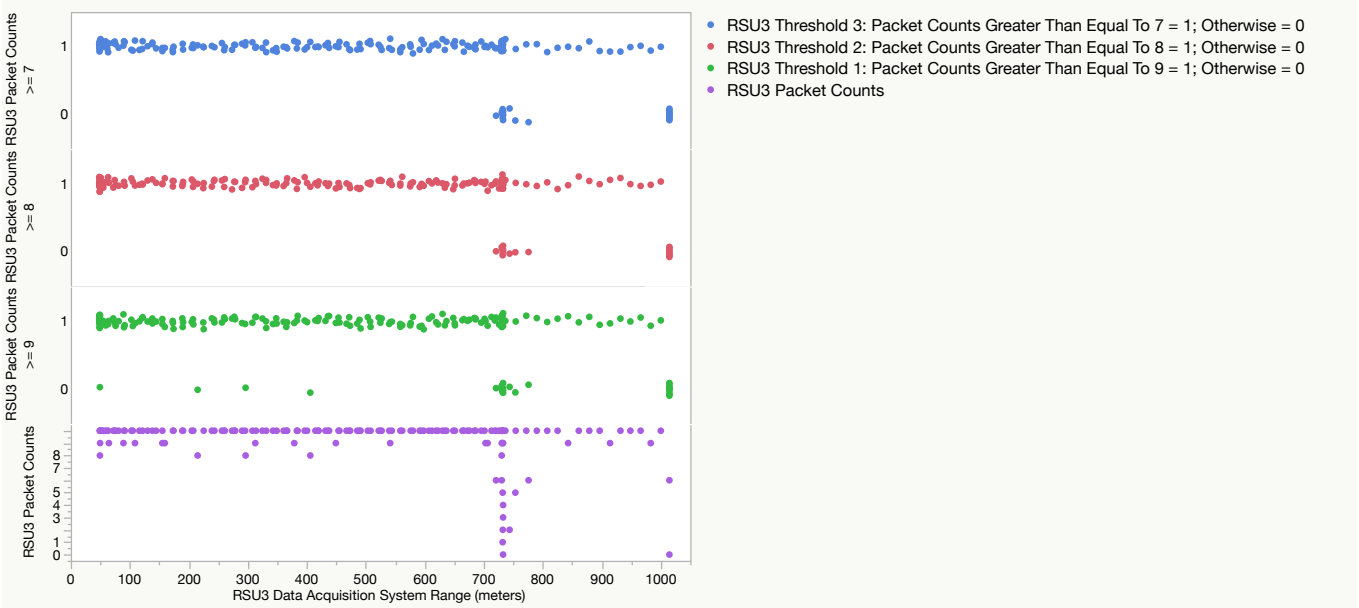

Figure 5-5. The three thresholds for packet counts from DSRC RSU-3

The packet counts from RSU-5 are depicted around a circular test track, in Figure 5-6, which is installed approximately 3.048 meters (or 10 feet) from the ground. The packet counts are

detected near the DSRC RSU. At a rate of 10 times per second, the data acquisition system collected information from the DSRC RSU in a single test run (i.e., there were 10 data points per second). The 10 data points were averaged over one second because the data acquisition system had limited storage space. In Figure 4-13, the packet counts are plotted against the vehicle travel distance to determine the potential null points based on three thresholds. For RSU-5, the three thresholds are for: a) Threshold 1 - packet counts greater than equal to 9, b) Threshold 2 - packet counts greater than equal to 8, and c) Threshold 3 - packet counts greater than equal to 7.

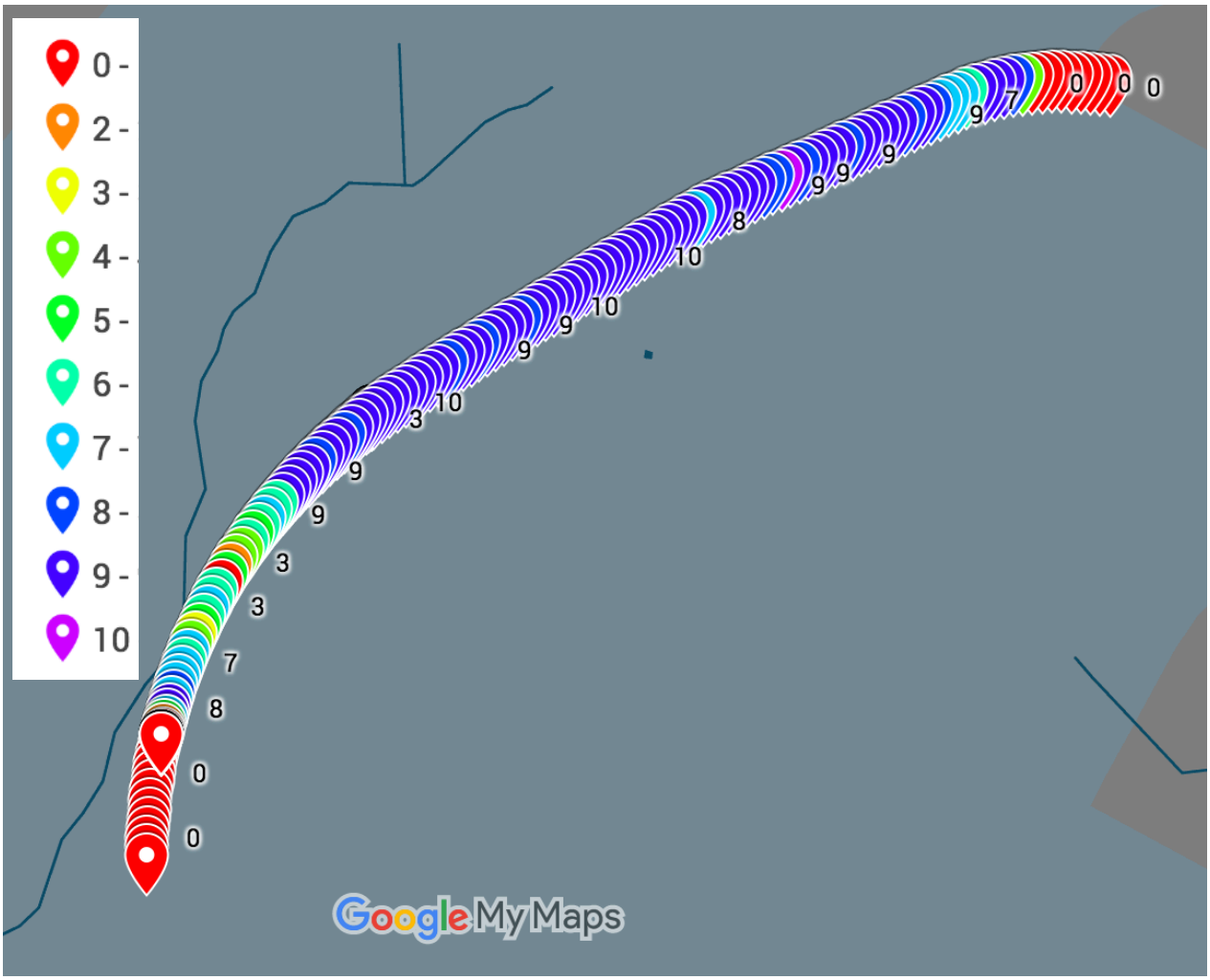

Figure 5-6. Packet counts from RSU-5 around a circular test track using Google My Maps.

Figure 5-7. The three thresholds for packet counts from DSRC RSU-5

The packet counts from RSU-7 are depicted around a circular test track, in Figure 5-8, which is installed approximately 3.048 meters (or 10 feet) from the ground. The packet counts are detected near the DSRC RSU. At a rate of 10 times per second, the data acquisition system collected information from the DSRC RSU in a single test run (i.e., there were 10 data points per second). The 10 data points were averaged over one second because the data acquisition system had limited storage space. In Figure 4-13, the packet counts are plotted against the vehicle travel distance to determine the potential null points based on three thresholds. For RSU-7, the three thresholds are for: a) Threshold 1 - packet counts greater than equal to 9, b) Threshold 2 - packet counts greater than equal to 8, and c) Threshold 3 - packet counts greater than equal to 7.

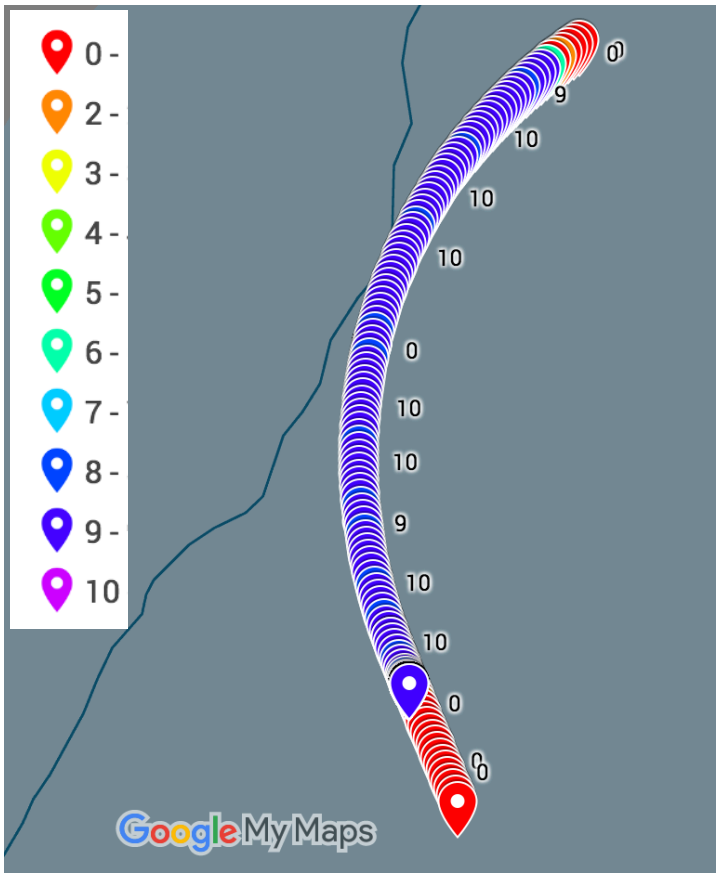

Figure 5-8. Packet counts from RSU-7 around a circular test track using Google My Maps.

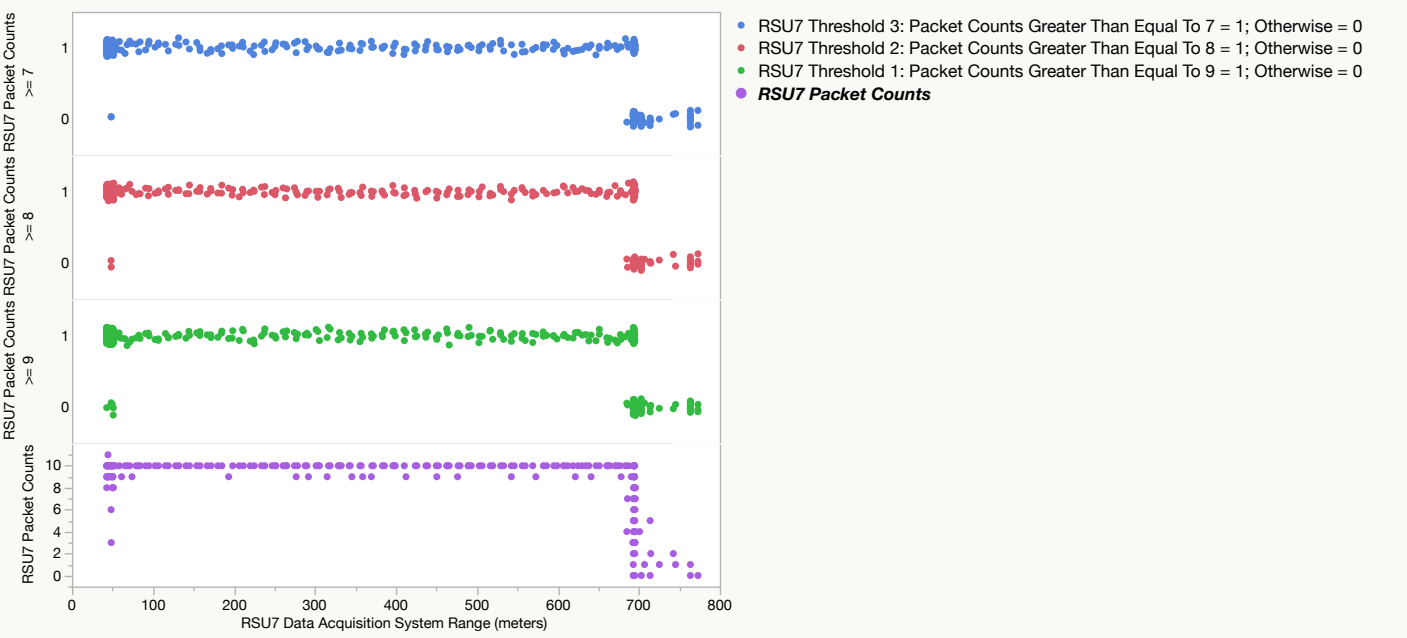

Figure 5-9. The three thresholds for packet counts from DSRC RSU-7

The packet counts from RSU-9 are depicted around a circular test track, in Figure 5-10, which is installed approximately 3.048 meters (or 10 feet) from the ground. The packet counts are detected near the DSRC RSU. At a rate of 10 times per second, the data acquisition system collected information from the DSRC RSU in a single test run (i.e., there were 10 data points per second). The 10 data points were averaged over one second because the data acquisition system had limited storage space. In Figure 4-13, the packet counts are plotted against the vehicle travel distance to determine the potential null points based on three thresholds. For RSU-9, the three thresholds are for: a) Threshold 1 - packet counts greater than equal to 9, b) Threshold 2 - packet counts greater than equal to 8, and c) Threshold 3 - packet counts greater than equal to 7.

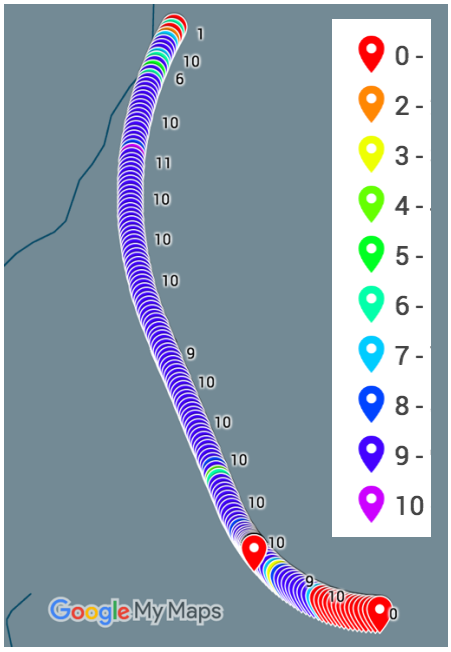

Figure 5-10. Packet counts from RSU-9 around a circular test track using Google My Maps.

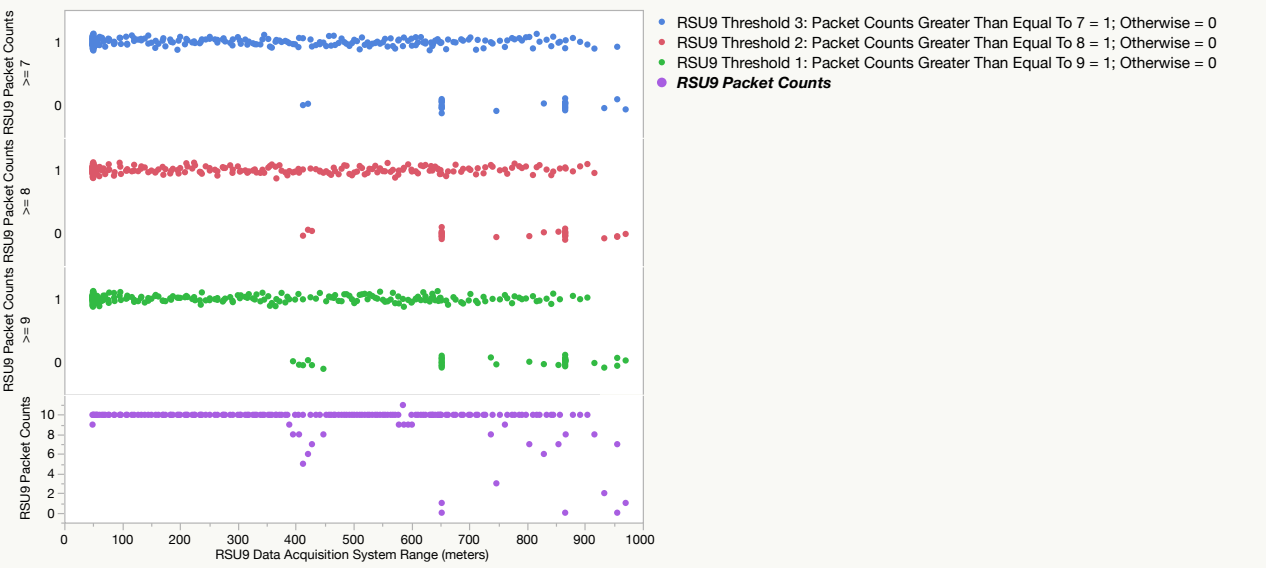

Figure 5-11. The three thresholds for packet counts from DSRC RSU-9

The packet counts from RSU-11 are depicted around a circular test track, in Figure 5-12, which is installed approximately 3.048 meters (or 10 feet) from the ground. The packet counts are detected near the DSRC RSU. At a rate of 10 times per second, the data acquisition system collected information from the DSRC RSU in a single test run (i.e., there were 10 data points per second). The 10 data points were averaged over one second because the data acquisition system had limited storage space. In Figure 4-13, the packet counts are plotted against the vehicle travel distance to determine the potential null points based on three thresholds. For RSU-13, the three thresholds are for: a) Threshold 1 -packet counts greater than equal to 9, b) Threshold 2 - packet counts greater than equal to 8, and c) Threshold 3 - packet counts greater than equal to 7.

Figure 5-12. Packet counts from RSU-11 around a circular test track using Google My Maps.

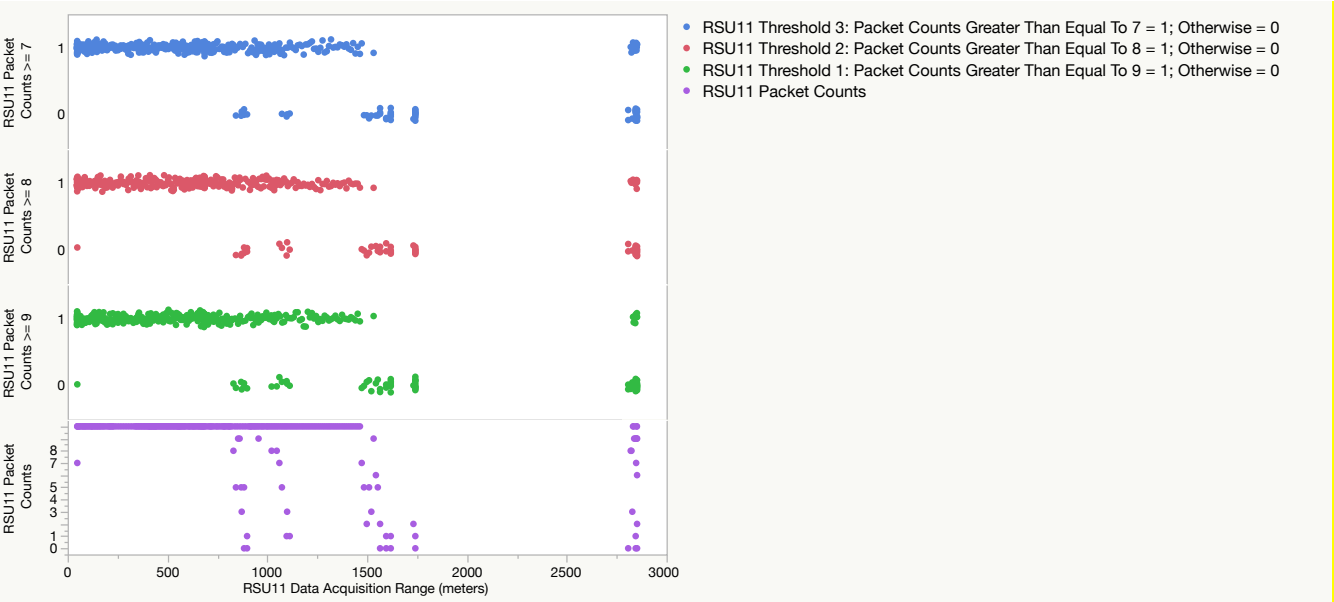

Figure 5-13. The three thresholds for packet counts from DSRC RSU-11

The packet counts from RSU-13 is depicted around a circular test track, in Figure 5-14, which is installed approximately 6.096 meters (or 20 feet) from the ground. The packet counts are detected near the DSRC RSU. The packet counts are detected near the DSRC RSU and 2,000 meters due to line-of-sight RF propagation. At a rate of 10 times per second, the data acquisition system collected information from the DSRC RSU in a single test run (i.e., there were 10 data points per second). In Figure 4-13, the packet counts are plotted against the vehicle travel distance to determine the potential null points based on three thresholds. For RSU-13, the three thresholds are for: a) Threshold 1 -packet counts greater than equal to 9, b) Threshold 2 - packet counts greater than equal to 8, and c) Threshold 3 - packet counts greater than equal to 7.

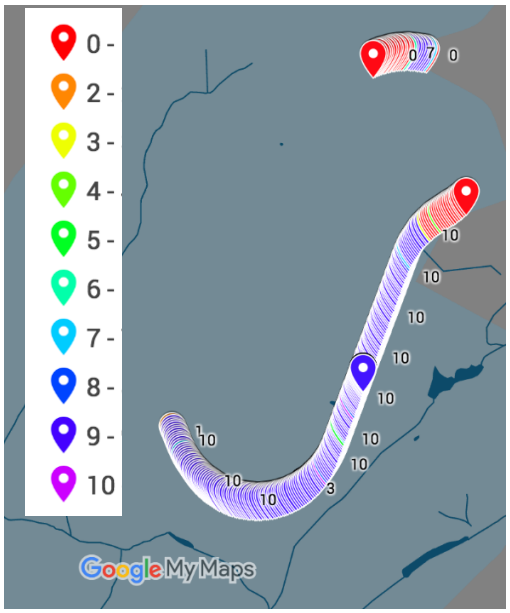

Figure 5-14. Packet counts from RSU-13 around a circular test track using Google My Maps.

Figure 5-15. The three thresholds for packet counts from DSRC RSU-13

The packet counts from RSU-15 are depicted around a circular test track, in Figure 5-16, which is installed approximately 6.096 meters (or 20 feet) from the ground. The packet counts are detected near the DSRC RSU. At a rate of 10 times per second, the data acquisition system collected information from the DSRC RSU in a single test run (i.e., there were 10 data points per second). The 10 data points were averaged over one second because the data acquisition system had limited storage space. In Figure 4-13, the packet counts are plotted against the vehicle travel distance to determine the potential null points based on three thresholds. For RSU-15, the three

thresholds are for: a) Threshold 1 -packet counts greater than equal to 9, b) Threshold 2 - packet counts greater than equal to 8, and c) Threshold 3 - packet counts greater than equal to 7.

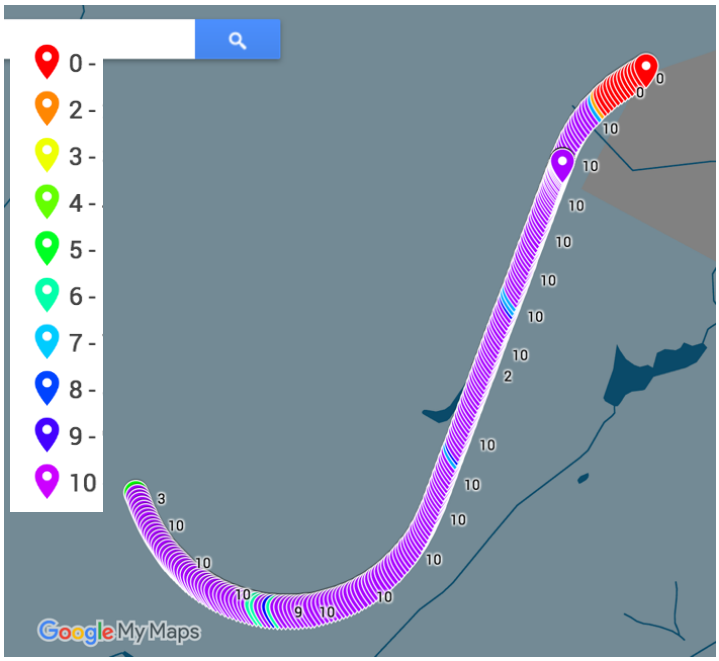

Figure 5-16. Packet counts from RSU-15 around a circular test track using Google My Maps.

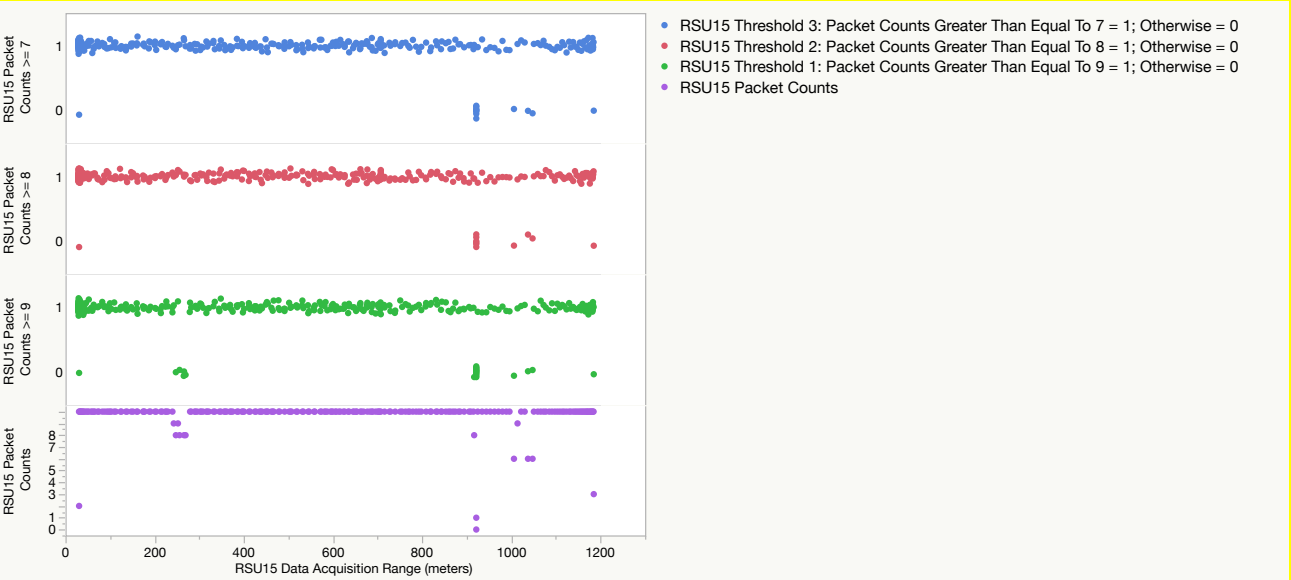

Figure 5-17. The three thresholds for packet counts from DSRC RSU-15

The packet counts from RSU-17 are depicted around a circular test track, in Figure 5-18, which is installed approximately 6.096 meters (or 20 feet) from the ground. The packet counts are detected near the DSRC RSU. At a rate of 10 times per second, the data acquisition system collected information from the DSRC RSU in a single test run (i.e., there were 10 data points per second). The 10 data points were averaged over one second because the data acquisition system

had limited storage space. In Figure 4-13, the packet counts are plotted against the vehicle travel distance to determine the potential null points based on three thresholds. For RSU-17, the three thresholds are for: a) Threshold 1 -packet counts greater than equal to 9, b) Threshold 2 - packet counts greater than equal to 8, and c) Threshold 3 - packet counts greater than equal to 7.

Figure 5-18. Packet counts from RSU-17 around a circular test track using Google My Maps.

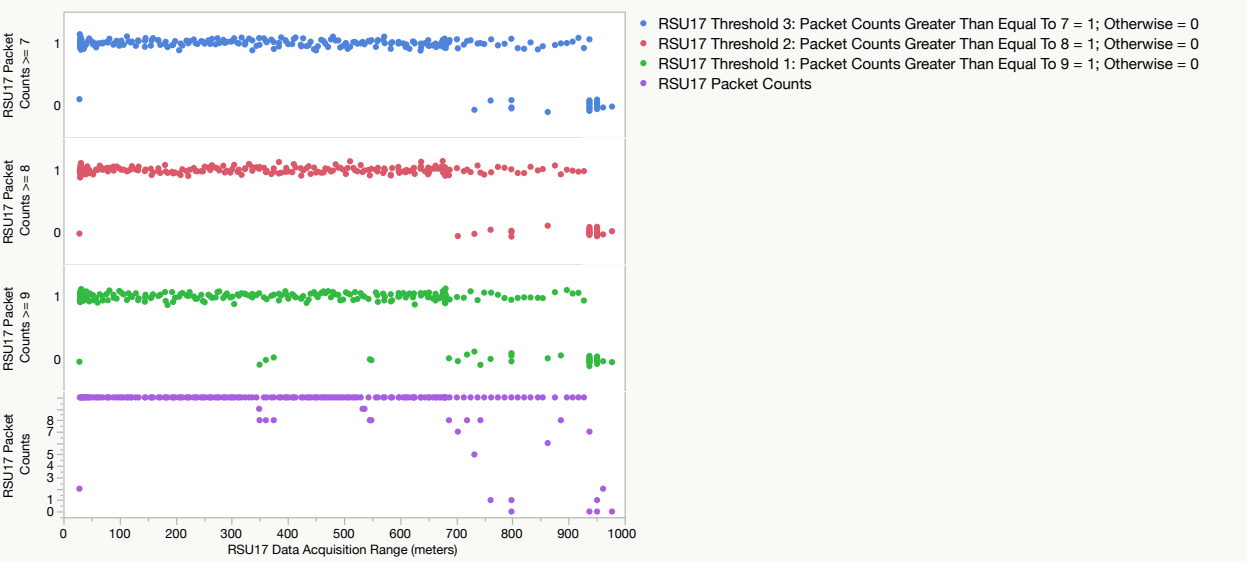

Figure 5-19. The three thresholds for packet counts from DSRC RSU-17

The packet counts from RSU-19 are depicted around a circular test track, in Figure 5-20, which is installed approximately 6.096 meters (or 20 feet) from the ground. The packet counts are

detected near the DSRC RSU. At a rate of 10 times per second, the data acquisition system collected information from the DSRC RSU in a single test run (i.e., there were 10 data points per second). The 10 data points were averaged over one second because the data acquisition system had limited storage space. In Figure 4-13, the packet counts are plotted against the vehicle travel distance to determine the potential null points based on three thresholds. For RSU-19, the three thresholds are for: a) Threshold 1 -packet counts greater than equal to 9, b) Threshold 2 - packet counts greater than equal to 8, and c) Threshold 3 - packet counts greater than equal to 7.

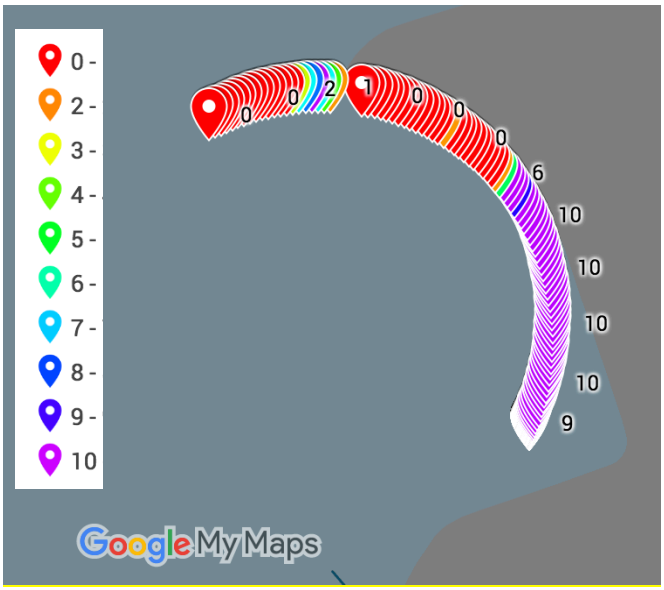

Figure 5-20. Packet counts from RSU-19 around a circular test track using Google My Maps.

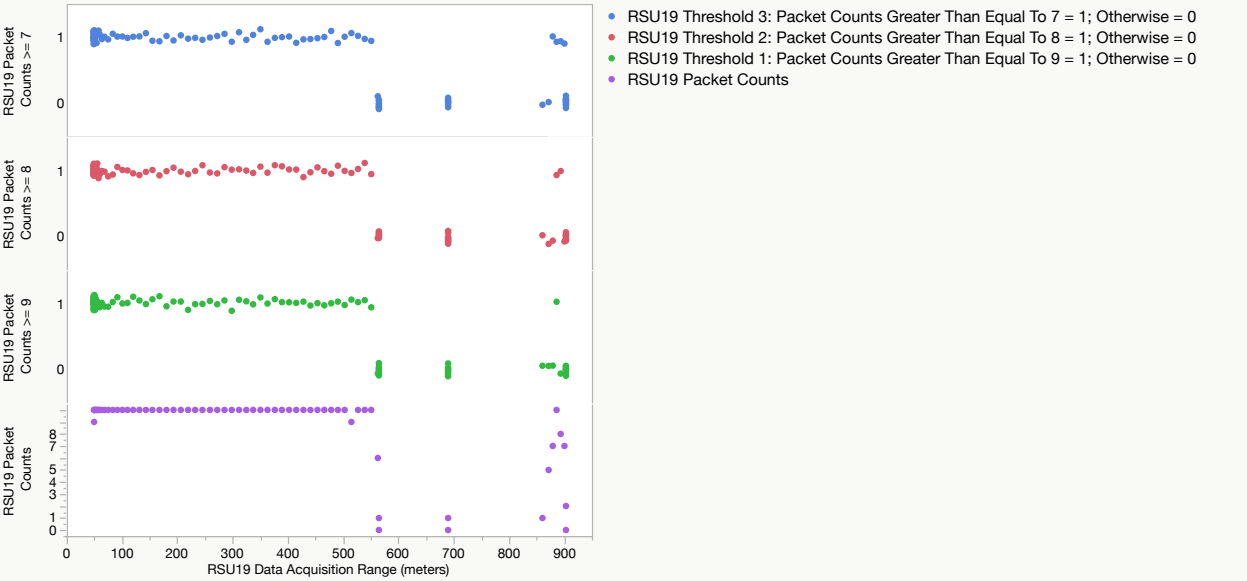

Figure 5-21. The three thresholds for packet counts from DSRC RSU-19

Section 5.4.2. Developing Categorical Models Using Packet Counts and Signal Strength Threshold (Step 6)

This subsection utilizes a statistical categorical variable model to develop a predictive formula by converting results of the packet counts into binary data (i.e., one or zero). Based on the previous chapter, the neural network model is utilized on the new data set, from a different location, to test our extended horizontal and vertical polarization models based on packet counts. The confusion matrix is used to measure the effectiveness of the neural network model from a different location.

In Figure 5-22 (top), neural network models are generated for DSRC RSU1 using three thresholds: a) Threshold 1 = packet counts greater than and equal to 9, b) Threshold 2 = packet counts greater than and equal to 8, and c) Threshold 3 = packet counts greater than and equal to 7. The objective is to compare the predictive ability of each model and measure the fit. Therefore, each row corresponds to a different model. The misclassification rates are 0.1206, 0.1143, and 0.1143, respectively. In Figure 5-22 (bottom), a predication graph is depicted with the neural network's probability profile for a logic 1 and logic 0 based on the three thresholds. From the right, the predication graph is for RSU1 using Threshold 1 for a logic 1 and logic 0. The two center predication graphs are for RSU1 using Threshold 2 for a logic 1 and logic 0. On the left, the predication graph is for RSU1 using Threshold 3 for a logic 1 and logic 0. To mitigate overfitting, the neural network model uses K-Fold to divide the original data into K subsets and each of the K sets is used to validate the model fit on the rest of the data (i.e., fitting a total of K models).

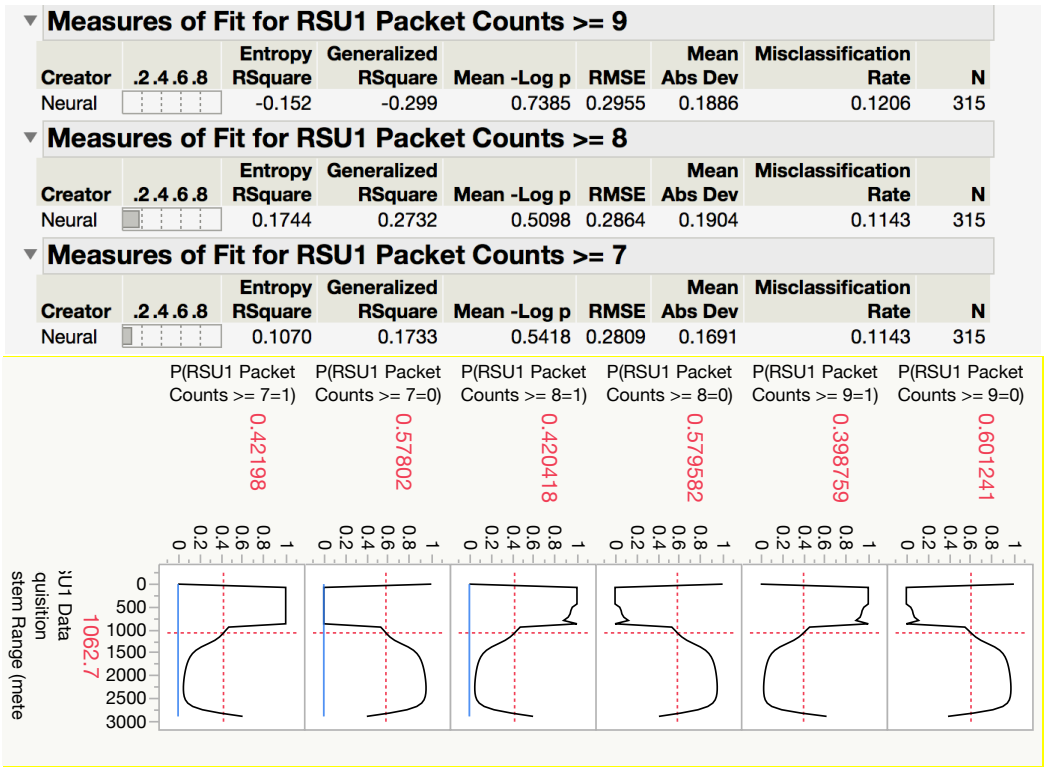

Measures of Fit for RSU1 Packet Counts >= 9

Creator	.2 .4 .6 .8	Entropy RSquare	Generalized RSquare	Mean -Log p	RMSE	Mean Abs Dev	Misclassification Rate	N
Neural		-0.152	-0.299	0.7385	0.2955	0.1886	0.1206	315

Measures of Fit for RSU1 Packet Counts >= 8

Creator	.2 .4 .6 .8	Entropy RSquare	Generalized RSquare	Mean -Log p	RMSE	Mean Abs Dev	Misclassification Rate	N
Neural		0.1744	0.2732	0.5098	0.2864	0.1904	0.1143	315

Measures of Fit for RSU1 Packet Counts >= 7

Creator	.2 .4 .6 .8	Entropy RSquare	Generalized RSquare	Mean -Log p	RMSE	Mean Abs Dev	Misclassification Rate	N
Neural		0.1070	0.1733	0.5418	0.2809	0.1691	0.1143	315

Figure 5-22. Using neural networks models on DSRC RSU1 data set, a comparison of three thresholds is generated along with the misclassification rating [top image] and predication graph for each threshold for both a logic 0 and logic 1 [bottom image].

In Figure 5-23 (top), neural network models are generated for DSRC RSU3 using three thresholds: a) Threshold 1 = packet counts greater than and equal to 9, b) Threshold 2 = packet counts greater than and equal to 8, and c) Threshold 3 = packet counts greater than and equal to 7. The objective is to compare the predictive ability of each model and measure the fit. Therefore, each row corresponds to a different model. The misclassification rates are 0.0860, 0.0588, and 0.0588, respectively. In Figure 5-23 (bottom), a predication graph is depicted with the neural network's probability profile for a logic 1 and logic 0 based on the three thresholds. From the right, the predication graph is for RSU3 using Threshold 1 for a logic 1 and logic 0. The two center predication graphs are for RSU3 using Threshold 2 for a logic 1 and logic 0. On the left, the predication graph is for RSU3 using Threshold 3 for a logic 1 and logic 0. To mitigate overfitting, the neural network model uses K-Fold to divide the original data into K subsets, and each of the K sets is used to validate the model fit on the rest of the data (i.e., fitting a total of K models).

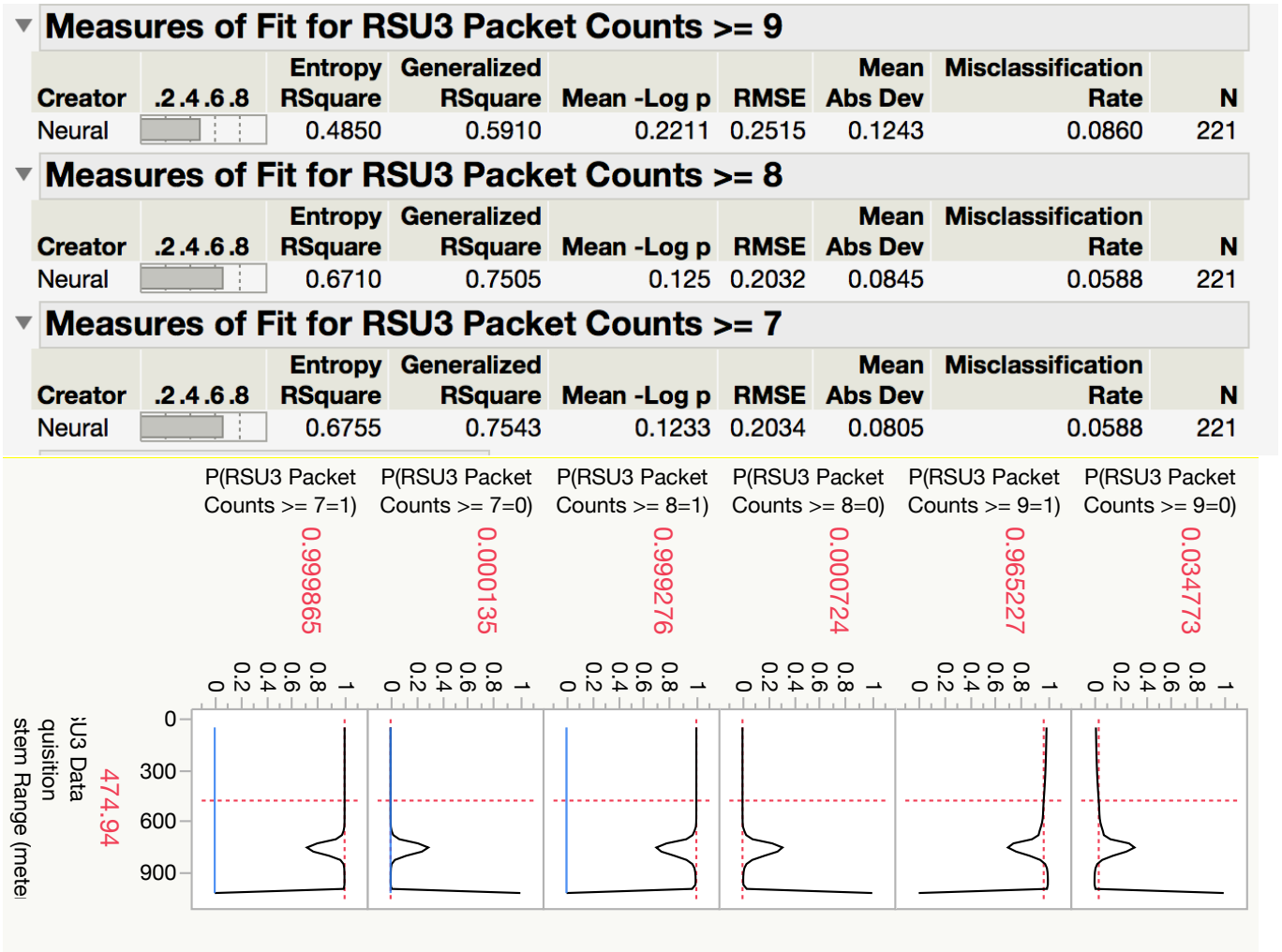

Measures of Fit for RSU3 Packet Counts >= 9

Creator	.2 .4 .6 .8	Entropy RSquare	Generalized RSquare	Mean -Log p	RMSE	Mean Abs Dev	Misclassification Rate	N
Neural		0.4850	0.5910	0.2211	0.2515	0.1243	0.0860	221

Measures of Fit for RSU3 Packet Counts >= 8

Creator	.2 .4 .6 .8	Entropy RSquare	Generalized RSquare	Mean -Log p	RMSE	Mean Abs Dev	Misclassification Rate	N
Neural		0.6710	0.7505	0.125	0.2032	0.0845	0.0588	221

Measures of Fit for RSU3 Packet Counts >= 7

Creator	.2 .4 .6 .8	Entropy RSquare	Generalized RSquare	Mean -Log p	RMSE	Mean Abs Dev	Misclassification Rate	N
Neural		0.6755	0.7543	0.1233	0.2034	0.0805	0.0588	221

Figure 5-23. Using neural networks models on DSRC RSU3 data set, a comparison of three thresholds is generated along with the misclassification rating [top image] and predication graph for each threshold for both a logic 0 and logic 1 [bottom image].

In Figure 5-24 (top), neural network models are generated for DSRC RSU5 using three thresholds: a) Threshold 1 = packet counts greater than and equal to 9, b) Threshold 2 = packet counts greater than and equal to 8, and c) Threshold 3 = packet counts greater than and equal to 7. The objective is to compare the predictive ability of each model and measure the fit. Therefore, each row corresponds to a different model. The misclassification rates are 0.1171, 0.0927, and 0.0707, respectively. In Figure 5-24 (bottom), a predication graph is depicted with the neural network's probability profile for a logic 1 and logic 0 based on the three thresholds. From the right, the predication graph is for RSU5 using Threshold 1 for a logic 1 and logic 0. The two center predication graphs are for RSU5 using Threshold 2 for a logic 1 and logic 0. On the left, the predication graph is for RSU5 using Threshold 3 for a logic 1 and logic 0. To mitigate overfitting, the neural network model uses K-Fold to divide the original data into K subsets, and each of the K sets is used to validate the model fit on the rest of the data (i.e., fitting a total of K models).

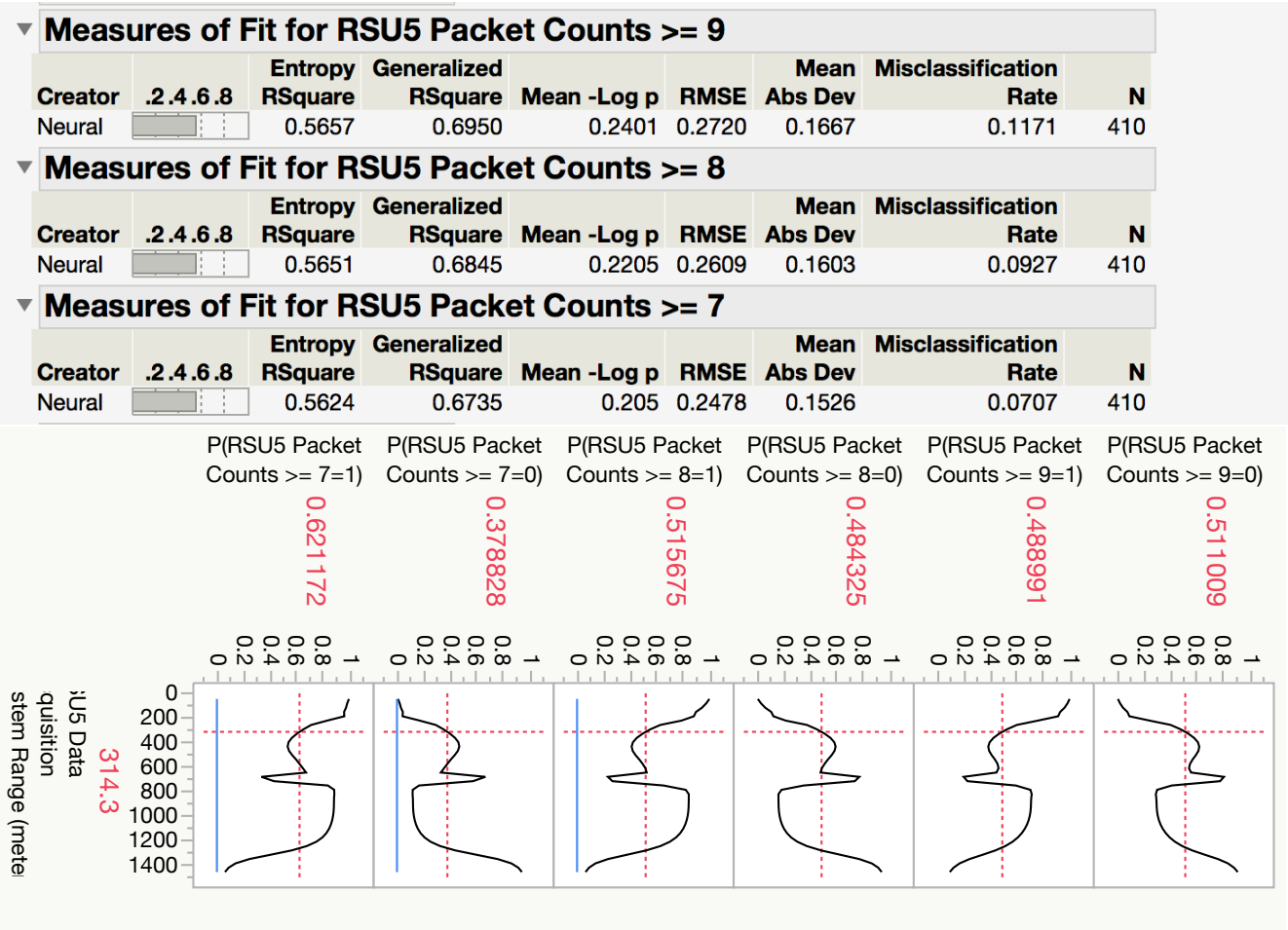

Figure 5-24. Using neural networks models on DSRC RSU5 data set, a comparison of three thresholds is generated along with the misclassification rating [Top image] and predication graph for each threshold for both a logic 0 and logic 1.

In Figure 5-25 (top), neural network models are generated for DSRC RSU7 using three thresholds: a) Threshold 1 = packet counts greater than and equal to 9, b) Threshold 2 = packet counts greater than and equal to 8, and c) Threshold 3 = packet counts greater than and equal to 7. The objective is to compare the predictive ability of each model and measure the fit. Therefore, each row corresponds to a different model. The misclassification rates are 0.1248, 0.1280, and 0.1137, respectively. In Figure 5-25 (bottom), a predication graph is depicted with the neural network's probability profile for a logic 1 and logic 0 based on the three thresholds. From the right, the predication graph is for RSU7 using Threshold 1 for a logic 1 and logic 0. The two center predication graphs are for RSU7 using Threshold 2 for a logic 1 and logic 0. On the left, the predication graph is for RSU7 using Threshold 3 for a logic 1 and logic 0. To mitigate overfitting, the neural network model uses K-Fold to divide the original data into K subsets, and each of the K sets is used to validate the model fit on the rest of the data (i.e., fitting a total of K models).

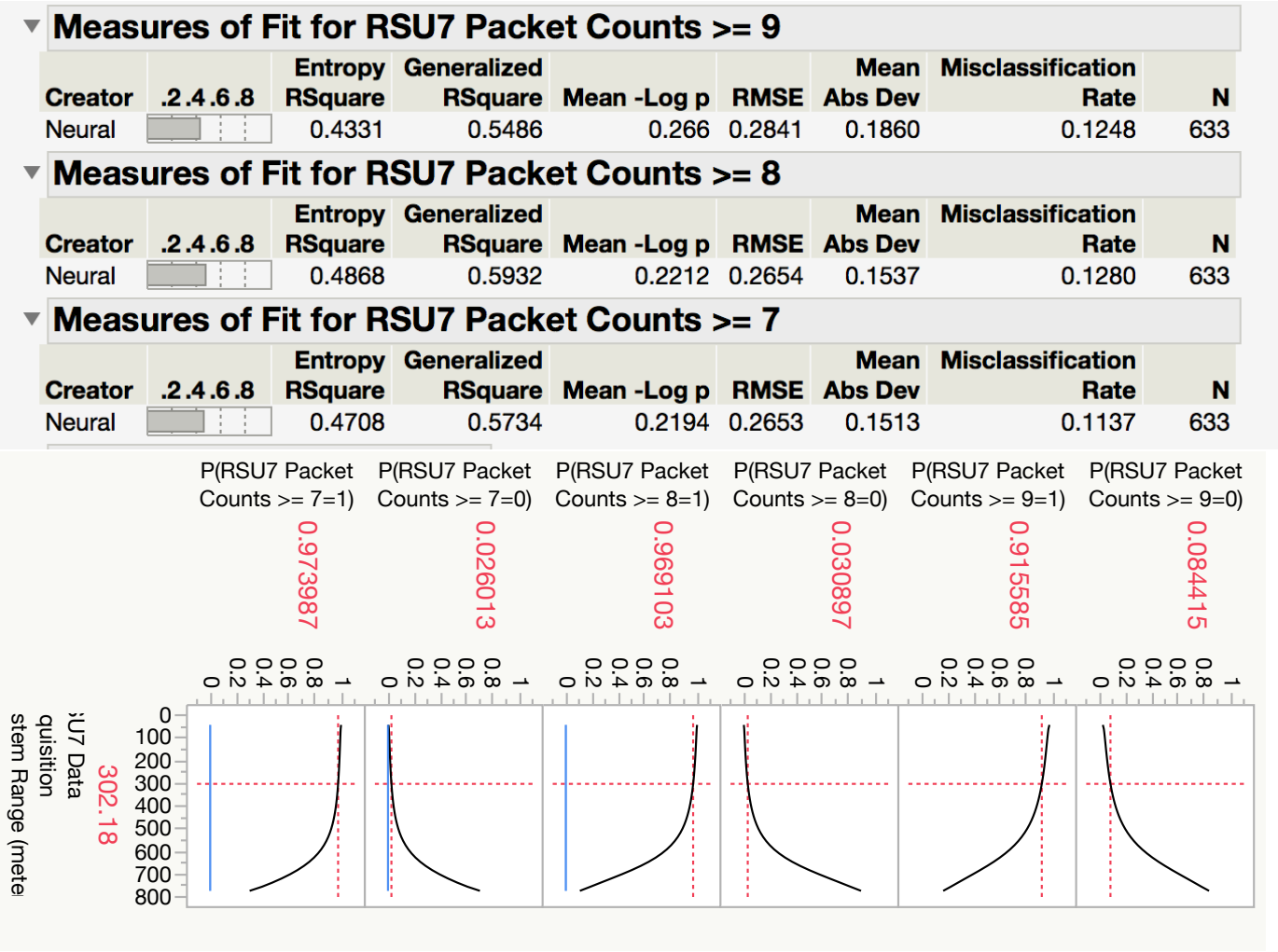

Figure 5-25. Using neural networks models on DSRC RSU7 data set, a comparison of three thresholds is generated along with the misclassification rating [Top image] and predication graph for each threshold for both a logic 0 and logic 1.

In Figure 5-26 (top), neural network models are generated for DSRC RSU9 using three thresholds: a) Threshold 1 = packet counts greater than and equal to 9, b) Threshold 2 = packet counts greater than and equal to 8, and c) Threshold 3 = packet counts greater than and equal to 7. The objective is to compare the predictive ability of each model and measure the fit. Therefore, each row corresponds to a different model. The misclassification rates are 0.0705, 0.0992, and 0.0914, respectively. In Figure 5-26 (bottom), a predication graph is depicted with the neural network's probability profile for a logic 1 and logic 0 based on the three thresholds. From the right, the predication graph is for RSU9 using Threshold 1 for a logic 1 and logic 0. The two center predication graphs are for RSU9 using Threshold 2 for a logic 1 and logic 0. On the left, the predication graph is for RSU9 using Threshold 3 for a logic 1 and logic 0. To mitigate overfitting, the neural network model uses K-Fold to divide the original data into K subsets, and each of the K sets is used to validate the model fit on the rest of the data (i.e., fitting a total of K models).

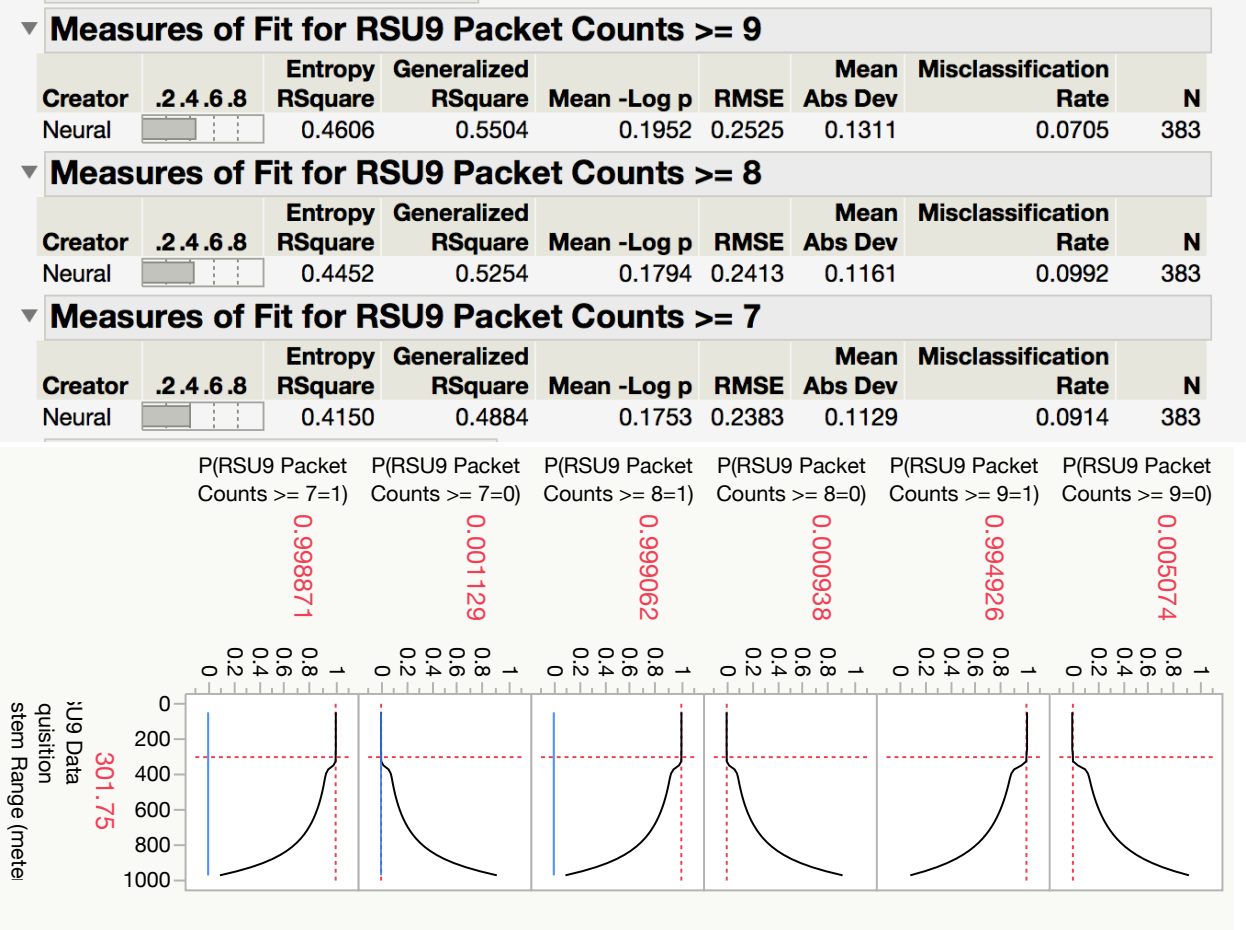

Measures of Fit for RSU9 Packet Counts >= 9

Creator	.2 .4 .6 .8	Entropy RSquare	Generalized RSquare	Mean -Log p	RMSE	Mean Abs Dev	Misclassification Rate	N
Neural		0.4606	0.5504	0.1952	0.2525	0.1311	0.0705	383

Measures of Fit for RSU9 Packet Counts >= 8

Creator	.2 .4 .6 .8	Entropy RSquare	Generalized RSquare	Mean -Log p	RMSE	Mean Abs Dev	Misclassification Rate	N
Neural		0.4452	0.5254	0.1794	0.2413	0.1161	0.0992	383

Measures of Fit for RSU9 Packet Counts >= 7

Creator	.2 .4 .6 .8	Entropy RSquare	Generalized RSquare	Mean -Log p	RMSE	Mean Abs Dev	Misclassification Rate	N
Neural		0.4150	0.4884	0.1753	0.2383	0.1129	0.0914	383

Figure 5-26. Using neural networks models on DSRC RSU9 data set, a comparison of three thresholds is generated along with the misclassification rating [Top image] and predication graph for each threshold for both a logic 0 and logic 1.

In Figure 5-27 (top), a neural network models are generated for DSRC RSU11 using three thresholds: a) Threshold 1 = packet counts greater than and equal to 9, b) Threshold 2 = packet

counts greater than and equal to 8, and c) Threshold 3 = packet counts greater than and equal to 7. The objective is to compare the predictive ability of each model and measure the fit. Therefore, each row corresponds to a different model. The misclassification rates are 0.0619, 0.0597, and 0.0553, respectively. In Figure 5-27 (bottom), a predication graph is depicted with the neural network's probability profile for a logic 1 and logic 0 based on the three thresholds. From the right, the predication graph is for RSU11 using Threshold 1 for a logic 1 and logic 0. The two center predication graphs are for RSU11 using Threshold 2 for a logic 1 and logic 0. On the left, the predication graph is for RSU11 using Threshold 3 for a logic 1 and logic 0. To mitigate overfitting, the neural network model uses K-Fold to divide the original data into K subsets, and each of the K sets is used to validate the model fit on the rest of the data (i.e., fitting a total of K models).

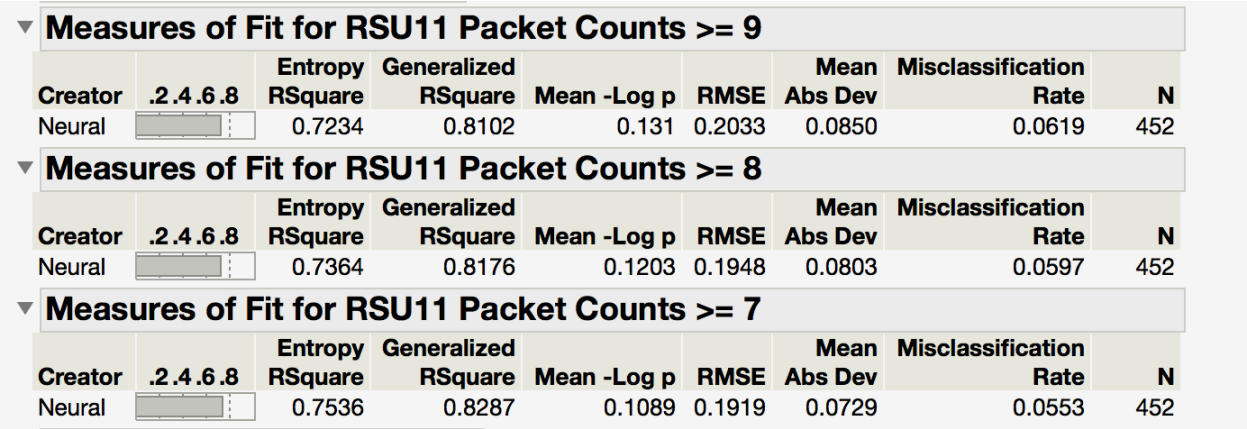

Measures of Fit for RSU11 Packet Counts >= 9

Creator	.2 .4 .6 .8	Entropy RSquare	Generalized RSquare	Mean -Log p	RMSE	Mean Abs Dev	Misclassification Rate	N
Neural		0.7234	0.8102	0.131	0.2033	0.0850	0.0619	452

Measures of Fit for RSU11 Packet Counts >= 8

Creator	.2 .4 .6 .8	Entropy RSquare	Generalized RSquare	Mean -Log p	RMSE	Mean Abs Dev	Misclassification Rate	N
Neural		0.7364	0.8176	0.1203	0.1948	0.0803	0.0597	452

Measures of Fit for RSU11 Packet Counts >= 7

Creator	.2 .4 .6 .8	Entropy RSquare	Generalized RSquare	Mean -Log p	RMSE	Mean Abs Dev	Misclassification Rate	N
Neural		0.7536	0.8287	0.1089	0.1919	0.0729	0.0553	452

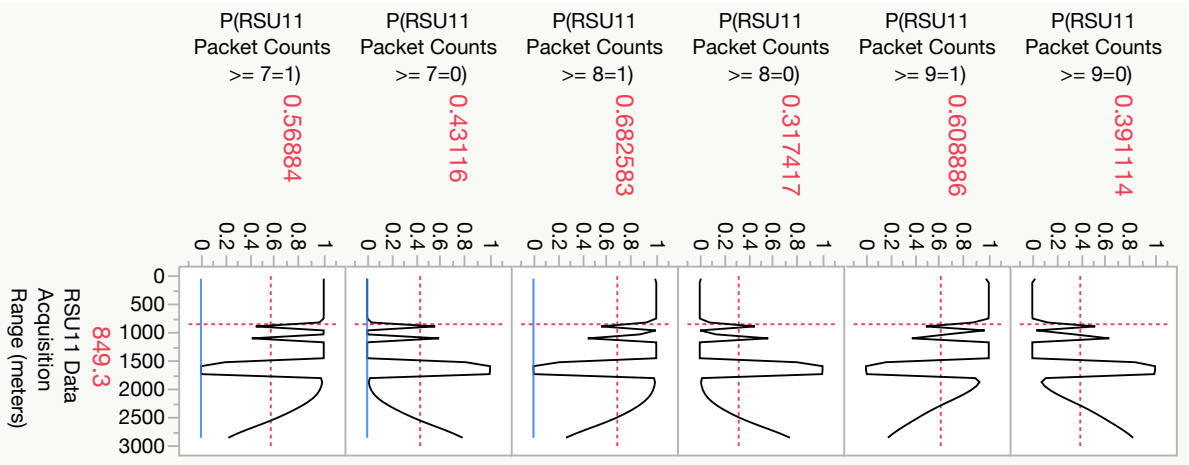

Figure 5-27. Using neural networks models on DSRC RSU11 data set, a comparison of three thresholds is generated along with the misclassification rating [Top image] and predication graph for each threshold for both a logic 0 and logic 1.

In Figure 5-28 (top), neural network models are generated for DSRC RSU13 using three thresholds: a) Threshold 1 = packet counts greater than and equal to 9, b) Threshold 2 = packet counts greater than and equal to 8, and c) Threshold 3 = packet counts greater than and equal to 7. The objective is to compare the predictive ability of each model and measure the fit.

Therefore, each row corresponds to a different model. The misclassification rates are 0.0411, 0.0329, and 0.0356, respectively. In Figure 5-28 (bottom), a predication graph is depicted with the neural network's probability profile for a logic 1 and logic 0 based on the three thresholds. From the right, the predication graph is for RSU13 using Threshold 1 for a logic 1 and logic 0. The two center predication graphs are for RSU13 using Threshold 2 for a logic 1 and logic 0. On the left, the predication graph is for RSU13 using Threshold 3 for a logic 1 and logic 0. To mitigate overfitting, the neural network model uses K-Fold to divide the original data into K subsets, and each of the K sets is used to validate the model fit on the rest of the data (i.e., fitting a total of K models).

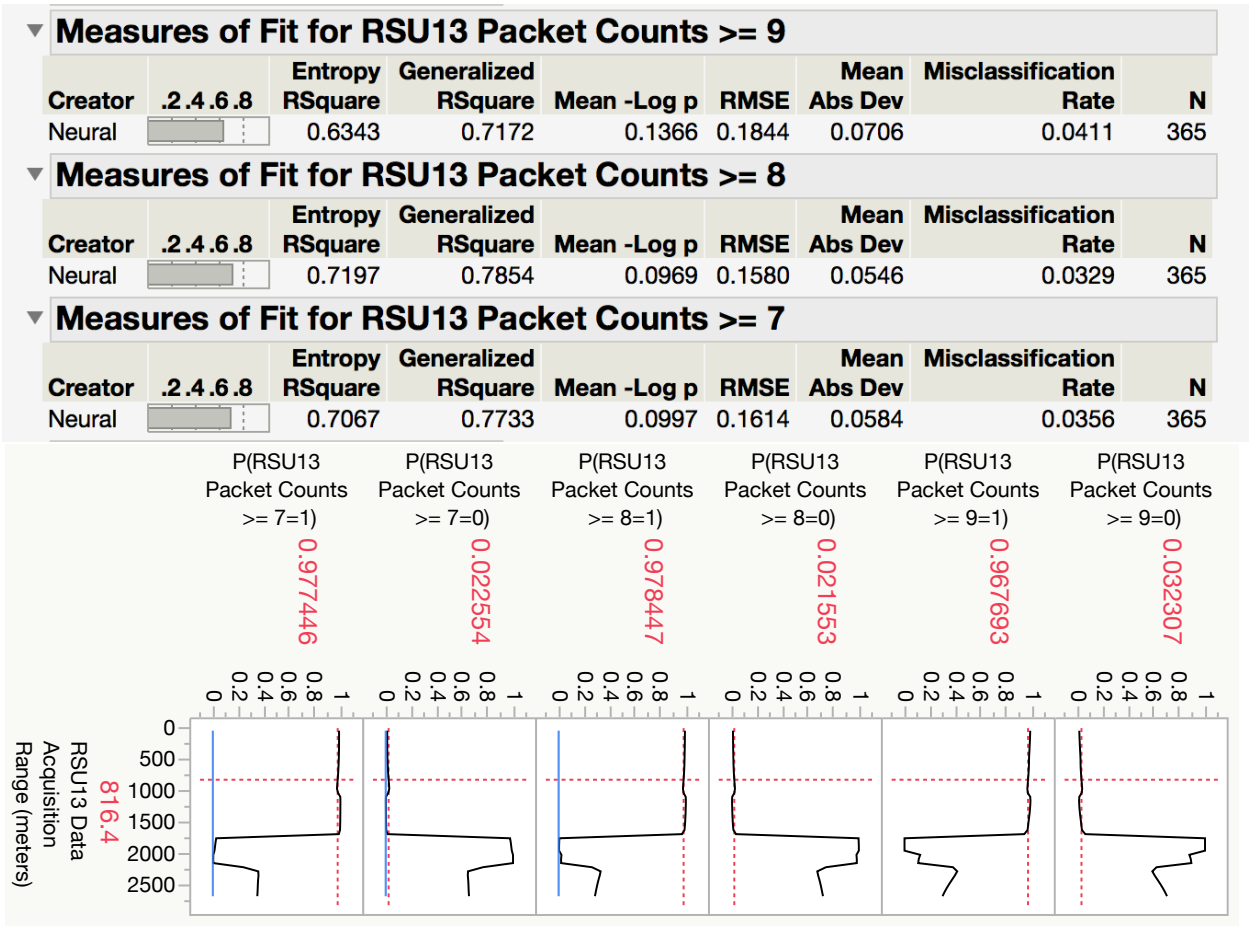

Figure 5-28. Using neural networks models on DSRC RSU13 data set, a comparison of three thresholds is generated along with the misclassification rating [Top image] and predication graph for each threshold for both a logic 0 and logic 1.

In Figure 5-29 (top), a neural network models are generated for DSRC RSU15 using three thresholds: a) Threshold 1 = packet counts greater than and equal to 9, b) Threshold 2 = packet counts greater than and equal to 8, and c) Threshold 3 = packet counts greater than and equal to 7. The objective is to compare the predictive ability of each model and measure the fit. Therefore, each row corresponds to a different model. The misclassification rates are 0.0352, 0.0282, and 0.0258, respectively. In Figure 5-29 (bottom), a predication graph is depicted with

the neural network's probability profile for a logic 1 and logic 0 based on the three thresholds. From the right, the predication graph is for RSU15 using Threshold 1 for a logic 1 and logic 0. The two center predication graphs are for RSU15 using Threshold 2 for a logic 1 and logic 0. On the left, the predication graph is for RSU15 using Threshold 3 for a logic 1 and logic 0. To mitigate overfitting, the neural network model uses K-Fold to divide the original data into K subsets, and each of the K sets is used to validate the model fit on the rest of the data (i.e., fitting a total of K models).

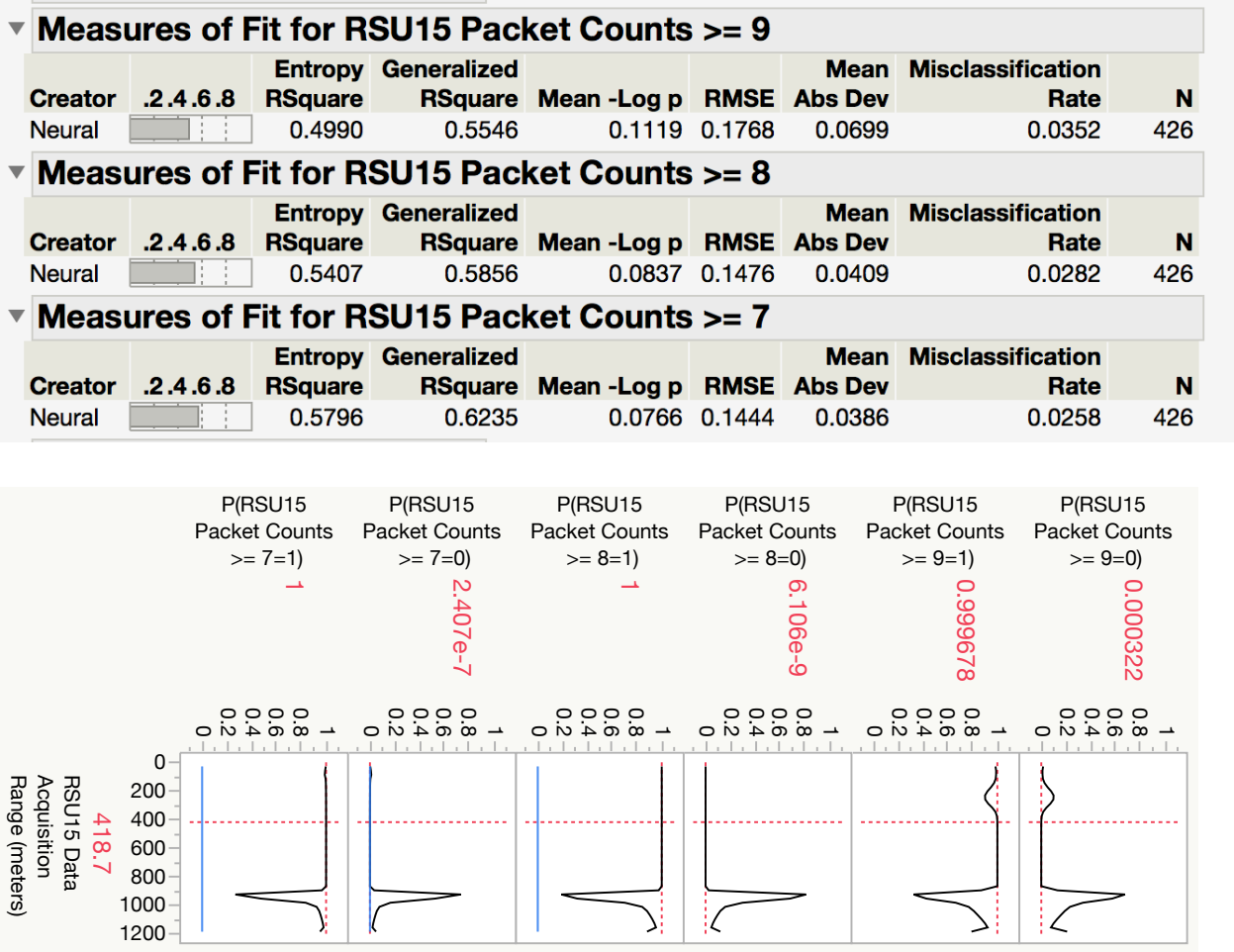

Measures of Fit for RSU15 Packet Counts >= 9

Creator	.2 .4 .6 .8	Entropy RSquare	Generalized RSquare	Mean -Log p	RMSE	Mean Abs Dev	Misclassification Rate	N
Neural		0.4990	0.5546	0.1119	0.1768	0.0699	0.0352	426

Measures of Fit for RSU15 Packet Counts >= 8

Creator	.2 .4 .6 .8	Entropy RSquare	Generalized RSquare	Mean -Log p	RMSE	Mean Abs Dev	Misclassification Rate	N
Neural		0.5407	0.5856	0.0837	0.1476	0.0409	0.0282	426

Measures of Fit for RSU15 Packet Counts >= 7

Creator	.2 .4 .6 .8	Entropy RSquare	Generalized RSquare	Mean -Log p	RMSE	Mean Abs Dev	Misclassification Rate	N
Neural		0.5796	0.6235	0.0766	0.1444	0.0386	0.0258	426

Figure 5-29. Using neural networks models on DSRC RSU15 data set, a comparison of three thresholds is generated along with the misclassification rating [Top image] and predication graph for each threshold for both a logic 0 and logic 1.

In Figure 5-30 (top), a neural network models are generated for DSRC RSU17 using three thresholds: a) Threshold 1 = packet counts greater than and equal to 9, b) Threshold 2 = packet counts greater than and equal to 8, and c) Threshold 3 = packet counts greater than and equal to 7. The objective is to compare the predictive ability of each model and measure the fit. Therefore, each row corresponds to a different model. The misclassification rates are 0.0919, 0.0662, and 0.0625, respectively. In Figure 5-30 (bottom), a predication graph is depicted with the neural network's probability profile for a logic 1 and logic 0 based on the three thresholds. From the right, the predication graph is for RSU17 using Threshold 1 for a logic 1 and logic 0.

The two center predication graphs are for RSU17 using Threshold 2 for a logic 1 and logic 0. On the left, the predication graph is for RSU17 using Threshold 3 for a logic 1 and logic 0. To mitigate overfitting, the neural network model uses K-Fold to divide the original data into K subsets, and each of the K sets is used to validate the model fit on the rest of the data (i.e., fitting a total of K models).

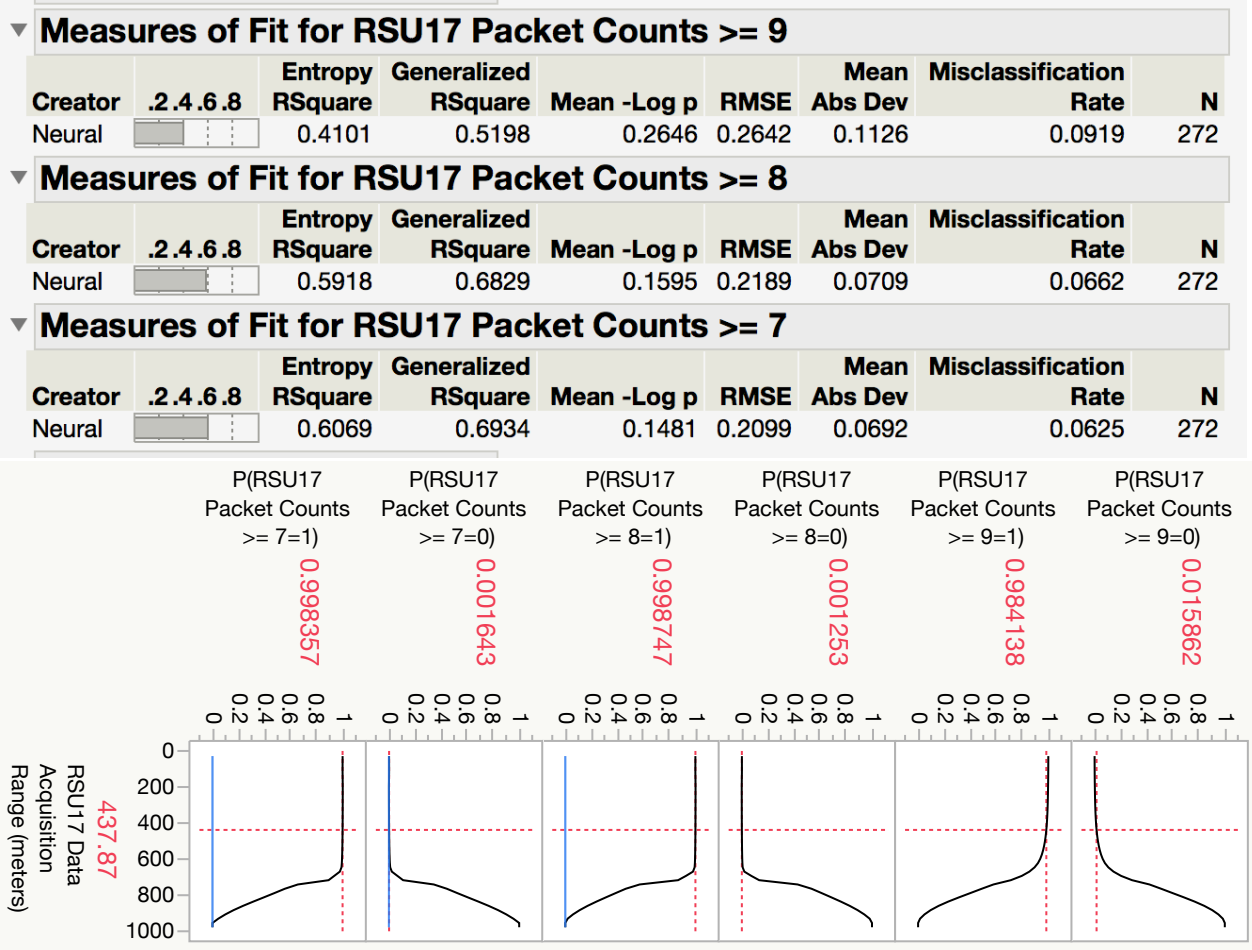

Figure 5-30. Using neural networks models on DSRC RSU17 data set, a comparison of three thresholds is generated along with the misclassification rating [Top image] and predication graph for each threshold for both a logic 0 and logic 1.

In Figure 5-31 (top), neural network models are generated for DSRC RSU19 using three thresholds: a) Threshold 1 = packet counts greater than and equal to 9, b) Threshold 2 = packet counts greater than and equal to 8, and c) Threshold 3 = packet counts greater than and equal to 7. The objective is to compare the predictive ability of each model and measure the fit. Therefore, each row corresponds to a different model. The misclassification rates are 0.0060, 0.000, and 0.000, respectively. In Figure 5-31 (bottom), a predication graph is depicted with the neural network's probability profile for a logic 1 and logic 0 based on the three thresholds. From the right, the predication graph is for RSU19 using Threshold 1 for a logic 1 and logic 0. The two center predication graphs are for RSU19 using Threshold 2 for a logic 1 and logic 0. On the left, the predication graph is for RSU19 using Threshold 3 for a logic 1 and logic 0. To mitigate

overfitting, the neural network model uses K-Fold to divide the original data into K subsets, and each of the K sets is used to validate the model fit on the rest of the data (i.e., fitting a total of K models).

Measures of Fit for RSU19 Packet Counts >= 9

Creator	.2 .4 .6 .8	Entropy RSquare	Generalized RSquare	Mean -Log p	RMSE	Mean Abs Dev	Misclassification Rate	N
Neural		0.9812	0.9901	0.0112	0.0558	0.0085	0.0060	166

Measures of Fit for RSU19 Packet Counts >= 8

Creator	.2 .4 .6 .8	Entropy RSquare	Generalized RSquare	Mean -Log p	RMSE	Mean Abs Dev	Misclassification Rate	N
Neural		0.9930	0.9963	0.0041	0.0223	0.0038	0.0000	166

Measures of Fit for RSU19 Packet Counts >= 7

Creator	.2 .4 .6 .8	Entropy RSquare	Generalized RSquare	Mean -Log p	RMSE	Mean Abs Dev	Misclassification Rate	N
Neural		0.9979	0.9989	0.0012	0.0035	0.0012	0.0000	166

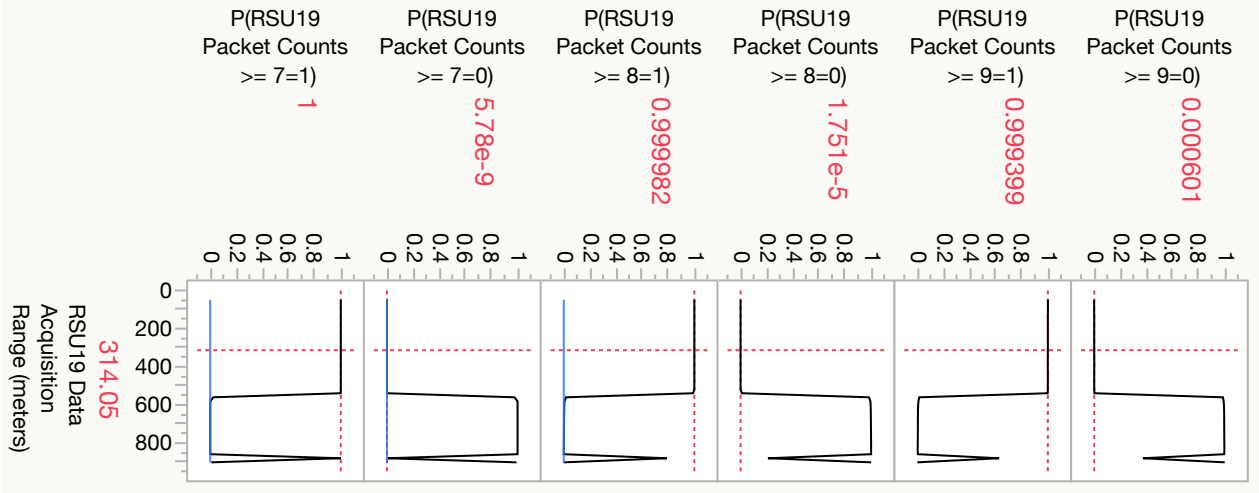

Figure 5-31. Using neural networks models on DSRC RSU19 data set, a comparison of three thresholds is generated along with the misclassification rating [Top image] and predication graph for each threshold for both a logic 0 and logic 1.

In the final chapter, the conclusion and future research are discussed in detail.

Chapter 6. Conclusions and Future Research

Section 6.1. Conclusion, Limitations, and Future Research

Section 6.1.1. Conclusion on Research Objectives

When deploying DSRC RSUs, it is essential to account for null points along the propagation pathways. The null points will have an impact on information transmitted and received between the DSRC RSU and the vehicle's OBU. For example, a designer of a V2I safety application may require a minimum rate of data (or packet counts) to effectively implement a V2I safety application such as RSZW. The RSZW safety application alerts or warns drivers, in a CACC platoon, who are approaching a work zone. If a CACC platoon is operating above the posted work zone speed limit, it is essential to maintain a minimum rate of data (or packet counts) between the vehicle and infrastructure to warn the drivers approaching a work zone.

The research motivation focuses on developing an empirical method of calculating the null points of a DSRC RSU for V2I communication at a highway on/off-ramp. The intent is to improve safety, mobility, and environmental applications since a map of the null points can be plotted against the distance between the DSRC RSU and a vehicle's OBU. The main research question asks: "What is a more robust empirical method, compared to the horizontal and vertical laws of reflection formula, in determining the null points from a DSRC RSU on a highway on/off ramp?"

There were three research objectives achieved:

1. Explain where and why null points occur from a DSRC RSU
2. Apply the existing horizontal and vertical polarization model in a real-world scenario along a highway on/off ramp
3. Introduce an extended horizontal and vertical polarization null point model using empirical data.

Section 6.1.2. Conclusion Regarding Research Objective 1

The null points for a DSRC RSU occurs because the direct and reflective waves produce a destructive interference (i.e., decrease in signal strength) when the two waves collide. A DSRC RSU's electric and magnetic fields can be depicted as two sinusoidal waves: direct and reflective waves (i.e., also known as a two-ray model). The reflective wave will propagate at an angle in the direction of the earth's surface. A portion of the electric and magnetic fields will transmit into the earth surface while the remaining electric and magnetic fields will reflect off the earth's surface. The reflected electric and magnetic fields will shift in phase then collide with the direct wave. A zero-degree phase shift will produce a constructive interference with the direct wave, and a 180-degree phase shift will produce a destructive interference with the direct wave. The destructive interference will produce a decrease in the signal strength of the direct wave, which is termed a null point. In other words, the direct and reflective waves will cancel each other when they are 180 degrees out of phase.

Using a two-ray model, the null points can be located using Pythagorean theorem for the direct and reflective waves. Using a modified Pythagorean theorem, a slightly modified model can be used to locate the null points both for a horizontal and vertical polarized DSRC RSU antenna. However, the modified Pythagorean theorem will provide only one null point, whereby our field test has shown several null points along the FSPL of V2I communication.

Section 6.1.3. Conclusion Regarding Research Objective 2

In a real-world V2I deployment, the RSU's mounting height may be restricted by the existing roadway infrastructure surrounding limitations (e.g., a fixed highway gantry height or fixed height of traffic signal enclosure). In 2009, Miucic provided key formulas to predict several null points in correlation to the height of the DSRC RSU that is based on a geometric triangle RF reflection model. But, Miucic's model does not account for several null points as the vehicle's OBU travels far from the DSRC RSU (i.e., the model only accounts for null points within a few hundred meters of the DSRC RSU).

After calculating the null points for several DSRC RSU heights, there is a noticeable limitation of the existing horizontal and vertical polarization models that is related to the full length of the FSPL model. Using Google Maps and Google MyMaps, the calculated horizontal and vertical null points were overlaid against empirical packet counts from a DSRC RSU at a mounting height of 7.620 meters. At a rate of 10 times per second, the data points were averaged over one second because the data acquisition system had limited storage space (i.e., there were 10 data points per second). The empirical DSRC RSU packet counts confirmed a null point for a horizontal polarization at K=0. Moreover, the empirical DSRC RSU packet count data spanned the full length of the FSPL. Based on the empirical DSRC RSU packet count data, there were several null points beyond K=0 as well as null points between K=0 to K=5.

The limitation of the horizontal and vertical polarization model does not account for the DSRC RSU signal strength, which will decrease with the square of the separation distance because of the decrease in power flux density. Likewise, the antenna gain for the radio hardware transmitter (source) and receiver (target) must be accounted for similar to the FSPL model.

Section 6.1.4. Conclusion Regarding Research Objective 3

Therefore, an extended horizontal and vertical polarization model was developed that calculates the null point from a DSRC RSU along the full path of the FSPL. The process introduced an extended horizontal and vertical polarization model to ascertain the null points from a DSRC RSU. The packet count and signal strength were used to determine thresholds to investigate potential DSRC RSU null points using statistical analysis. However, the packet counts and signal strength threshold criteria must be determined by the developer of the V2I safety application before implementing the extended horizontal and vertical polarization models.

First, the DSRC RSU signal strength was analyzed against the FSPL model using a fit smoothing spline on field data based on at least lambda value. The error term of the spline model has more weight, and the fit becomes more flexible and curved when the value of lambda decreases. On the other hand, the fit becomes stiff that approaches a straight line when the value of lambda increases. The developer of the V2I safety application must determine the best signal strength threshold criterion based on the desired results. Second, the DSRC RSU packet counts were analyzed against the FSPL model utilizing a histogram and outlier box plot because the data set are discrete values that can be easily quantified.

After determining a threshold for the signal strength and packet counts, a statistical categorical variable model was developed for several predictive formulas by converting results of the packet counts and/or signal strength into binary data (i.e., one or zero). Three categorical models were used to develop several predictive formulas: Classification (Decision) Tree, Logistic Regression, and Neural Networks.

The classification (decision) tree model recursively partitions data according to a relationship between the predictors and response values to generate a decision tree. The algorithm searches all possible splits of predictors to best predict the response. The logistic regression model establishes a relationship between a binary packet count and a predictor travel distance variable. Then, the prediction formulas model the logit-transformed probability as a linear relationship with the predictor travel distance. When the packet counts are subdivided based on the Quantiles, a binary packet count can be represented as a zero/one or failure/success. While a neural network model uses at least three multi-layer functions: a) Tangent Hyperbolic, b) Linear, and c) Gaussian.

The KFold validation method was implemented for each neural network model, which divides the original data into K subsets thus fitting a total of K models. Also, the train-validate-test method is used to build various categorical models using the DSRC RSU data set. The validation process uses part of a data set to estimate model parameters and the other part to assess the predictive ability of the model. The train set was 59 percent, the validate set was set to 21 percent, and the test set was at 20 percent.

The confusion matrix was used to measure the effectiveness of the classification tree, logistic regression, and neural networks. There were 18 model comparisons of the packet counts and signal strengths, for the best predictive fit, for at least three thresholds. In general, the neural network model provided the most effective (or smallest) misclassification count with a misclassification rate of 0.0743 at a threshold of logic packet count greater than or equal to 377.

Section 6.1.5. Applying the Neural Network Model to a New DSRC RSU Data Set

Based on the previous chapters, the neural network model was applied to 10 different DSRC RSU data sets at 10 unique locations around a circular test track with packet counts ranging from 0 to 11. The DSRC RSUs were installed approximately 800 meters apart with six RSUs mounted approximately 3.048 meters (or 10 feet) from the ground and four RSUs mounted approximately

6.096 meters (or 20 feet) from the ground. The DSRC RSU sample rate was 10 times per second, which was averaged over one second because the data acquisition system had limited storage space. The packet counts are detected near the DSRC RSU and 2,000 meters as discussed due to line-of-sight RF propagation from the FSPL model.

Neural network models were generated for 10 DSRC RSUs using three thresholds: a) Threshold 1 = packet counts greater than and equal to 9, b) Threshold 2 = packet counts greater than and equal to 8, and c) Threshold 3 = packet counts greater than and equal to 7. The objective was to compare the predictive ability of each model and measure the fit.

Based on 30 models at 10 unique locations, the highest misclassification was 0.1248, while the lowest misclassification was 0.000. There were six RSUs mounted at 3.048 (or 10 feet) from the ground with a misclassification rate that ranged from 0.1248 to 0.0553. Out of 18 models, seven had a misclassification rate greater than 0.110, while the remaining misclassification rates were less than 0.0993.

There were four RSUs mounted at 6.096 meters (or 20 feet) from the ground with a misclassification rate that ranged from 0.919 to 0.000. Out of 12 models, four had a misclassification rate greater than 0.0590, while the remaining misclassification rates were less than 0.0412.

Section 6.2. Limitations

There are two major limitations in the research: 1) the most effective key parameter is packet counts, which often require expensive data acquisition equipment to obtain the information and 2) the categorical type (i.e., decision tree, logistic regression, and neural network) will vary based on the packet counts or signal strength threshold that is dictated by the threshold criteria.

1. Normally, researchers and DSRC RSU deployers will utilize signal strength to plan, design, and test the effectiveness of the V2I communication between the DSRC RSUs and the vehicle's OBU. The manufacturers of DSRC RSUs provide simplistic software tools to measure the signal strength. However, it is extremely challenging to evaluate the null points using signal strength because of the sinusoidal nature of an electric and magnetic wave. Therefore, the packet counts require expensive data acquisition equipment to obtain the information.
2. When conducting an 18-model comparison, there was a slight difference in the categorical model that obtains the best fit based for various packet counts or signal strength threshold, which is dictated by the threshold criteria. The neural network provided the best fit for most threshold criteria, but the decision tree showed competitive models in lower thresholds (e.g., greater than or equal to 377 and greater than or equal to lambda at 0.110).

Section 6.3. Future Research

There are at least two future research areas that correspond to this body of work: 1) there is a need to leverage the extended horizontal and vertical polarization null point model on multiple DSRC RSUs along a highway on/off ramp and 2) there is a need to apply and validate different electric and magnetic (or propagation) models.

1. Because of limited research in this area, there is a strong need to leverage the extended horizontal and vertical polarization null point model when two or more DSRC RSUs are deployed in close proximity. Normally, DSRC RSUs are deployed with overlapping electric and magnetic (propagation) waves to account for free space path loss over distance. Therefore, the null points are offered hidden (or masked) by the overlapping propagation waves. This should be the next area of research investigation and validation.
2. There is a need to apply and validate different electric and magnetic (or propagation) models. There are propagation models for various frequencies (e.g., microwave to sonar), algorithms (e.g., ray tracing), and hybrid statistical models. The propagation models can be segmented into indoor and outdoor applications; therefore, the models can render different results for different environments. Thus, there is a need for future research that investigates and validates difference propagation models for null points.

Appendices

Appendix A. The Fundamental Principles of Antenna Theory for V2I Deployments

Appendix A.1 Abstract

This appendix is a theoretical explanation and visual perspective of antenna theory used in a V2I deployment through an RSU. At times, there are ways to leverage existing ITS roadside equipment as an upgrade to V2I technology. On the other hand, the optimal location of the roadside equipment maybe physically infeasible to be repositioned or limited by cost and/or the deployment schedule. This appendix expounds on:

4. The electromagnetic waves as the energy departs the antenna
5. The antenna patterns
6. Significant characteristics in antenna patterns
7. Common antenna patterns
8. Free space antenna path loss
9. The antenna location on a vehicle and an RSU.

A few real-world scenarios will be observed that have a significant impact on the V2I deployment. The major goal is to assist design engineers, owner/operators, or closely related professions with realistic V2I deployment expectations and the theoretical limitations due to the electromagnetic principles imposed on V2I a deployment.

Appendix A.2 Introduction

This appendix introduces the propagation characteristics—the process of spreading to a larger area—of electromagnetic waves that are transmitted by an antenna used in a V2I deployment by an RSU. The intent of this appendix is to provide a simplistic explanation of antenna theory with a concentration on 2-dimensional and 3-dimensional pictorial representations of a V2I deployment. It targets those with little or no knowledge of antenna theory but who are responsible for planning, managing, or owning a V2I deployment. The fundamental principles of electromagnetic waves normally start with Maxwell's equations along with the study of electric and magnetic fields as a variable of time. These principles and antenna theory are topics that can be found in most electrical engineering or radio communication textbooks. Thus, this appendix summarizes the basic concepts related to electromagnetic waves and focuses on the application of antenna theory in a V2I deployment as the signal propagates from an RSU.

The antenna has become an effective means of distributing electrical charges and current in a specific direction for wireless communications. The electromagnetic waves can be transmitted over a short distance (e.g., indoors or outdoors) or a long distance (e.g., a satellite that is orbiting the earth). An antenna's components will force the electric charges to oscillate when a changing power is applied to the wire(s) of an antenna. There are general concepts that a non-engineer can comprehend based on a few mathematical formulae and visual pictures. Similarly, the general

concepts may prevent costly design changes, inaccurate procurement orders, and improper antenna placement.

Regarding V2I wireless communication, an antenna is designed to distribute the electromagnetic waves from the radio hardware (source of energy) to an end device (target) that may be running a safety application. There is a need to maintain a reliable wireless connection between the source and target so that the safety application can perform properly. For example, the Red Light Violation Warning (RLVW) application enables a connected vehicle approaching an instrumented signalized intersection to receive information from the infrastructure (e.g., RSU) regarding the signal timing and the geometry of the intersection (e.g., SPaT). The CVRIA states that there is a mechanism to obtain the vehicle location and motion of the surrounding vehicles from the RSU. A poor wireless connection could obstruct the RLVW application from alerting the driver in time to avoid the traffic conflict.

In Figure A-1, an RLVW scenario is depicted with electromagnetic waves emitting from the RSU, which are represented by the vertical and horizontal sinusoidal waves. The RSU is electrically wired to the signalized lights and the RSU has radio hardware that transmit SPaT information within the electromagnetic waves. The two SUVs have an antenna that receives the electromagnetic waves from the RSUs. The two concentric patterns represent the reception coverage of electromagnetic waves by the radio hardware in the SUVs. Then, the V2I safety application utilizes the SPaT information to alert the driver of a traffic conflict. Likewise, the concentric patterns could represent the transmission coverage of electromagnetic waves to the RSU. The latter representation will be discussed in a section subtopic titled concentric pattern and FSPL pattern. In reality, the reception coverage is much larger in size than depicted by the concentric patterns in the figure. Nevertheless, the reception coverage was reduced in sized, within the figure, to generate a clear image that was not overwhelmed with a concentric pattern.

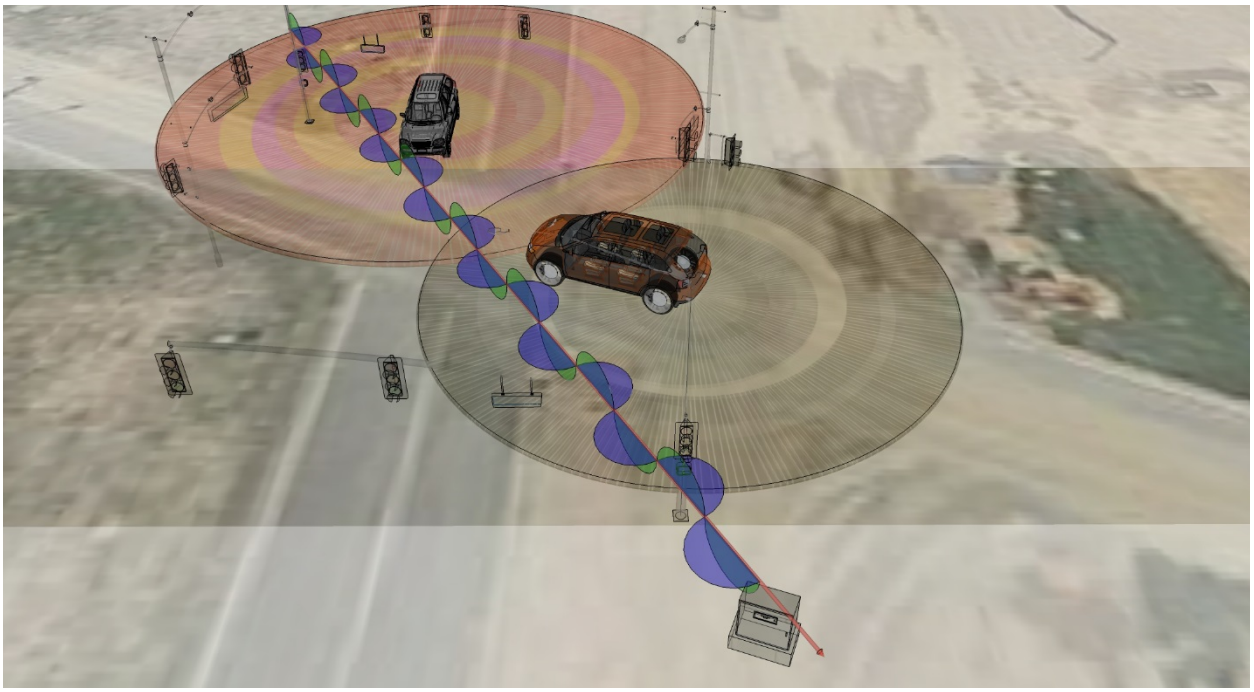

Figure A-1. A RLVW scenario with two approaching vehicles that transmit and receive electromagnetic waves from/to the RSUs.

In a V2I deployment using RSUs, there are several scenarios that require a basic understanding of antenna theory to ensure the system meets expectations. In Table A-1, there are four scenarios that appear to be reasonable decisions when installing, procuring, and specifying an antenna in a V2I deployment. Nevertheless, each of these scenarios may have a significant impact on the V2I deployment in a negative manner that will be addressed after the general concepts are explained.

Table A-1. Four scenarios that appear to be reasonable decisions when installing, procuring, and specifying an antenna in a V2I deployment.

Scenario	Description
1	A project manager may find it reasonable to hire a well-known electrical company to design or install a V2I communication system.
2	A procurement officer may accept the lowest bid for a set of replacement antennas.
3	A traffic engineer may justify mounting the V2I antenna inside an RSU to prevent the equipment from being vandalized and rotating the antenna by 90 degrees to fit in the equipment cabinet.
4	A design engineer could write a technical specification requiring the white antenna housing and the associated mounting hardware coated with a non-glossy green paint to appease the planning commission.

The major objective of each subtopic is to assist individuals such as design engineers, owner/operators, or closely related professions with realistic deployment expectations and the

limitations of certain electromagnetic principles that depart the antenna. This will be achieved by explaining the electromagnetic waves as the energy departs departing the antenna, the antenna patterns, significance characteristics in antenna patterns, common antenna patterns, free space antenna path loss, and the antenna location on a vehicle and an RSU.

Appendix A.3 Antenna Patterns

The antenna pattern is a graphical representation of electromagnetic waves (or energy) departing the antenna, which provides a means of estimating how the energy is distributed. Typically, the manufacturer will draw the antenna patterns in 2-dimensions, while the academic communities have developed innovative ways to plot the antenna pattern in 3-dimensions for various analyses. Although the antenna radiates in 3-dimensional space, the manufacturer's 2-dimensional drawings are represented in a *principal plane pattern* by rendering two slices through the 3-dimensional pattern. The two patterns are frequently plotted in polar coordinates and called the *azimuth plane pattern* and *elevation pattern*. The azimuth pattern represents the "horizontal" plane, and the elevation pattern represents the "vertical" plane.

An elevation pattern and azimuth pattern are represented in Figure A-2 and Figure A-3, respectively. In Figure A-2, the elevation pattern has electromagnetic radiation that propagates in the horizontal direction of zero and 180 degrees, which is perpendicular to the antenna in the direction of 90 degrees. In Figure A-3, the azimuth plane pattern has the z-axis in the center of the graph and extends from the paper. Both figures have a hypothetical shape that does not exist in real life; however, the shape is used to characterize a pattern using a mathematical formula.

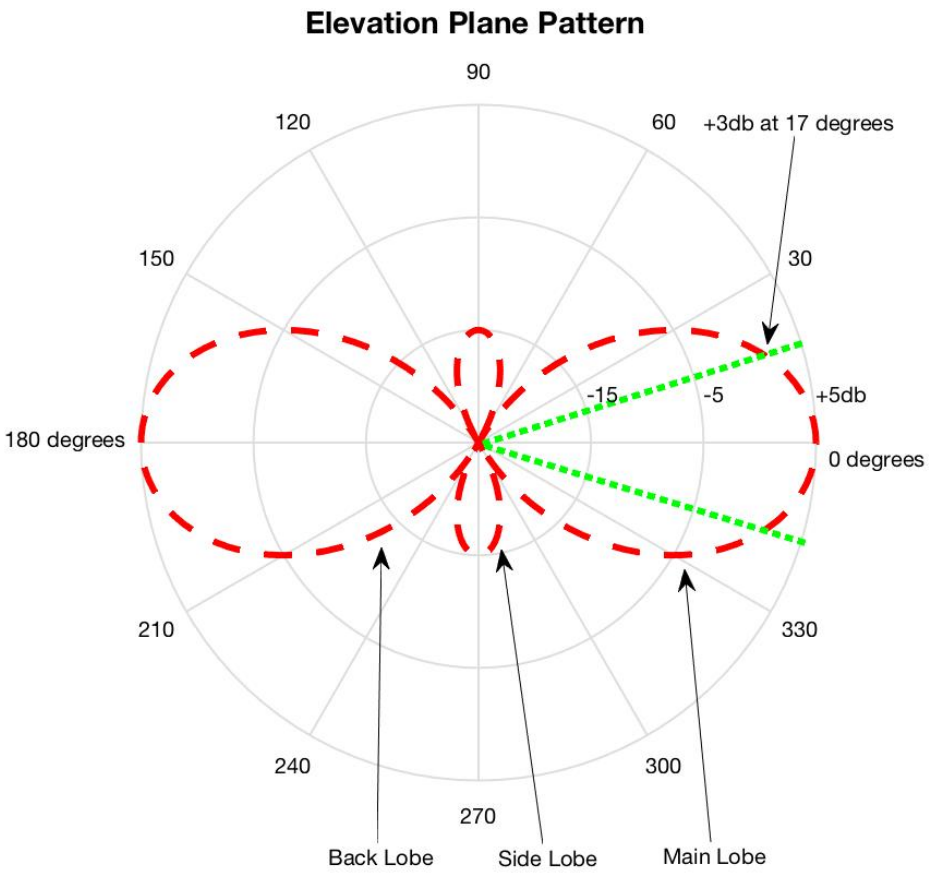

Figure A-2. The elevation plane pattern of a directional antenna that is plotted in polar coordinates as a function of 1 + 2 cos (2θ).

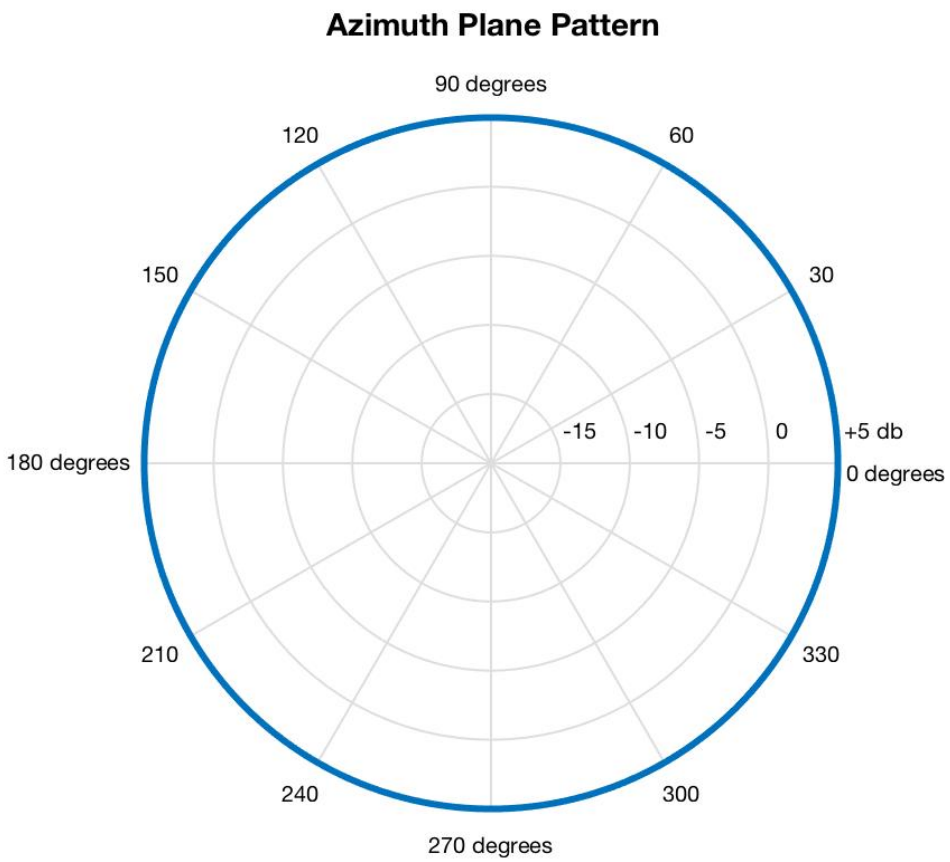

Figure A-3. The azimuth plane pattern of a directional antenna that is plotted in polar coordinates as a function of one from 0 to 360 degrees.

As an example, the graphical representation of the elevation plane pattern was plotted using a Lemniscate of Bernoulli – Two-leaved rose curve (i.e., the red curve):

$$\boldsymbol{r^2 = a^2 \cos 2\theta} \quad \text{or} \quad \boldsymbol{r = a + 2 \cos 2\theta}$$

whereby *a* is the size of the two-leaved rose along 90 and 270 degrees. When *a* is equal to zero, the two-leaved rose at 90 and 270 degrees will be of equal diameter to the leaved rose at 0 and 180 degrees. Then, the diameter will decrease to zero as the value approaches the cosine multiplier (i.e., the number 2). In Figure A-2, the elevation plane pattern is a function of 1 + 2 cos (2θ).

As discussed later, the signal strength of an electromagnetic wave is not uniform over distance. Nearly all electromagnetic energy has a limitation that is inversely proportional to the distance squared. This limitation must be accounted for in technical requirements when designing and deploying V2I system. So, the antenna's principal plane pattern is essential for the traffic

engineer or design engineer because the graph provides a means of estimating the area of effective (or ineffective) coverage for a V2I application.

Appendix A.4 Significance Characteristics in Antenna Patterns

The following describes four significance characteristics in antenna patterns, based on Figure A-2 and Figure A-3.

Lobes

In Figure A-3, the azimuth plane is a hypothetical antenna pattern with a signal strength of +5 decibels relative to isotropic (or +5dbi). The term isotropic has origins from "iso" meaning the same and "tropic" meaning direction. The isotropic antenna has a pattern that is equal in radiation all directions. In Figure A-2, the antenna pattern is characterized in terms of lobes: the main lobe, side lobe, and back lobe. The main lobe radiates in the direction of zero degrees if we continue to assume the antenna is orientated in the direction of 90 degrees while the back lobe is radiating in the direction of 180 degrees. The maximum radiation is in the direction of zero degrees. The signal strength becomes weaker when moving in the direction of 30 and 330 degrees. In other words, there is a tremendous signal loss when a measurement is made outside of the two-leaved rose curve. In this hypothetical case, the back lobe is identical to the main lobe in signal strength and in the opposite direction. The side lobes radiate in the direction of 90 degrees and 180 degrees with a signal strength at -15dbi. The side lobes are a region of undesirable radiation and are several times lower in magnitude than the maximum radiation power of the main beam. In reality, the antenna pattern may be comprised of several side lobes but the manufacturer's technical specification may only list the first and nearest (or highest) side lobe to the main beam.

3-dB Beamwidth

The 3-dB beamwidth is defined as the angle between the points of the main lobe that are down from the maximum gain by 3dB (or half-power). Normally, the decrease is experienced as the target moves away from the source; since, the signal strength is inversely proportional to the distance squared. In Figure A-2, the 3-dB beamwidth is located from 17 degrees to 343 degrees for a total of 34 degrees (i.e., the distance between the green lines).

Polarization

In the simplest form, an electromagnetic wave is comprised of two sinusoidal signals in the horizontal and vertical planes traveling through space, which are the electric and magnetic fields. A traveling wave is considered vertically (or linearly) polarized if the electrical field is moving vertically polarized through space. An example of a vertical antenna is an antenna on an automobile, which is perpendicular to the Earth's surface. A polarized antenna is sensitive to the mounting position and provides the best transmission/reception when the electrical fields are on the same plane.

In Figure A-4, the SUV antenna is linearly polarized with the electrical field traveling perpendicular (i.e., the left signal moving up and down) to the Earth's surface. The RSU antenna is linearly polarized, but the electrical field is traveling parallel (i.e., the right signal moving side to side) to the Earth's surface. Therefore, the electrical fields are not propagating on the same plane. In this scenario, a linearly polarized RSU antenna will receive the most energy from the SUV antenna when both antennas are physically mounted in the same direction and the electrical fields are traveling on the same plane (i.e., perpendicular to the Earth's surface).

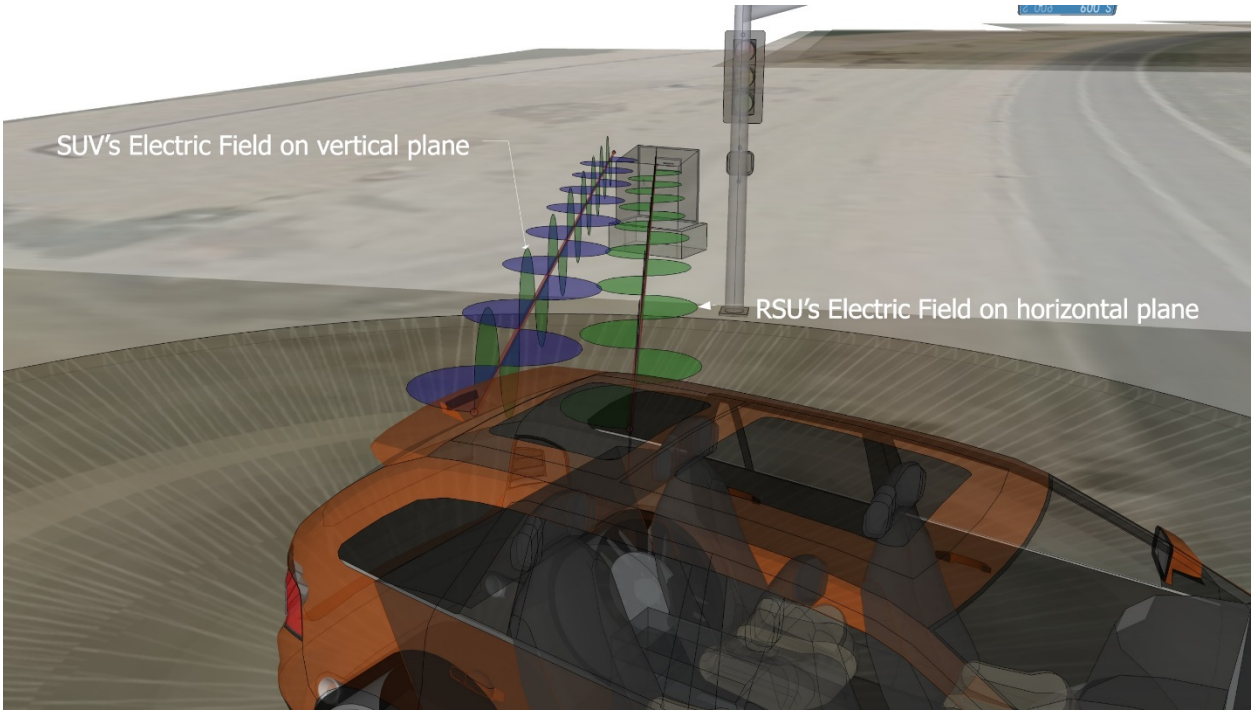

Figure A-4. The SUV and RSU antennas are linearly polarized; however, the electromagnetic waves are not propagating on the same plane.

The polarization is directly related to the propagation direction (e.g., horizontal or vertical) of the electrical fields that depart the antenna. An antenna can be designed with a sensitivity to the mounting direction, which implies the transmitting and receiving antennas must retain the same polarization for the best transmission/reception path. If the mounting direction is not observed during installation, the target will experience at least a 3-dB loss because the electrical fields are not propagating on the same plane. Ordinarily, the antenna manufacturer will provide a directional marking on the exterior body of the antenna such as an arrow to ensure the antennas are installed properly.

Appendix A.5 Hypothetical Antenna Patterns

When studying antenna theory, there are hypothetical antenna patterns that capture the core of a propagation waves. Moreover, the V2I application will determine the characteristic of the antenna or the orientation of a particular pattern. The following are four hypothetical antenna

patterns with electromagnetic energy departing from an RSU, which are depicted in 3-dimension:

1. RSU 1 is an isotropic antenna based on a hypothetical lossless antenna that distributes the energy equally in all directions.
2. RSU 2 is a monopole antenna, manufactured as a single wire element, with a shape similar to half-a-donut that is parallel to the earth's surface.
3. RSU 3 is a dipole antenna, manufactured as two wire elements, that has a non-directional (or circular) pattern in a given plane and a directional pattern in the perpendicular plane.
4. RSU 4 is a directional antenna, which is more effective in a specific direction and has a main lobe as well as minor lobe(s).

Figure A-5 is a top view (or the 3-dimensional azimuth plane pattern) as the electromagnetic energy depart from the RSU's antenna. The 3-dimensional azimuth plane is a circular antenna pattern for RSU 1, RSU 2, and RSU 3, while RSU 4 has a concentrated antenna pattern in one direction.

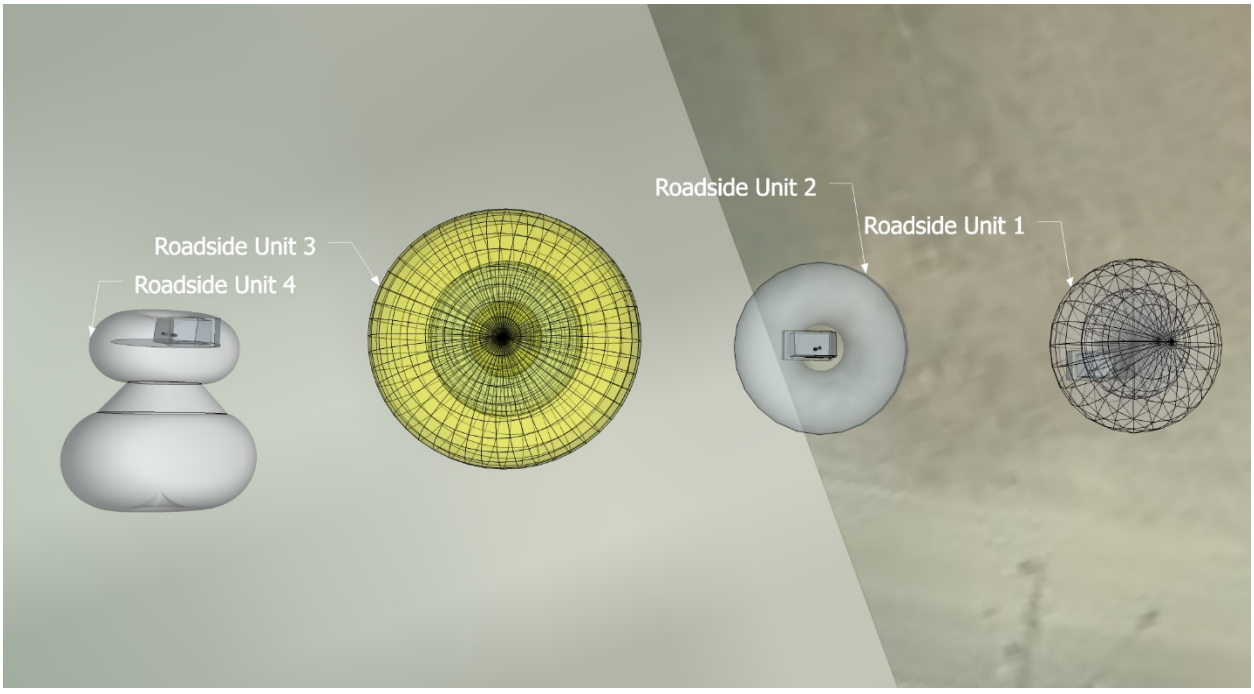

Figure A-5. A 3-dimensional azimuth plane pattern with electromagnetic waves departing from RSU 1 (isotropic antenna), RSU 2 (monopole antenna), RSU 3 (dipole antenna), and RSU 4 (directional antenna).

Figure A-6 and Figure A-7 are front viewpoints (or the 3-dimensional elevation plane pattern) as the electromagnetic waves travel from the RSU's antenna along the earth's horizon plane. Figure A-6 is a close-up of RSU 1 and RSU 2 with the electromagnetic waves propagating outward along the horizon, while Figure A-7 is a close-up of RSU 3 and RSU 4. RSU 1 has a spherical radiation pattern and serves as a 3-dimensional isotropic antenna. RSU 2 has radiation above the

height of the physical antenna with no radiation below the RSU, ideally. RSU 3 has radiation in all directions along the earth's horizon plane and has a shape similar to a donut. RSU 4 has a main lobe in front of the RSU with some radiation from the back and side lobes.

Figure A-6. A 3-dimensional elevation plane pattern with electromagnetic waves along the earth's horizon plane for RSU 1 and RSU 2.

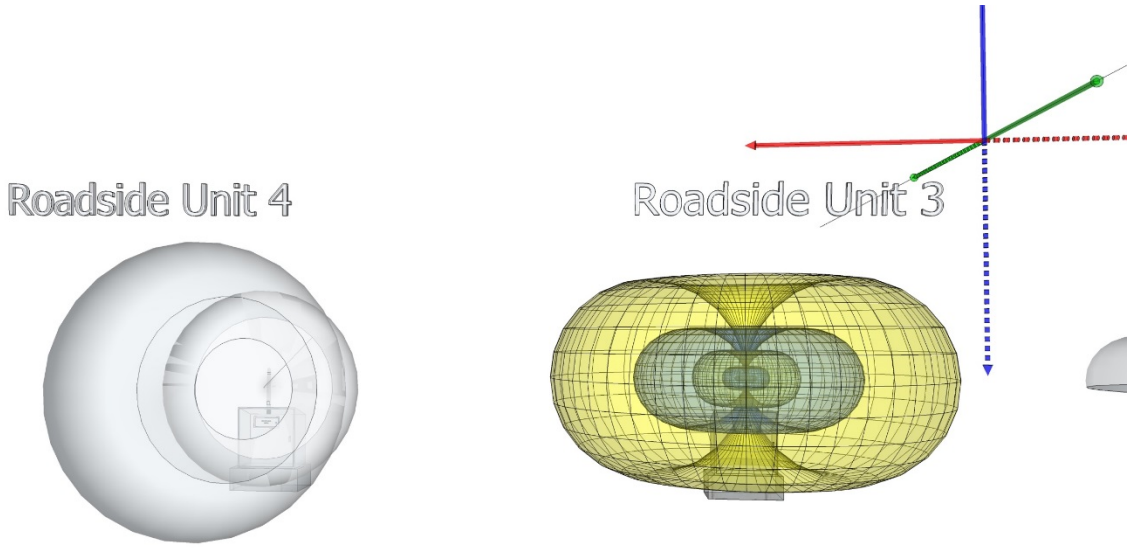

Figure A-7. A 3-dimensional elevation plane pattern with electromagnetic waves along the earth's horizon plane for RSU 3 and RSU 4.

Appendix A.6 Concentric Pattern and FSPL Patterns

At times, the azimuth plane pattern is represented by concentric circles with several annuli—ring-shaped regions that are bounded by two concentric circles. In Figure A-8, the concentric circles represent two elements of radiation: 1) propagation of the electromagnetic waves along the horizontal plane from the source and 2) the FSPL, which is the decrease in signal strength of an electromagnetic wave in the open air. The 3-dimensional dipole sphere has several mini-spheres within the larger sphere. Furthermore, the larger sphere represents the outer boundary of an azimuth plane pattern. For example, the larger sphere could represent +5dB; similar to the azimuth plane pattern on Figure A-3. Accordingly, the mini-spheres represent inner circles within the polar coordinate graph such as 0dB, -5dB, and -10dB. As stated earlier, the signal strength (or reception coverage) was reduced in sized, within the figure, to produce a clear image that was not inundated with a concentric pattern.

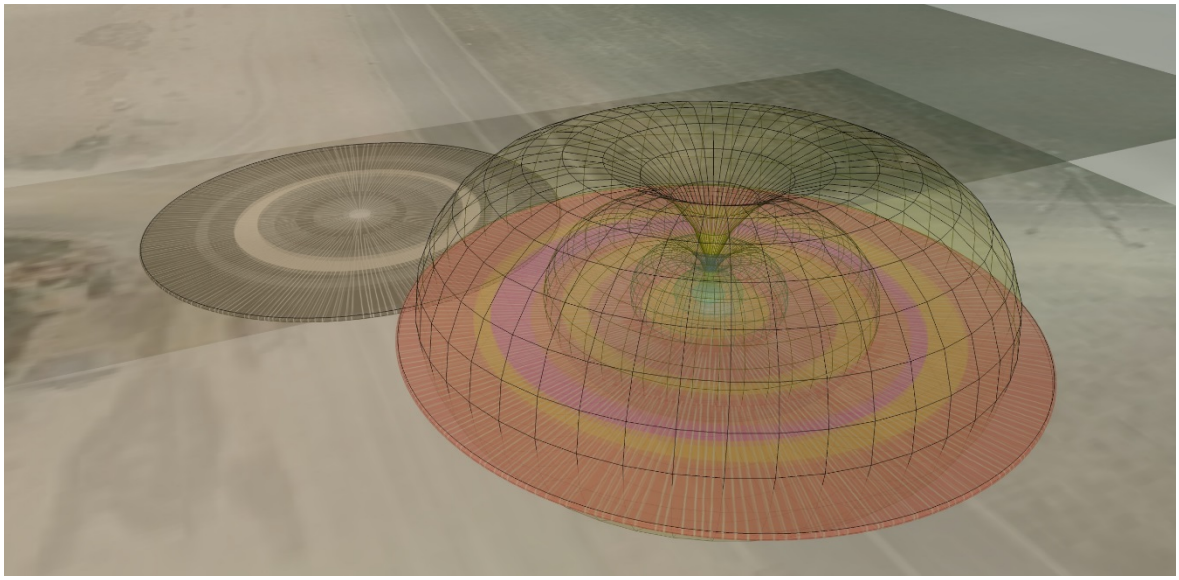

Figure A-8. An azimuth plane pattern is represented as a 3-dimensional dipole sphere and as a 2-dimensioanl concentric circle.

Also, the sphere and concentric circle depict the FSPL which is "not due to dissipation, but rather to the fact that the power flux density decreases with the square of the separation distance" as quoted from the IEEE standard 145-1993. The equation for FSPL is derived below in terms of dB:

$$\boldsymbol{FSPL = \left(\frac{4\pi df}{c}\right)}$$

$$\boldsymbol{FSPL(dB) = 20Log_{10}\left(\frac{4\pi df}{c}\right)}$$

$$\boldsymbol{FSPL(dB) = 20Log_{10}(d) + 20Log_{10}(f) + 20Log_{10}\left(\frac{4\pi}{c}\right)}$$

$$\boldsymbol{FSPL(dB) = 20Log_{10}(d) + 20Log_{10}(f) + 92.45}$$

where *c* is the speed of light (3 x 10^8 m/s), *d* is the distance from the transmitter (in kilometers), and *f* is the signal frequency (in GHz).

Normally, a manufacturer will produce an antenna with gain in reference to an isotropic antenna. The antenna gain for the radio hardware transmitter (source) and receiver (target) must be accounted for in the FSPL such that

$$\boldsymbol{FSPL(dB) = 20Log_{10}(d) + 20Log_{10}(f) + 92.45 - GTx - GRx}$$

whereby *d* is the distance from the transmitter (in kilometers), *f* is the signal frequency (in GHz), GTx is the transmitter gain (in dBi), and GRx is the receiver gain (in dBi). The antenna gain for the transmitter and receiver can be different in value, but the designer of the V2I system will make the final decision, which is often based on the V2I application or surrounding environment.

In Figure A-9, four graphs depict using the FSPL formula to show the effect of frequency and antenna gain. The top graph (in green) has a frequency of 5.9 GHz with no antenna gain for the transmitter or receiver. Just below, the next graph (in purple) has a frequency of 5.9 GHz with an antenna gain of +5dB for the radio transmitter and zero for the receiver. The third graph from the top (in blue) has a frequency of 2.4 GHz with no antenna gain for the transmitter or receiver. Just below, the next graph (in purple) has a frequency of 2.4 GHz with an antenna gain of +5dB for the transmitter and zero for the receiver.

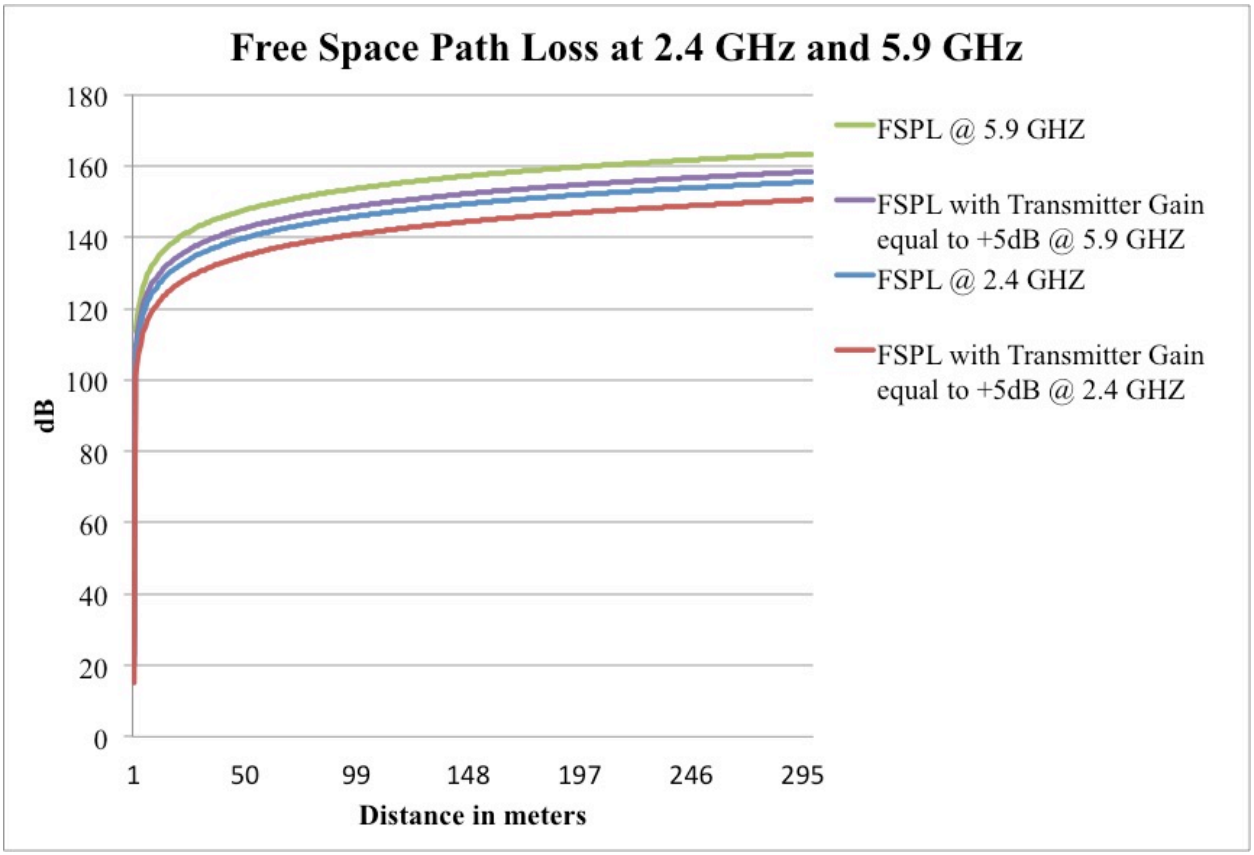

Figure A-9. The FSPL to show the effect of frequency (2.4GHz vs. 5.9GHz) and antenna gain (0dB vs. +5dB).

This scenario shows how the path loss will increase as the frequency increases; consequently, the frequency will have an impact on the reception and transmission coverage of a V2I deployment. A designer can estimate the signal strengths that may be expected in a given V2I deployment. In addition, the FSPL has a major impact on the number of RSUs and the spacing of RSUs; a V2I application requires contiguous wireless coverage.

Appendix A.7 Antenna Location on a Vehicle and an RSU

The antenna placement is a critical aspect to the reception and transmission coverage of electromagnetic energy since the signal strength of an electromagnetic wave is not equal (or infinite) over distance. In a V2I deployment, the location of the vehicle and roadside antennas are critical for the initial and continuous wireless communication over time.

In regard to vehicle installation, the car manufacturers have developed techniques to mount an antenna on the rooftop with minimum signal strength loss. When an antenna is mounted inside the vehicle, the signal strength is attenuated (or reduced) because the electromagnetic energy must propagate through a layer of glass, metal, or fiberglass. Usually, the mounting location on the rooftop is positioned in the rear-center, but the front or center rooftop positions are sufficient if there are no vehicles accessories (e.g., ski racks, luggage racks, and a taxi advertisement sign).

When considering a roadside installation, the antenna is typically mounted on (or near) the RSU, traffic light signal pole, or highway gantry. In Figure A-10, the antenna is mounted on the RSU and the concentric pattern represents the transmission coverage of electromagnetic energy (i.e., the source) with several annuli—ring-shaped regions that are bounded by two concentric circles. The RSU is in the center of the concentric pattern and each annulus represents the FSPL as the signal strength decreases in the open air. Each SUV is approximately 110 meters from the street's intersection or a total of 200 meters apart. On a similar note, one SUV is 88 meters from the RSU, and the second is 132 meters from the RSU because radio hardware is located several meters from the street intersection. The closest SUV will receive a stronger signal strength and potentially a better wireless connection if there is a clear line-of-sight. In other words, the electromagnetic waves will travel a direct path from the source (RSU) to the target (SUV) with no (or very little) obstruction.

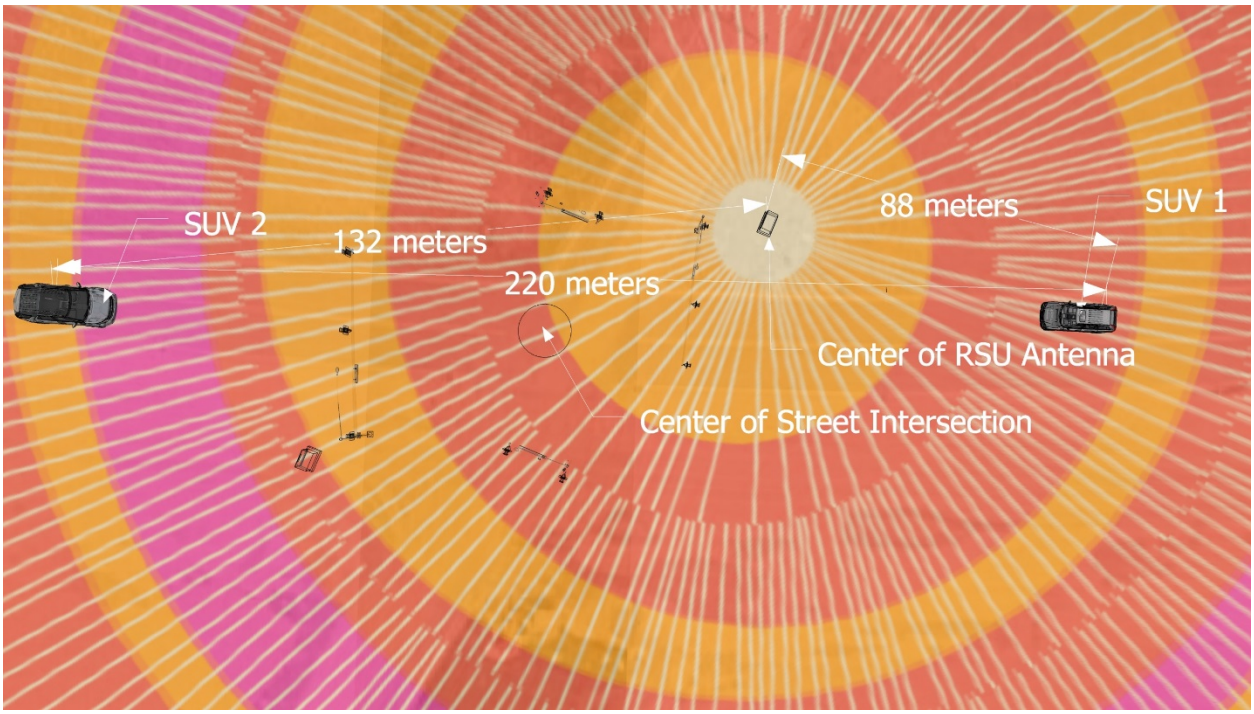

Figure A-10. The concentric pattern represents the transmission coverage from the RSU's antenna, which is closer to SUV 1 even though SUV 1 and SUV 2 are equal distance from the center of the street intersection.

In Figure A-11, the antenna for the RSU is located on the traffic light signal pole. When the antenna is located on a signal pole or highway gantry, the electromagnetic energy is radiated more homogeneously along the street intersection and the transmission coverage is aligned with both driving directions. In turn, the signal strength will be similar as well as the wireless communication data rate. Conversely, the polarization is a vital component when mounting the antenna on a signal pole and highway gantry (source) because the antenna polarization of source

must match the vehicle antenna (target). Because the vehicle is moving, there will be a misalignment between the source and target at various points on the highway (or street).

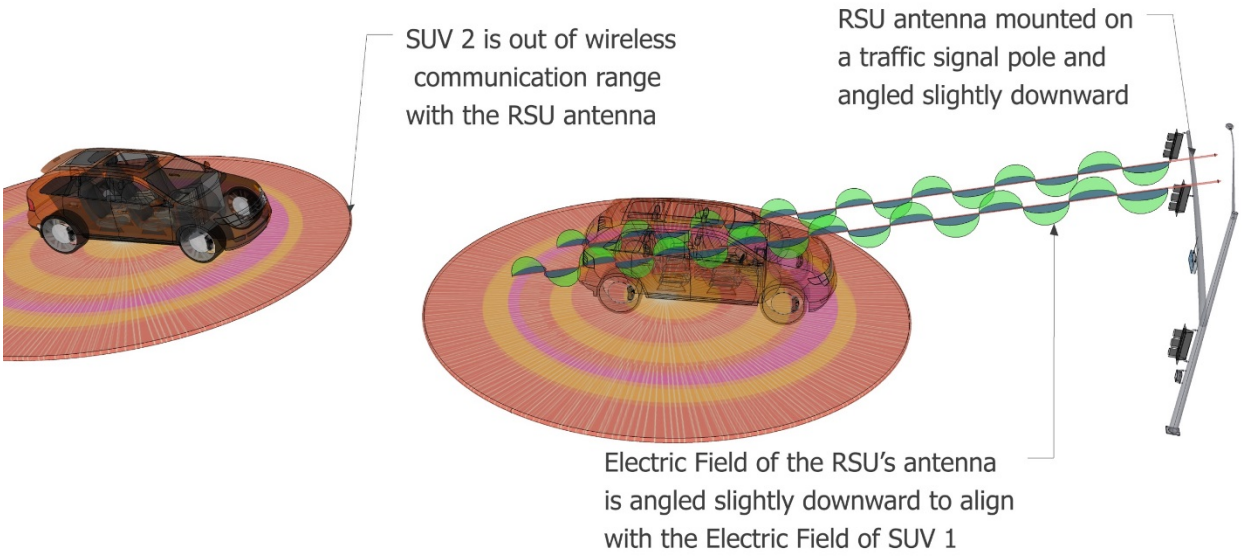

Figure A-11. To maximize electromagnetic energy, the RSU antenna is mounted on the traffic light signal pole and angled slightly downward to match the SUV's antenna polarization.

In Figure A-11, the electric field of the RSU's antenna is angled slightly downward to align with the antenna polarization of SUV 1. The purpose of mounting the RSU's antenna at a slight angle is to maximize the amount of electric field energy received by the SUV's antenna from the RSU. SUV 1 has a concentric pattern that represents the reception coverage of electromagnetic energy (i.e., the target), which depicts the signal strength of wireless communication coverage. SUV 2 has a concentric pattern as well to represent the wireless reception coverage. Once again, the signal strength (or reception coverage) was reduced in sized, within the figure, to produce a clear image that was not inundated with a concentric pattern. SUV 1 is within wireless communication range of the RSU's antenna, while SUV 2 is out of wireless communication range with the RSU's electromagnetic field. The relative polarization will change as each vehicle approaches and departs from the signal pole, which will impact the total signal strength. The source antenna must be mounted in a tilted fashion to initiate and maintain wireless communication before the vehicle is underneath the signal light pole. In a V2I application such as RLVW, there is a need to initiate and maintain wireless communication before the SUV is underneath the signal light to provide ample warning to the driver. The speed of the SUV will determine if ample to initiate or maintain wireless communication. For example, a vehicle traveling at twice the posted speed limit will have less time to initiate and maintain wireless communication compared to a vehicle moving at one-half the posted speed limit.

Appendix A.8 Conclusion

There are numerous subtopics related to antenna theory that are not discussed in this appendix. The intent is to provide a simplistic explanation of fundamental principles on antenna theory and utilize 2-dimensional and 3-dimensional image representations of a V2I deployment using an RSU. The antenna of an RSU has become an effective means of distributing electrical energy and maintaining a reliable wireless connection if the equipment is mounted properly. Thus, there are subtle mistakes, which may lead to an ineffective V2I deployment. In Table A-2, the four scenarios apply our knowledge of antenna theory in real-world mistakes that could significantly impact the V2I deployment.

Table A-2. Four scenarios appear to be reasonable decisions; but, there is a significant impact to each scenario, which may impact the wireless communication of the V2I deployment.

Scenario	Description	Significant Impact on the V2I Deployment
1	A project manager may find it reasonable to hire a well-known electrical company to design or install a V2I communication system.	The average electrical company may not have the experience or knowledge of antenna theory. Hence, the electrical company could produce costly delays such as: a) purchasing the wrong antenna for the application, b) installing an insufficient number of antennas to maintain a reliable wireless communication, or c) purchasing a 2.4 GHz antenna when the application requires a 5.9 GHz antenna.
2	A procurement officer may accept the lowest bid for a set of replacement antennas.	The replacement antenna may be a directional antenna whereby the application requires a dipole antenna. Consequently, the procurement officer's decision may impact the reception and transmission coverage of a V2I deployment.
3	A traffic engineer may justify mounting the V2I antenna inside an RSU to prevent the equipment from being vandalized and rotating the antenna by 90 degrees to fit in the equipment cabinet.	A vertically polarized antenna is sensitive to the mounting position and rotating the antenna 90 degrees will impact the maximum amount of electric field energy received by the SUV's antenna

Scenario	Description	Significant Impact on the V2I Deployment
		from the RSU. When the antenna is mounted in the equipment cabinet, the electromagnetic energy will experience a signal strength loss because the electromagnetic waves must penetrate the metal cabinet before traveling in open air.
4	A design engineer could write a technical specification requiring the white antenna housing and the associated mounting hardware coated with a non-glossy green paint to appease the planning commission.	The antenna's manufacturer discourages painting the antenna housing because the signal strength will be attenuated (or reduced) since the electromagnetic waves must propagate through a layer of paint. Also, there are some paints that contain lead, and the lead may affect the antenna pattern.

Appendix A.9 References

[1] J. Walker and K. Heaslip, "A Low-Cost Real-World Planning Strategy For Deploying a Dedicated Short-Range Communications Roadside Unit on a Highway Off-Ramp," *Transportation Research Board*, pp. 1–19, 2017.

[2] J. Walker, "The Fundamental Principles of Antenna Theory for (V2I) Deployments," in *Vehicle-to-Vehicle and Vehicle-to-Infrastructure Communications: A Technical Approach*, F. Hu, Ed. Boca Raton: CRC Press: Taylor & Francis Group, 2018, pp. 207–220.

[3] M. T. Hayat, H. Park, and B. L. Smith, "Connected Vehicle Enabled Freeway Merge Assistance system-field test: Preliminary results of driver compliance to advisory," *IEEE Intelligent Vehicle Symposium Proceedings*, no. Iv, pp. 1017–1022, 2014.

[4] S. E. Shladover, C. Nowakowski, X.-Y. Lu, and R. Ferlis, "Cooperative Adaptive Cruise Control (CACC) Definitions and Operating Concepts," no. November 2014. p. 27.

[5] J. Fishelson, "Platooning Safety and Capacity in Automated Electric Transportation," Utah State University, 2013.

[6] E. Meissner, T. Chantem, and K. Heaslip, "Optimizing Departures of Automated Vehicles From Highways While Maintaining Mainline Capacity," *IEEE Transactions on Intelligent Transportation Systems.*, vol. 17, no. 12, pp. 3498–3511, Dec. 2016.

[7] D. Desiraju, T. Chantem, and K. Heaslip, "Minimizing the Disruption of Traffic Flow of Automated Vehicles During Lane Changes," *IEEE Transactions on Intelligent Transportation Systems.*, vol. 16, no. 3, pp. 1249–1258, Jun. 2015.

[8] National Highway Traffic Safety Administration (NHTSA), "Federal Motor Vehicle Safety Standards; V2V Communications." National Highway Traffic Safety Administration (NHTSA), Department of Transportation (DOT) ACTION:, Washington, D.C., pp. 1–392, 2016.

[9] Federal Highway Administration, "Crash Data Analyses for Vehicle-to- Infrastructure Communications for Safety Applications," Washington, D.C., 2012.

[10] J. Harding, G. Powell, R. Yoon, J. Fikentscher, C. Doyle, D. Sade, M. Lukuc, J. Simons, and J. Wang, "Vehicle-to-Vehicle Communications : Readiness of V2V Technology for Application," no. August. p. 327, 2014.

[11] National Highway Traffic Safety Administration (NHTSA), "Vehicle Safety Communications Project Final Report DOT HS 810 591," 2006.

[12] Federal Highway Administration, "2015 FHWA Vehicle to Infrastructure Deployment Guidance and Products." Washington, D.C., p. 30, 2014.

[13] D. Ou, Y. Yang, L. Xue, and D. Dong, "Optimal Connectivity-Based Deployment of Roadside Units for Vehicular Networks in Urban Areas," *Transportation Research Record: Journal of the Transportation Research Board*, vol. 2559, no. 2559, pp. 46–56, Jan. 2016.

[14] G. G. M. Nawaz Ali, P. H. J. Chong, S. K. Samantha, and E. Chan, "Efficient data dissemination in cooperative multi-RSU Vehicular Ad Hoc Networks (VANETs)," *Journal of Systems and Software*, vol. 117, pp. 508–527, Jul. 2016.

[15] M. Kafsi, P. Papadimitratos, O. Dousse, T. Alpcan, and J.-P. Hubaux, "VANET Connectivity Analysis," 2009.

[16] T. Yan, W. Zhang, G. Wang, and Y. Zhang, "Access Points Planning in Urban Area for Data Dissemination to Drivers," *IEEE Transactions on Vehicular Technology*, vol. 63, no. 1, pp. 390–402, Jan. 2014.

[17] C. M. Silva, W. Meira, and J. F. M. Sarubbi, “Non-Intrusive Planning the Roadside Infrastructure for Vehicular Networks,” *IEEE Transactions on Intelligent Transportation Systems.*, vol. 17, no. 4, pp. 938–947, 2016.
[18] O. Trullols, M. Fiore, C. Casetti, C. F. Chiasserini, and J. M. Barcelo Ordinas, “Planning roadside infrastructure for information dissemination in intelligent transportation systems,” *Computer Communications*, vol. 33, no. 4, pp. 432–442, 2010.
[19] V. D. Khairnar and S. N. Pradhan, “Simulation Based Evaluation of Highway Road Scenario between DSRC/802.11p MAC Protocol and STDMA for Vehicle-to-Vehicle Communication,” *Journal of Transportation Technologies*, vol. 3, no. 1, pp. 88–104, 2013.
[20] M. Shulman and R. K. Deering, “Third Annual Report of the Crash Avoidance Metrics Partnership, April 2003 - March 2004,” Washington, D.C., 2005.
[21] R. Miucic, Z. Popovic, and S. M. Mahmud, “Experimental characterization of DSRC signal strength drops,” in *2009 12th International IEEE Conference on Intelligent Transportation Systems*, 2009, pp. 1–5.
[22] E. Zöchmann, K. Guan, and M. Rupp, “Two-Ray Models in mmWave Communications,” pp. 225–229, 2017.
[23] IEEE Vehicular Technology Society Sponsored, *IEEE Standard for Wireless Access in Vehicular Environments (WAVE)— Networking Services IEEE*. New York: The Institute of Electrical and Electronics Engineers, Inc., 2016.
[24] V. Shivaldova, A. Winkelbauer, and C. F. Mecklenbrauker, “Signal-to-noise ratio modeling for vehicle-to-infrastructure communications,” *2014 IEEE 6th International Symposium on Wireless Vehicular Communications WiVeC 2014 - Proc.*, 2014.
[25] V. Shivaldova, A. Winkelbauer, and C. F. Mecklenbrauker, “Vehicular Link Performance: From Real-World Experiments to Reliability Models and Performance Analysis,” *IEEE Vehicular Technology Magazine*, vol. 8, no. 4, pp. 35–44, 2013.
[26] V. Shivaldova and C. F. Mecklenbräuker, “Quantization-based Complexity Reduction for Range-dependent Modified Gilbert Model,” *Proc. IEEE Sens. Array Multichannel Signal Process. Work.*, pp. 345–348, 2014.
[27] V. Shivaldova, A. Winkelbauer, and C. F. Mecklenbr, “Realistic Performance Model for Vehicle-to-Infrastructure Communications,” no. c, pp. 557–561, 2014.
[28] V. Shivaldova, A. Paier, D. Smely, and C. F. Mecklenbräuker, “On roadside unit antenna measurements for vehicle-to-infrastructure communications,” *IEEE International Symposium on Personal, Indoor and Mobile Radio Communications PIMRC*, pp. 1295–1299, 2012.
[29] W. H. Hayt, Jr., *Engineering Electromagnetics*, Fifth Edit. New York: McGraw-Hill, Inc., 1989.
[30] L. V. Bewley, *Two Dimensional Fields in Electrial Engineering*, 1st ed. New York: Dover Publications, 1963.
[31] D. Corson and P. Lorrain, *Introducing to Electromagnetic Fields and Waves*. San Franscisco: W.H. Freeman, 1962.
[32] R. Wilson, “Propagation Losses Through Common Building Materials 2.4 GHz vs 5 GHz,” *Magis Network, Inc.*, pp. 1–28, 2002.
[33] R. E. Collins, *Antennas and Radio Wave Propagation*. New York: McGraw-Hill, Inc., 2014.
[34] S. L. Salas and E. Hille, *Calculus: One and Several Variables*, 3rd ed. John Wiley and

Sons, Inc., 1978.
[35] R. Plonsey and R. E. Collin, *Principles and Applications of Electromagnetic Fields*. McGraw-Hill, Inc., 1961.
[36] M. Javid and P. M. Brown, *Field Analysis and Electromagnetics*. New York: McGraw-Hill, Inc., 1963.
[37] E. C. Jordan and K. G. Balmain, *Electromagnetic Waves and Radiating Systems*, 2nd ed. Englewood Cliffs: Dorling Kindesley Pearson Education, 2015.
[38] J. D. Kraus, *Electromagnetics*, 4th ed. New York: McGraw-Hill, Inc., 1992.
[39] J. E. Parton, S. J. . Owen, and M. S. Raven, *Applied Electromagnetics*. Palgrave Macmillan, 1985.
[40] D. T. Paris and F. K. Hurd, *Basic Electromagnetic Theory*. McGraw-Hill, Inc., 1969.
[41] R. C. Weast and S. M. Selby, Eds., *Standard Mathematical Tables*, Seventeent. The Chemical Rubber Co., 1969.
[42] S. Ramo, J. R. Whinnery, and T. Van Duzer, *Fields and Waves in Communication Electronics*, 3rd ed. New York: John Wiley and Sons, Inc., 2008.
[43] K. F. Sander and G. A. L. Reed, *Transmission and Propagation of Electromagnetic Waves*, 2nd ed. New York: Cambridge University Press, 1986.
[44] D. K. Cheng, *Field and Wave Electromagnetics*, Second Edi. Reading, Mass.: The Addison-Wesley, 1989.
[45] R. Valenzuela, "A ray tracing approach to predicting indoor wireless transmission," *IEEE 43rd Veh. Technol. Conf.*, pp. 214–218, 1993.
[46] A. M. Bodzin and L. Cirucci, "A Land-Use-Planning Simulation Using Google Earth.," *Sci. Scope*, vol. 32, no. 7, pp. 30–38, 2009.
[47] I. Janssen and A. Rosu, "Measuring sidewalk distances using Google earth," *BMC Med. Res. Methodol.*, vol. 12, no. 39, p. 10, 2012.
[48] S. Bayless, A. Guan, A. Shaw, M. Johnson, G. Pruitt, and B. Abernathy, "Recommended Practices for DSRC Licensing and Spectrum Management: A Guide for Management, Regulation, Deployment, and Administration for Connected Vehicle Environment.," 2015.
[49] F. C. Commission, "Equipment Authorization Order & Accredited Testing Laboratories FCC Equipment Authorization Process," 2017. [Online]. Available: https://transition.fcc.gov/oet/ea/presentations/files/may17/10-EA_Accredited-Labs-GT-Final.pdf.
[50] C. Kwok, R. F. Jr. Cleveland, and D. L. Means, "Evaluating Compliance with FCC Guidelines for Human Exposure to Radiofrequency Electromagnetic Fields Supplement C," 1997.
[51] J. D. M. S. J. L. U. Robert F. Cleveland and Standards, "OET bulletin 65: Evaluating compliance with FCC guidelines for human exposure to radiofrequency electromagnetic fields," 1997.
[52] Cisco Systems, "White Paper on Antenna Patterns and Their Meaning," San Jose, 2007.
[53] Linx Technology, "Application Note," Merlin, 2012.
[54] A. S. C. of the I. A. and Propagation and Society, "IEEE Standard Definitions of Terms for Antennas," 1993.
[55] Campbell Scientific, "The Link Budget and Fade Margin (Application Notes)." Campbell Scientific, Inc., Logan, 2016.
[56] T. Vincenty, "Direct and Inverse Solutions of Geodesics on the Ellipsoid With Application of Nested Equations," *Surv. Rev.*, vol. 23, no. 176, pp. 88–93, 1975.

[57] T. Vincenty, “Geodetic inverse solution between antipodal points,” *Richard Rapp Geodetic Science Ohio State University*. 1975.

Appendix B. Parsing Raw Data Using Python Script and Formatting as a .csv File

Appendix B.1 Overview of Parsing and Formatting Process

The following steps were utilized to parse and format FHWA's DSRC RSU data:

A. Using a Python script, the raw data was parsed from a text file (see section B.2 and B.4)

B. The text file was imported to structured .csv file format (see section B.3)

C. Using Jupyter Notebook open-source software, a second Python was used to calculate the greater circle distance and Vincenty distance with GeoPy (see section B.5).

Notes

1. Jupyter Notebook is an open-source web application that allows creation of live code, equations, visualizations, and narrative text.
2. GeoPy is a Python 2 and 3 client for several popular geocoding web services. Geopy can calculate geodesic distance between two points using the Vincenty distance (https://en.wikipedia.org/wiki/Vincenty's_formulae) and great-circle distance (https://en.wikipedia.org/wiki/Great-circle_distance) formulas.

Appendix B.2 Sample of Data File

Header
--RemoteHost localhost
--RemotePort 37008
--SnapLen 4096
--BufLen 4194304
--UpdatePeriod 1
--Interface cw-mon-rxa
--HdrLen 46
--HdrTag 0x00
--Meta
--RxPos=127.0.0.1:2947
--LogMode CW14
{"epoch" : 1505327128.713449,
 "mac" : Removed to maintain device privacy,
 "TestPkt_CW14_RxData" : {
  "coding_rate"   : 10
 },
 "MultiModeData" : {
  "ThisMode"   : 0,

"NumModes" : 1,
"TxPower_dBm" : 41,
"TxAntenna" : 1
},
"Dot11Header" : {
"FrameCtrl" : 136
},
"PacketMetaData" : {
"PayloadLen" : 338,
"RateID" : 10
},
"data" : {}
}

Epoch Frame

{"epoch" : 1505327128.714001, "Pkts": 1, "Bytes": 338, "Delta": 1505327104.00, "comment": "
Removed data to maintain device privacy", "header":
"mac[#mode|_rate] : latitude longitude range max age sig_A noise_A sig_B
noise_B num loss% kBps","data":{
" Removed data to maintain device privacy":[Removed data to maintain location privacy, -1.00,
0.00, 0.00, -66.00, -101.00, 0.00, 0.00, 1, 99, 0.000]
} }

Rcap Frame

rcap: [cw-mon-rxa] Rx:129 RxChanEst:0 RxNoChanEst:0 RxErr:0 Tx:0 TxErr:0 TxPos:0 BuffAllocErr:0 MinPkt:390 MaxPkt:390 ps_recv:135 ps_drop:0, Filt:129 RxPwrA:-66 RxPwrB:-16384

Epoch Frame

{"epoch" : 1505327129.003994, "Pkts": 128, "Bytes": 43264, "Delta": 0.29, "comment": null,
"header":
"mac[#mode|_rate] : latitude longitude range max age sig_A noise_A sig_B
noise_B num loss% kBps","data":{
" Removed data to maintain device privacy":[Removed data to maintain location privacy, 2.75,
2.75, 0.00, -65.27, -101.87, 0.00, 0.00, 128, 0, 149.190]
} }

Rcap Frame

rcap: [cw-mon-rxa] Rx:529 RxChanEst:0 RxNoChanEst:0 RxErr:0 Tx:0 TxErr:0 TxPos:0 BuffAllocErr:0 MinPkt:390 MaxPkt:390 ps_recv:535 ps_drop:0, Filt:529 RxPwrA:-66 RxPwrB:-16384

The epoch and rcap frames are repeated with the essential data set until the data acquisition system (or test run) is halted.

Appendix B.3 Sample of Formatted .csv file

Epoch Time	Time (HH:mm:ss)	Eastern Std Time (HH:mm:ss)	Latitude	Longitude	Receiver	Receiver Channel Estimate	Receiver No Channel Estimate	Receiver Error	Transmit
1505327129	6:25:29 PM	1:25:29 PM	39.4450322	-76.2051195	129	0	0	0	0
1505327130	6:25:30 PM	1:25:30 PM	39.445032	-76.2051193	529	0	0	0	0

Transmit Error	Transmit Positive	Buff Allocation Error	Miniumum Packet (Kbps)	Maximum Packet (Kbps)	PS Receive	PS Drop	Filt	Receive Power A (dBm)	Receive Power B (dBm)
0	0	0	390	390	135	0	129	-66	-16384
0	0	0	390	390	535	0	529	-66	-16384

Packets Counts	Bytes	Delta	Mac Address	Range (meters)	Maximum	Age	Signal A (dBm)	Noise A (dBm)	Signal - Noise	Signal B
128	43264	0.29	04:e5:48:01:9c:10	2.75	2.75	0	-65.27	-101.87	36.6	0
400	135200	1	04:e5:48:01:9c:10	2.65	2.75	0	-65.89	-101.66	35.77	0

Noise B	Number of Loss %	kBps	Data Rate (Kbps)	Distances	V Distances
0	128	0	149.19	0	0
0	400	0	135.186	0.028106117	0.028076058

Appendix B.4 Python Script

```
#!/usr/bin/python
# Written by Tom Gilmore, Ph.D. and Jonathan Walker, Sr., P.E.

import re

#Counts the number of new lines in one complete set of data (e.g., The set of data is compressed
of 5 newlines (\n)).
num_lines = sum(1 for line in open('Cohda_DSRC_RSU_RxMaxDistanceSteps.txt'))

#open the file titled ... and store the data in variable f (input file)
f = open('Cohda_DSRC_RSU_RxMaxDistanceSteps.txt', 'r')

#open the file titled ... and store the data in variable f2 (output file)
f2 = open('Cohda_DSRC_RSU_RxMaxDistanceSteps.csv','w')

#Loop through each new line
for i in range(num_lines):

      #Read the 1st line and assign the data to part1
         part1 = f.readline()

         if len(part1) > 1:

            #Read the 2nd, 3rd, 4th, and 5th line and assign the data to part2, part3, part4, and
part5
                  part2 = f.readline()
                  part3 = f.readline()
                  part4 = f.readline()
                  part5 = f.readline()

            #Combine the 5 new lines with a space between each new line
                  line = part1.rstrip() + ' ' +  part2.rstrip() + ' ' + part3.rstrip() + part4.rstrip() + part5

                  Rx = re.search('Rx:(.+?) ', line).group(1)
            RxChanEst = re.search('RxChanEst:(.+?) ', line).group(1)
            RxNoChanEst = re.search('RxNoChanEst:(.+?) ', line).group(1)
            RxErr = re.search('RxErr:(.+?) ', line).group(1)
            Tx = re.search('Tx:(.+?) ', line).group(1)
            TxErr = re.search('TxErr:(.+?) ', line).group(1)
            TxPos = re.search('TxPos:(.+?) ', line).group(1)
            BuffAllocErr = re.search('BuffAllocErr:(.+?) ', line).group(1)
```

```
            MinPkt = re.search('MinPkt:(.+?) ', line).group(1)
            MaxPkt = re.search('MaxPkt:(.+?) ', line).group(1)
            ps_recv = re.search('ps_recv:(.+?) ', line).group(1)
            ps_drop = re.search('ps_drop:(.+?),', line).group(1)
            Filt = re.search('Filt:(.+?) ', line).group(1)
                RxPwrA = re.search('RxPwrA:(.+?) ', line).group(1)
            RxPwrB = re.search('RxPwrB:(.+?) ', line).group(1)
                epoch = re.search('epoch\" : (.+?),', line).group(1)
                Pkts = re.search('Pkts\": (.+?),', line).group(1)
                Bytes = re.search('Bytes\": (.+?),', line).group(1)
                Delta = re.search('Delta\": (.+?),', line).group(1)
                mac = re.search('data\": {\"(.+?)#', line).group(1)

                remainder = re.search('#0000\":(.+?)]', line).group(1)
                remainder = remainder[2:].replace(' ',")

                data =
Rx+","+RxChanEst+","+RxNoChanEst+","+RxErr+","+Tx+","+TxErr+","+TxPos+","+BuffAllo
cErr+","+MinPkt+","+MaxPkt+","+ps_recv+","+ps_drop+","+Filt+","+RxPwrA+","+RxPwrB+"
,"+epoch+","+Pkts+","+Bytes+","+Delta+","+mac+","+remainder
                #print Rx, RxChanEst, RxNoChanEst, RxErr, Tx, TxErr, TxPos, BuffAllocErr,
MinPkt, MaxPkt, ps_recv, ps_drop, Filt, RxPwrA, RxPwrB, epoch, Pkts, Bytes, Delta, mac
                #print data
                f2.write(data + "\n")

f.close()
f2.close()
```

Appendix B.5 Python Script Using Jupyter Interface

```
# Written by Tom Gilmore, Ph.D. and Jonathan Walker, Sr., P.E.

import numpy as np
import pandas as pd
from geopy.distance import vincenty
from geopy.distance import great_circle

try:
   data = pd.read_csv("Cohda_DSRC_RSU_RxMaxDistanceSteps.csv")
   print "Dataset has {} samples with {} features each.".format(*data.shape)
except:
   print "Dataset could not be loaded."

data2 = data[['Latitude','Longitude']]

data2.head()

data2.describe()

location1 = (data2['Latitude'][0], data2['Longitude'][0])

location1

location2 = (data2['Latitude'][1], data2['Longitude'][1])

location2

print(great_circle(location1, location2).meters)

dists = []
vicents = []

for i in range(1,len(data2)):
      location1 = (data2['Latitude'][i-1], data2['Longitude'][i-1])
      location2 = (data2['Latitude'][i], data2['Longitude'][i])
      dists.append(great_circle(location1, location2).meters)
      vicents.append(vincenty(location1, location2).meters)

dists = map(str,dists)
vicents = map(str,vicents)
```

```
print len(dists)
print len(vicents)

data['Distances'] = [0] * len(data)
data['Distances'][1:len(data)+1] = dists

data['V Distances'] = [0] * len(data)
data['V Distances'][1:len(data)+1] = vicents

data.to_csv("Cohda_DSRC_RSU_RxMaxDistanceSteps.csv", encoding='utf-8', index=False)
```

Appendix C. Python Script for an Extended Horizontal and Vertical Polarization Neural Network Model

Appendix C.1 Overview of Neural Network Model and Code

The objective of the extended horizontal and vertical polarization neural network model is to provide the probability for packet counts =1 when greater than or equal to 377. The probability is mapped against the total Vincenty distance on the x-axis.

The following permissions are granted provided that the SAS copyright and this notice appear in the score code and any related documentation. Permission to copy, modify, and distribute the score code generated using JMP(R) software is limited to customers of SAS Institute Inc. ("SAS") and successive third parties, all without any warranty, express or implied, or any other obligation by SAS.SAS and all other SAS Institute Inc. product and service names are registered trademarks or trademarks of SAS Institute Inc.in the USA and other countries. Except as contained in this notice, the name of the SAS Institute Inc. and JMP shall not be used in the advertising or promotion of products or services without prior written authorization from SAS Institute Inc.

Copyright(C) 2016 SAS Institute Inc. All rights reserved.

```
 ======================================================================== """

""" Python code generated by JMP v13.0.0 """


""" ========================================================================


def getModelMetadata():
        return {"creator": "Neural", "modelName": "", "predicted": "Logic Packet Counts = 1
When Greater Than or Equal To 377", "table":
"DataPoints130_306CohdaDSRCRSURev1d.jmp", "version": "13.0.0", "timestamp": "2018-07-
23T23:06:11Z"}


def getInputMetadata():
   return {
      "Total Vincenty Distances (meters)": "float"
         }


def getOutputMetadata():
   return {
```

```
    "Probability( Logic Packet Counts = 1 When Greater Than or Equal To 377=0 )": "float",
    "Probability( Logic Packet Counts = 1 When Greater Than or Equal To 377=1 )": "float",
    "Most Likely Logic Packet Counts = 1 When Greater Than or Equal To 377": "float"
      }


def score(indata, outdata):
  # H2_1
  # H2_2
  # H2_3
  # H2_4
  # H2_5
  # H2_6
  # H2_7
  # H2_8
  # H2_9
  # H2_10
  # H2_11
  # H2_12
  # H2_13
  # H2_14
  # H2_15
  # H2_16
  # H2_17
  # H2_18
  # H2_19
  # H2_20
  # H2_21
  # H2_22
  # H2_23
  # H2_24
  # H2_25
  # H2_26
  # H2_27
  # H2_28
  # H2_29
  # H2_30
  # H2_31
  # H2_32
  # H2_33
  # H2_34
  # H2_35
  # H2_36
```

```
# H2_37
# H2_38
# H2_39
# H2_40
# H1_1
_temp0 = 0.79664742641267
# H1_2
_temp1 = 0.370355409364551
# H1_3
_temp2 = -0.0491365571521895
# H1_4
_temp3 = 0.607560711381847
# H1_5
_temp4 = -78.5547293311769
# H1_6
_temp5 = 18.3667252652515
# H1_7
_temp6 = -47.4746097605407
# H1_8
_temp7 = -18.923593614816
# H1_9
_temp8 = 0.127678451601765
# H1_10
_temp9 = -0.148338672826113
# H1_11
_temp10 = 17.0638729387307
# H1_12
_temp11 = -8.88188773948294
# H1_13
_temp12 = -0.949481560574027
# H1_14
_temp13 = 18.4760804606341
# H1_15
_temp14 = -4.2670071588794
# H1_16
_temp15 = -2.05096864569143
# H1_17
_temp16 = -1.93408022640442
# H1_18
_temp17 = -0.457822931029797
# H1_19
_temp18 = 1.08465371110467
# H1_20
```

```
_temp19 = -0.766284689697397
# H1_21
_temp20 = 4.69966331638114
# H1_22
_temp21 = -12.0220270383968
# H1_23
_temp22 = 1.37981380901557
# H1_24
_temp23 = -11.763188492274
# H1_25
_temp24 = -2.80086349746033
# H1_26
_temp25 = 0.32942893748421
# H1_27
_temp26 = -3.74025677825604
# H1_28
_temp27 = 0.815546122705591
# H1_29
_temp28 = 1.4840514172451
# H1_30
_temp29 = 1.13059488617096
# H1_31
_temp30 = -0.160001034291794
# H1_32
_temp31 = -0.872702379297501
# H1_33
_temp32 = 4.49525306150021
# H1_34
_temp33 = 13.2584141150118
# H1_35
_temp34 = 0.544982773818705
# H1_36
_temp35 = -2.40342873420703
# H1_37
_temp36 = 0.749631697255862
# H1_38
_temp37 = -0.542680914160098
# H1_39
_temp38 = 0.107214056407581
# H1_40
_temp39 = -0.896839068944877
_temp40 = 0.378454810089775
_temp41 = 0.378454810089775
```

```
    _temp42 = 0.378454810089775
    # _temp43
    _temp44 = [0 for i in range(2)]
    _temp45 = None

    H2_1 = tanh((0.5 * (0.857363133442572 + -3.21216816322781 * log(((indata['Total Vincenty
Distances (meters)'] - -65.7633356189583) / (3689.20417323271 - indata['Total Vincenty
Distances (meters)']))))))

    H2_2 = tanh((0.5 * (-0.610194592013816 + -0.68003134345508 * log(((indata['Total
Vincenty Distances (meters)'] - -65.7633356189583) / (3689.20417323271 - indata['Total
Vincenty Distances (meters)']))))))

    H2_3 = tanh((0.5 * (2.63063321425099 + -1.51824057345476 * log(((indata['Total Vincenty
Distances (meters)'] - -65.7633356189583) / (3689.20417323271 - indata['Total Vincenty
Distances (meters)']))))))

    H2_4 = tanh((0.5 * (-0.420776594362368 + 0.440272370819754 * log(((indata['Total
Vincenty Distances (meters)'] - -65.7633356189583) / (3689.20417323271 - indata['Total
Vincenty Distances (meters)']))))))

    H2_5 = tanh((0.5 * (-37.7987947345588 + 103.526027348194 * log(((indata['Total Vincenty
Distances (meters)'] - -65.7633356189583) / (3689.20417323271 - indata['Total Vincenty
Distances (meters)']))))))

    H2_6 = tanh((0.5 * (-13.9022883654872 + 6.65226216213189 * log(((indata['Total Vincenty
Distances (meters)'] - -65.7633356189583) / (3689.20417323271 - indata['Total Vincenty
Distances (meters)']))))))

    H2_7 = tanh((0.5 * (1.00800709554725 + -1.20946848174347 * log(((indata['Total Vincenty
Distances (meters)'] - -65.7633356189583) / (3689.20417323271 - indata['Total Vincenty
Distances (meters)']))))))

    H2_8 = tanh((0.5 * (24.2877806324375 + -104.053230023731 * log(((indata['Total Vincenty
Distances (meters)'] - -65.7633356189583) / (3689.20417323271 - indata['Total Vincenty
Distances (meters)']))))))

    H2_9 = tanh((0.5 * (22.7944327226168 + -17.3455073110539 * log(((indata['Total Vincenty
Distances (meters)'] - -65.7633356189583) / (3689.20417323271 - indata['Total Vincenty
Distances (meters)']))))))
```

```
    H2_10 = tanh((0.5 * (-10.5232645939659 + -25.5122325562095 * log(((indata['Total
Vincenty Distances (meters)'] - -65.7633356189583) / (3689.20417323271 - indata['Total
Vincenty Distances (meters)']))))))

    H2_11 = tanh((0.5 * (86.2177402121353 + -16.8819497986111 * log(((indata['Total Vincenty
Distances (meters)'] - -65.7633356189583) / (3689.20417323271 - indata['Total Vincenty
Distances (meters)']))))))

    H2_12 = tanh((0.5 * (0.45875340063702 + 13.4438264757575 * log(((indata['Total Vincenty
Distances (meters)'] - -65.7633356189583) / (3689.20417323271 - indata['Total Vincenty
Distances (meters)']))))))

    H2_13 = tanh((0.5 * (55.6978361177562 + -88.6475653733629 * log(((indata['Total Vincenty
Distances (meters)'] - -65.7633356189583) / (3689.20417323271 - indata['Total Vincenty
Distances (meters)']))))))

    H2_14 = tanh((0.5 * (2.92796055696259 + 0.393596107791808 * log(((indata['Total
Vincenty Distances (meters)'] - -65.7633356189583) / (3689.20417323271 - indata['Total
Vincenty Distances (meters)']))))))

    H2_15 = tanh((0.5 * (-23.1478009686313 + 20.0057647284366 * log(((indata['Total Vincenty
Distances (meters)'] - -65.7633356189583) / (3689.20417323271 - indata['Total Vincenty
Distances (meters)']))))))

    H2_16 = tanh((0.5 * (-14.0432898426385 + -5.64188272966226 * log(((indata['Total
Vincenty Distances (meters)'] - -65.7633356189583) / (3689.20417323271 - indata['Total
Vincenty Distances (meters)']))))))

    H2_17 = tanh((0.5 * (-2.57282867824696 + -1.89239580660054 * log(((indata['Total
Vincenty Distances (meters)'] - -65.7633356189583) / (3689.20417323271 - indata['Total
Vincenty Distances (meters)']))))))

    H2_18 = tanh((0.5 * (-0.666211636181071 + -0.839754566493371 * log(((indata['Total
Vincenty Distances (meters)'] - -65.7633356189583) / (3689.20417323271 - indata['Total
Vincenty Distances (meters)']))))))

    H2_19 = tanh((0.5 * (0.517768443297628 + -0.0545196624947596 * log(((indata['Total
Vincenty Distances (meters)'] - -65.7633356189583) / (3689.20417323271 - indata['Total
Vincenty Distances (meters)']))))))

    H2_20 = tanh((0.5 * (-0.204196880922019 + 0.101934294785167 * log(((indata['Total
Vincenty Distances (meters)'] - -65.7633356189583) / (3689.20417323271 - indata['Total
Vincenty Distances (meters)']))))))
```

```
    H2_21 = tanh((0.5 * (-29.580921791295 + 11.5574789762162 * log(((indata['Total Vincenty
Distances (meters)'] - -65.7633356189583) / (3689.20417323271 - indata['Total Vincenty
Distances (meters)']))))))

    H2_22 = tanh((0.5 * (-3.32192323311978 + -1.92907619020791 * log(((indata['Total
Vincenty Distances (meters)'] - -65.7633356189583) / (3689.20417323271 - indata['Total
Vincenty Distances (meters)']))))))

    H2_23 = tanh((0.5 * (16.3149987349477 + -3.89812376954703 * log(((indata['Total Vincenty
Distances (meters)'] - -65.7633356189583) / (3689.20417323271 - indata['Total Vincenty
Distances (meters)']))))))

    H2_24 = tanh((0.5 * (3.92702037494339 + 0.291775082538617 * log(((indata['Total
Vincenty Distances (meters)'] - -65.7633356189583) / (3689.20417323271 - indata['Total
Vincenty Distances (meters)']))))))

    H2_25 = tanh((0.5 * (-7.58120700643604 + 59.131957789841 * log(((indata['Total Vincenty
Distances (meters)'] - -65.7633356189583) / (3689.20417323271 - indata['Total Vincenty
Distances (meters)']))))))

    H2_26 = tanh((0.5 * (-0.166493224386744 + -1.03109934588228 * log(((indata['Total
Vincenty Distances (meters)'] - -65.7633356189583) / (3689.20417323271 - indata['Total
Vincenty Distances (meters)']))))))

    H2_27 = tanh((0.5 * (2.72942795843569 + -2.24090373436115 * log(((indata['Total Vincenty
Distances (meters)'] - -65.7633356189583) / (3689.20417323271 - indata['Total Vincenty
Distances (meters)']))))))

    H2_28 = tanh((0.5 * (-2.95320741590675 + 4.06917555864697 * log(((indata['Total Vincenty
Distances (meters)'] - -65.7633356189583) / (3689.20417323271 - indata['Total Vincenty
Distances (meters)']))))))

    H2_29 = tanh((0.5 * (-2.18617429119737 + 14.6761701367385 * log(((indata['Total Vincenty
Distances (meters)'] - -65.7633356189583) / (3689.20417323271 - indata['Total Vincenty
Distances (meters)']))))))

    H2_30 = tanh((0.5 * (1.28558406318601 + 1.30205152289237 * log(((indata['Total Vincenty
Distances (meters)'] - -65.7633356189583) / (3689.20417323271 - indata['Total Vincenty
Distances (meters)']))))))
```

```
    H2_31 = tanh((0.5 * (-0.409192010029739 + -0.0114850306393101 * log(((indata['Total
Vincenty Distances (meters)'] - -65.7633356189583) / (3689.20417323271 - indata['Total
Vincenty Distances (meters)']))))))

    H2_32 = tanh((0.5 * (-1.47656576904351 + 2.27785592345645 * log(((indata['Total Vincenty
Distances (meters)'] - -65.7633356189583) / (3689.20417323271 - indata['Total Vincenty
Distances (meters)']))))))

    H2_33 = tanh((0.5 * (12.4814414113197 + -12.5956572883369 * log(((indata['Total Vincenty
Distances (meters)'] - -65.7633356189583) / (3689.20417323271 - indata['Total Vincenty
Distances (meters)']))))))

    H2_34 = tanh((0.5 * (5.42787391809287 + -5.22745257948279 * log(((indata['Total Vincenty
Distances (meters)'] - -65.7633356189583) / (3689.20417323271 - indata['Total Vincenty
Distances (meters)']))))))

    H2_35 = tanh((0.5 * (-1.87881675802321 + 1.8497062088686 * log(((indata['Total Vincenty
Distances (meters)'] - -65.7633356189583) / (3689.20417323271 - indata['Total Vincenty
Distances (meters)']))))))

    H2_36 = tanh((0.5 * (-2.03664176904169 + 4.47146263674033 * log(((indata['Total Vincenty
Distances (meters)'] - -65.7633356189583) / (3689.20417323271 - indata['Total Vincenty
Distances (meters)']))))))

    H2_37 = tanh((0.5 * (-0.639169638487311 + 5.11003074988251 * log(((indata['Total
Vincenty Distances (meters)'] - -65.7633356189583) / (3689.20417323271 - indata['Total
Vincenty Distances (meters)']))))))

    H2_38 = tanh((0.5 * (-0.626979082066627 + 0.279536273505492 * log(((indata['Total
Vincenty Distances (meters)'] - -65.7633356189583) / (3689.20417323271 - indata['Total
Vincenty Distances (meters)']))))))

    H2_39 = tanh((0.5 * (-0.95799496905267 + -0.246131213756424 * log(((indata['Total
Vincenty Distances (meters)'] - -65.7633356189583) / (3689.20417323271 - indata['Total
Vincenty Distances (meters)']))))))

    H2_40 = tanh((0.5 * (1.88872626578627 + 0.999716925778541 * log(((indata['Total
Vincenty Distances (meters)'] - -65.7633356189583) / (3689.20417323271 - indata['Total
Vincenty Distances (meters)']))))))

    _temp0 += 0.300569041792547 * H2_1
    _temp0 += 1.74533151070861 * H2_2
    _temp0 += 1.56849040268515 * H2_3
```

```
_temp0 += 3.77586451185533 * H2_4
_temp0 += 0 * H2_5
_temp0 += 0 * H2_6
_temp0 += 0 * H2_7
_temp0 += 0 * H2_8
_temp0 += 0 * H2_9
_temp0 += 0 * H2_10
_temp0 += 0 * H2_11
_temp0 += 0 * H2_12
_temp0 += 0 * H2_13
_temp0 += 0 * H2_14
_temp0 += 0 * H2_15
_temp0 += 0 * H2_16
_temp0 += 0 * H2_17
_temp0 += 0 * H2_18
_temp0 += 0 * H2_19
_temp0 += 0 * H2_20
_temp0 += 0 * H2_21
_temp0 += 0 * H2_22
_temp0 += 0 * H2_23
_temp0 += 0 * H2_24
_temp0 += 0 * H2_25
_temp0 += 0 * H2_26
_temp0 += 0 * H2_27
_temp0 += 0 * H2_28
_temp0 += 0 * H2_29
_temp0 += 0 * H2_30
_temp0 += 0 * H2_31
_temp0 += 0 * H2_32
_temp0 += 0 * H2_33
_temp0 += 0 * H2_34
_temp0 += 0 * H2_35
_temp0 += 0 * H2_36
_temp0 += 0 * H2_37
_temp0 += 0 * H2_38
_temp0 += 0 * H2_39
_temp0 += 0 * H2_40
H1_1 = tanh((0.5 * _temp0))

_temp1 += 1.8102499945118 * H2_1
_temp1 += -0.329160923897948 * H2_2
_temp1 += 1.36542079672709 * H2_3
_temp1 += -1.29839663121996 * H2_4
```

```
_temp1 += 0 * H2_5
_temp1 += 0 * H2_6
_temp1 += 0 * H2_7
_temp1 += 0 * H2_8
_temp1 += 0 * H2_9
_temp1 += 0 * H2_10
_temp1 += 0 * H2_11
_temp1 += 0 * H2_12
_temp1 += 0 * H2_13
_temp1 += 0 * H2_14
_temp1 += 0 * H2_15
_temp1 += 0 * H2_16
_temp1 += 0 * H2_17
_temp1 += 0 * H2_18
_temp1 += 0 * H2_19
_temp1 += 0 * H2_20
_temp1 += 0 * H2_21
_temp1 += 0 * H2_22
_temp1 += 0 * H2_23
_temp1 += 0 * H2_24
_temp1 += 0 * H2_25
_temp1 += 0 * H2_26
_temp1 += 0 * H2_27
_temp1 += 0 * H2_28
_temp1 += 0 * H2_29
_temp1 += 0 * H2_30
_temp1 += 0 * H2_31
_temp1 += 0 * H2_32
_temp1 += 0 * H2_33
_temp1 += 0 * H2_34
_temp1 += 0 * H2_35
_temp1 += 0 * H2_36
_temp1 += 0 * H2_37
_temp1 += 0 * H2_38
_temp1 += 0 * H2_39
_temp1 += 0 * H2_40
H1_2 = tanh((0.5 * _temp1))

_temp2 += 2.70653416962 * H2_1
_temp2 += 0.606885680721196 * H2_2
_temp2 += 0.809119442030925 * H2_3
_temp2 += 0.515064493340598 * H2_4
_temp2 += 0 * H2_5
```

```
_temp2 += 0 * H2_6
_temp2 += 0 * H2_7
_temp2 += 0 * H2_8
_temp2 += 0 * H2_9
_temp2 += 0 * H2_10
_temp2 += 0 * H2_11
_temp2 += 0 * H2_12
_temp2 += 0 * H2_13
_temp2 += 0 * H2_14
_temp2 += 0 * H2_15
_temp2 += 0 * H2_16
_temp2 += 0 * H2_17
_temp2 += 0 * H2_18
_temp2 += 0 * H2_19
_temp2 += 0 * H2_20
_temp2 += 0 * H2_21
_temp2 += 0 * H2_22
_temp2 += 0 * H2_23
_temp2 += 0 * H2_24
_temp2 += 0 * H2_25
_temp2 += 0 * H2_26
_temp2 += 0 * H2_27
_temp2 += 0 * H2_28
_temp2 += 0 * H2_29
_temp2 += 0 * H2_30
_temp2 += 0 * H2_31
_temp2 += 0 * H2_32
_temp2 += 0 * H2_33
_temp2 += 0 * H2_34
_temp2 += 0 * H2_35
_temp2 += 0 * H2_36
_temp2 += 0 * H2_37
_temp2 += 0 * H2_38
_temp2 += 0 * H2_39
_temp2 += 0 * H2_40
H1_3 = tanh((0.5 * _temp2))

_temp3 += -4.65353695752121 * H2_1
_temp3 += -1.09859178878904 * H2_2
_temp3 += -0.176768290079901 * H2_3
_temp3 += 1.26484435306261 * H2_4
_temp3 += 0 * H2_5
_temp3 += 0 * H2_6
```

```
_temp3 += 0 * H2_7
_temp3 += 0 * H2_8
_temp3 += 0 * H2_9
_temp3 += 0 * H2_10
_temp3 += 0 * H2_11
_temp3 += 0 * H2_12
_temp3 += 0 * H2_13
_temp3 += 0 * H2_14
_temp3 += 0 * H2_15
_temp3 += 0 * H2_16
_temp3 += 0 * H2_17
_temp3 += 0 * H2_18
_temp3 += 0 * H2_19
_temp3 += 0 * H2_20
_temp3 += 0 * H2_21
_temp3 += 0 * H2_22
_temp3 += 0 * H2_23
_temp3 += 0 * H2_24
_temp3 += 0 * H2_25
_temp3 += 0 * H2_26
_temp3 += 0 * H2_27
_temp3 += 0 * H2_28
_temp3 += 0 * H2_29
_temp3 += 0 * H2_30
_temp3 += 0 * H2_31
_temp3 += 0 * H2_32
_temp3 += 0 * H2_33
_temp3 += 0 * H2_34
_temp3 += 0 * H2_35
_temp3 += 0 * H2_36
_temp3 += 0 * H2_37
_temp3 += 0 * H2_38
_temp3 += 0 * H2_39
_temp3 += 0 * H2_40
H1_4 = tanh((0.5 * _temp3))

_temp4 += 0 * H2_1
_temp4 += 0 * H2_2
_temp4 += 0 * H2_3
_temp4 += 0 * H2_4
_temp4 += -0.629327586008451 * H2_5
_temp4 += -9.57030477975966 * H2_6
_temp4 += -17.8408010563176 * H2_7
```

```
_temp4 += -73.3867395088319 * H2_8
_temp4 += 0 * H2_9
_temp4 += 0 * H2_10
_temp4 += 0 * H2_11
_temp4 += 0 * H2_12
_temp4 += 0 * H2_13
_temp4 += 0 * H2_14
_temp4 += 0 * H2_15
_temp4 += 0 * H2_16
_temp4 += 0 * H2_17
_temp4 += 0 * H2_18
_temp4 += 0 * H2_19
_temp4 += 0 * H2_20
_temp4 += 0 * H2_21
_temp4 += 0 * H2_22
_temp4 += 0 * H2_23
_temp4 += 0 * H2_24
_temp4 += 0 * H2_25
_temp4 += 0 * H2_26
_temp4 += 0 * H2_27
_temp4 += 0 * H2_28
_temp4 += 0 * H2_29
_temp4 += 0 * H2_30
_temp4 += 0 * H2_31
_temp4 += 0 * H2_32
_temp4 += 0 * H2_33
_temp4 += 0 * H2_34
_temp4 += 0 * H2_35
_temp4 += 0 * H2_36
_temp4 += 0 * H2_37
_temp4 += 0 * H2_38
_temp4 += 0 * H2_39
_temp4 += 0 * H2_40
H1_5 = tanh((0.5 * _temp4))

_temp5 += 0 * H2_1
_temp5 += 0 * H2_2
_temp5 += 0 * H2_3
_temp5 += 0 * H2_4
_temp5 += 23.5075748745771 * H2_5
_temp5 += 83.5329619499037 * H2_6
_temp5 += -36.3551874461466 * H2_7
_temp5 += -8.31279547945436 * H2_8
```

```
_temp5 += 0 * H2_9
_temp5 += 0 * H2_10
_temp5 += 0 * H2_11
_temp5 += 0 * H2_12
_temp5 += 0 * H2_13
_temp5 += 0 * H2_14
_temp5 += 0 * H2_15
_temp5 += 0 * H2_16
_temp5 += 0 * H2_17
_temp5 += 0 * H2_18
_temp5 += 0 * H2_19
_temp5 += 0 * H2_20
_temp5 += 0 * H2_21
_temp5 += 0 * H2_22
_temp5 += 0 * H2_23
_temp5 += 0 * H2_24
_temp5 += 0 * H2_25
_temp5 += 0 * H2_26
_temp5 += 0 * H2_27
_temp5 += 0 * H2_28
_temp5 += 0 * H2_29
_temp5 += 0 * H2_30
_temp5 += 0 * H2_31
_temp5 += 0 * H2_32
_temp5 += 0 * H2_33
_temp5 += 0 * H2_34
_temp5 += 0 * H2_35
_temp5 += 0 * H2_36
_temp5 += 0 * H2_37
_temp5 += 0 * H2_38
_temp5 += 0 * H2_39
_temp5 += 0 * H2_40
H1_6 = tanh((0.5 * _temp5))

_temp6 += 0 * H2_1
_temp6 += 0 * H2_2
_temp6 += 0 * H2_3
_temp6 += 0 * H2_4
_temp6 += -141.086005649992 * H2_5
_temp6 += -41.3854537418617 * H2_6
_temp6 += -72.058397403622 * H2_7
_temp6 += -32.5661507603619 * H2_8
_temp6 += 0 * H2_9
```

```
_temp6 += 0 * H2_10
_temp6 += 0 * H2_11
_temp6 += 0 * H2_12
_temp6 += 0 * H2_13
_temp6 += 0 * H2_14
_temp6 += 0 * H2_15
_temp6 += 0 * H2_16
_temp6 += 0 * H2_17
_temp6 += 0 * H2_18
_temp6 += 0 * H2_19
_temp6 += 0 * H2_20
_temp6 += 0 * H2_21
_temp6 += 0 * H2_22
_temp6 += 0 * H2_23
_temp6 += 0 * H2_24
_temp6 += 0 * H2_25
_temp6 += 0 * H2_26
_temp6 += 0 * H2_27
_temp6 += 0 * H2_28
_temp6 += 0 * H2_29
_temp6 += 0 * H2_30
_temp6 += 0 * H2_31
_temp6 += 0 * H2_32
_temp6 += 0 * H2_33
_temp6 += 0 * H2_34
_temp6 += 0 * H2_35
_temp6 += 0 * H2_36
_temp6 += 0 * H2_37
_temp6 += 0 * H2_38
_temp6 += 0 * H2_39
_temp6 += 0 * H2_40
H1_7 = tanh((0.5 * _temp6))

_temp7 += 0 * H2_1
_temp7 += 0 * H2_2
_temp7 += 0 * H2_3
_temp7 += 0 * H2_4
_temp7 += 98.0119014531861 * H2_5
_temp7 += -70.9075620798307 * H2_6
_temp7 += -1.54568668153401 * H2_7
_temp7 += 43.1025820363088 * H2_8
_temp7 += 0 * H2_9
_temp7 += 0 * H2_10
```

```
_temp7 += 0 * H2_11
_temp7 += 0 * H2_12
_temp7 += 0 * H2_13
_temp7 += 0 * H2_14
_temp7 += 0 * H2_15
_temp7 += 0 * H2_16
_temp7 += 0 * H2_17
_temp7 += 0 * H2_18
_temp7 += 0 * H2_19
_temp7 += 0 * H2_20
_temp7 += 0 * H2_21
_temp7 += 0 * H2_22
_temp7 += 0 * H2_23
_temp7 += 0 * H2_24
_temp7 += 0 * H2_25
_temp7 += 0 * H2_26
_temp7 += 0 * H2_27
_temp7 += 0 * H2_28
_temp7 += 0 * H2_29
_temp7 += 0 * H2_30
_temp7 += 0 * H2_31
_temp7 += 0 * H2_32
_temp7 += 0 * H2_33
_temp7 += 0 * H2_34
_temp7 += 0 * H2_35
_temp7 += 0 * H2_36
_temp7 += 0 * H2_37
_temp7 += 0 * H2_38
_temp7 += 0 * H2_39
_temp7 += 0 * H2_40
H1_8 = tanh((0.5 * _temp7))

_temp8 += 0 * H2_1
_temp8 += 0 * H2_2
_temp8 += 0 * H2_3
_temp8 += 0 * H2_4
_temp8 += 0 * H2_5
_temp8 += 0 * H2_6
_temp8 += 0 * H2_7
_temp8 += 0 * H2_8
_temp8 += -12.261529064192 * H2_9
_temp8 += 10.1996553936984 * H2_10
_temp8 += 0.526848607104603 * H2_11
```

```
_temp8 += -20.342460041019 * H2_12
_temp8 += 0 * H2_13
_temp8 += 0 * H2_14
_temp8 += 0 * H2_15
_temp8 += 0 * H2_16
_temp8 += 0 * H2_17
_temp8 += 0 * H2_18
_temp8 += 0 * H2_19
_temp8 += 0 * H2_20
_temp8 += 0 * H2_21
_temp8 += 0 * H2_22
_temp8 += 0 * H2_23
_temp8 += 0 * H2_24
_temp8 += 0 * H2_25
_temp8 += 0 * H2_26
_temp8 += 0 * H2_27
_temp8 += 0 * H2_28
_temp8 += 0 * H2_29
_temp8 += 0 * H2_30
_temp8 += 0 * H2_31
_temp8 += 0 * H2_32
_temp8 += 0 * H2_33
_temp8 += 0 * H2_34
_temp8 += 0 * H2_35
_temp8 += 0 * H2_36
_temp8 += 0 * H2_37
_temp8 += 0 * H2_38
_temp8 += 0 * H2_39
_temp8 += 0 * H2_40
H1_9 = tanh((0.5 * _temp8))

_temp9 += 0 * H2_1
_temp9 += 0 * H2_2
_temp9 += 0 * H2_3
_temp9 += 0 * H2_4
_temp9 += 0 * H2_5
_temp9 += 0 * H2_6
_temp9 += 0 * H2_7
_temp9 += 0 * H2_8
_temp9 += 0.0155708624898591 * H2_9
_temp9 += -3.68475589169318 * H2_10
_temp9 += -0.100382148281777 * H2_11
_temp9 += 14.4563849787454 * H2_12
```

```
_temp9 += 0 * H2_13
_temp9 += 0 * H2_14
_temp9 += 0 * H2_15
_temp9 += 0 * H2_16
_temp9 += 0 * H2_17
_temp9 += 0 * H2_18
_temp9 += 0 * H2_19
_temp9 += 0 * H2_20
_temp9 += 0 * H2_21
_temp9 += 0 * H2_22
_temp9 += 0 * H2_23
_temp9 += 0 * H2_24
_temp9 += 0 * H2_25
_temp9 += 0 * H2_26
_temp9 += 0 * H2_27
_temp9 += 0 * H2_28
_temp9 += 0 * H2_29
_temp9 += 0 * H2_30
_temp9 += 0 * H2_31
_temp9 += 0 * H2_32
_temp9 += 0 * H2_33
_temp9 += 0 * H2_34
_temp9 += 0 * H2_35
_temp9 += 0 * H2_36
_temp9 += 0 * H2_37
_temp9 += 0 * H2_38
_temp9 += 0 * H2_39
_temp9 += 0 * H2_40
H1_10 = tanh((0.5 * _temp9))

_temp10 += 0 * H2_1
_temp10 += 0 * H2_2
_temp10 += 0 * H2_3
_temp10 += 0 * H2_4
_temp10 += 0 * H2_5
_temp10 += 0 * H2_6
_temp10 += 0 * H2_7
_temp10 += 0 * H2_8
_temp10 += -20.9664584314721 * H2_9
_temp10 += -8.41127995397991 * H2_10
_temp10 += -29.1847731471165 * H2_11
_temp10 += 19.4082394781292 * H2_12
_temp10 += 0 * H2_13
```

```
_temp10 += 0 * H2_14
_temp10 += 0 * H2_15
_temp10 += 0 * H2_16
_temp10 += 0 * H2_17
_temp10 += 0 * H2_18
_temp10 += 0 * H2_19
_temp10 += 0 * H2_20
_temp10 += 0 * H2_21
_temp10 += 0 * H2_22
_temp10 += 0 * H2_23
_temp10 += 0 * H2_24
_temp10 += 0 * H2_25
_temp10 += 0 * H2_26
_temp10 += 0 * H2_27
_temp10 += 0 * H2_28
_temp10 += 0 * H2_29
_temp10 += 0 * H2_30
_temp10 += 0 * H2_31
_temp10 += 0 * H2_32
_temp10 += 0 * H2_33
_temp10 += 0 * H2_34
_temp10 += 0 * H2_35
_temp10 += 0 * H2_36
_temp10 += 0 * H2_37
_temp10 += 0 * H2_38
_temp10 += 0 * H2_39
_temp10 += 0 * H2_40
H1_11 = tanh((0.5 * _temp10))

_temp11 += 0 * H2_1
_temp11 += 0 * H2_2
_temp11 += 0 * H2_3
_temp11 += 0 * H2_4
_temp11 += 0 * H2_5
_temp11 += 0 * H2_6
_temp11 += 0 * H2_7
_temp11 += 0 * H2_8
_temp11 += -26.0642623941954 * H2_9
_temp11 += 1.79463026923561 * H2_10
_temp11 += -21.2203562368336 * H2_11
_temp11 += 6.35966025371559 * H2_12
_temp11 += 0 * H2_13
_temp11 += 0 * H2_14
```

```
_temp11 += 0 * H2_15
_temp11 += 0 * H2_16
_temp11 += 0 * H2_17
_temp11 += 0 * H2_18
_temp11 += 0 * H2_19
_temp11 += 0 * H2_20
_temp11 += 0 * H2_21
_temp11 += 0 * H2_22
_temp11 += 0 * H2_23
_temp11 += 0 * H2_24
_temp11 += 0 * H2_25
_temp11 += 0 * H2_26
_temp11 += 0 * H2_27
_temp11 += 0 * H2_28
_temp11 += 0 * H2_29
_temp11 += 0 * H2_30
_temp11 += 0 * H2_31
_temp11 += 0 * H2_32
_temp11 += 0 * H2_33
_temp11 += 0 * H2_34
_temp11 += 0 * H2_35
_temp11 += 0 * H2_36
_temp11 += 0 * H2_37
_temp11 += 0 * H2_38
_temp11 += 0 * H2_39
_temp11 += 0 * H2_40
H1_12 = tanh((0.5 * _temp11))

_temp12 += 0 * H2_1
_temp12 += 0 * H2_2
_temp12 += 0 * H2_3
_temp12 += 0 * H2_4
_temp12 += 0 * H2_5
_temp12 += 0 * H2_6
_temp12 += 0 * H2_7
_temp12 += 0 * H2_8
_temp12 += 0 * H2_9
_temp12 += 0 * H2_10
_temp12 += 0 * H2_11
_temp12 += 0 * H2_12
_temp12 += 3.99586227348622 * H2_13
_temp12 += 0.0958429261564822 * H2_14
_temp12 += 8.79954706457756 * H2_15
```

```
_temp12 += 12.3665837154673 * H2_16
_temp12 += 0 * H2_17
_temp12 += 0 * H2_18
_temp12 += 0 * H2_19
_temp12 += 0 * H2_20
_temp12 += 0 * H2_21
_temp12 += 0 * H2_22
_temp12 += 0 * H2_23
_temp12 += 0 * H2_24
_temp12 += 0 * H2_25
_temp12 += 0 * H2_26
_temp12 += 0 * H2_27
_temp12 += 0 * H2_28
_temp12 += 0 * H2_29
_temp12 += 0 * H2_30
_temp12 += 0 * H2_31
_temp12 += 0 * H2_32
_temp12 += 0 * H2_33
_temp12 += 0 * H2_34
_temp12 += 0 * H2_35
_temp12 += 0 * H2_36
_temp12 += 0 * H2_37
_temp12 += 0 * H2_38
_temp12 += 0 * H2_39
_temp12 += 0 * H2_40
H1_13 = tanh((0.5 * _temp12))

_temp13 += 0 * H2_1
_temp13 += 0 * H2_2
_temp13 += 0 * H2_3
_temp13 += 0 * H2_4
_temp13 += 0 * H2_5
_temp13 += 0 * H2_6
_temp13 += 0 * H2_7
_temp13 += 0 * H2_8
_temp13 += 0 * H2_9
_temp13 += 0 * H2_10
_temp13 += 0 * H2_11
_temp13 += 0 * H2_12
_temp13 += 24.5912043410209 * H2_13
_temp13 += 8.04018123624971 * H2_14
_temp13 += -22.5338429956479 * H2_15
_temp13 += -2.34030699783377 * H2_16
```

```
_temp13 += 0 * H2_17
_temp13 += 0 * H2_18
_temp13 += 0 * H2_19
_temp13 += 0 * H2_20
_temp13 += 0 * H2_21
_temp13 += 0 * H2_22
_temp13 += 0 * H2_23
_temp13 += 0 * H2_24
_temp13 += 0 * H2_25
_temp13 += 0 * H2_26
_temp13 += 0 * H2_27
_temp13 += 0 * H2_28
_temp13 += 0 * H2_29
_temp13 += 0 * H2_30
_temp13 += 0 * H2_31
_temp13 += 0 * H2_32
_temp13 += 0 * H2_33
_temp13 += 0 * H2_34
_temp13 += 0 * H2_35
_temp13 += 0 * H2_36
_temp13 += 0 * H2_37
_temp13 += 0 * H2_38
_temp13 += 0 * H2_39
_temp13 += 0 * H2_40
H1_14 = tanh((0.5 * _temp13))

_temp14 += 0 * H2_1
_temp14 += 0 * H2_2
_temp14 += 0 * H2_3
_temp14 += 0 * H2_4
_temp14 += 0 * H2_5
_temp14 += 0 * H2_6
_temp14 += 0 * H2_7
_temp14 += 0 * H2_8
_temp14 += 0 * H2_9
_temp14 += 0 * H2_10
_temp14 += 0 * H2_11
_temp14 += 0 * H2_12
_temp14 += -0.281630744795144 * H2_13
_temp14 += -0.815095166103845 * H2_14
_temp14 += -7.87151624565874 * H2_15
_temp14 += -1.62558011442175 * H2_16
_temp14 += 0 * H2_17
```

```
_temp14 += 0 * H2_18
_temp14 += 0 * H2_19
_temp14 += 0 * H2_20
_temp14 += 0 * H2_21
_temp14 += 0 * H2_22
_temp14 += 0 * H2_23
_temp14 += 0 * H2_24
_temp14 += 0 * H2_25
_temp14 += 0 * H2_26
_temp14 += 0 * H2_27
_temp14 += 0 * H2_28
_temp14 += 0 * H2_29
_temp14 += 0 * H2_30
_temp14 += 0 * H2_31
_temp14 += 0 * H2_32
_temp14 += 0 * H2_33
_temp14 += 0 * H2_34
_temp14 += 0 * H2_35
_temp14 += 0 * H2_36
_temp14 += 0 * H2_37
_temp14 += 0 * H2_38
_temp14 += 0 * H2_39
_temp14 += 0 * H2_40
H1_15 = tanh((0.5 * _temp14))

_temp15 += 0 * H2_1
_temp15 += 0 * H2_2
_temp15 += 0 * H2_3
_temp15 += 0 * H2_4
_temp15 += 0 * H2_5
_temp15 += 0 * H2_6
_temp15 += 0 * H2_7
_temp15 += 0 * H2_8
_temp15 += 0 * H2_9
_temp15 += 0 * H2_10
_temp15 += 0 * H2_11
_temp15 += 0 * H2_12
_temp15 += -2.21737765235428 * H2_13
_temp15 += -0.360815926894465 * H2_14
_temp15 += -5.97867981940379 * H2_15
_temp15 += -6.99496621670163 * H2_16
_temp15 += 0 * H2_17
_temp15 += 0 * H2_18
```

```
_temp15 += 0 * H2_19
_temp15 += 0 * H2_20
_temp15 += 0 * H2_21
_temp15 += 0 * H2_22
_temp15 += 0 * H2_23
_temp15 += 0 * H2_24
_temp15 += 0 * H2_25
_temp15 += 0 * H2_26
_temp15 += 0 * H2_27
_temp15 += 0 * H2_28
_temp15 += 0 * H2_29
_temp15 += 0 * H2_30
_temp15 += 0 * H2_31
_temp15 += 0 * H2_32
_temp15 += 0 * H2_33
_temp15 += 0 * H2_34
_temp15 += 0 * H2_35
_temp15 += 0 * H2_36
_temp15 += 0 * H2_37
_temp15 += 0 * H2_38
_temp15 += 0 * H2_39
_temp15 += 0 * H2_40
H1_16 = tanh((0.5 * _temp15))

_temp16 += 0 * H2_1
_temp16 += 0 * H2_2
_temp16 += 0 * H2_3
_temp16 += 0 * H2_4
_temp16 += 0 * H2_5
_temp16 += 0 * H2_6
_temp16 += 0 * H2_7
_temp16 += 0 * H2_8
_temp16 += 0 * H2_9
_temp16 += 0 * H2_10
_temp16 += 0 * H2_11
_temp16 += 0 * H2_12
_temp16 += 0 * H2_13
_temp16 += 0 * H2_14
_temp16 += 0 * H2_15
_temp16 += 0 * H2_16
_temp16 += 0.468203309336794 * H2_17
_temp16 += -0.113366935164924 * H2_18
_temp16 += 0.89201252249722 * H2_19
```

```
_temp16 += 1.55412552582064 * H2_20
_temp16 += 0 * H2_21
_temp16 += 0 * H2_22
_temp16 += 0 * H2_23
_temp16 += 0 * H2_24
_temp16 += 0 * H2_25
_temp16 += 0 * H2_26
_temp16 += 0 * H2_27
_temp16 += 0 * H2_28
_temp16 += 0 * H2_29
_temp16 += 0 * H2_30
_temp16 += 0 * H2_31
_temp16 += 0 * H2_32
_temp16 += 0 * H2_33
_temp16 += 0 * H2_34
_temp16 += 0 * H2_35
_temp16 += 0 * H2_36
_temp16 += 0 * H2_37
_temp16 += 0 * H2_38
_temp16 += 0 * H2_39
_temp16 += 0 * H2_40
H1_17 = tanh((0.5 * _temp16))

_temp17 += 0 * H2_1
_temp17 += 0 * H2_2
_temp17 += 0 * H2_3
_temp17 += 0 * H2_4
_temp17 += 0 * H2_5
_temp17 += 0 * H2_6
_temp17 += 0 * H2_7
_temp17 += 0 * H2_8
_temp17 += 0 * H2_9
_temp17 += 0 * H2_10
_temp17 += 0 * H2_11
_temp17 += 0 * H2_12
_temp17 += 0 * H2_13
_temp17 += 0 * H2_14
_temp17 += 0 * H2_15
_temp17 += 0 * H2_16
_temp17 += -1.29226136016536 * H2_17
_temp17 += -1.91424364372117 * H2_18
_temp17 += -0.311520000862641 * H2_19
_temp17 += 0.25835163770618 * H2_20
```

```
_temp17 += 0 * H2_21
_temp17 += 0 * H2_22
_temp17 += 0 * H2_23
_temp17 += 0 * H2_24
_temp17 += 0 * H2_25
_temp17 += 0 * H2_26
_temp17 += 0 * H2_27
_temp17 += 0 * H2_28
_temp17 += 0 * H2_29
_temp17 += 0 * H2_30
_temp17 += 0 * H2_31
_temp17 += 0 * H2_32
_temp17 += 0 * H2_33
_temp17 += 0 * H2_34
_temp17 += 0 * H2_35
_temp17 += 0 * H2_36
_temp17 += 0 * H2_37
_temp17 += 0 * H2_38
_temp17 += 0 * H2_39
_temp17 += 0 * H2_40
H1_18 = tanh((0.5 * _temp17))

_temp18 += 0 * H2_1
_temp18 += 0 * H2_2
_temp18 += 0 * H2_3
_temp18 += 0 * H2_4
_temp18 += 0 * H2_5
_temp18 += 0 * H2_6
_temp18 += 0 * H2_7
_temp18 += 0 * H2_8
_temp18 += 0 * H2_9
_temp18 += 0 * H2_10
_temp18 += 0 * H2_11
_temp18 += 0 * H2_12
_temp18 += 0 * H2_13
_temp18 += 0 * H2_14
_temp18 += 0 * H2_15
_temp18 += 0 * H2_16
_temp18 += -2.76981726019547 * H2_17
_temp18 += -0.477443165293951 * H2_18
_temp18 += 0.139643590994897 * H2_19
_temp18 += 0.0158176389007988 * H2_20
_temp18 += 0 * H2_21
```

```
_temp18 += 0 * H2_22
_temp18 += 0 * H2_23
_temp18 += 0 * H2_24
_temp18 += 0 * H2_25
_temp18 += 0 * H2_26
_temp18 += 0 * H2_27
_temp18 += 0 * H2_28
_temp18 += 0 * H2_29
_temp18 += 0 * H2_30
_temp18 += 0 * H2_31
_temp18 += 0 * H2_32
_temp18 += 0 * H2_33
_temp18 += 0 * H2_34
_temp18 += 0 * H2_35
_temp18 += 0 * H2_36
_temp18 += 0 * H2_37
_temp18 += 0 * H2_38
_temp18 += 0 * H2_39
_temp18 += 0 * H2_40
H1_19 = tanh((0.5 * _temp18))

_temp19 += 0 * H2_1
_temp19 += 0 * H2_2
_temp19 += 0 * H2_3
_temp19 += 0 * H2_4
_temp19 += 0 * H2_5
_temp19 += 0 * H2_6
_temp19 += 0 * H2_7
_temp19 += 0 * H2_8
_temp19 += 0 * H2_9
_temp19 += 0 * H2_10
_temp19 += 0 * H2_11
_temp19 += 0 * H2_12
_temp19 += 0 * H2_13
_temp19 += 0 * H2_14
_temp19 += 0 * H2_15
_temp19 += 0 * H2_16
_temp19 += 0.367578754848451 * H2_17
_temp19 += -1.70442569526778 * H2_18
_temp19 += -0.187371644154435 * H2_19
_temp19 += -0.743145337241529 * H2_20
_temp19 += 0 * H2_21
_temp19 += 0 * H2_22
```

```
_temp19 += 0 * H2_23
_temp19 += 0 * H2_24
_temp19 += 0 * H2_25
_temp19 += 0 * H2_26
_temp19 += 0 * H2_27
_temp19 += 0 * H2_28
_temp19 += 0 * H2_29
_temp19 += 0 * H2_30
_temp19 += 0 * H2_31
_temp19 += 0 * H2_32
_temp19 += 0 * H2_33
_temp19 += 0 * H2_34
_temp19 += 0 * H2_35
_temp19 += 0 * H2_36
_temp19 += 0 * H2_37
_temp19 += 0 * H2_38
_temp19 += 0 * H2_39
_temp19 += 0 * H2_40
H1_20 = tanh((0.5 * _temp19))

_temp20 += 0 * H2_1
_temp20 += 0 * H2_2
_temp20 += 0 * H2_3
_temp20 += 0 * H2_4
_temp20 += 0 * H2_5
_temp20 += 0 * H2_6
_temp20 += 0 * H2_7
_temp20 += 0 * H2_8
_temp20 += 0 * H2_9
_temp20 += 0 * H2_10
_temp20 += 0 * H2_11
_temp20 += 0 * H2_12
_temp20 += 0 * H2_13
_temp20 += 0 * H2_14
_temp20 += 0 * H2_15
_temp20 += 0 * H2_16
_temp20 += 0 * H2_17
_temp20 += 0 * H2_18
_temp20 += 0 * H2_19
_temp20 += 0 * H2_20
_temp20 += 5.69788365654628 * H2_21
_temp20 += -1.19058827742183 * H2_22
_temp20 += 4.75604867652631 * H2_23
```

```
_temp20 += 0.716636486889683 * H2_24
_temp20 += 0 * H2_25
_temp20 += 0 * H2_26
_temp20 += 0 * H2_27
_temp20 += 0 * H2_28
_temp20 += 0 * H2_29
_temp20 += 0 * H2_30
_temp20 += 0 * H2_31
_temp20 += 0 * H2_32
_temp20 += 0 * H2_33
_temp20 += 0 * H2_34
_temp20 += 0 * H2_35
_temp20 += 0 * H2_36
_temp20 += 0 * H2_37
_temp20 += 0 * H2_38
_temp20 += 0 * H2_39
_temp20 += 0 * H2_40
H1_21 = tanh((0.5 * _temp20))

_temp21 += 0 * H2_1
_temp21 += 0 * H2_2
_temp21 += 0 * H2_3
_temp21 += 0 * H2_4
_temp21 += 0 * H2_5
_temp21 += 0 * H2_6
_temp21 += 0 * H2_7
_temp21 += 0 * H2_8
_temp21 += 0 * H2_9
_temp21 += 0 * H2_10
_temp21 += 0 * H2_11
_temp21 += 0 * H2_12
_temp21 += 0 * H2_13
_temp21 += 0 * H2_14
_temp21 += 0 * H2_15
_temp21 += 0 * H2_16
_temp21 += 0 * H2_17
_temp21 += 0 * H2_18
_temp21 += 0 * H2_19
_temp21 += 0 * H2_20
_temp21 += 33.3083083454135 * H2_21
_temp21 += -3.7066728555188 * H2_22
_temp21 += -16.2582083670967 * H2_23
_temp21 += 16.3090244172886 * H2_24
```

```
_temp21 += 0 * H2_25
_temp21 += 0 * H2_26
_temp21 += 0 * H2_27
_temp21 += 0 * H2_28
_temp21 += 0 * H2_29
_temp21 += 0 * H2_30
_temp21 += 0 * H2_31
_temp21 += 0 * H2_32
_temp21 += 0 * H2_33
_temp21 += 0 * H2_34
_temp21 += 0 * H2_35
_temp21 += 0 * H2_36
_temp21 += 0 * H2_37
_temp21 += 0 * H2_38
_temp21 += 0 * H2_39
_temp21 += 0 * H2_40
H1_22 = tanh((0.5 * _temp21))

_temp22 += 0 * H2_1
_temp22 += 0 * H2_2
_temp22 += 0 * H2_3
_temp22 += 0 * H2_4
_temp22 += 0 * H2_5
_temp22 += 0 * H2_6
_temp22 += 0 * H2_7
_temp22 += 0 * H2_8
_temp22 += 0 * H2_9
_temp22 += 0 * H2_10
_temp22 += 0 * H2_11
_temp22 += 0 * H2_12
_temp22 += 0 * H2_13
_temp22 += 0 * H2_14
_temp22 += 0 * H2_15
_temp22 += 0 * H2_16
_temp22 += 0 * H2_17
_temp22 += 0 * H2_18
_temp22 += 0 * H2_19
_temp22 += 0 * H2_20
_temp22 += -2.10444135324781 * H2_21
_temp22 += 0.148493013012874 * H2_22
_temp22 += -10.294725325666 * H2_23
_temp22 += 8.47828352928663 * H2_24
_temp22 += 0 * H2_25
```

```
_temp22 += 0 * H2_26
_temp22 += 0 * H2_27
_temp22 += 0 * H2_28
_temp22 += 0 * H2_29
_temp22 += 0 * H2_30
_temp22 += 0 * H2_31
_temp22 += 0 * H2_32
_temp22 += 0 * H2_33
_temp22 += 0 * H2_34
_temp22 += 0 * H2_35
_temp22 += 0 * H2_36
_temp22 += 0 * H2_37
_temp22 += 0 * H2_38
_temp22 += 0 * H2_39
_temp22 += 0 * H2_40
H1_23 = tanh((0.5 * _temp22))

_temp23 += 0 * H2_1
_temp23 += 0 * H2_2
_temp23 += 0 * H2_3
_temp23 += 0 * H2_4
_temp23 += 0 * H2_5
_temp23 += 0 * H2_6
_temp23 += 0 * H2_7
_temp23 += 0 * H2_8
_temp23 += 0 * H2_9
_temp23 += 0 * H2_10
_temp23 += 0 * H2_11
_temp23 += 0 * H2_12
_temp23 += 0 * H2_13
_temp23 += 0 * H2_14
_temp23 += 0 * H2_15
_temp23 += 0 * H2_16
_temp23 += 0 * H2_17
_temp23 += 0 * H2_18
_temp23 += 0 * H2_19
_temp23 += 0 * H2_20
_temp23 += -48.5163132663767 * H2_21
_temp23 += -5.88282200454063 * H2_22
_temp23 += -18.2042162019721 * H2_23
_temp23 += 7.97290319535305 * H2_24
_temp23 += 0 * H2_25
_temp23 += 0 * H2_26
```

```
_temp23 += 0 * H2_27
_temp23 += 0 * H2_28
_temp23 += 0 * H2_29
_temp23 += 0 * H2_30
_temp23 += 0 * H2_31
_temp23 += 0 * H2_32
_temp23 += 0 * H2_33
_temp23 += 0 * H2_34
_temp23 += 0 * H2_35
_temp23 += 0 * H2_36
_temp23 += 0 * H2_37
_temp23 += 0 * H2_38
_temp23 += 0 * H2_39
_temp23 += 0 * H2_40
H1_24 = tanh((0.5 * _temp23))

_temp24 += 0 * H2_1
_temp24 += 0 * H2_2
_temp24 += 0 * H2_3
_temp24 += 0 * H2_4
_temp24 += 0 * H2_5
_temp24 += 0 * H2_6
_temp24 += 0 * H2_7
_temp24 += 0 * H2_8
_temp24 += 0 * H2_9
_temp24 += 0 * H2_10
_temp24 += 0 * H2_11
_temp24 += 0 * H2_12
_temp24 += 0 * H2_13
_temp24 += 0 * H2_14
_temp24 += 0 * H2_15
_temp24 += 0 * H2_16
_temp24 += 0 * H2_17
_temp24 += 0 * H2_18
_temp24 += 0 * H2_19
_temp24 += 0 * H2_20
_temp24 += 0 * H2_21
_temp24 += 0 * H2_22
_temp24 += 0 * H2_23
_temp24 += 0 * H2_24
_temp24 += -2.70399696762067 * H2_25
_temp24 += 1.0888808375831 * H2_26
_temp24 += -0.705945103890998 * H2_27
```

```
_temp24 += -2.12862368017978 * H2_28
_temp24 += 0 * H2_29
_temp24 += 0 * H2_30
_temp24 += 0 * H2_31
_temp24 += 0 * H2_32
_temp24 += 0 * H2_33
_temp24 += 0 * H2_34
_temp24 += 0 * H2_35
_temp24 += 0 * H2_36
_temp24 += 0 * H2_37
_temp24 += 0 * H2_38
_temp24 += 0 * H2_39
_temp24 += 0 * H2_40
H1_25 = tanh((0.5 * _temp24))

_temp25 += 0 * H2_1
_temp25 += 0 * H2_2
_temp25 += 0 * H2_3
_temp25 += 0 * H2_4
_temp25 += 0 * H2_5
_temp25 += 0 * H2_6
_temp25 += 0 * H2_7
_temp25 += 0 * H2_8
_temp25 += 0 * H2_9
_temp25 += 0 * H2_10
_temp25 += 0 * H2_11
_temp25 += 0 * H2_12
_temp25 += 0 * H2_13
_temp25 += 0 * H2_14
_temp25 += 0 * H2_15
_temp25 += 0 * H2_16
_temp25 += 0 * H2_17
_temp25 += 0 * H2_18
_temp25 += 0 * H2_19
_temp25 += 0 * H2_20
_temp25 += 0 * H2_21
_temp25 += 0 * H2_22
_temp25 += 0 * H2_23
_temp25 += 0 * H2_24
_temp25 += -2.4731320106112 * H2_25
_temp25 += 0.298565176700032 * H2_26
_temp25 += -2.05225539803987 * H2_27
_temp25 += 2.43511526429564 * H2_28
```

```
_temp25 += 0 * H2_29
_temp25 += 0 * H2_30
_temp25 += 0 * H2_31
_temp25 += 0 * H2_32
_temp25 += 0 * H2_33
_temp25 += 0 * H2_34
_temp25 += 0 * H2_35
_temp25 += 0 * H2_36
_temp25 += 0 * H2_37
_temp25 += 0 * H2_38
_temp25 += 0 * H2_39
_temp25 += 0 * H2_40
H1_26 = tanh((0.5 * _temp25))

_temp26 += 0 * H2_1
_temp26 += 0 * H2_2
_temp26 += 0 * H2_3
_temp26 += 0 * H2_4
_temp26 += 0 * H2_5
_temp26 += 0 * H2_6
_temp26 += 0 * H2_7
_temp26 += 0 * H2_8
_temp26 += 0 * H2_9
_temp26 += 0 * H2_10
_temp26 += 0 * H2_11
_temp26 += 0 * H2_12
_temp26 += 0 * H2_13
_temp26 += 0 * H2_14
_temp26 += 0 * H2_15
_temp26 += 0 * H2_16
_temp26 += 0 * H2_17
_temp26 += 0 * H2_18
_temp26 += 0 * H2_19
_temp26 += 0 * H2_20
_temp26 += 0 * H2_21
_temp26 += 0 * H2_22
_temp26 += 0 * H2_23
_temp26 += 0 * H2_24
_temp26 += 8.27470691283592 * H2_25
_temp26 += 1.48683335248394 * H2_26
_temp26 += -6.26343581172309 * H2_27
_temp26 += -2.56308610887932 * H2_28
_temp26 += 0 * H2_29
```

```
_temp26 += 0 * H2_30
_temp26 += 0 * H2_31
_temp26 += 0 * H2_32
_temp26 += 0 * H2_33
_temp26 += 0 * H2_34
_temp26 += 0 * H2_35
_temp26 += 0 * H2_36
_temp26 += 0 * H2_37
_temp26 += 0 * H2_38
_temp26 += 0 * H2_39
_temp26 += 0 * H2_40
H1_27 = tanh((0.5 * _temp26))

_temp27 += 0 * H2_1
_temp27 += 0 * H2_2
_temp27 += 0 * H2_3
_temp27 += 0 * H2_4
_temp27 += 0 * H2_5
_temp27 += 0 * H2_6
_temp27 += 0 * H2_7
_temp27 += 0 * H2_8
_temp27 += 0 * H2_9
_temp27 += 0 * H2_10
_temp27 += 0 * H2_11
_temp27 += 0 * H2_12
_temp27 += 0 * H2_13
_temp27 += 0 * H2_14
_temp27 += 0 * H2_15
_temp27 += 0 * H2_16
_temp27 += 0 * H2_17
_temp27 += 0 * H2_18
_temp27 += 0 * H2_19
_temp27 += 0 * H2_20
_temp27 += 0 * H2_21
_temp27 += 0 * H2_22
_temp27 += 0 * H2_23
_temp27 += 0 * H2_24
_temp27 += 0.586111930200343 * H2_25
_temp27 += -0.318010777300626 * H2_26
_temp27 += 0.406189344729985 * H2_27
_temp27 += 0.0707456713524507 * H2_28
_temp27 += 0 * H2_29
_temp27 += 0 * H2_30
```

```
_temp27 += 0 * H2_31
_temp27 += 0 * H2_32
_temp27 += 0 * H2_33
_temp27 += 0 * H2_34
_temp27 += 0 * H2_35
_temp27 += 0 * H2_36
_temp27 += 0 * H2_37
_temp27 += 0 * H2_38
_temp27 += 0 * H2_39
_temp27 += 0 * H2_40
H1_28 = tanh((0.5 * _temp27))

_temp28 += 0 * H2_1
_temp28 += 0 * H2_2
_temp28 += 0 * H2_3
_temp28 += 0 * H2_4
_temp28 += 0 * H2_5
_temp28 += 0 * H2_6
_temp28 += 0 * H2_7
_temp28 += 0 * H2_8
_temp28 += 0 * H2_9
_temp28 += 0 * H2_10
_temp28 += 0 * H2_11
_temp28 += 0 * H2_12
_temp28 += 0 * H2_13
_temp28 += 0 * H2_14
_temp28 += 0 * H2_15
_temp28 += 0 * H2_16
_temp28 += 0 * H2_17
_temp28 += 0 * H2_18
_temp28 += 0 * H2_19
_temp28 += 0 * H2_20
_temp28 += 0 * H2_21
_temp28 += 0 * H2_22
_temp28 += 0 * H2_23
_temp28 += 0 * H2_24
_temp28 += 0 * H2_25
_temp28 += 0 * H2_26
_temp28 += 0 * H2_27
_temp28 += 0 * H2_28
_temp28 += -2.97940500093091 * H2_29
_temp28 += -1.06823073985758 * H2_30
_temp28 += 0.281486909706899 * H2_31
```

```
_temp28 += 0.0253692500825705 * H2_32
_temp28 += 0 * H2_33
_temp28 += 0 * H2_34
_temp28 += 0 * H2_35
_temp28 += 0 * H2_36
_temp28 += 0 * H2_37
_temp28 += 0 * H2_38
_temp28 += 0 * H2_39
_temp28 += 0 * H2_40
H1_29 = tanh((0.5 * _temp28))

_temp29 += 0 * H2_1
_temp29 += 0 * H2_2
_temp29 += 0 * H2_3
_temp29 += 0 * H2_4
_temp29 += 0 * H2_5
_temp29 += 0 * H2_6
_temp29 += 0 * H2_7
_temp29 += 0 * H2_8
_temp29 += 0 * H2_9
_temp29 += 0 * H2_10
_temp29 += 0 * H2_11
_temp29 += 0 * H2_12
_temp29 += 0 * H2_13
_temp29 += 0 * H2_14
_temp29 += 0 * H2_15
_temp29 += 0 * H2_16
_temp29 += 0 * H2_17
_temp29 += 0 * H2_18
_temp29 += 0 * H2_19
_temp29 += 0 * H2_20
_temp29 += 0 * H2_21
_temp29 += 0 * H2_22
_temp29 += 0 * H2_23
_temp29 += 0 * H2_24
_temp29 += 0 * H2_25
_temp29 += 0 * H2_26
_temp29 += 0 * H2_27
_temp29 += 0 * H2_28
_temp29 += 0.441070005874754 * H2_29
_temp29 += 0.842450570133094 * H2_30
_temp29 += -0.0442533085765791 * H2_31
_temp29 += -3.85116843527979 * H2_32
```

```
_temp29 += 0 * H2_33
_temp29 += 0 * H2_34
_temp29 += 0 * H2_35
_temp29 += 0 * H2_36
_temp29 += 0 * H2_37
_temp29 += 0 * H2_38
_temp29 += 0 * H2_39
_temp29 += 0 * H2_40
H1_30 = tanh((0.5 * _temp29))

_temp30 += 0 * H2_1
_temp30 += 0 * H2_2
_temp30 += 0 * H2_3
_temp30 += 0 * H2_4
_temp30 += 0 * H2_5
_temp30 += 0 * H2_6
_temp30 += 0 * H2_7
_temp30 += 0 * H2_8
_temp30 += 0 * H2_9
_temp30 += 0 * H2_10
_temp30 += 0 * H2_11
_temp30 += 0 * H2_12
_temp30 += 0 * H2_13
_temp30 += 0 * H2_14
_temp30 += 0 * H2_15
_temp30 += 0 * H2_16
_temp30 += 0 * H2_17
_temp30 += 0 * H2_18
_temp30 += 0 * H2_19
_temp30 += 0 * H2_20
_temp30 += 0 * H2_21
_temp30 += 0 * H2_22
_temp30 += 0 * H2_23
_temp30 += 0 * H2_24
_temp30 += 0 * H2_25
_temp30 += 0 * H2_26
_temp30 += 0 * H2_27
_temp30 += 0 * H2_28
_temp30 += 0.548268385413295 * H2_29
_temp30 += -2.03323279502144 * H2_30
_temp30 += -0.170707423184607 * H2_31
_temp30 += -2.50183933074792 * H2_32
_temp30 += 0 * H2_33
```

```
_temp30 += 0 * H2_34
_temp30 += 0 * H2_35
_temp30 += 0 * H2_36
_temp30 += 0 * H2_37
_temp30 += 0 * H2_38
_temp30 += 0 * H2_39
_temp30 += 0 * H2_40
H1_31 = tanh((0.5 * _temp30))

_temp31 += 0 * H2_1
_temp31 += 0 * H2_2
_temp31 += 0 * H2_3
_temp31 += 0 * H2_4
_temp31 += 0 * H2_5
_temp31 += 0 * H2_6
_temp31 += 0 * H2_7
_temp31 += 0 * H2_8
_temp31 += 0 * H2_9
_temp31 += 0 * H2_10
_temp31 += 0 * H2_11
_temp31 += 0 * H2_12
_temp31 += 0 * H2_13
_temp31 += 0 * H2_14
_temp31 += 0 * H2_15
_temp31 += 0 * H2_16
_temp31 += 0 * H2_17
_temp31 += 0 * H2_18
_temp31 += 0 * H2_19
_temp31 += 0 * H2_20
_temp31 += 0 * H2_21
_temp31 += 0 * H2_22
_temp31 += 0 * H2_23
_temp31 += 0 * H2_24
_temp31 += 0 * H2_25
_temp31 += 0 * H2_26
_temp31 += 0 * H2_27
_temp31 += 0 * H2_28
_temp31 += 0.939698383963261 * H2_29
_temp31 += 0.0658209936317344 * H2_30
_temp31 += -0.197014123960453 * H2_31
_temp31 += -0.8704006724575 * H2_32
_temp31 += 0 * H2_33
_temp31 += 0 * H2_34
```

```
_temp31 += 0 * H2_35
_temp31 += 0 * H2_36
_temp31 += 0 * H2_37
_temp31 += 0 * H2_38
_temp31 += 0 * H2_39
_temp31 += 0 * H2_40
H1_32 = tanh((0.5 * _temp31))

_temp32 += 0 * H2_1
_temp32 += 0 * H2_2
_temp32 += 0 * H2_3
_temp32 += 0 * H2_4
_temp32 += 0 * H2_5
_temp32 += 0 * H2_6
_temp32 += 0 * H2_7
_temp32 += 0 * H2_8
_temp32 += 0 * H2_9
_temp32 += 0 * H2_10
_temp32 += 0 * H2_11
_temp32 += 0 * H2_12
_temp32 += 0 * H2_13
_temp32 += 0 * H2_14
_temp32 += 0 * H2_15
_temp32 += 0 * H2_16
_temp32 += 0 * H2_17
_temp32 += 0 * H2_18
_temp32 += 0 * H2_19
_temp32 += 0 * H2_20
_temp32 += 0 * H2_21
_temp32 += 0 * H2_22
_temp32 += 0 * H2_23
_temp32 += 0 * H2_24
_temp32 += 0 * H2_25
_temp32 += 0 * H2_26
_temp32 += 0 * H2_27
_temp32 += 0 * H2_28
_temp32 += 0 * H2_29
_temp32 += 0 * H2_30
_temp32 += 0 * H2_31
_temp32 += 0 * H2_32
_temp32 += -0.281952405014332 * H2_33
_temp32 += -4.05269697036467 * H2_34
_temp32 += 2.49358981684101 * H2_35
```

```
_temp32 += -2.26470387062786 * H2_36
_temp32 += 0 * H2_37
_temp32 += 0 * H2_38
_temp32 += 0 * H2_39
_temp32 += 0 * H2_40
H1_33 = tanh((0.5 * _temp32))

_temp33 += 0 * H2_1
_temp33 += 0 * H2_2
_temp33 += 0 * H2_3
_temp33 += 0 * H2_4
_temp33 += 0 * H2_5
_temp33 += 0 * H2_6
_temp33 += 0 * H2_7
_temp33 += 0 * H2_8
_temp33 += 0 * H2_9
_temp33 += 0 * H2_10
_temp33 += 0 * H2_11
_temp33 += 0 * H2_12
_temp33 += 0 * H2_13
_temp33 += 0 * H2_14
_temp33 += 0 * H2_15
_temp33 += 0 * H2_16
_temp33 += 0 * H2_17
_temp33 += 0 * H2_18
_temp33 += 0 * H2_19
_temp33 += 0 * H2_20
_temp33 += 0 * H2_21
_temp33 += 0 * H2_22
_temp33 += 0 * H2_23
_temp33 += 0 * H2_24
_temp33 += 0 * H2_25
_temp33 += 0 * H2_26
_temp33 += 0 * H2_27
_temp33 += 0 * H2_28
_temp33 += 0 * H2_29
_temp33 += 0 * H2_30
_temp33 += 0 * H2_31
_temp33 += 0 * H2_32
_temp33 += -2.76433946650708 * H2_33
_temp33 += -10.1493158397865 * H2_34
_temp33 += -4.86363688188127 * H2_35
_temp33 += -11.8820757642353 * H2_36
```

```
_temp33 += 0 * H2_37
_temp33 += 0 * H2_38
_temp33 += 0 * H2_39
_temp33 += 0 * H2_40
H1_34 = tanh((0.5 * _temp33))

_temp34 += 0 * H2_1
_temp34 += 0 * H2_2
_temp34 += 0 * H2_3
_temp34 += 0 * H2_4
_temp34 += 0 * H2_5
_temp34 += 0 * H2_6
_temp34 += 0 * H2_7
_temp34 += 0 * H2_8
_temp34 += 0 * H2_9
_temp34 += 0 * H2_10
_temp34 += 0 * H2_11
_temp34 += 0 * H2_12
_temp34 += 0 * H2_13
_temp34 += 0 * H2_14
_temp34 += 0 * H2_15
_temp34 += 0 * H2_16
_temp34 += 0 * H2_17
_temp34 += 0 * H2_18
_temp34 += 0 * H2_19
_temp34 += 0 * H2_20
_temp34 += 0 * H2_21
_temp34 += 0 * H2_22
_temp34 += 0 * H2_23
_temp34 += 0 * H2_24
_temp34 += 0 * H2_25
_temp34 += 0 * H2_26
_temp34 += 0 * H2_27
_temp34 += 0 * H2_28
_temp34 += 0 * H2_29
_temp34 += 0 * H2_30
_temp34 += 0 * H2_31
_temp34 += 0 * H2_32
_temp34 += -0.911235853034649 * H2_33
_temp34 += -1.21062234580154 * H2_34
_temp34 += 1.5825558833083 * H2_35
_temp34 += 3.37233704374699 * H2_36
_temp34 += 0 * H2_37
```

```
_temp34 += 0 * H2_38
_temp34 += 0 * H2_39
_temp34 += 0 * H2_40
H1_35 = tanh((0.5 * _temp34))

_temp35 += 0 * H2_1
_temp35 += 0 * H2_2
_temp35 += 0 * H2_3
_temp35 += 0 * H2_4
_temp35 += 0 * H2_5
_temp35 += 0 * H2_6
_temp35 += 0 * H2_7
_temp35 += 0 * H2_8
_temp35 += 0 * H2_9
_temp35 += 0 * H2_10
_temp35 += 0 * H2_11
_temp35 += 0 * H2_12
_temp35 += 0 * H2_13
_temp35 += 0 * H2_14
_temp35 += 0 * H2_15
_temp35 += 0 * H2_16
_temp35 += 0 * H2_17
_temp35 += 0 * H2_18
_temp35 += 0 * H2_19
_temp35 += 0 * H2_20
_temp35 += 0 * H2_21
_temp35 += 0 * H2_22
_temp35 += 0 * H2_23
_temp35 += 0 * H2_24
_temp35 += 0 * H2_25
_temp35 += 0 * H2_26
_temp35 += 0 * H2_27
_temp35 += 0 * H2_28
_temp35 += 0 * H2_29
_temp35 += 0 * H2_30
_temp35 += 0 * H2_31
_temp35 += 0 * H2_32
_temp35 += -5.03232443298946 * H2_33
_temp35 += 2.05025057856504 * H2_34
_temp35 += 2.17479612900866 * H2_35
_temp35 += 4.52913053252561 * H2_36
_temp35 += 0 * H2_37
_temp35 += 0 * H2_38
```

```
_temp35 += 0 * H2_39
_temp35 += 0 * H2_40
H1_36 = tanh((0.5 * _temp35))

_temp36 += 0 * H2_1
_temp36 += 0 * H2_2
_temp36 += 0 * H2_3
_temp36 += 0 * H2_4
_temp36 += 0 * H2_5
_temp36 += 0 * H2_6
_temp36 += 0 * H2_7
_temp36 += 0 * H2_8
_temp36 += 0 * H2_9
_temp36 += 0 * H2_10
_temp36 += 0 * H2_11
_temp36 += 0 * H2_12
_temp36 += 0 * H2_13
_temp36 += 0 * H2_14
_temp36 += 0 * H2_15
_temp36 += 0 * H2_16
_temp36 += 0 * H2_17
_temp36 += 0 * H2_18
_temp36 += 0 * H2_19
_temp36 += 0 * H2_20
_temp36 += 0 * H2_21
_temp36 += 0 * H2_22
_temp36 += 0 * H2_23
_temp36 += 0 * H2_24
_temp36 += 0 * H2_25
_temp36 += 0 * H2_26
_temp36 += 0 * H2_27
_temp36 += 0 * H2_28
_temp36 += 0 * H2_29
_temp36 += 0 * H2_30
_temp36 += 0 * H2_31
_temp36 += 0 * H2_32
_temp36 += 0 * H2_33
_temp36 += 0 * H2_34
_temp36 += 0 * H2_35
_temp36 += 0 * H2_36
_temp36 += 2.02625035418046 * H2_37
_temp36 += -1.09358784793566 * H2_38
_temp36 += -0.118242608797789 * H2_39
```

```
_temp36 += -1.0081088600916 * H2_40
H1_37 = tanh((0.5 * _temp36))

_temp37 += 0 * H2_1
_temp37 += 0 * H2_2
_temp37 += 0 * H2_3
_temp37 += 0 * H2_4
_temp37 += 0 * H2_5
_temp37 += 0 * H2_6
_temp37 += 0 * H2_7
_temp37 += 0 * H2_8
_temp37 += 0 * H2_9
_temp37 += 0 * H2_10
_temp37 += 0 * H2_11
_temp37 += 0 * H2_12
_temp37 += 0 * H2_13
_temp37 += 0 * H2_14
_temp37 += 0 * H2_15
_temp37 += 0 * H2_16
_temp37 += 0 * H2_17
_temp37 += 0 * H2_18
_temp37 += 0 * H2_19
_temp37 += 0 * H2_20
_temp37 += 0 * H2_21
_temp37 += 0 * H2_22
_temp37 += 0 * H2_23
_temp37 += 0 * H2_24
_temp37 += 0 * H2_25
_temp37 += 0 * H2_26
_temp37 += 0 * H2_27
_temp37 += 0 * H2_28
_temp37 += 0 * H2_29
_temp37 += 0 * H2_30
_temp37 += 0 * H2_31
_temp37 += 0 * H2_32
_temp37 += 0 * H2_33
_temp37 += 0 * H2_34
_temp37 += 0 * H2_35
_temp37 += 0 * H2_36
_temp37 += -0.665294488783435 * H2_37
_temp37 += 0.312427387573377 * H2_38
_temp37 += 0.381516770841108 * H2_39
_temp37 += -0.106951539220484 * H2_40
```

```
H1_38 = tanh((0.5 * _temp37))

_temp38 += 0 * H2_1
_temp38 += 0 * H2_2
_temp38 += 0 * H2_3
_temp38 += 0 * H2_4
_temp38 += 0 * H2_5
_temp38 += 0 * H2_6
_temp38 += 0 * H2_7
_temp38 += 0 * H2_8
_temp38 += 0 * H2_9
_temp38 += 0 * H2_10
_temp38 += 0 * H2_11
_temp38 += 0 * H2_12
_temp38 += 0 * H2_13
_temp38 += 0 * H2_14
_temp38 += 0 * H2_15
_temp38 += 0 * H2_16
_temp38 += 0 * H2_17
_temp38 += 0 * H2_18
_temp38 += 0 * H2_19
_temp38 += 0 * H2_20
_temp38 += 0 * H2_21
_temp38 += 0 * H2_22
_temp38 += 0 * H2_23
_temp38 += 0 * H2_24
_temp38 += 0 * H2_25
_temp38 += 0 * H2_26
_temp38 += 0 * H2_27
_temp38 += 0 * H2_28
_temp38 += 0 * H2_29
_temp38 += 0 * H2_30
_temp38 += 0 * H2_31
_temp38 += 0 * H2_32
_temp38 += 0 * H2_33
_temp38 += 0 * H2_34
_temp38 += 0 * H2_35
_temp38 += 0 * H2_36
_temp38 += 0.230155377782323 * H2_37
_temp38 += -0.155255193821996 * H2_38
_temp38 += -0.620870223275214 * H2_39
_temp38 += 0.781736800208992 * H2_40
H1_39 = tanh((0.5 * _temp38))
```

```
_temp39 += 0 * H2_1
_temp39 += 0 * H2_2
_temp39 += 0 * H2_3
_temp39 += 0 * H2_4
_temp39 += 0 * H2_5
_temp39 += 0 * H2_6
_temp39 += 0 * H2_7
_temp39 += 0 * H2_8
_temp39 += 0 * H2_9
_temp39 += 0 * H2_10
_temp39 += 0 * H2_11
_temp39 += 0 * H2_12
_temp39 += 0 * H2_13
_temp39 += 0 * H2_14
_temp39 += 0 * H2_15
_temp39 += 0 * H2_16
_temp39 += 0 * H2_17
_temp39 += 0 * H2_18
_temp39 += 0 * H2_19
_temp39 += 0 * H2_20
_temp39 += 0 * H2_21
_temp39 += 0 * H2_22
_temp39 += 0 * H2_23
_temp39 += 0 * H2_24
_temp39 += 0 * H2_25
_temp39 += 0 * H2_26
_temp39 += 0 * H2_27
_temp39 += 0 * H2_28
_temp39 += 0 * H2_29
_temp39 += 0 * H2_30
_temp39 += 0 * H2_31
_temp39 += 0 * H2_32
_temp39 += 0 * H2_33
_temp39 += 0 * H2_34
_temp39 += 0 * H2_35
_temp39 += 0 * H2_36
_temp39 += 1.34043347029519 * H2_37
_temp39 += 0.847485389246957 * H2_38
_temp39 += -0.866263103850933 * H2_39
_temp39 += 1.07345891136857 * H2_40
H1_40 = tanh((0.5 * _temp39))
```

```
_temp40 += 7.81696633926759 * H1_1
_temp40 += -6.55624717875302 * H1_2
_temp40 += 7.18515621973926 * H1_3
_temp40 += 3.95210863384018 * H1_4
_temp40 += 21.0178170478464 * H1_5
_temp40 += 0.914165633348978 * H1_6
_temp40 += 13.8093630354397 * H1_7
_temp40 += -7.14529189379519 * H1_8
_temp40 += 0.640135862640473 * H1_9
_temp40 += 0.680683889159819 * H1_10
_temp40 += 0.896112369169927 * H1_11
_temp40 += -1.26851068460609 * H1_12
_temp40 += -0.256467223728002 * H1_13
_temp40 += -0.701156598830882 * H1_14
_temp40 += 0.230782832634894 * H1_15
_temp40 += 1.26114014935077 * H1_16
_temp40 += -0.0193723586158285 * H1_17
_temp40 += 0.166347082989199 * H1_18
_temp40 += -0.227311228540184 * H1_19
_temp40 += 0.190152737298724 * H1_20
_temp40 += -2.30285342572461 * H1_21
_temp40 += 2.05041430719741 * H1_22
_temp40 += 2.57871471816594 * H1_23
_temp40 += 0.171055686104518 * H1_24
_temp40 += 0.500572176932325 * H1_25
_temp40 += -0.21104989985949 * H1_26
_temp40 += 0.709967986939336 * H1_27
_temp40 += -0.185128212988592 * H1_28
_temp40 += -0.166088221826469 * H1_29
_temp40 += -0.198640109280141 * H1_30
_temp40 += 0.251439299940001 * H1_31
_temp40 += 0.0900813643012787 * H1_32
_temp40 += -1.10522288276921 * H1_33
_temp40 += 1.17209980129227 * H1_34
_temp40 += -0.122129342033025 * H1_35
_temp40 += 0.731434769396121 * H1_36
_temp40 += 1.56418318563915 * H1_37
_temp40 += 0.101916080281168 * H1_38
_temp40 += -1.19704817994047 * H1_39
_temp40 += 0.0509686208272469 * H1_40
_temp41 += 7.81696633926759 * H1_1
_temp41 += -6.55624717875302 * H1_2
_temp41 += 7.18515621973926 * H1_3
```

```
    _temp41 += 3.95210863384018 * H1_4
    _temp41 += 21.0178170478464 * H1_5
    _temp41 += 0.914165633348978 * H1_6
    _temp41 += 13.8093630354397 * H1_7
    _temp41 += -7.14529189379519 * H1_8
    _temp41 += 0.640135862640473 * H1_9
    _temp41 += 0.680683889159819 * H1_10
    _temp41 += 0.896112369169927 * H1_11
    _temp41 += -1.26851068460609 * H1_12
    _temp41 += -0.256467223728002 * H1_13
    _temp41 += -0.701156598830882 * H1_14
    _temp41 += 0.230782832634894 * H1_15
    _temp41 += 1.26114014935077 * H1_16
    _temp41 += -0.0193723586158285 * H1_17
    _temp41 += 0.166347082989199 * H1_18
    _temp41 += -0.227311228540184 * H1_19
    _temp41 += 0.190152737298724 * H1_20
    _temp41 += -2.30285342572461 * H1_21
    _temp41 += 2.05041430719741 * H1_22
    _temp41 += 2.57871471816594 * H1_23
    _temp41 += 0.171055686104518 * H1_24
    _temp41 += 0.500572176932325 * H1_25
    _temp41 += -0.21104989985949 * H1_26
    _temp41 += 0.709967986939336 * H1_27
    _temp41 += -0.185128212988592 * H1_28
    _temp41 += -0.166088221826469 * H1_29
    _temp41 += -0.198640109280141 * H1_30
    _temp41 += 0.251439299940001 * H1_31
    _temp41 += 0.0900813643012787 * H1_32
    _temp41 += -1.10522288276921 * H1_33
    _temp41 += 1.17209980129227 * H1_34
    _temp41 += -0.122129342033025 * H1_35
    _temp41 += 0.731434769396121 * H1_36
    _temp41 += 1.56418318563915 * H1_37
    _temp41 += 0.101916080281168 * H1_38
    _temp41 += -1.19704817994047 * H1_39
    _temp41 += 0.0509686208272469 * H1_40
    outdata['Probability( Logic Packet Counts = 1 When Greater Than or Equal To 377=0 )'] =
jmp.exp(_temp40) / (1 + jmp.exp(_temp41))

    _temp42 += 7.81696633926759 * H1_1
    _temp42 += -6.55624717875302 * H1_2
    _temp42 += 7.18515621973926 * H1_3
```

```
    _temp42 += 3.95210863384018 * H1_4
    _temp42 += 21.0178170478464 * H1_5
    _temp42 += 0.914165633348978 * H1_6
    _temp42 += 13.8093630354397 * H1_7
    _temp42 += -7.14529189379519 * H1_8
    _temp42 += 0.640135862640473 * H1_9
    _temp42 += 0.680683889159819 * H1_10
    _temp42 += 0.896112369169927 * H1_11
    _temp42 += -1.26851068460609 * H1_12
    _temp42 += -0.256467223728002 * H1_13
    _temp42 += -0.701156598830882 * H1_14
    _temp42 += 0.230782832634894 * H1_15
    _temp42 += 1.26114014935077 * H1_16
    _temp42 += -0.0193723586158285 * H1_17
    _temp42 += 0.166347082989199 * H1_18
    _temp42 += -0.227311228540184 * H1_19
    _temp42 += 0.190152737298724 * H1_20
    _temp42 += -2.30285342572461 * H1_21
    _temp42 += 2.05041430719741 * H1_22
    _temp42 += 2.57871471816594 * H1_23
    _temp42 += 0.171055686104518 * H1_24
    _temp42 += 0.500572176932325 * H1_25
    _temp42 += -0.21104989985949 * H1_26
    _temp42 += 0.709967986939336 * H1_27
    _temp42 += -0.185128212988592 * H1_28
    _temp42 += -0.166088221826469 * H1_29
    _temp42 += -0.198640109280141 * H1_30
    _temp42 += 0.251439299940001 * H1_31
    _temp42 += 0.0900813643012787 * H1_32
    _temp42 += -1.10522288276921 * H1_33
    _temp42 += 1.17209980129227 * H1_34
    _temp42 += -0.122129342033025 * H1_35
    _temp42 += 0.731434769396121 * H1_36
    _temp42 += 1.56418318563915 * H1_37
    _temp42 += 0.101916080281168 * H1_38
    _temp42 += -1.19704817994047 * H1_39
    _temp42 += 0.0509686208272469 * H1_40
    outdata['Probability( Logic Packet Counts = 1 When Greater Than or Equal To 377=1 )'] = 1 /
(1 + jmp.exp(_temp42))

    _temp44[0] = outdata['Probability( Logic Packet Counts = 1 When Greater Than or Equal To
377=0 )']
```

```
    _temp44[1] = outdata['Probability( Logic Packet Counts = 1 When Greater Than or Equal To
377=1 )']
    _temp43 = jmp.max_array(2, _temp44)
    if (_temp43 == 0):
        _temp45 = 0
    elif (_temp43 == 1):
        _temp45 = 1
    else:
        _temp45 = None
    outdata['Most Likely Logic Packet Counts = 1 When Greater Than or Equal To 377'] =
_temp45

    return outdata['Most Likely Logic Packet Counts = 1 When Greater Than or Equal To 377']
```